EXPERIMENTAL INVESTIGATION AND CFD MODELLING OF A THERMOSYPHON-EQUIPPED HEAT EXCHANGER USED IN LOW-GRADE WASTE HEAT RECOVERY

JOÃO AFONSO GOUVEIA SOARES BARRETO RAMOS

A submission presented in fulfilment of the requirements
of the University of South Wales / Prifysgol De Cymru
for the degree of Doctor of Philosophy

This work is part-funded by the European Social Fund (ESF) through the European Union's Convergence programme administered by the Welsh Government and carried out in collaboration with Econotherm UK Ltd.

July 2016

University of South Wales
Prifysgol De Cymru

Graduate **R**esearch **O**ffice
Swyddfa Ymchwil Graddedigion

Certificate of Research

This is to certify that, except where specific reference is made, the work described in this thesis is the result of the candidate's research. Neither this thesis, nor any part of it, has been presented, or is currently submitted, in candidature for any degree at any other University.

Signed ……..…
Candidate (Joao Ramos)

Date ……....

Signed ……
Director of Studies (Dr Alex Chong)

Date ……

Abstract

Energy lost in the form of heat is reported to account for more than 50% of the total energy waste in industry. Due to renewed environmental policies with focus on promoting sustainability and reducing wasted energy, new measures have been put in place to reduce these energy losses. In industry, waste heat is recovered through the use of heat exchangers installed at the outlets of high temperature exhausts, recovering heat energy and meanwhile helping reduce the overall exhaust temperature with the objective of increasing the overall efficiency of the process.

The heat exchanger under study is equipped with wickless heat pipes, tubular devices filled with a working fluid and sealed in vacuum. Heat pipes are commonly found in modern electrical equipment due to their high rate of heat transfer per unit area and lack of outer energy source. Wickless heat pipes, also known as two-phase closed thermosyphons, lack a sintered wick structure within and are therefore easier to manufacture in large quantities making them ideal heat sinks in macroscopic applications such as industrial waste heat recovery.

The subject of this work is the creation of an analytical prediction model to predict the thermal behaviour of heat exchangers equipped with heat pipes. To that end, three tests were conducted, one on a single thermosyphon, another on a heat exchanger equipped with thermosyphons and the last one on a heat exchanger with returned flow on a second pass over the thermosyphons. CFD is also used using data from the prediction model in order to obtain a visualisation of the results.

The results of the analytical and CFD models were found to be in good agreement with the experimental results and a recommendation is made to implement the same model to larger heat exchangers equipped with more thermosyphons. The model will benefit the company partner, Econotherm, who shall use it in the modelling of future heat exchangers.

Acknowledgements

I would like to start by expressing my sincere gratitude to my supervisors Dr Alex Chong, the Director of Studies of this research project, as well as Dr CK Tan and Dr Jason Matthews for their incredible support, especially towards the submission date.

I would also like to extend my gratitude to Dr Hussam Jouhara for coming out of his way to give me a hand during the toughest part of the work. His support and academic know-how resulted in an *applied crash course academics* which I am most grateful for and I will remember for years to come.

I would also like to thank KESS for the excellent opportunity for newly-graduated students especially to Leanne and Alison who I dealt with several times.

A special mention to the people at Econotherm and a thanks especially to Mr Mark Boocock for the all the help and support which I hope one day I will be able to repay. David Jenkins for being a really good friend and companion during our trips to Bridgend. The technicians, Peter, Stefan, Vio and Tibi for their companionship.

A thank you to my closest colleagues and friends, Palani, Francisco, Lena and Paul for the company during long lunch time reviews, and to colleagues across different schools, Hassan and Quentin with whom I worked and aspire to work with again.

This work would not have been made possible without the initiative of Prof Albino Reis to contact the University of Glamorgan, without whom I would have never taken the first step towards studying abroad, and without whom I may not even have undertaken a PhD.

Mas mais do que tudo, gostava de agradecer aos meus queridos pais e queridos manos, pois sem o seu incentivo e apoio constante nunca teria sido capaz de me aventurar por terras de Sua Magestade para tirar um curso e eventualmente um Doutoramento. Obrigado por tudo!

Last but not least, I would also like to thank my dearest Noa as without her inspiring presence I would have never been able to gather the courage to finish the project nor the thesis. Thank you from the bottom of my heart!

Dedicado ao Zé e ao Luís, que este trabalho os inspire a seguir os seus sonhos!

Table of Contents

List of Figures

List of Tables

Nomenclature

Abbreviations

CFD	Computational Fluid Dynamics
EU	European Union
HP	Heat Pipe
HPHX	Heat Pipe-equipped Heat Exchanger
HPHS	Heat Pipe-Heat Sink
HS	Heat Sink
HX	Heat Exchanger
LMTD	Logarithmic Mean Temperature Difference
NTU	Number of Transfer Units
PCM	Phase-change Materials
TS	Thermosyphon
TSHX	Thermosyphon-equipped Heat Exchanger

Symbols

A	(m^2)	Area
C	($W.K^{-1}$)	Heat capacity ($\dot{m}c_p$)
c_p	($J.kg^{-1}K^{-1}$)	Specific heat at constant pressure
c_{sf}		Constant/coefficient used in the boiling equation
g	($m.s^{-2}$)	Acceleration of gravity
h	($W.m^{-2}K^{-1}$)	Average heat transfer coefficient
h_{fg}	($J.kg^{-1}$)	Latent heat
k	($W.m^{-1}K^{-1}$)	Thermal conductivity
L	(m)	Length/Characteristic dimension
$\dot{m}$	($kg.s^{-1}$)	Mass flow rate
n		Constant whose significance changes depending on equation
Nu		Nusselt number
N_L		Constant representing number of rows
Pr		Prandtl number
Q	(W)	Heat transfer rate
q''	($W.m^{-2}$)	Heat flux

Re		Reynolds number
R_{th}	($K.W^{-1}$)	Thermal resistance
r	(m)	Radius
T	(K)	Temperature
U	($W.m^{-2}K^{-1}$)	Overall heat transfer coefficient
v	($m.s^{-1}$)	Average velocity
Δ		Difference
ΔT_{LM}	(K)	LMTD – Logarithmic Mean Temperature Difference
α	($m^2.s$)	Thermal diffusivity
μ	($kg.m^{-1}s^{-1}$)	Dynamic (absolute) viscosity
v	($m^2.s$)	Kinematic viscosity (μ / ρ)
π	~3.141592	Pi
ρ	$Kg.m^{-3}$	Density
σ	($N.m^{-1}$)	Surface tension
Φ	($W.m^{-2}$)	Heat Flux

Subscripts

avg	average
b	boiling
c	Cold side/Condenser side
e	Evaporator section
h	Hot side
i	Inlet
l	Liquid phase
o	Outlet
s	Surface (temperature)
sat	Saturation (temperature)
T	Total
ts	Thermosyphon
v	Vapour/Gas phase

Chapter 1

Introduction

Ever since the discovery of fire, humanity has regarded heat as a source of energy, for warmth, protection and especially comfort. With the advent of the industrial revolution and especially the discovery and development of the steam engine, heat energy quickly became the central protagonist in energy production. Even to this day, the main source for electrical energy generation is heat produced from coal, gas or oil-fuelled furnaces (Coal Industry Advisory Board, 2008; BP, 2015; Valliappan, 2015).

Unfortunately, heat energy is not desirable for the environment; the recent increase in the earth's global temperature (Brahic, 2007), has caused a great number of changes in our planet, ranging from melting of the ice caps to changes in oceanic currents (PISCO, 2010). The rise in temperature aligns with the recent increase in the amount of carbon dioxide (CO_2) in the atmosphere, in itself a result of industrialisation.

Fortunately, the term *sustainability* has been finding increased use as a keyword for change (Vandermeersch, et al., 2014) resulting in new environmental policies (EU, 2013; European Commission, 2014) that countries in the European Union (EU) are required to follow. Sustainability is related to the efforts made to guarantee sustenance for future generations so they will not have to bear with the fruits of bad resource management. These efforts translate into the reduction of primary energy consumption and reduction of overall energy wastage.

In the case of heat energy, one area of CO_2 reduction is through energy efficiency enhancement of industrial processes, specifically through the reduction of the temperature of exhaust gases. Energy recovery can be done through the installation of a heat exchanger, a device employed to recover exiting heat energy. The recovered heat energy may be reused or stored for later use.

Heat exchangers are tailor-suited to fit their specific application and therefore heat exchanger types are as varied as their applications. The most common type of heat exchanger is the shell-and-tube heat exchanger. The shell-and-tube is so common that it is often referred to as a "conventional" heat exchanger. It has been studied in great detail and most of the empirical expressions available in literature relate to it, it is the benchmark for current heat exchanger analysis.

As previously mentioned, there are other types of heat exchangers that find moderate usage in industry, once again depending on their particular application. One of such types is the heat pipe-based heat exchanger, which refers to a heat exchanger equipped with heat pipes. Heat pipes are effectively superconductors with a thermal conductivity many times that of copper (Faghri, 1995). The application of heat exchangers to waste heat recovery is a relatively novel technology and specific knowledge is required in this subject area in order to design and build these units.

It is in low- to medium-grade heat (temperatures ranging from 100 °C to 400 °C) that 90% of the wasted heat energy is found, as shown graphically in Figure 1-1 (Haddad, et al., 2014). It is in this environment that heat exchangers equipped with thermosyphons are finding increasing use due to an array of inherent advantages discussed in great detail in the literature review. Thermosyphons are devices sealed in vacuum and partially filled with a working fluid; heat transfer takes place axially through the phase change process of the working fluid (Reay & Kew, 2006; Yau, 2008; Jouhara, et al., 2009) (a schematic can be seen in Figure 2-1, page 7).

The challenge is to build a simplified design tool able to predict the performance of heat exchangers equipped with thermosyphons for a range of different inlet temperatures and mass flow rates.

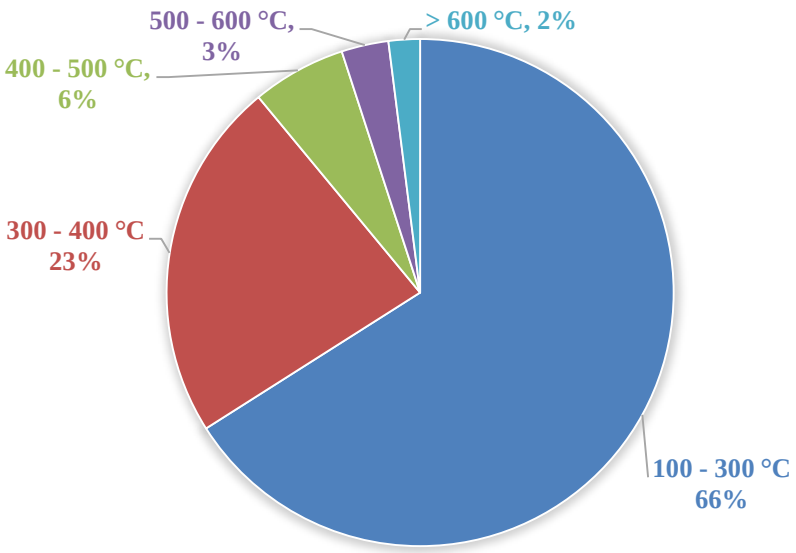

Figure 1-1 – Industrial waste heat temperature distribution in the EU (Haddad, et al., 2014)

This thesis was carried out in partnership with Econotherm UK Ltd, an associate company of Spirax Sarco Plc., which specialises in thermosyphon-equipped heat exchangers employed in the waste heat recovery industry. This study intends to simplify the design process by considering the thermosyphons as super-conductors of a set thermal conductivity which is a function of the inlet conditions. To assess the approach, a custom-built experimental rig was created and tested for low-grade heat.

Up to this point, the term “thermosyphon” has been liberally interchanged with the term “heat pipe”. It is important to note that the heat exchangers Econotherm currently designs and sells are equipped with two-phase closed thermosyphons. The term “thermosyphon” shall be used from this point onward to refer to the wickless heat pipe.

1.1 Aim and Objectives

The main aim of this study is to develop a prediction tool that measures the heat transfer performance of a thermosyphon-equipped heat exchanger through use and adaption of a combination of current theoretical expressions. A comprehensive yet approachable scientific method to characterise thermosyphon-equipped heat exchangers is still missing in this field of study and could help attract greater interest towards this type of devices.

From this aim the following objectives were derived:

- The first objective focusses on developing a working knowledge of the heat transfer processes inside the tubular thermosyphon, with an emphasis on boiling and condensation heat transfer.
- The second objective is to create a prediction tool based on empirical formulae that will allow the prediction of the outlet conditions of thermosyphon-equipped heat exchangers.
- The third objective is to create a CFD model for the performance prediction of a thermosyphon-equipped heat exchanger. The model's boundary conditions are extracted from the prediction tool. The model will help the design of thermosyphon-equipped heat exchangers.
- The fourth objective is to validate the theoretical results from the prediction tool and the results from the CFD simulation against experimental results obtained from a purpose-built experimental rig.

1.2 Relevance to Science and Industry

Heat pipes have been finding increased use as heat sinks in small electrical equipment due to their size and lack of need of external power (Jouhara & Meskimmon, 2014; Mroué, et al., 2015). Due to their popularity, literature on these devices is extensive (Vasiliev, 2005; Chan, et al., 2015). Larger thermosyphons have started receiving renewed interest as waste heat recovery equipment due to recent environmental policies and cheapest manufacturing costs, however, there is not a large amount of recent literature on the subject, additionally very little mention of its application in heat exchangers used in low to medium grade waste heat recovery equipment (up to 300 °C) has been made.

1.3 Organisation and structure of the thesis

The thesis is organised in the following sequence:

Chapter 1 provides an overview of the background of the work: the current climate problems resulting in renewed environmental policies and how heat exchangers are currently used as waste heat recovery devices. The use of thermosyphon-equipped heat exchangers is also introduced, as well as the concept of the heat pipe/thermosyphon.

Chapter 2 reviews the current status of literature concerning the modelling and prediction of the performance of thermosyphons and heat exchangers equipped with thermosyphons, with an emphasis on the different aspects of heat transfer within the devices. The necessary ingredients to create the simplified prediction tool are also presented.

Chapter 3 contains a thorough review of the method(s) used to characterise a heat exchanger equipped with heat pipes or thermosyphons with emphasis on the thermal network analysis method.

Chapter 4 contains a description of the experimental set-up, portraying meticulously the steps taken to conduct the experiments with a single thermosyphon and the small heat exchanger. It also lists the instrumentation required.

Chapter 5 presents the experimental results and discussion for all the tests conducted, the single thermosyphon, the heat exchanger in single pass and the heat exchanger double pass. It proceeds to compare the results to the prediction model.

Chapter 6 contains all the information related to the CFD simulation, including the mesh setup, the model design, the boundary conditions and the results, including plots of the velocity and temperature profile within the heat exchanger. At the end of the chapter, a discussion of the the results presented is included.

In chapter 7 the final conclusions are drawn and recommendations for future work are made.

Chapter 2

Literature Review

This section outlines relevant work done in the field of heat exchangers equipped with thermosyphons, extending to literature on thermosyphons and CFD simulations of heat exchangers.

The section starts by introducing the tubular thermosyphon and the heat exchanger equipped with thermosyphons. On the latter, different applications for the thermosyphon-equipped heat pipe are presented. The chapter closes with after presenting and reviewing previous work in the field similar to the current study.

2.1 The tubular heat pipe and the thermosyphon

A thermosyphon, also known as two-phase closed thermosyphon or wickless heat pipe, consists of a tube partially filled with a working fluid and sealed in vacuum. Applying heat to the lower section of the tube (the evaporator) causes the fluid within to evaporate, forcing it to travel in gaseous form to the upper section (the condenser). Contact with the colder wall on the upper section causes the vapour to condense and flow back to the base in liquid form, thus completing the thermodynamic cycle.

This principle of two-phase heat transfer (liquid-gas) allows for high quantities of heat to be transferred at essentially constant temperature as the working fluid is constantly at its saturation temperature (Faghri, 1995; Faghri, 2012). As long as the warmer end of the tube is within the saturation temperature of the working fluid at the tube's working

pressure and there is a temperature difference between the two sections, a large amount of heat can be transferred based on the latent heat of evaporation of the fluid within.

As can be seen in Figure 2-1, the thermosyphon is customarily divided into three sections: evaporator, adiabatic and condenser sections; the denomination of each section is derived from the respective external thermal boundary conditions. Heat is received by the working fluid at the condenser section, causing it to evaporate and flow through the adiabatic section to the lower temperature condenser where the captive heat is released.

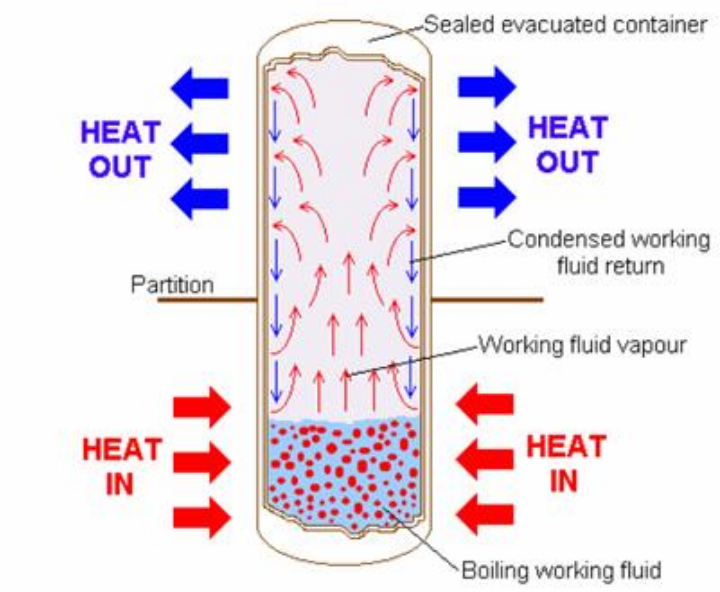

Figure 2-1 – Schematic representation of a thermosyphon (ForSTEEL Ltd., 2008)

The energy transfer through a heat pipe is said to be several times that of copper (Faghri, 1995), and that is due to the change of internal energy associated with the phase change of a system. This energy is called *latent heat* and it is very large in the evaporation and condensation processes (Çengel, 2002; Hagens, et al., 2007). Under equilibrium conditions, large amounts of heat can be transferred at essentially constant temperature and pressure thus giving the thermosyphon a very high effective thermal conductance. The pressure inside the thermosyphon adjusts itself in order to better accommodate outer temperature conditions and maintain a constant evaporation-condensation of the working fluid (Carvajal-Mariscal, et al., 2012).

Before delving further into the heat transfer characteristics of thermosyphons, it is important to outline the difference between a thermosyphon and a heat pipe. The most common type of heat pipe is the wicked heat pipe, represented in Figure 2-2 on the left.

Equipped with a porous wick structure, it is able to function against the force of gravity. This capability is a result of the high difference in pressure between the evaporator and the condenser which is able to push the condensed fluid to the walls of the pipe into the wick, and back to the evaporator. The "wick" is an internal porous structure used to move the liquefied working fluid to the evaporator when the force of gravity is not present to do so. Heat pipes (equipped with an inner wick) have been popularised as effective heat transfer equipment in space and in the computing industry (Vasiliev, 2005) and their popularity has made it so that the term "heat pipe" applies to all devices that rely on phase change to transport heat. In a thermosyphon, the condenser section must always be located above the evaporator section (i.e. the hot flow section), as the device relies on gravity to pull the condensate back to the evaporator, as can be seen in Figure 2-2 on the right.

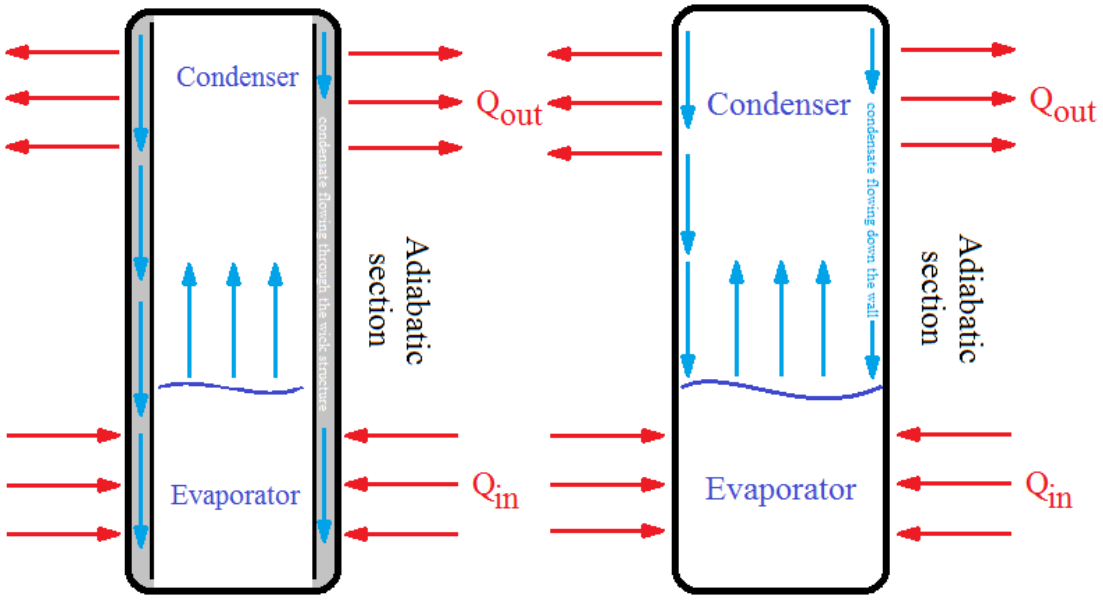

Figure 2-2 – Schematic comparison between a heat pipe (L) and a thermosyphon (R)

The use of the term "thermosyphon" to refer to two-phase evacuated devices dates from as early as 1960 (Lock, 1992) and the discoveries made on thermosyphon technology eventually gave rise to modern wicked heat pipes. Additionally, thermosyphons are preferred to wicked heat pipes outside the computing and space industry due to the lack of a wick structure, which does not hinder their heat transfer capabilities at a bigger scale and keeps its manufacturing price down (Vasiliev, 2005).

2.1.1 Working fluids

The choice of working fluid always comes first and, if price is not considered an issue, it is dictated by the saturation temperature of the fluid and the future working conditions, in particular the difference in temperature between the evaporator and the condenser. Common working fluids include: water, helium, hydrogen, toluene, methanol, ammonia, sodium and silver. Table 2-1 lists the physical properties of most of the working fluids that may be found inside a common thermosyphon. The most important are latent heat (h_{fg}) and surface tension (σ), therefore, acetone, diethyl ether, ethanol, methanol, and water are the most recommended fluids (Chen, et al., 2016). In general, water is preferred due to its high latent heat, suitable boiling point and availability (Hughes, et al., 2014) but depending on the working conditions and on the compatibility with the shell material, other fluids may be considered as well.

Table 2-1 – Properties of different working fluids

Adapted from several sources (Incropera & DeWitt, 1996; M. Conde Engineering, 2004; Bar-Cohen, et al., 2006; Chen, et al., 2016)

No	Name	ρ (kg/m^3)	T_b (°C)	h_{fg} (J/kg.K)	c_p (J/kg.K)	k (W/mK)	σ (N/m)	μ (kg/m.s)
1	Acetic acid ($C_2H_40_2$)	1049	118	390	1960	0.180	27.6	1.219×10^{-3}
2	Acetone (C_3H_60)	780	57	520	2210	0.161	23.7	0.324×10^{-3}
3	Benzene (C_6H_6)	879	80	400	1700	0.140	28.9	0.647×10^{-3}
4	Bromine (Br)	3100	59	183	460		41.5	0.993×10^{-3}
5	Carbon disulphide (CS_2)	1293	46	360	1000	0.144	32.3	0.375×10^{-3}
6	Carbon tetrachloride	1632	77	190	840	0.103	26.8	0.972×10^{-3}
7	Chloroform ($CHC1_3$)	1490	61	250	960	0.121	27.1	0.569×10^{-3}
8	Ether, diethyl ($C_4H_{10}O$)	714	35	350	2300	0.127	17	0.242×10^{-3}
9	Ethyl alcohol (C_2H_60)	789	79	850	2500	0.177	22.3	1.197×10^{-3}
10	Methyl alcohol (CH_40)	791	64	1120	2500	0.201	22.6	0.594×10^{-3}
11	Toluene ($C7H_8$)	867	111	350	1670	0.134	28.4	0.585×10^{-3}
12	Turpentine	870	156	290	1760	0.136	27	1.490×10^{-3}
13	Water (H_2O)	958	100	2257	4217	0.68	58.9	0.279×10^{-3}
14	Ammonia	681	-33	1369	1463.9			
15	R134		-27	215			91.2	
16	FC-40	1870	156	711.6			16	3.540×10^{-3}
17	FC-72	1623	56	85.0	1098		8.4	0.457×10^{-3}
18	HFE-7100	1500	61	125.6	1180		14	0.610×10^{-3}
19	HFE-7200	1430	76	122.6	1210		14	0.610×10^{-3}

2.1.2 Materials used for outer shell casing

The choice of materials for the outer shell and its compatibility with the inside surface must be carefully considered especially if a wick is placed inside the heat pipe. The wick found within a heat pipe must resist the constant flowing of the working fluid and is commonly composed of the following materials: copper, stainless steel, nickel, bronze, titanium, carbon fibres and cloths. The material is chosen after the working fluid. In addition, the wick may also have different configurations which allow more or less wetting of the internal walls of the thermosyphon. Typical wick configurations include: screens, grooves, sintered powders, felt (fibrous media) or foams.

In order to insure a long life for the two-phase closed thermosyphon, it is important to ensure that internal and external fluids are compatible with the shell of the tube. Common materials for the thermosyphon wall (the shell): copper, stainless steel, nickel, aluminium, titanium. (Faghri, 1995).

2.1.3 Types of heat pipes

Heat pipes come in many shapes and sizes, most commonly with a circular cross section but may also be found, depending on the application, with rectangular cross-sections. Regardless of the different shapes and designs, the heat pipe always operates under the same principle of phase change of the working fluid.

Size wise, heat pipes can be as small as 10 μm (Sobhan, et al., 2007) and as long as 100 m (Faghri, 2012). The temperature range depends on the working fluid and on the thermal capacity of the outer shell, ranging from as low as -200 °C up to 2000 °C (Thermacore, 2016)

Types of heat pipes include two-phase closed thermosyphons (more commonly referred to as thermosyphons), capillary-driven heat pipes (cylindrical heat pipes with a wick), annular heat pipes, vapour chamber heat pipes (flat shaped), rotating heat pipes, gas-loaded heat pipes, loop heat pipes, capillary pumped loop heat pipes, pulsating heat pipes, micro and miniature heat pipes and inverted meniscus heat pipes (Faghri, 1995; Reay & Kew, 2006).

In terms of working life, heat pipes have reported lives as high as 13 years (Rosenfeld, et al., 2003) or even 20 (Econotherm, 2012).

2.1.4 Heat pipe operating limits

The heat pipe is a self-contained device operating at essentially constant temperature and pressure; as the temperature increases, the pressure adjusts itself in order to keep the heat pipe in working order. However, if the power source happens to exceed the heat transport limitations, a catastrophic temperature increase may occur which may in turn damage or even destroy the heat pipe seal and the device itself (Noie-Baghban & Majideian, 2000; Faghri, 1995; Peterson, 1994; Terpstra & Veen, 1987).

In a heat pipe-equipped heat exchanger, the limitation that restricts the operation of the assembly is determined by the heat pipe with the lowest heat transfer rate at a specific working temperature. Depending on the working conditions, several limits to heat pipe health have been identified in literature and are listed below. A graphical representation of the limits with respect to Heat flux and temperature is presented graphically in Figure 2-3.

(1) Viscous limit – a result of low temperature at the evaporator section, a temperature too low to allow complete evaporation of the working fluid. Due to the insufficient difference in vapour pressure between the evaporator and the condenser, the evaporated working fluid is incapable of moving up the tube and to overcome the fluid's viscous forces thus not being able to complete the thermodynamic cycle.

(2) Sonic limit – common during start-up, as the temperature increases, the vapour velocity continuously increases until it reaches the speed of sound. A barrier is created between the evaporator and the condenser at this point.

(3) Wicking or capillary limit (Heat pipe only) – This limit takes place when the capillary pressure is too low for the condenser to provide sufficient liquid to the evaporator, which leads to dry-out in the evaporator. Dry-out prevents the thermodynamic cycle from continuing, and the heat pipe to function properly.

(4) Entrainment limit (Heat pipe only) – at high vapour velocities, droplets of liquid in the wick are pulled from the wick and sent into the vapour, which results in dry-out at the evaporator section.

(5) Boiling limit – dry-out occurs when the radial heat flux into the heat pipe causes the liquid in the wick or in the surface of the pipe to boil and evaporate at a faster rate than it returns to the evaporator. The boiling limit may also be expressed as burnout or critical

heat flux (CHF). After the limit has been reached, a vapour blanket is created thus creating an extra resistance to heat transfer (Revellin & Thome, 2008).

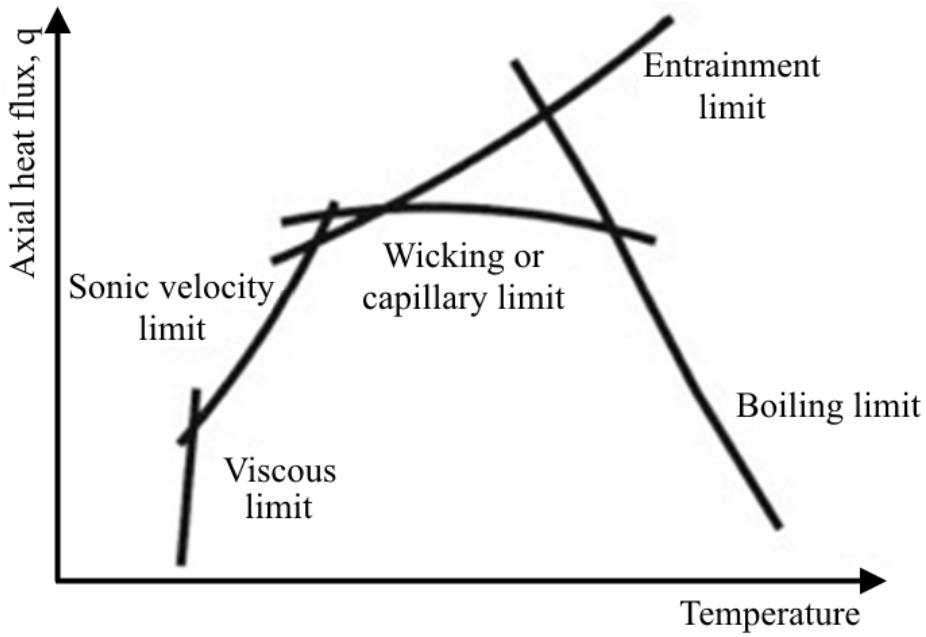

Figure 2-3 – Operating limits of the heat pipe (Reay & Kew, 2006)

2.1.5 Characterisation of the performance of a working thermosyphon

One of the most widely accepted methods of characterisation of a thermosyphon is the thermal network analysis (Shabgard, et al., 2015). In this approach, an analogy is made comparing the thermosyphon to an electrical circuit. The different heat transfer modes are interpreted as different thermal resistances.

In order to identify the highest and lowest resistances to heat transfer, just imagine an assembly such as that found in a car radiator. The working fluid inside the pipe is hot and it is cooled through contact with outside air. The greatest thermal resistances are the convection inside and outside the tube and the conduction across the tube, which may even be neglected for thin-walled tubes. The same approach may be used in a thermosyphon, with the addition of evaporation and condensation processes taking place within the tube and the movement of particles from the evaporator to the condenser section, the latter dependent on tube length.

Looking at a simple thermosyphon in cross flow, as can be seen in Figure 2-4, the thermal resistances are in series as the heat moves from the evaporator to the condenser section following a strict order of convection to the pipe wall ($R_{h,e}$), conduction across the pipe wall ($R_{k,e}$), convection to the working fluid causing evaporation on the evaporator side (R_b), the movement of the fluid particles from the evaporator to the condenser section (R_{in}), condensation on the wall of the pipe (R_{cd}), conduction across the pipe wall ($R_{k,c}$) and finally convection to the outside medium ($R_{h,c}$). There is also axial conduction across the thermosyphon ($R_{k,t}$) but that may be neglected in the analysis of long heat pipes with small cross-sectional areas (Hagens, et al., 2007).

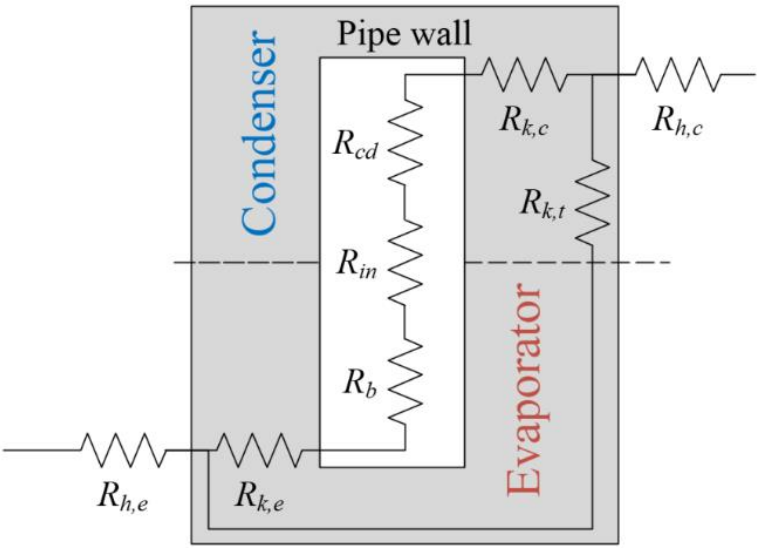

Figure 2-4 – Schematic of the thermal resistances within the thermosyphon

A detailed breakdown of the characterisation of a heat pipe is given in Chapter 3 – Theoretical Analysis.

2.2 Heat exchangers

In the words of Shah & Sekulić a heat exchanger may be defined as "*a device that is used to transfer thermal energy between two or more fluids or between a solid surface and a fluid… The fluids need to be at different temperatures and there must be thermal contact*" (Shah & Sekulić, 2003).

The purpose of a heat exchanger is to extract heat from where it is undesired and to transfer it somewhere where it may be useful. Heat exchangers find use in a variety of fields but the three main areas of application are in: Energy production, Heating, Ventilation and Air Conditioning (HVAC), and Waste heat recovery.

Heat exchanger design varies according to the specified working conditions and requirements; a lower pressure drop, a higher exposure area, the presence of a high percentage of unwanted particles, etc. In industrial waste heat recovery, it is not uncommon for the flow to have a high level of particulates, which in turn poses a threat of fouling in the heat exchanger. The flow may even contain corrosive substances which may decrease the working life of the heat exchanger or even cause full failure through cross-contamination. Heat exchangers equipped with thermosyphons are employed to tackle these problems through a number of inherent advantages.

2.2.1 Heat exchangers equipped with thermosyphons

The typical design goals for these devices as for all heat exchangers are to maximise heat transfer rates and effectiveness all the while minimising the cost, usually by minimising the size, weight, but also the pressure drop and the overall thermal resistance. Secondary objectives include minimising corrosion and fouling and preventing freezing. All of the design objectives have a direct effect on one another as size affects cost, pressure drop affects heat transfer rate and fouling, fouling affects the heat transfer and so on.

According to Shabgard et al (2015), the most basic form of a heat pipe-equipped heat exchanger (HPHX) is shown in Figure 2-5(a), in which a hot fluid and a cold fluid are in contact through the medium of a heat pipe or thermosyphon placed in between them. As can be seen in Figure 2-5(b), the adiabatic section is not necessary and may be removed allowing the heat pipe to function in parallel with the plate placed in between the two fluids.

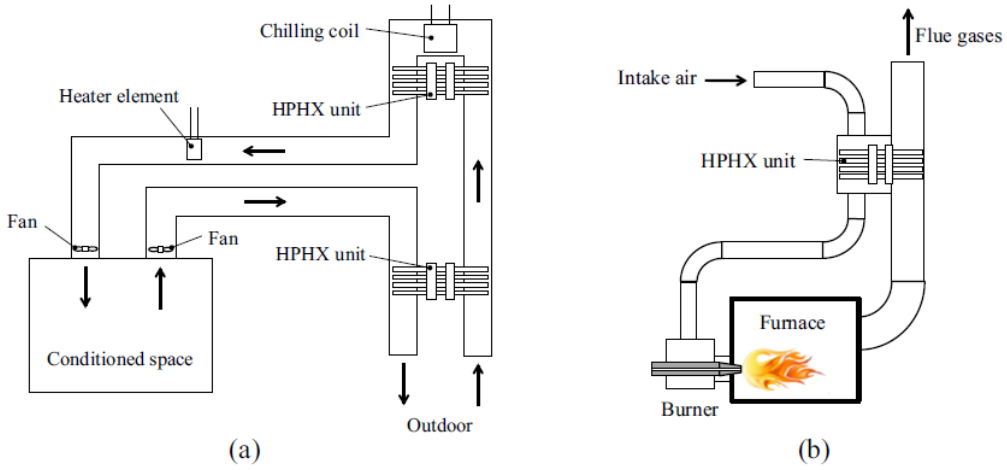

Figure 2-5 – Applications of HPHX systems (a) HVAC, (b) waste heat recovery.

(adapted from Shabgard et al. (2015))

Heat exchangers equipped with heat pipes or thermosyphons offer many advantages when used as waste heat recovery devices and those advantages are widely highlighted in literature (Nuntaphan, et al., 2001; Noie, 2005; Vasiliev, 2005; Hagens, et al., 2007; Econotherm, 2012; Shabgard, et al., 2015) and presented below:

- *Increased redundancy and reliability*: In waste heat recovery, the inlet flows are often dirty and have a high percentage of small sediments. These particles may cause fouling inside the heat exchanger. Fouling reduces the heat exchanger's performance and can even damage it. In a thermosyphon-equipped heat exchanger, fouling is mitigated by replacing the thermosyphons regularly and in case of failure of a single thermosyphon, it can just as easily be replaced by another device.
- *Ease of cleaning*: All the thermosyphons can be easily removed after being installed, facilitating access to hard-to-reach areas within the heat exchanger.
- *No additional power input to the system*: After installed, the thermal energy extraction takes place without any need for external power input to the system;

the thermosyphons will be active as long as there is a difference in temperature between the two streams.

- *Reduced risk of cross-contamination*: The thermosyphon functions thanks to the phase-change process of the working fluid. In the mid-section, where the working fluid is travelling to either end of the thermosyphon, there is no heat transfer taking place as long as the section is kept insulated. A complete separation of the two streams is possible as the heat pipes are the heat transfer medium between the hot and cold flow.
- *No moving parts*: The thermosyphons themselves are individual devices and each carry their own maximum performance. Under operation all of them are sealed and carry no moving parts.
- *Reduced production costs of heat pipes*: Due to increased production of heat pipes and thermosyphons and the know-how of their production, prices have reduced tenfold in the past 20 years.

Heat exchangers equipped with heat pipes are superior to conventional heat exchangers when: (i) applications require great distances between the hot and cold streams as the thermosyphons may be built longer and kept at constant temperature across the adiabatic section, or when (ii) the hot and cold fluids have different properties and require different exposure areas; traditionally, fins are used but it is common knowledge that fin efficiency decreases with length.

2.2.2 Applications of heat exchangers equipped with heat pipes and thermosyphons

Applications of heat pipe-equipped heat exchangers (HPHX) are broadening due to their versatility and the ease with which different designs may be obtained. Over the course of this chapter, a thermosyphon is seen as a type of heat pipe as it can be employed in the same situations as long as anti-gravitational heat flow is not required. The next sub-chapters will focus on giving the reader a look into what applications better suit the use of HPHX.

2.2.2.1 Applications to Baking

HPHX have been tried and tested as waste heat recovery devices in high temperature baking ovens. Before bread is baked, it is often allowed to rise in a low-temperature

oven maintained at 40°C ad 95% relative humidity. Akbarzadeh and Dube (2001) conducted an experimental and analytical study (using the ε-NTU method) of a loop thermosyphon heat exchanger to recover waste heat from a high temperature baking oven to heat a low temperature proofing oven (where the bread is raised). The TSHX was able to supply the heat required in the proofing oven therefore eliminating the requirement of heating system. The payback period in this application was reported to be less than 3.5 years.

2.2.2.2 Applications with PCMs

A heat pipe heat exchanger equipped with a phase-change material (PCM) is another relatively common configuration. The PCM is usually equipped to the adiabatic section of the HP, the purpose of the PCM is to store thermal energy and the HP is used to increase the rate at which the PCM stores or discharges thermal energy (Sharifi, et al., 2014).

2.2.2.3 Data centre cooling

Data centres often generate a high amount of heat and often require cooling in order to function properly. The thermal management of data centres often takes between 10-50% of the total power used by the facilities (Sawyer, 2004). A possibility is to use cool air from outdoors during cold times of the year. Zhou et al. (2013) looked at the possibility of installing TSHX on Chinese telecommunication base stations during winter months. It was concluded that a difference of 3°C was sufficient for the TSHX to operate in this environment and to achieve energy savings that offset the cost of the fan required to force air through the TSHX tubes.

In another work by Wu et al. (2011) a TSHX was used in parallel with a chiller in order to cool a water tank. As long as the surrounding air was cooler than the water the thermosyphon handled most of the cooling load. As long as the outside temperature was a bit higher, the chiller would turn on and ensure the water stayed at the required temperature. Energy savings were on the order of 60% as the TSHX handled 60% of the yearly cooling load.

2.2.2.4 Electronics cooling using HPHX

HPHX may also be used as heat sinks to cool down electronic equipment. These applications tend to be smaller than the other examples in this list with cross-sections on the order of millimetres. Heat pipe heat sinks (HPHS) are mostly found as CPU coolers in laptop computers. This is due to the impracticability of direct cooling of the CPU due to the limited space available inside the casing. The HP is then used as a medium to transfer heat from the CPU to a remotely located heat sink. The HP is used due to its lower thermal resistance when compared to solid materials (Shabgard, et al., 2015). One might argue that the internal resistances of the thermosyphon creates a larger overall thermal resistance. However, the convective thermal resistance may be reduced through the use of fins at the condenser section. This arrangement has been proven to reduce the overall thermal resistance by addition of multiple finned HPs (Wang, 2008; Anandan & Bhaskaran, 2012). Kim and Kim (2014) conducted an experiment in which an ECU was cooled with a flat heat pipe and it was found that the integrated circuit (IC) temperature was reduced by 42°C by using the HP when compared to an IC merely exposed to ambient air in both vertical and horizontal orientations.

2.2.2.5 Heating, ventilation and air conditioning (HVAC) systems

One of the most common applications of heat pipe-equipped heat exchangers is in thermal energy recovery of HVAC systems, using air on both external fluid sides. HPHX used in HVAC systems can either (a) recover coolness from exhaust air in hot climates or (b) recover heat from exhaust air in cold climates. Due to their simplicity, installation is an easy task even in existing HVAC systems.

It was found by Yau (2007) that the sensible heating ratio of a HVAC system, defined as the ratio of sensible to total heat load, could be reduced from 0.856 to 0.188 by the addition of a HPHX system.

In hot and humid weather typical of tropical climates it is conventional to use a chilling coil around which condensation occurs which in place reduces the moisture in the air. However, the chilling coil has been found to overcool the hot air which then requires an electric heater to heat the air to the desired temperature. A HPHX may be installed instead to reheat the air after it comes back from the chilling coil. This application has been studied extensively in the literature surveyed (Yau & Tucker, 2003; Yau, 2008b; Jouhara, 2009; Yau, 2010).

In a study by El-Baky and Mohamed (2007) different mass flow rates across the evaporator and condenser streams were investigated for the same operating temperatures and it was found that a higher ratio between return air and fresh air resulted in greater cooling of the fresh air, a result of the higher heat transfer coefficient of the shell-side flow.In an experimental study conducted by Jouhara and Merchant (2012), the influence of the inclination angle and hot air inlet temperature on the effectiveness was investigated and it was found that the effectiveness increases the closer the thermosyphon is from a vertical displacement as well as by increasing the inlet air temperature. However, in a similar study using a heat pipe-equipped heat exchanger the inclination angles were found to have little effect on the performance of the HPHX (Yau & Ahmadzadehtalatapeh, 2010). A horizontal displacement was still recommended since vertical external fins facilitated drainage.

A numerical study using a multi-phase flow was conducted by Hughes et al. (2014) on horizontally oriented heat pipes for passive energy recovery in natural ventilation air systems. He reported that air could be passively pre-cooled and pre-heated by more than 15.6°C and 3.3°C, respectively.

The use of HPHX has also been recommended in hospitals due to the high degree of flow separation which ensures clean conditions in surgery rooms (operating theatres) and where air is required to change up to 40 times per hour (Noie-Baghban & Majideian, 2000). Using a schematic model of a HPHX used in conjunction with the HVAC system of an operating theatre, Yau and Ng (2011) found that the HPHX is capable of reducing the energy consumption by over 50% with a payback period of less than one year (0.95 years).

An analytical study of a relatively large thermosyphon-equipped heat exchanger (TSHX) currently used in a shopping mall in Beijing was studied by Ma et al. (2013). The heat exchanger was equipped with 192 copper thermosyphons measuring 1.34 m and 16 mm of outer diameter with 1 mm wall thickness. During summer, the TSHX transferred heat from exhaust air to fresh intake air and during winter vice-versa. Through tests it was proven that the TSHX saved approximately 24,000 kWh and 3200 kWh of electrical energy during winter and summer (respectively) and the estimated payback period was of 2.65 years.

Another application worthy of note is that of pulsating heat pipes, continuous devices consisting of an uninterrupted full cycle constantly undergoing evaporation and condensation at different rates. Due to the relatively high surface areas in contact with external air flows and relatively small overall system volume, they are promising in the field of HVAC (Zhang & Faghri, 2008; Srimuang & Amatachaya, 2012).

2.2.2.6 Metal forging

A conventional HPHX was used by Yodrak et al. (2010) to recover waste heat from a furnace of a hot brass forging process. In a simple loop, the exhaust gas is used to pre-heat the incoming air into the furnace. The analysis was made using a combination of the thermal network analysis method in conjunction with the LMTD in order to predict the heat transfer rate in the HPHX. It was found that an increase in the inlet gas temperature resulted in an increased heat transfer rate. Furnace fuel consumption using the HPHX was reduced by about 20%.

2.2.2.7 Nuclear applications

Mochizuki et al. (2013) investigated the application of a passive TSHX cooling system for thermal management of spent fuel at the Fukushima Daiichi nuclear reactor in Japan. It was concluded that the HPHX would be effective and perhaps safer in dissipating heat from the spent fuel when compared to current techniques.

2.2.2.8 Power plant cooling towers

Power plants, where electricity is created through the movement of steam can also benefit from the use of HPHX or TSHX as either to cool the steam after expansion or cooling the water upstream of a wet cooling tower. Robertson and Cady (1980) investigated the application of HPHX to dry coolers using ammonia HPs ranging in length from 8 to 23 m. Significant operating advantages were observed over the course of 18 months relative to conventional designs and due to the reduced cost of heat pipes, cost-competitive with other methods of dry cooling.

2.2.2.9 Solar power applications

HPHXs may also be applied to solar collectors as a medium to transfer the heat energy from the collector to an external fluid (usually water). This application of heat pipes has been recommended in literature as efficient heat transport mechanisms for use in solar collectors (Chougule, et al., 2013). Rassamakin et al. (2013) proposed a new HPHX design consisting of modules comprising of cylindrical heat pipes equipped to a flat

plate solar collector as one piece. The heat pipe was used to cool the solar collector and to heat water and HP thermal resistances were found to be as low as 0.02 °C/W. A similar work has been presented by Jouhara et al. (2015) in which solar panels were cooled by flat plate heat pipes. The solar panels were found to have a greater efficiency when equipped with the flat plate heat pipes as they were cooler and the flat plate HPHX equipped to the solar panels were found to warm up the water on the condenser side at a faster rate as the solar panels have a higher solar absorption rate.

2.2.2.10 Stabilisation of permafrost

The application of heat pipes to permafrost stabilisation has already been proven to work as shown by the oil pipeline in Alaska, installed 2 decades ago (Reay & Kew, 2006). The idea is to employ the thermosyphons vertically, evaporator below, which ensures the heat from the surrounding warm weather is absorbed and the ice maintained. It has been proven that the operation can be maintained with a temperature difference between the evaporator and the condenser as low as 0.2 °C (Zhang, et al., 2013). Another advantage for this application is the ease of maintenance (Zhi, et al., 2005; Bayasan, et al., 2008).

2.2.2.11 Thermal management of spacecraft

Heat pipes first found popularity from the application to spacecraft due to their ability to dissipate heat efficiently regardless of their orientation and of any surrounding forces such as gravity (Vasiliev, 2005). And the applications of HPs keeps expanding, as shown by Kim et al. (2013), using PCM-HPHS to aid in the thermal management of spacecraft control systems. The heat sinks (HS) were divided into two; a lower half containing a HP and an upper half containing a phase-change material. The HS was integrated into the heated baseplate. A reduction on the component operating temperature by 28°C was observed due to redistribution of the temporal peak heat over the whole orbit period.

2.2.3 *Characterisation of the performance of a heat exchanger equipped with thermosyphons*

One of the most common approaches to analysing the performance of a thermosyphon-equipped heat exchanger is the thermal network analysis, represented in Figure 2-6. It is also the most common and simplest approach to characterising a heat pipe or a thermosyphon (Shabgard, et al., 2015). Other methods are used in addition to the thermal network analysis such as the logarithmic mean temperature difference (LMTD) and the effectiveness NTU (ε-NTU) method, both described in more detail in Chapter 3 – Theoretical Analysis.

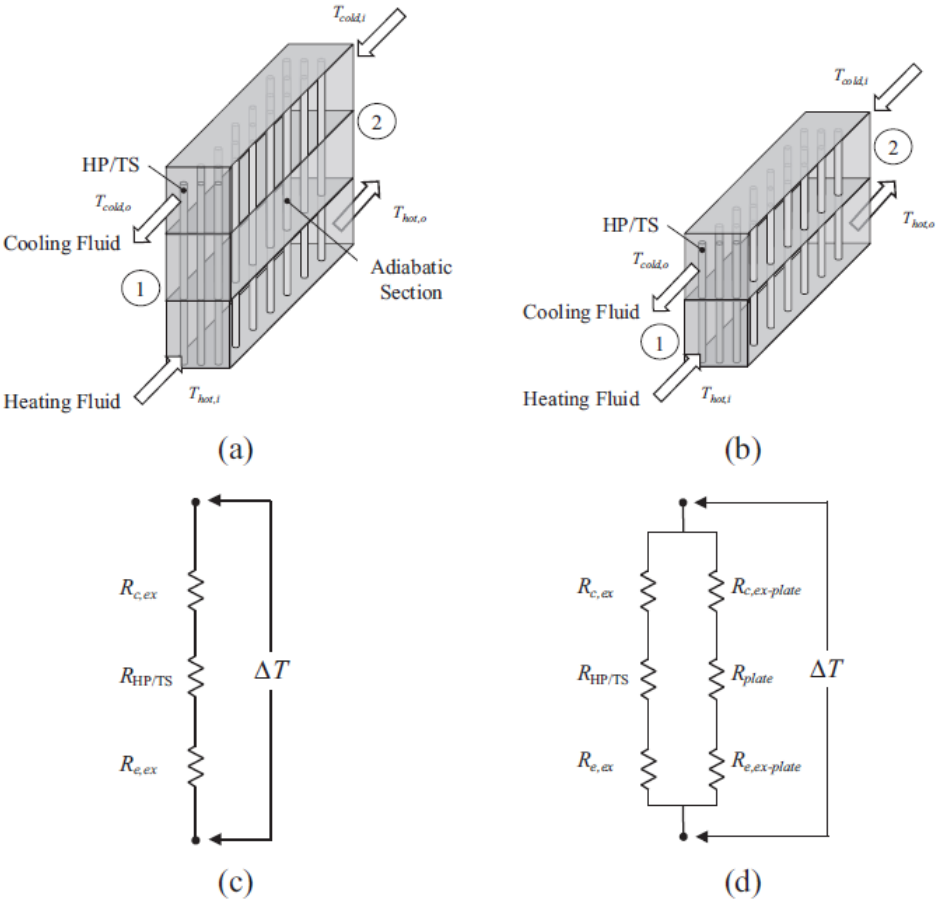

Figure 2-6 – Conventional HPHX and respective thermal circuits (Shabgard, et al., 2015)

(a) a conventional HPHX including an adiabatic section, (b) a conventional HPHX without the HP adiabatic section, (c) module thermal resistance network for (a) including the adiabatic section, (d) module thermal resistance network for (b) not including the adiabatic section.

The thermal network analysis has proven to be very accurate for steady state applications as the small fluctuation periods in the operation of heat exchangers are averaged and not taken into account in the resistance value which results in a slight under-representation of the actual value of heat transfer. However, this method still provides a relatively accurate representation of the system at steady state through a relatively simple and straightforward method.

Figure 2-6 represents a typical heat exchanger equipped with thermosyphons/heat pipes. The main difference between (a) and (b) is the presence of an adiabatic section. On (b), there is no adiabatic section, therefore the heat pipes provide a parallel route to heat transfer adding to the heat transfer via the plate between the two fluids as can be seen in Figure 2-6 (d).

The ΔT in Figure 2-6 represents the difference in temperature between the average temperature across the evaporator and condenser sections of the thermosyphons. Since each thermosyphon is operating at a different working temperature, the logarithmic mean temperature difference (ΔT_{LM}) is used instead, which represents the averaged difference in temperature across the heat exchanger.

2.3 Computational Fluid Dynamics

CFD is a numerical method of solving complex engineering problems. It provides numerical solutions of partial differential equations capable of carrying out in-depth analysis of relevant variables in fluid flow analysis. In simple terms, CFD breaks down a continuous problem into small sections resembling a grid and solves the continuity equations for each point in this grid in an iterative manner until balance is achieved. For most cases, the numerical error decreases as the number of grid points increases.

The turbulent equations are derived from Navier-Stokes continuity equations (Temam, 2012) which do not have an exact solution (Claymath, 2015) but simplification holds up remarkably well, mimicking fluid flow in all their turbulent complexity. By making various assumptions and modelling decisions, it is possible to approximate real world fluid flow around and through complex shapes such as aircraft and cars.

Bhutta et al. (2012) conducted a review of existing CFD applications across several heat exchanger designs and came to the conclusion that CFD emerged in the industry as an addition-alternative to complete physical testing, extremely expensive and slow in today's competitive market. Although CFD cannot completely replace physical testing, it can facilitate the process by avoiding unnecessary testing. Current CFD simulators can be up to 98% accurate and in accordance with experimental data (Ozden & Tari, 2010). CFD can predict problems involving laminar flow fairly well as they have been studied extensively and their behaviour is somewhat predictable (Incropera & DeWitt, 1996). However, turbulence and natural convection are more challenging to predict through numerical methods due to the intrinsic chaos (Ramos, et al., 2014b; Gillespie, 2015).

In a CFD simulation, the turbulence/shear stresses are modelled in terms of two turbulence parameters, the turbulent kinetic energy k and the turbulent energy dissipation ε. These parameters form a family of models generally known as k-ε (k-epsilon) proposed by Launder and Spalding (1972), which are the basis for most CFD packages. It is a semi-empirical model only applicable to fully turbulent flows. Other models are available that can simulate at a larger range of Reynolds numbers, the more famous one being the k-ω, based on the work of Wilcox (1998). This model incorporates some modifications for lower Reynolds numbers, compressibility and flow shearing. The ω stands for the specific dissipation rate, a ratio of ε to k (Smith, 2008).

2.3.1 Previous related works

(i) CFD simulation of the phase change inside the thermosyphon

Studies by Ekambara et al. (2006; 2008) have shown that it is rather efficient to use *k-ε* multiphase turbulence models to predict the heat transfer performance in horizontal pipes during boiling. The results proved satisfactory and a recommendation was made to attempt the same technique for tubes arranged vertically.

Two-dimensional modelling of a thermosyphon in CFD has been attempted by Alizadehdakhel et al. (2010) and Fadhl et al. (2013). A custom code was created to simulate the start-up process of the thermosyphon using the Volume of Fraction (VOF) method (Hirt & Nichols, 1981) to model the phase change process. The outcome of the model was positive as the results agreed with previous experimental results. The only limitation reported was the long time required to conduct the simulations ranging from 3 to 4 months per simulation for a small 2D model. More recently, the same method has been successfully applied to a 3D model to simulate Geyser boiling in the heat pipe (Jouhara, et al., 2016). Geyser boiling usually takes place at low heat input, when a large amount of evaporated fluid bubbles starts to form below the liquid bulk. When the pressure difference between the bubble and the liquid bulk becomes too great, the liquid is projected into the top of the thermosyphon (Negishi & Sawada, 1983; Khazaee, et al., 2010).

A numerical model of a thermosyphon using a combination of Matlab and Ansys Fluent was simulated by Nair et al (2016). In this work, the saturation temperature was created as a function of the local vapour pressure instead of being considered constant as in the previous works. The results were even more accurate than that of previous simulations.

CFD has also been used to calculate the optimum filling ratio for a thermosyphon by calculating the quantity that will allow the shortest response time and lowest thermal resistance (Shabgard, et al., 2014). In the end, it was recommended that an extra 5-10% of fluid is inserted in the pipe to prevent breakdown of the liquid film from the thermosyphon wall.

A three-dimensional numerical study simulating multi-phase flow inside horizontally oriented heat pipes was conducted by Hughes et al. (2014) for steady-state conditions. In this study, a multiphase flow with coupled heat and mass transfer was used. In order to predict the performance of the heat pipes, the effectiveness of the heat exchanger was

determined through an experimental study. A good correlation was found between the results from the CFD model and the experimental results for the same operating conditions.

(ii) CFD simulation of the shell-side flow in a HPHX

Overall, a progression is being observed in the application of CFD to the simulation of HPHXs but it seems there is not much literature on the study of the shell-side flow within HPHXs.

Selma et al (Selma, et al., 2014) investigated the optimisation of the design of an existing heat pipe heat exchanger (HPHX) using an open-source CFD code. A 3-dimensional model was created to investigate the flow on the shell side of the heat exchanger. The results from the simulation showed good agreement with both experimental results and the commercial CFD release showing the great potential of using CFD as a design improvement tool for HPHXs.

Peng et al (2012) conducted a CFD study on the effect of fin shape on the air-side heat transfer performance of a fin-plate thermosyphon used in electronics cooling. The results from the CFD model were within 15% error of the experimental results.

CFD has also been employed to simulate the feasibility of installing heat pipes within a wind tower. In a study by Calautita et al (2013), the heat pipes were modelled as having a constant surface temperature, a reasonable assumption taking into account there is little difference in the temperature of the working fluid inside the pipe. The results showed that the incorporation of heat pipes in this application is capable of improving the reduction in inlet air temperature.

More studies of the heat transfer performance in the shell-side of a HPHX have been conducted by Ramos et al. (2014b; 2015) and Mroué et al. (2015) and have been made available in Appendix B.

2.4 Summary of literature review

It was concluded that heat pipes and thermosyphons are passive systems that require no power to operate, therefore HPHXs have great potential for application in both commercial and industrial markets. Advantages include the complete flow separation which eliminates any cross-leakage between the streams, compactness and lightweightness, passive application, reliability and ease of assembly. Their versatility is also a very important aspect of their success as they may also be retrofitted into existing systems.

CFD has recently started being used as a tool in the prediction of thermosyphon behaviour. In order to predict their behaviour, literature seems to favour the volume of fraction (VOF) method. In terms of equipping thermosyphons to heat exchangers and simulating the ensemble, there is not much literature available as it is a growing area of research. Of the literature encountered, none of it models both the thermosyphons and the heat exchanger together. The outer surface of the thermosyphons is modelled as the boundary condition, usually at constant temperature.

It is concluded that there is a gap in the literature surveyed and no attempt made at simulating the thermosyphons and the heat exchanger in the same simulation. Other than the VOF method, there were no other recommendations in terms of alternative methods of simulating the thermosyphons using, for example, the thermal network analogy. The author therefore recommends the application of the thermal network analogy in order to predict the thermal conductivity of the thermosyphons and feeding that value as a boundary condition into the CFD model of the TSHX. This analysis takes place over the next chapter.

Chapter 3

Theoretical Analysis

This section's aim is to describe in greater detail the prediction models introduced in the surveyed literature which may be used in the characterisation of thermosyphons and heat exchangers.

The reader is presented a review of essential concepts in the field of thermodynamics that are used in the characterisation of thermosyphons and heat exchangers. After the acquaintance process, the preferred method of analysis for the heat exchanger is presented and the novelty in the work identified.

3.1 Essential concepts in heat exchanger characterisation

A heat exchanger is a device used to transfer heat between two separate flows at different temperatures. The performance of the heat exchanger is measured through its ability to extract heat from the hot flow and transfer it to the cold flow. There are a large number of factors affecting the rate of heat transfer within a heat exchanger, on the flow side it may be affected by the flow velocity, the temperature and the properties of the fluid. On the solid boundary it is mainly affected by the type of material and the condition of the surface. In order to simplify the prediction of heat transfer through the heat exchanger, an overall heat transfer coefficient is introduced, a variable which describes the potential for heat transfer within the heat exchanger (in J/kgK). This variable is a measure of how much heat is transferred in the heat exchanger per Area

and per difference in temperature across the streams, thus making it independent of the size of the heat exchanger as may be seen in equation (3-1):

$$U = \frac{Q}{A\Delta T_{LM}} \quad (Wm^{-2}K^{-1}) \qquad \text{(3-1) (Çengel, 2002)}$$

Q is the overall heat transfer rate (in *W*), a measure of the heat exchanger's performance. This is a simplified relation that only applies to heat exchangers using fluids with a constant specific heat capacity or very little variation and not undergoing phase change (Incropera & DeWitt, 1996).

3.1.1 The Effectiveness-NTU (ε-NTU) method

ε-NTU stands for *effectiveness-Number of Transfer Units* and it is another method of predicting the performance of a heat exchanger (Çengel, 2002). The number of transfer units is a dimensionless parameter widely used in heat exchanger analysis, generally defined as:

$$\text{NTU} \equiv \frac{UA}{C_{min}} \qquad \text{(3-2) (Incropera \& DeWitt, 1996)}$$

Where *U* represents the overall heat transfer coefficient, *A* the total heat transfer area and C_{min} the minimum heat capacity rate between the hot and cold flows. The heat capacity rate is a measure of the mass flow rate ($\dot{m}$ in *kg/s*) multiplied by the specific heat capacity (c_p in *J/kg.K*).

Effectiveness (ε) is the ratio of the actual heat transfer rate to the maximum possible heat transfer rate; which would be achieved if the temperature of the outlet of the cold flow would equal the inlet temperature of the hot flow (Jouhara & Merchant, 2012).

$$\varepsilon \equiv \frac{q_{act}}{q_{max}} \equiv \frac{C_h(T_{h,i} - T_{h,o})}{C_{min}(T_{h,i} - T_{c,i})} \quad \text{and} \quad \varepsilon = \frac{C_c(T_{c,o} - T_{c,i})}{C_{min}(T_{h,} - T_{c,i})} \qquad \text{(3-3)}$$

Where C_h and C_c represent the heat capacity of the hot and cold flows, respectively, and C_{min} the smallest heat capacity. By definition, effectiveness is dimensionless and must be valued between 0 and 1; theoretically only a heat exchanger of infinite length would be able to achieve an effectiveness of 1.

It is common place to compare the effectiveness of different heat exchangers as it is a unitless parameter, it may be used to compare units of difference sizes and it is

commonly used in the analysis of heat exchangers equipped with heat pipes as a prediction tool.

3.1.2 Logarithmic mean temperature difference

The Logarithmic Mean Temperature Difference (LMTD or ΔT_{LM}) in equation (3-1) is the average temperature difference between the hot and cold flow across the entire heat exchanger. It is logarithmic and not arithmetic due to the non-linearity of the change in temperature between both flows as can be seen in Figure 3-1.

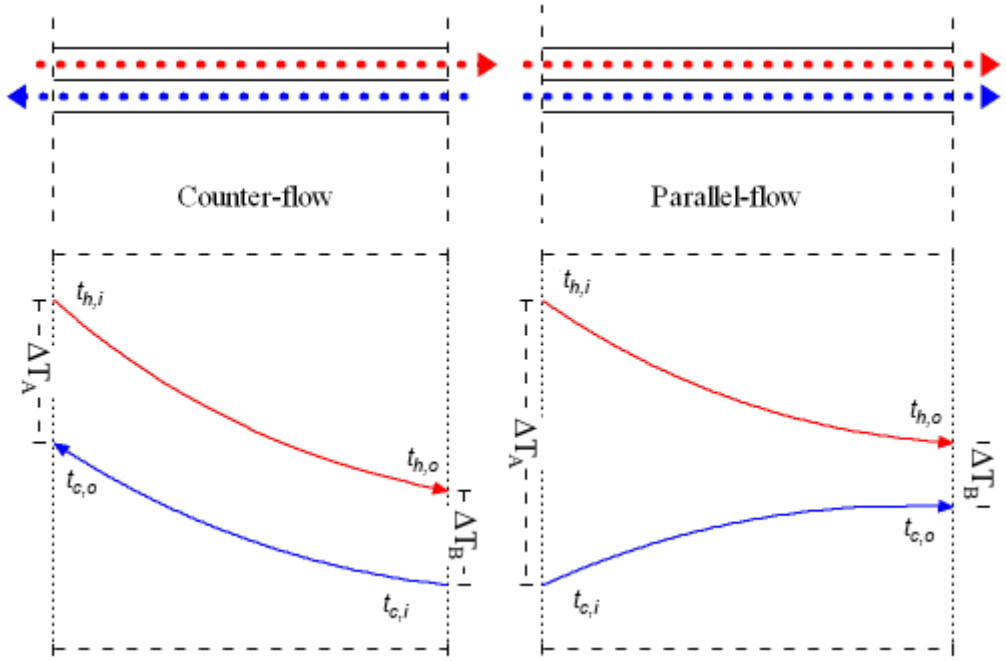

Figure 3-1 –Temperature profile of two flows travelling through different heat exchangers Adapted from The Engineering Toolbox (2012)

The heat exchanger is the medium through which heat transfer from the hot flow to the cold flow. At steady state, the logarithmic mean temperature difference can be found from:

$$\Delta T_{LM} = \frac{\Delta T_A - \Delta T_B}{\ln\left(\frac{\Delta T_A}{\Delta T_B}\right)} \qquad \text{(3-4) (Çengel, 2002)}$$

Where ΔT_A and ΔT_B represent the differences in temperature at *Side A* and *Side B*, sides in accordance with the convention shown in Figure 3-1; the subscripts h and c referring to the hot flow and cold flow, respectively.

For a cross flow heat exchanger, equation (3-5) is used:

$$\Delta T_{m,crossflow} = \frac{\left(T_{h,i} - T_{c,o}\right) - \left(T_{h,o} - T_{c,i}\right)}{ln\left(\frac{T_{h,i} - T_{c,o}}{T_{h,o} - T_{c,i}}\right)} \qquad \text{(3-5) (Çengel, 2002)}$$

The LMTD method assumes the fluids have a constant specific heat (c_p); a condition only met in small temperature ranges. In addition, the LMTD does not apply if any of the shell side fluids (the fluids whose temperatures are displayed in Figure 3-1) is undergoing phase change. In the case of a heat exchanger equipped with thermosyphons this is not limiting, as the phase change process takes place uniquely within each thermosyphon and not in the shell-side fluid.

A correction factor may also be applied to the LMTD in cases where the flows are not parallel to each other or in cases where the heat exchanger includes more than one fluid pass. This correction factor will depend on the heat exchanger being considered.

In order to determine the logarithmic mean temperature difference, the temperatures of the flow on the hot side and on the cold side must be known. The hot side flow and the cold side flow are referred to multiple times over the course of this chapter and generally throughout the thesis. They refer to the flow external to the pipes; the hot side flow referring to the evaporator section and the cold side flow referring to the condenser section.

3.1.3 Thermal network analysis

The thermal network analysis is a simplified method to observe and analyse the thermal boundaries within heat exchangers in which the thermal. In the thermal network analysis method an analogy is established between electric current and heat energy transfer, in other words, the resistance for heat energy is expressed as the ratio of the diving potential (temperature) to the transfer rate between two points (heat). If a direct comparison is made between the diffusion of heat and electrical charge, then thermal resistance is to the conduction of heat what electrical resistance is to the conduction of electricity as shown in equation (3-6):

$$R = \frac{V}{I} \quad so \quad R_{th} = \frac{\Delta T_{LM}}{Q} \qquad \text{(3-6) (Çengel, 2002)}$$

Since this analysis focusses on the characterisation of a heat exchanger equipped with thermosyphons or heat pipes, the difference in temperature between the hot and the cold

side do not refer to a local measurement but rather to a logarithmic mean average temperature or through knowledge of the effectiveness of the thermosyphon-equipped heat exchanger (covered in chapter 3.3.2)

In general, a thermal element is characterised by a thermal resistance and a thermal capacitance. In steady state conditions, since the thermal properties are constant, there is no internal heat generation, the thermal element solely consists of a thermal resistance (Shabgard, et al., 2010).

3.1.4 Overall heat transfer coefficient

The overall heat transfer coefficient ($\underline{U}$ in equation (3-1)) is often used in complex heat exchanger systems as an overall measure of a system's performance. In a heat exchanger, it is a function of all the different heat transfer mechanisms involved in the transfer of heat. As a result, it is not a straightforward variable to determine. However, by applying the thermal network analogy, the overall heat transfer coefficient can be determined.

Replacing Q from equation (3-6) into equation (3-1), the thermal resistance is found to be inversely proportional to the overall heat transfer coefficient and takes the form:

$$R_{th} = \frac{1}{UA} \quad (K/W) \qquad \text{(3-7) (Çengel, 2002)}$$

If the overall heat transfer coefficient is a function of all the heat transfer coefficients within the heat exchanger, then it follows that the total thermal resistance can also be a sum of all the thermal resistances within the heat exchanger. Using the thermal network analogy and assuming all the thermal resistances are known, the overall heat transfer coefficient may be found by re-arranging equation (3-7).

$$R_{th,T} = R_{convection} + R_{conduction} + \cdots \quad (K/W) \qquad \text{(3-8) (Çengel, 2002)}$$

3.1.5 Heat transfer rate for fluid flow

The overall heat transfer rate (Q) refers to the entire heat exchanger; but each flow may also be individually analysed in order to have a good idea of how much heat has entered or left a specific flow.

Equation (3-9) shows the heat transfer for each flow within the heat exchanger:

$$Q = \dot{m} c_p \Delta T \quad (W) \qquad \text{(3-9) (Çengel, 2002)}$$

Where $\dot{m}$ is the mass flow rate of the flow, c_p the specific heat at constant pressure and ΔT the temperature difference between the inlet and the outlet of the flow. The specific heat is assumed constant in this expression and it tends to take the value of the specific heat for the average temperature of the flow.

3.2 Predicting the performance of a thermosyphon

A thermosyphon is, in many ways, a miniature heat exchanger; so it is only natural to approach it the same way a heat exchanger is approached. The most reported method of predicting the performance of a thermosyphon is through the thermal network analogy (Reay & Kew, 2006; Hagens, et al., 2007; Mroué, et al., 2015; Shabgard, et al., 2015), also approached in this study. In this analogy, the thermosyphon is broken down into its inner thermal resistances, conduction, boiling, condensation, etc.

The thermal resistances within a thermosyphon are represented graphically in Figure 3-2. With the exception of $R_{k,t}$, all the thermal barriers are displayed in series. The subscripts are also explained in the figure.

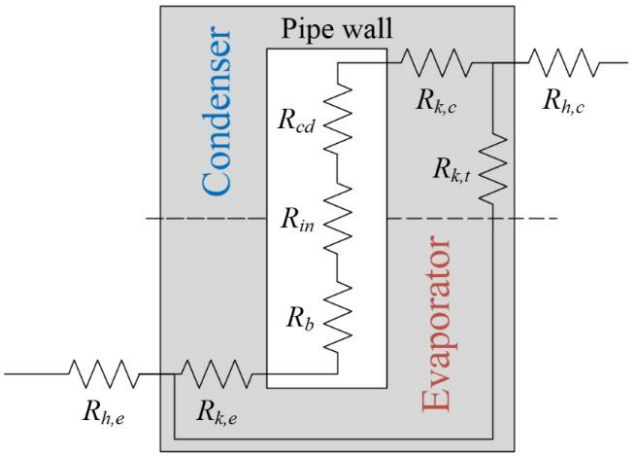

$R_{h,e}$	Thermal resistance from convection on outside of evaporator section
$R_{k,e}$	Thermal resistance from conduction across wall of evaporator section
R_b	Thermal resistance from boiling on TS wall
R_{in}	Thermal resistance from change in pressure between top and bottom
R_{cd}	Thermal resistance from condensation on TS wall
$R_{k,c}$	Thermal resistance from conduction across wall of condenser section
$R_{h,c}$	Thermal resistance from convection on outside of condenser section
$R_{k,t}$	Thermal resistance from Axial conduction across thermosyphon

Figure 3-2 – Schematic of the thermal resistances within the thermosyphon

Treating the circuit displayed in Figure 3-2 as an electrical circuit; the total thermal resistance for the thermosyphon is found through equation (3-10):

$$\frac{1}{R_T} = \frac{1}{R_{h,e} + R_{k,e} + R_b + R_{in} + R_{cd} + R_{k,c} + R_{h,c}} + \frac{1}{R_{k,t}} \qquad \text{(3-10)}$$

In the case of a heat pipe, which is equipped with a wick structure, an additional parallel network of thermal resistances is added which includes the convection to enter the wick and the axial conductivity along the length of the device.

The axial thermal conductivity along thin-walled thermosyphons with long adiabatic sections may be considered negligible (Reay & Kew, 2006; Hagens, et al., 2007) therefore equation (3-10) may be simplified to:

$$R_T = R_{h,e} + R_{k,e} + R_b + R_{in} + R_{cd} + R_{k,c} + R_{h,c} \qquad (3\text{-}11)$$

Which is graphically represented in Figure 3-3:

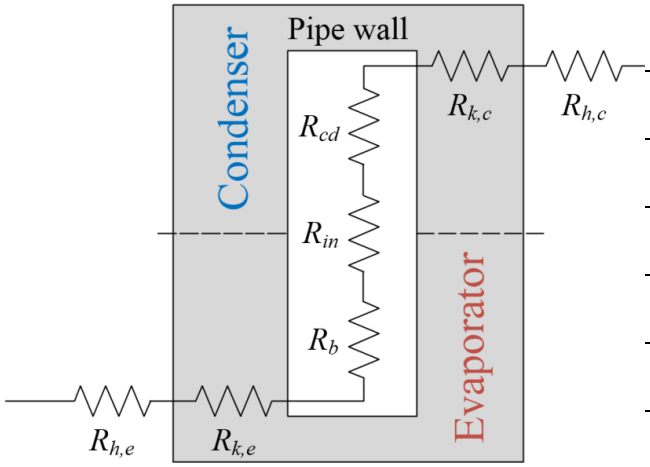

$R_{h,e}$	Thermal resistance from convection on outside of evaporator section
$R_{k,e}$	Thermal resistance from conduction across wall of evaporator section
R_b	Thermal resistance from boiling on TS wall
R_{in}	Thermal resistance from change in pressure between top and bottom
R_{cd}	Thermal resistance from condensation on TS wall
$R_{k,c}$	Thermal resistance from conduction across wall of condenser section
$R_{h,c}$	Thermal resistance from convection on outside of condenser section

Figure 3-3 – Schematic of the thermal resistances within the thermosyphon without axial conduction

Each of the components included in equation (3-11) and Figure 3-3 and shall now be broken down and explained, starting with thermal conduction – both radial and axial ($R_{k,e}$/$R_{k,c}$ and $R_{k,t}$) then moving on to the convection on the shell-side flow ($R_{h,e}$ and $R_{h,c}$), inner thermal resistance from the vapour pressure difference (R_{in}) and finally the boiling and condensation expressions (R_b and R_{cd}).

3.2.1 Conduction through the thermosyphon walls

Thermal resistance from conduction ($R_{k,e}$, $R_{k,c}$ and $R_{k,t}$ in equation (3-2)) take place mainly on zones where the thermosyphon wall is present. Conduction takes place as heat is brought into the thermosyphon or out of the thermosyphon through the thermosyphon wall. Heat transfer by axial conduction is found through the following expression, also known as Fourier's Law (Incropera & DeWitt, 1996):

$$Q_k = \frac{kA}{L}(T_1 - T_2) \quad (W) \tag{3-12}$$

Where *k* is the thermal conductivity of the material, *A* the area normal to the direction of heat travel, which in the case of a solid pipe is the cross-sectional area and *L* the distance through which the heat travels. Axial conduction takes place across the thermosyphon from the evaporator to the condenser. It is often neglected in heat pipes with long adiabatic sections and small cross sections due to its small contribution towards the overall heat transfer rate (Hagens, et al., 2007).

The inverse of equation (3-12) reflects the thermal resistance from axial conduction and takes the form:

$$R_k = \frac{L}{kA} \quad (K/W) \tag{3-13}$$

For tubes with a circular cross-section, equation (3-13) changes to:

$$R_k = \frac{L_a}{k\pi\left(r_o^2 - r_i^2\right)} \quad (K/W) \tag{3-14}$$

Worth of mention is that (3-14) may also be applied to axial conduction through the liquid film at the adiabatic section. However, this mode of heat transfer is very small and the resistance tends to be neglected (Shabgard, et al., 2015).

Heat transfer by radial conduction takes place from the outside to the inside of a tube or vice-versa, equation (3-13) is slightly altered into equation (3-14) to take into account the radial heat transfer with r_o and r_i referring to the outer and inner radii, respectively (Incropera & DeWitt, 1996):

$$Q_k = \frac{2\pi kL}{\ln(r_o/r_i)}(T_1 - T_2) \quad (W) \tag{3-15}$$

Equation (3-15) may also be inverted in order to reveal the conduction resistance from the radial flow of heat, which takes the form (Incropera & DeWitt, 1996):

$$R_k = \frac{\ln(r_o/r_i)}{2\pi kL} \quad (K/W) \tag{3-16}$$

3.2.2 Convection resistance on the outside of the thermosyphon

Thermal resistance from convection ($R_{h,e}$ and $R_{h,c}$ in Figure 3-3) is found mainly on the shell-side of the thermosyphon. Heat transfer by convection takes place between the outer surface of the thermosyphon and the shell-side fluid. It is found to be directly related to the heat transfer coefficient (h), a variable dependent on the solid-fluid combination.

It has the general form (Incropera & DeWitt, 1996):

$$Q_h = hA(T_\infty - T_s) \quad (W) \tag{3-17}$$

Where A is the total area of exposure and ΔT the difference between the average fluid temperature (T_∞) and the surface temperature (T_s).

The inverse of (3-17) is the thermal resistance from convection which takes the following form:

$$R_{convection,h} = \frac{1}{h_{o,e}A_{o,e}} \quad (K/W) \qquad \text{(3-18) (Çengel, 2002)}$$

The subscript o indicates *outer*. The expression is the same for the condenser section:

$$R_{convection,c} = \frac{1}{h_{o,c}A_{o,c}} \quad (K/W) \qquad \text{(3-19) (Çengel, 2002)}$$

3.2.2.1 The average heat transfer coefficient

The h in equation (3-17) stands for *average heat transfer coefficient*, a function of a combination of fluid conditions which make it a very complex variable. An average value for the heat transfer coefficient is necessary, as it fluctuates from point to point depending on the local flow properties and the proximity to the wall of the thermosyphon.

The average heat transfer coefficient h is determined solely from empirical study (Incropera & DeWitt, 1996). It is a function of a large number of flow properties, but most authors seem to agree that the most important are the temperature gradient at the surface, the turbulence and the momentum and thermal diffusivity; the latter being related to the other two. These three variables are measured by the dimensionless Nusselt number, the Reynolds number and the Prandtl number, respectively (Incropera & DeWitt, 1996).

The Nusselt number is a measure of the temperature gradient at the surface and is therefore directly related to the heat transfer coefficient. It is often used as a means to determine the heat transfer coefficient through empirical study.

The Nusselt number may be determined using the following expression:

$$Nu = \frac{hL}{k} \qquad \text{(3-20) (Çengel, 2002)}$$

Where h is the average heat transfer coefficient, L is a characteristic dimension and k is the thermal conductivity of the fluid. The Nusselt number may also be related to the Reynolds number and the Prandtl number through empirical study. A general equation has the form:

$$Nu = C\ Re^m\ Pr^n \qquad \text{(3-21) (Incropera \& DeWitt, 1996)}$$

Where the variables C, m and n depend on the working conditions. This equation is widely used in the prediction of the heat transfer coefficient for shell-side flow in heat exchangers (Incropera & DeWitt, 1996; Hagens, et al., 2007; Ramos, et al., 2014a).

The Reynolds number is a measure of turbulence and it is found by establishing a relation between the density (ρ in kg/m^3), velocity (v in m/s), viscosity (μ in Pa.s), and a characteristic dimension (L in metres) as shown in equation (3-22):

$$Re = \frac{\rho v L}{\mu} \qquad \text{(3-22) (Çengel, 2002)}$$

The Reynolds number is mainly used to predict the flow profile; Reynolds numbers higher than 6000 usually represent a turbulent flow and lower than 4000 a laminar flow (non-turbulent). In between is situated the transition zone where the flow is a mix between laminar and turbulent.

The Pr in equation (3-24) refers to the Prandtl number, which according to Incropera is a *"ratio of the momentum and thermal diffusivities"* (Incropera & DeWitt, 1996). The Prandtl number has the general form:

$$Pr = \frac{\nu}{\alpha} = \frac{c_p \mu}{k} \qquad \text{(3-23) (Çengel, 2002)}$$

ν is the dynamic viscosity (m^2/s) and α the thermal diffusivity. The expression on the right relates the specific heat (c_p), the static viscosity (μ) and the thermal conductivity (k) and is more commonly used in experimental studies as that information is readily available from fluid property tables.

Most of the empirical formulae found in literature include a combination of the Reynolds and Prandtl number with the same form as (3-21) and the most widely used correlations are those by Zhukauskas as they are found to be the most accurate and apply to a broader range of Reynolds numbers (Zhukauskas, 1972; Zhukauskas & Ulinskas, 1988; Incropera & DeWitt, 1996). Additional correlations are available in the heat transfer literature and are not reported as they were not found to be as accurate for the range of Reynolds numbers investigated.

3.2.2.2 Convection resistance on the outside of a single thermosyphon

The heat transfer by convection outside the thermosyphon has been extensively studied in the literature as the thermosyphon behaves as a vertical cylinder in cross-flow. The thermosyphon is considered by many sources to be effectively isothermal as the difference in temperature between the evaporator and the condenser is very small.

The most widely used correlation for external flow over a single cylinder is that of Zhukauskas (1972):

$$Nu = C\ Re^m\ Pr^n \left(\frac{Pr}{Pr_s}\right)^{1/4} \qquad (3\text{-}24)$$

$$[0.7 < Pr < 500]$$

$$[1 < Re < 1 \times 10^6]$$

The constants *C* and *m* depend on the turbulence in the vicinity of the cylinder and are available in Table 3-1. All properties are evaluated at the arithmetic mean of the fluid inlet and outlet temperatures except for the properties marked with an *s*, which are evaluated at the boundary between the solid and the fluid.

Table 3-1 – Constants of equation (3-24) for a circular cylinder in cross flow – excerpt *(Zhukauskas, 1972)*

Re	C	m
1 – 40	0.75	0.4
40 – 1000	0.51	0.5
10^3 – 2×10^5	0.26	0.6
2×10^3 – 1×10^6	0.076	0.7

For finned tube bundles various correlations are also available (Kearney & Jacobi, 1995), and the most recommended by various sources is that of Schmidt (1963):

$$h = C_1 \left(\frac{k_{ex}}{2r_o}\right)\left(\frac{A_t}{A_b}\right)^{-3/8} Re_d^{5/8} Pr^{1/3} \tag{3-25}$$

The value of C_1 varies between 0.45 for staggered or 0.30 for inline tube arrangements. For Reynolds number use the tube diameter. The subscript *t* stands for the Total area exposed to the hot/cold external flow plus any fin surface area exposed to the fluid. The parameter A_b is the bare (finless) area in contact with the fluid.

3.2.2.3 Convection resistance on the outside of a bundle of thermosyphons

Equation (3-24) may be used to represent the heat transfer taking place in a setting in which the shell-side fluid flows through each pipe one at a time (Zhukauskas, 1972). However, the expression is not as accurate when used to determine the heat transfer coefficient of a bundle of thermosyphons.

The correlation suggested for a range of vertical tubes in a staggered arrangement is that of Grimison (1937) and applies to tube bundles of 10 or more rows:

$$Nu = 1.13\, C_1\, C_2\, Re_{max}^{m}\, Pr^{1/3}$$
$$[N_L \geq 10] \tag{3-26}$$
$$[2000 < Re_{max} < 40{,}000]$$
$$[Pr \geq 0.7]$$

All properties of the fluids used in equation (3-26) are evaluated at the mean film temperature. This expression accounts for the maximum turbulence and therefore Re_{max} is used, a variable based on the maximum fluid velocity. The maximum velocity occurs at the smallest area; transversally or diagonally between the tubes, according to Figure 3-4. C_1 and m depend on the geometry of the tube bundle and are taken from Table 3-2. C_2 is a correction factor used in case fewer than 10 rows of tubes are used and is available in Table 3-3.

In the heat exchanger textbooks surveyed (Incropera & DeWitt, 1996; Çengel, 2002) and literature (Selma, et al., 2014) a staggered arrangement of tubes is preferred to an aligned arrangement due to the increased exposure to the flow which results in a higher overall convective heat transfer coefficient at the cost of a higher pressure drop.

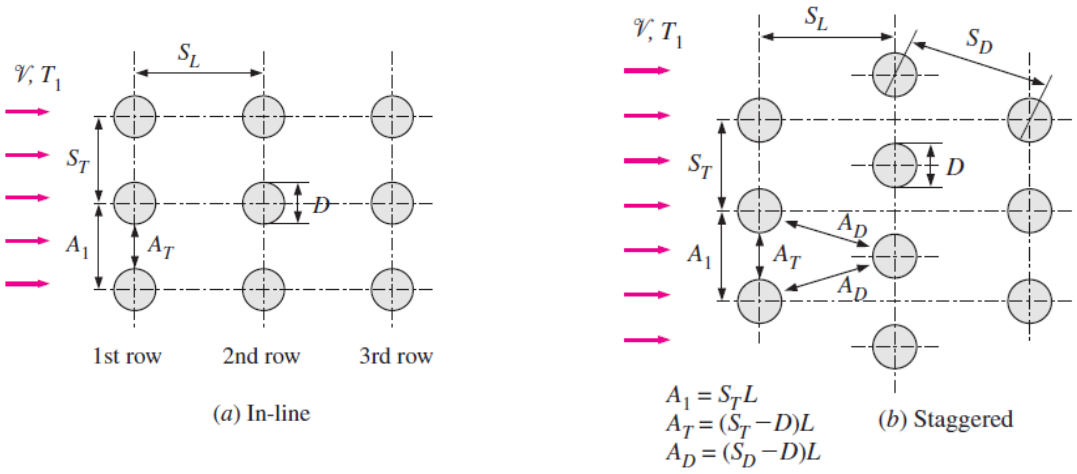

Figure 3-4 – Tube arrangements in a bank

(a) aligned and (b) staggered (Çengel, 2002)

Table 3-2 – Constants of equation (3-26) for airflow over a tube bank of >9 rows

excerpt (Grimison, 1937) – refers to Figure 3-4

	S_T/D			
	1.5		2.0	
S_L/D	C_1	m	C_1	m
Staggered				
1.25	0.505	0.554	0.519	0.556
1.50	0.460	0.562	0.452	0.568
2.00	0.416	0.568	0.482	0.556

Table 3-3 – Correction factor C_2 of equation (3-26) for N_L < 20 (Grimison, 1937)

N_L	1	2	3	4	5	6	7	8	9
Aligned	0.64	0.80	0.87	0.9	0.92	0.94	0.96	0.98	0.99
Staggered	0.68	0.75	0.83	0.89	0.92	0.95	0.97	0.98	0.99

A different expression was suggested by Zhukauskas (1972) as it also takes into account the flow conditions at the boundary between the solid and the fluid. This expression applies to 20 or more rows and it also includes a different correction factor in case there are less than 20 rows present (C_2 – Table 3-4)

$$Nu = C_1\, C_2\, Re_{max}^{m}\, Pr^{0.36} \left(\frac{Pr}{Pr_s}\right)^{1/4} \tag{3-27}$$

$$[N_L \geq 20]$$

$$[2000 < Re_{max} < 40{,}000]$$

$$[Pr \geq 0.7]$$

Table 3-4 – Correction factor C2 of equation (3-27) for NL < 20

(Zhukauskas, 1972)

N_L	1	2	3	4	5	6	7	8	9
Aligned	0.64	0.80	0.87	0.9	0.92	0.94	0.96	0.98	0.99
Staggered	0.68	0.75	0.83	0.89	0.92	0.95	0.97	0.98	0.99

Table 3-5 – Constants of equation (3-27) for airflow over a tube bank of >9 rows excerpt (Zhukauskas, 1972)

Configuration	Re_{max}	C_1	m
Aligned	$10–10^2$	0.80	0.40
Staggered	$10–10^2$	0.90	0.40
Aligned	$10^2–10^3$	Approximate as a single	
Staggered	$10^2–10^3$	(isolated) cylinder	
Aligned $S_T/S_L > 0.7$	$10^3–2 \times 10^5$	0.27	0.63
Staggered $S_T/S_L < 2$	$10^3–2 \times 10^5$	$0.35(S_T/S_L)^{1/5}$	0.60
Staggered $S_T/S_L > 2$	$10^3–2 \times 10^5$	0.40	0.60
Aligned	$2 \times 10^5–2 \times 10^6$	0.021	0.84
Staggered	$2 \times 10^5–2 \times 10^6$	0.022	0.84

3.2.3 Thermal resistance from vapour pressure drop

The thermal resistance from vapour pressure drop (R_{in} in Figure 3-3) changes as the vapour pressure decreases as it flows from the evaporator to the condenser section. The expression used for the vapour pressure drop is that of Faghri (1995) and takes the form:

$$R_v = \frac{8R_g\mu_v T_v^2}{\pi h_{fg}^2 P_v \rho_v}\left[\frac{(L_e + L_c)/2 + L_a}{r_i^4}\right] \tag{3-28}$$

Where R_g, h_{fg}, L_a, T_v, P_v, μ_v and ρ_v are the specific gas constant, latent heat of vaporisation of the working fluid, adiabatic section length and temperature, pressure, dynamic viscosity and density of the vapour phase, respectfully. The vapour temperature is the average temperature between the evaporator and condenser section temperatures and the vapour pressure is the saturation pressure correspondent to the vapour temperature.

3.2.4 Boiling

The key to the operating function of the thermosyphon is the boiling and condensation of the working fluid. The thermal resistance from boiling is represented as R_b in Figure 3-3. Boiling takes place when the temperature of the thermosyphon wall is higher than the saturation temperature of the fluid within it. The saturation temperature is the temperature required to cause a fluid to change phase; in the case of boiling, from liquid to gas.

In the literature reviewed (Incropera & DeWitt, 1996; Çengel, 2002; Piasecka, 2015), a variety of semi-empirical expressions were found, each referring to different boiling regimes and different physical aspect of the boiling process. Figure 3-5 represents a typical boiling curve for a fluid, in this particular case water, a preferred working fluid due to its high latent heat, suitable boiling point and availability (Hughes, et al., 2014). In Figure 3-5 the different boiling regimes are clearly demonstrated with respect to the difference between the saturation temperature and the temperature of the boiling surface. The saturation temperature is the temperature at which phase change occurs; in this case, from liquid to gas.

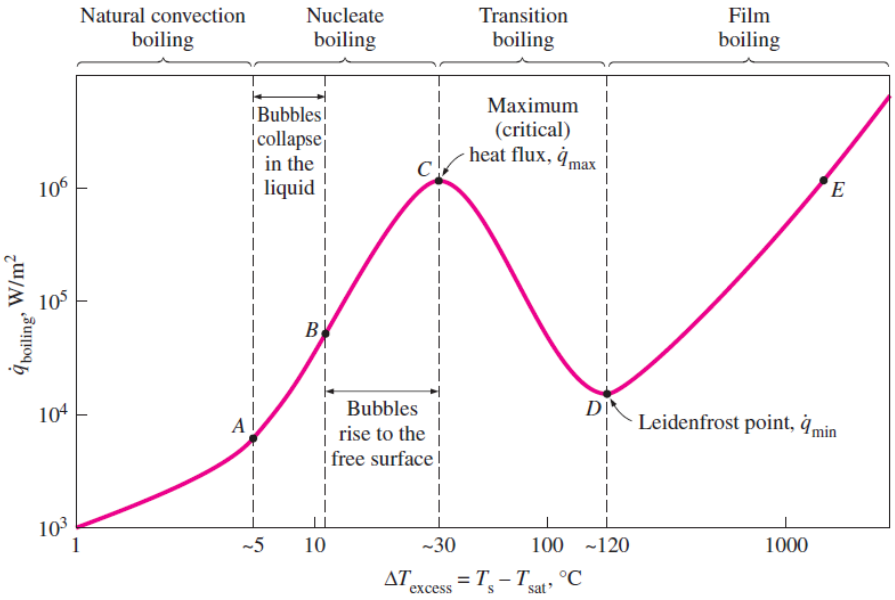

Figure 3-5 – Typical boiling curve for water at 1 atm (Çengel, 2002)

The boiling curve is a representation of the heat flux (W/m^2) plotted against the difference in temperature between the heating surface and the saturation temperature of a fluid in contact with that surface. As this temperature difference increases, a higher heat flux is possible up to a certain point, after which the bubbles start to form a "slug flow" – a state in which the presence of too many bubbles blocks the transfer of heat from the solid to the fluid medium (Çengel, 2002; Reay & Kew, 2006).

The critical heat flux for water at one atmosphere tends to be approximately 30 °C difference between the temperature of the heating surface and the saturation temperature ($T_s - T_{sat} = \Delta T_e$). At normal atmospheric conditions the saturation temperature of water is 100 °C, so having a container at 130 °C will maximise the heat transfer to the water (Çengel, 2002).

3.2.4.1 Nucleate pool boiling correlation

Boiling also depends on the quantity of fluid present; evaporation on a pool of liquid is different from evaporation of a liquid film. Depending on the location of the evaporator section in the thermosyphon, the expression used to characterise the process of boiling in the thermosyphon changes.

The thermosyphons under study were equipped with water and engineered to work in the nucleate boiling regime. The expression chosen to predict the heat transfer in nucleate pool boiling is that of Rohsenow & Hartnett (1952), found to be the most comprehensive correlation as it holds remarkably well and has been reported by much

of the literature; Reay & Kew (2006), Hagens et al. (2007), Mroué et al. (2015) and Ramos et al. (2015) reported the use of Rohsenow & Hartnett's expression (1952) to predict the heat transfer from nucleate pool boiling in thermosyphons. This expression has the form:

$$q'' = \mu_l h_{fg} \left[\frac{g(\rho_l - \rho_v)}{\sigma}\right]^{1/2} \left(\frac{c_{p,l}(T_{sat} - T_s)}{c_{sf} h_{fg} Pr_l^{\,n}}\right)^3 \quad (W/m^2) \tag{3-29}$$

q'' – Heat flux (W/m^2)

μ_l – Static viscosity of the liquid phase (Pa.s)

h_{fg} – Latent heat (J/kg)

g – Acceleration of gravity (m/s^2)

ρ – Density (kg/m^3)

σ – Surface tension at saturation temperature (N/m)

$c_{p,l}$ – Specific heat of the liquid phase (J/kgK)

$(T_{sat} - T_s)$ – Difference between surface temperature and the saturation temperature (K)

C_{sf} , n – Coefficients dependant on surface-liquid combination

The subscript *l* refers to the liquid phase and *v* to the gas phase as during boiling there is a mix of both. The coefficient c_{sf} and the exponent *n* depend on the surface-liquid combination and are given in Table 3-6 (Rohsenow, 1952).

The thermal resistance offered by the boiling process may be found from equation (3-30):

$$R_{b,pool} = \frac{T_s - T_{sat}}{q'' A_{e,inside}} \quad (K/W) \tag{3-30}$$

It is important to note that the Temperature of saturation of the fluid (T_{sat}) and the Temperature of the boundary (T_s) are required in order to solve the expressions related to the boiling and condensation of the working fluid. This is often resolved by employing thermocouples on the inside of the thermosyphon and on its surface.

Table 3-6 – Values of c_{sf} and n for various surface-fluid combinations *(Rohsenow, 1952)*

Surface-Fluid combination	c_{sf}	n
Water-copper		
Scored	0.0068	1.0
Polished	0.0130	1.0
Water-stainless steel		
Chemically treated	0.0130	1.0
Mechanically polished	0.0130	1.0
Ground and polished	0.0060	1.0
Water-brass	0.0060	1.0
Water-nickel	0.0060	1.0
Water-platinum	0.0130	1.0
n-Pentane-copper		
Polished	0.0154	1.7
Lapped	0.0049	1.7
Benzene-chromium	0.1010	1.7
Ethyl alcohol-chromium	0.0027	1.7

3.2.4.2 Nucleate film boiling correlation

In case the evaporator section of the thermosyphon is not entirely occupied by fluid, evaporation will take place on the liquid condensate flowing down the walls of the thermosyphon.

The heat transfer coefficient for nucleate film boiling may be found using the following expression (Zumbrunnen, et al., 1989):

$$\dot{q} = 1.155 \times 10^{-3}\, Nu_{\mu f}^{0.33}\, Pr_l^{0.35}\, K_p^{0.7} \left(\frac{q_e\, l_m}{\rho_V h_{fg} \upsilon_l}\right)^{0.7} \times \Delta T_b k/l_l \times A \qquad (3\text{-}31)$$

where K_p is a dimensionless parameter inverse to surface tension, l_m the bubble length scale and l_l the film thickness scale.

The thermal resistance for nucleate film boiling will then have the form:

$$R_{b,film} = \frac{T_s - T_{sat}}{\dot{q}\, A_{e,inside}} \quad (K/W) \qquad (3\text{-}32)$$

3.2.5 Condensation

At the top end of the thermosyphon, the colder flow in the condenser section causes the working fluid to condense against the walls of the thermosyphon. The thermal resistance from condensation is represented as R_{cd} in Figure 3-3.The condensation expression is mainly derived from Nusselt's film condensation theory (Nusselt, 1916), reported by Faghri et al (2006), Hagens et al. (2007) and Mroué et al. (2015). The equation has the form:

$$h_{condensation} = 0.943 \left[\frac{g\ \rho_l(\rho_l - \rho_v)\ k_l^3\ h'_{fg}}{\mu_l\ (T_{sat} - T_s)\ L} \right]^{1/4} \quad (W/m^2K) \tag{3-33}$$

g – Acceleration of gravity (m/s^2)

ρ – Density (kg/m^3)

k – Thermal conductivity of the working fluid (W/mK)

h'_{fg} – Modified latent heat (J/kg)

μ_l – Dynamic viscosity of the liquid phase (Pa.s)

L – Length of the condenser section (m)

Due to the nature of the process of condensation, the density of the liquid phase is far greater than that of the gas phase, $\rho_l \gg \rho_v$, which allows for some simplification of the expression.

Furthering this change, McAdams (1954) suggested that since experimental values are often 20% larger than theoretical values, the equation should be changed to:

$$h_m = 1.13 \times \left[\frac{g\ {\rho_l}^2 k_l^3\ h'_{fg}}{\mu_l\ (T_{sat} - T_s)\ L} \right]^{1/4} \quad (W/m^2K) \tag{3-34}$$

Where the subscript *m* depicts modified. The heat transfer coefficient is directly related to the conductivity of the working fluid (k) and the modified latent heat (h'_{fg}) but inverse to the viscosity of the fluid (μ_l) and the difference in temperature between the bulk fluid temperature and the surface temperature ($T_{sat} - T_s$). The modified latent heat is a suggestion by Rohsenow & Hartnett (1952) in order increase the accuracy of the expression and has the form:

$$h'_{fg} = h_{fg} + 0.68\ c_{p,l}(T_{sat} - T_s) \quad (J/kg) \tag{3-35}$$

The thermal resistance from condensation has the form:

$$R_{condensation} = \frac{1}{h_m \, A_{c,i}} \quad (W/m^2K) \tag{3-36}$$

Where the subscript $A_{c,i}$ represents the inside area of the condenser section of the thermosyphon.

The major contributors to the overall thermal resistance of a thermosyphon are the internal resistances at the condenser and the evaporator. Typically, the resistance due to vapour pressure and the resistance across the thermosyphon wall for thin-walled thermosyphons (thickness less than 5 times the diameter) are very small and may be neglected in most cases without great difference in the final result.

It is of note that due to the inherent chaotic nature of the process of evaporation and condensation, the actual heat transfer within thermosyphons may be largely difference from the predictions obtained through the use of the different correlations presented and large discrepancies may sometimes take place (Meyer & Dobson, 2006; Jouhara & Robinson, 2010).

3.3 Predicting the performance of a thermosyphon-based heat exchanger

In terms of predicting the performance of a heat exchanger equipped with thermosyphons, there are quite a few examples in literature; Azad & Geoola (1984) and Kays and London (1984) were some of the first to report the use of the effectiveness-Number of Transfer Units (ε-NTU) method to predict the performance of a heat exchanger equipped with thermosyphons to great effect. Even to this day authors continue using the same approach as it has provided satisfactory results; Lukitobudi et al. (1995) used it in an approach to recovering waste heat in bakeries, Noie (2006) used it in an investigation of an air-to-air heat exchanger used in heat recovery, and Jouhara & Merchant (2012) reported the same in their multi-use apparatus.

The thermal network analysis is the approach of choice to better visualise the thermal barriers within a heat exchanger equipped with thermosyphons (Ramos, et al., 2014a). Figure 3-6 visually represents the thermal circuit for the six-thermosyphon heat exchanger under study.

From a heat transfer perspective, the total thermal resistance for the heat exchanger would assume the six thermosyphons are in parallel with each other. This means that the overall thermal resistance would be smaller the more thermosyphons are included in the assembly. This is represented analytically in the following way:

$$\frac{1}{R_{6\ thermosyphons\ (TS)}} = \frac{1}{R_i} + \frac{1}{R_{ii}} + \frac{1}{R_{iii}} + \frac{1}{R_{iv}} + \frac{1}{R_v} + \frac{1}{R_{vi}} \tag{3-37}$$

The thermosyphons (TS) are assumed to have the same average internal thermal resistance thus simplifying the equation to:

$$\frac{1}{R_{6\,TSs}} = \frac{1}{R_{1\,TS}} \times 6 \quad \therefore \quad R_{6\,TS} = \frac{R_{1\,TS}}{6} \tag{3-38}$$

When looking at the larger picture as displayed in Figure 3-6, the overall thermal resistance for the thermosyphon-equipped heat exchanger ($R_{th,TSHX}$) may be found through the following expression:

$$R_{th,TSHX} = R_{h,e} + R_{6\,TSs} + R_{h,c} \tag{3-39}$$

The subscript *TS* stands for *thermosyphon*, *e* for evaporator, *c* for condenser and *o* for outer.

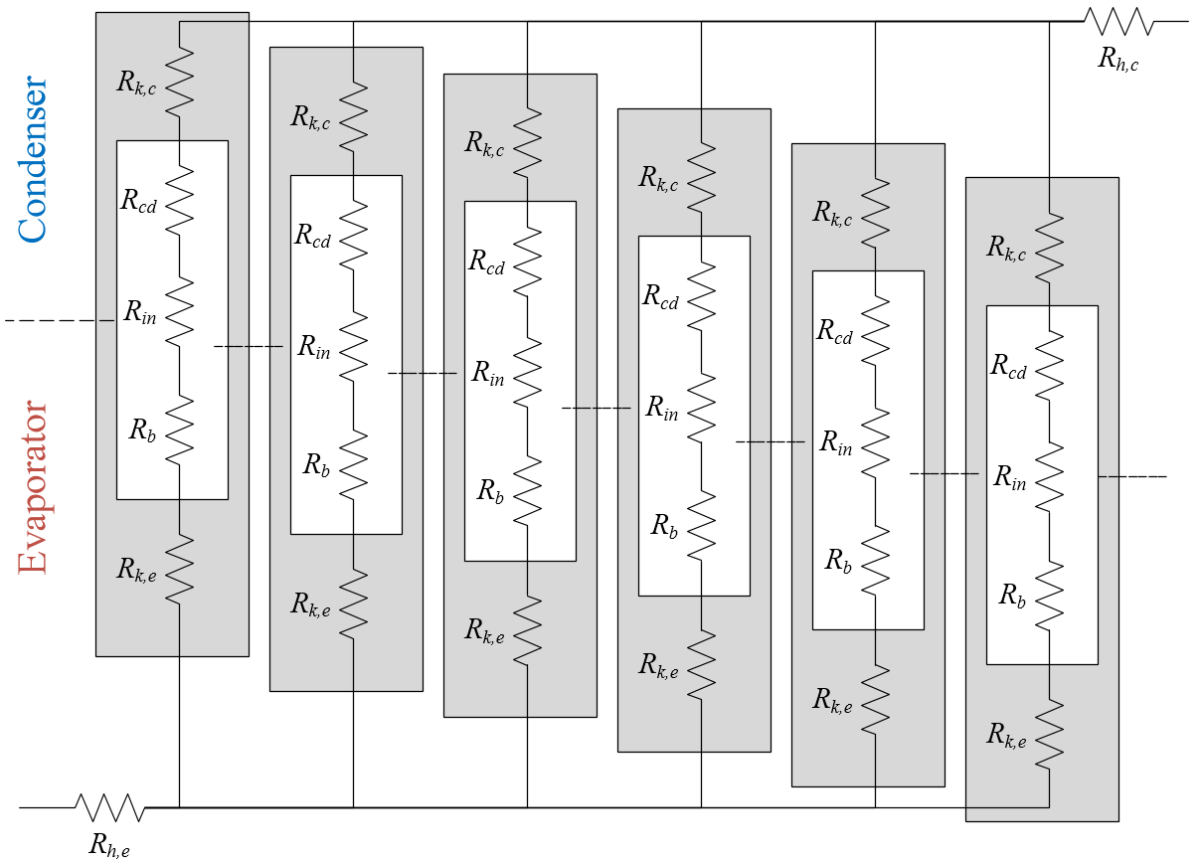

Figure 3-6 – Schematic of the thermal resistances within the thermosyphons equipped in the heat exchanger

The subscripts follow the same logic as Figure 3-3.

Placing equation (3-38) into equation (3-39):

$$R_{th,TSHX} = R_{h,e} + \frac{R_{1\,TS}}{6} + R_{h,c} \tag{3-40}$$

The thermal resistance of a thermosyphon is separated into all its different heat transfer modes, as equation (3-11) but without the external convection, already included in equation (3-40):

$$R_{1\,TS} = R_{k,e} + R_b + R_{in} + R_{cd} + R_{k,c} \tag{3-41}$$

Equation (3-41) applies to thermosyphons undergoing nucleate pool boiling. In case a combination of nucleate pool boiling and nucleate film boiling is present, when looking at the thermal network analysis, the two heat transfer modes are in parallel and equation (3-42) is used instead:

$$R_{1\,TS} = \left(\frac{1}{R_{k,e,1} + R_{b,pool}} + \frac{1}{R_{k,e,2} + R_{b,film}}\right)^{-1} + R_{in} + R_{cd} + R_{k,c} \qquad (3\text{-}42)$$

Where 1 and 2 refer to either flow.

3.3.1 Determination of the thermal conductivity of a single TS

If the thermosyphon is assumed to be a solid super-conductor, this means that the total axial conductivity of a single thermosyphon may be taken as the axial conduction through a solid pipe:

$$R_{1\,TS} = \frac{L}{kA} \quad (K/W) \qquad (3\text{-}43)$$

Where $R_{1\,TS}$ is the overall thermal resistance of a single thermosyphon, L is correlated to the length of the thermosyphon (in m), k is the effective thermal conductivity for a single thermosyphon (in W/mK) and A the cross sectional area (in m^2). Re-arranging the equation for k and considering the cross-sectional area of a circle, equation (3-44) is obtained:

$$k = \frac{L}{R_{1\,ts}\pi r^2} \quad (W/mK) \qquad (3\text{-}44)$$

Equation (3-44) represents the thermal conductivity for a thermosyphon if it is assumed to be a solid super conductor. This value is used as a boundary condition in the CFD simulation.

3.3.2 The Effectiveness-NTU prediction method applied to a TSHX

The *ε-NTU* analysis of a heat exchanger equipped with thermosyphons is done by separating it into two separate heat exchangers, the condenser and the evaporator, and consider them coupled by the thermosyphon working fluid (Azad & Geoola, 1984; Faghri, 1995; Noie, 2006).

The effectiveness of the evaporator and condenser sections of the heat exchanger is determined separately and is given by:

$$\varepsilon_e = 1 - e^{(-NTU_e)} \quad \text{and} \quad \varepsilon_c = 1 - e^{(-NTU_c)} \tag{3-45}$$

The number of transfer units for the evaporator and for the condenser is found through:

$$\mathrm{NTU}_e = \frac{U_e A_e}{C_e} \quad \text{and} \quad \mathrm{NTU}_c = \frac{U_c A_c}{C_c} \tag{3-46}$$

Where A refers to the total heat transfer area in the respective row or stage, and C_x represents the average heat capacity of the shell-side fluid for the evaporator (e) and the condenser (c).

The overall heat transfer coefficient U must be found for each section using the thermal network analysis:

$$\frac{1}{U_e A_e} = \frac{1}{h_e A_{ts}} + R_{ts,e} \tag{3-47}$$

$$\frac{1}{U_c A_c} = \frac{1}{h_c A_{ts}} + R_{ts,c} \tag{3-48}$$

The first term of both equation (3-47) and (3-48) consists of the thermal resistance for the outer convection between the flow and the pipe, where h is the heat transfer coefficient between the tubes and the flow and A_{ts} the outer heat transfer area (the area of the thermosyphon in contact with the flow). R_{ts} is the overall thermal resistance of the thermosyphon, given by equation (3-6).

From (3-6): $$R_{ts} = \frac{T_e - T_c}{Q_{ts}} \quad (K/W)$$

Faghri (1995) defined the effectiveness of an individual thermosyphon to be:

$$\varepsilon_{ts} = \left(\frac{1}{\varepsilon_{min}} + \frac{C_r}{\varepsilon_{max}}\right)^{-1}, \quad C_r = \frac{C_{min}}{C_{max}} \tag{3-49}$$

Where ε_{min} and ε_{max} take the minimum and maximum values of ε_e and ε_c. C_r is the heat capacity ratio and C_{min} and C_{max} follow the same logic of the effectiveness, taking the minimum and maximum values of C_e and C_c, respectively.

Incropera & DeWitt (1996) define the effectiveness of a multistage heat exchanger in counter flow for an *n* number of rows as:

$$\varepsilon = \frac{\left(\frac{1 - C_r\,\varepsilon_p}{1 - \varepsilon_p}\right)^n - 1}{\left(\frac{1 - C_r\,\varepsilon_p}{1 - \varepsilon_p}\right)^n - C_r} \tag{3-50}$$

Where C_r is the heat capacity ratio of the fluid streams on one side of the thermosyphon; the ratio between the heat capacity rate of the shell-side fluid to the heat capacity rate of the thermosyphon's working fluid.

This equation can be adapted to the thermosyphon-equipped heat exchanger as shown below:

$$\varepsilon_{e,n} = \frac{\left(\frac{1 - C_{r,e}\,\varepsilon_e}{1 - \varepsilon_e}\right)^n - 1}{\left(\frac{1 - C_{r,e}\,\varepsilon_e}{1 - \varepsilon_e}\right)^n - C_{r,e}} \tag{3-51}$$

$$\varepsilon_{c,n} = \frac{\left(\frac{1 - C_{r,c}\,\varepsilon_c}{1 - \varepsilon_c}\right)^n - 1}{\left(\frac{1 - C_{r,c}\,\varepsilon_c}{1 - \varepsilon_c}\right)^n - C_{r,c}} \tag{3-52}$$

Two equations are used, one referring to the evaporator section (3-51) and another referring to the condenser section (3-52). $C_{r,e}$ and $C_{r,c}$ represent the heat capacity ratio between the shell side and the working fluid. However, since the working fluid is at constant temperature, its specific heat and capacity rate is effectively infinite, making the variables $C_{r,e}$ and $C_{r,c}$ equal to zero (Kays & London, 1984). Equations (3-51) and (3-52) are then simplified into the forms seen in equation (3-53) and (3-54), respectively:

$$\varepsilon_{e,n} = 1 - (1 - \varepsilon_e)^n \tag{3-53}$$

$$\varepsilon_{c,n} = 1 - (1 - \varepsilon_c)^n \tag{3-54}$$

The overall effectiveness depends on which fluid side has the largest heat capacity; if the heat capacitance of the evaporator side fluid is the largest; $C_e > C_c$:

$$\varepsilon_t = \left(\frac{1}{\varepsilon_{c,n}} + \frac{C_c/C_e}{\varepsilon_{e,n}} \right)^{-1} \tag{3-55}$$

On the other hand, if $C_c > C_e$:

$$\varepsilon_t = \left(\frac{1}{\varepsilon_{e,n}} + \frac{C_e/C_c}{\varepsilon_{c,n}} \right)^{-1} \tag{3-56}$$

Using the overall effectiveness, the outlet temperatures for the evaporator and the condenser can be found from:

$$T_{h,out} = T_{h,in} - \varepsilon_t \frac{C_{min}}{C_e} \left(T_{h,in} - T_{c,in} \right) \tag{3-57}$$

$$T_{c,out} = T_{c,in} + \varepsilon_t \frac{C_{min}}{C_c} \left(T_{h,in} - T_{c,in} \right) \tag{3-58}$$

3.4 Summary of theoretical analysis

This chapter presented to the reader the most recommended prediction methods currently available in literature in order to characterise the behaviour of thermosyphons and heat exchangers. The thermal network analysis is widely recommended as it provides a simple yet surprisingly accurate method to predict the behaviour of thermosyphons and of heat exchangers and it allows the separation of the different heat transfer modes.

The approach may be applied to heat exchangers equipped with thermosyphons in order to clearly determine the heat transfer rate. In order to make the jump to CFD, the author recommends the determination of the thermal conductivity of the thermosyphons which may be used as a boundary condition in the CFD simulation.

Chapter 4

Experimental Methodology

This chapter describes the methodology employed in this study, explaining in detail the experimental procedures for each of the tests. All experimental testing took place at Econotherm UK Plc in Bridgend, Wales, UK over the period spanning January 2014 to September 2015 in separate occasions.

Three experimental tests were conducted, the first consisting of a single thermosyphon test. The second experiment involved a heat exchanger equipped with 6 thermosyphons and it furthers the experimental knowledge by extracting a value of average thermal conductivity (k) for the thermosyphons involved in the study using the thermal network analysis. Six thermosyphons were used for two main reasons; they represent a module that has been used for Econotherm (the funding body) for sizing purposes and it is also one of the smallest representations of a staggered arrangement for further study.

A third experiment took place involving the same heat exchanger as the second experiment but doubling the heat transfer area on the evaporator side through addition of a "second pass" on the evaporator-side. A flow chart of the three experiments is included in Figure 4-1.

Finally CFD was used to investigate the applicability of the model numerically, by using the thermal conductivity as a boundary condition, and to investigate fluid recirculation zones, areas where fouling is usually more likely to occur.

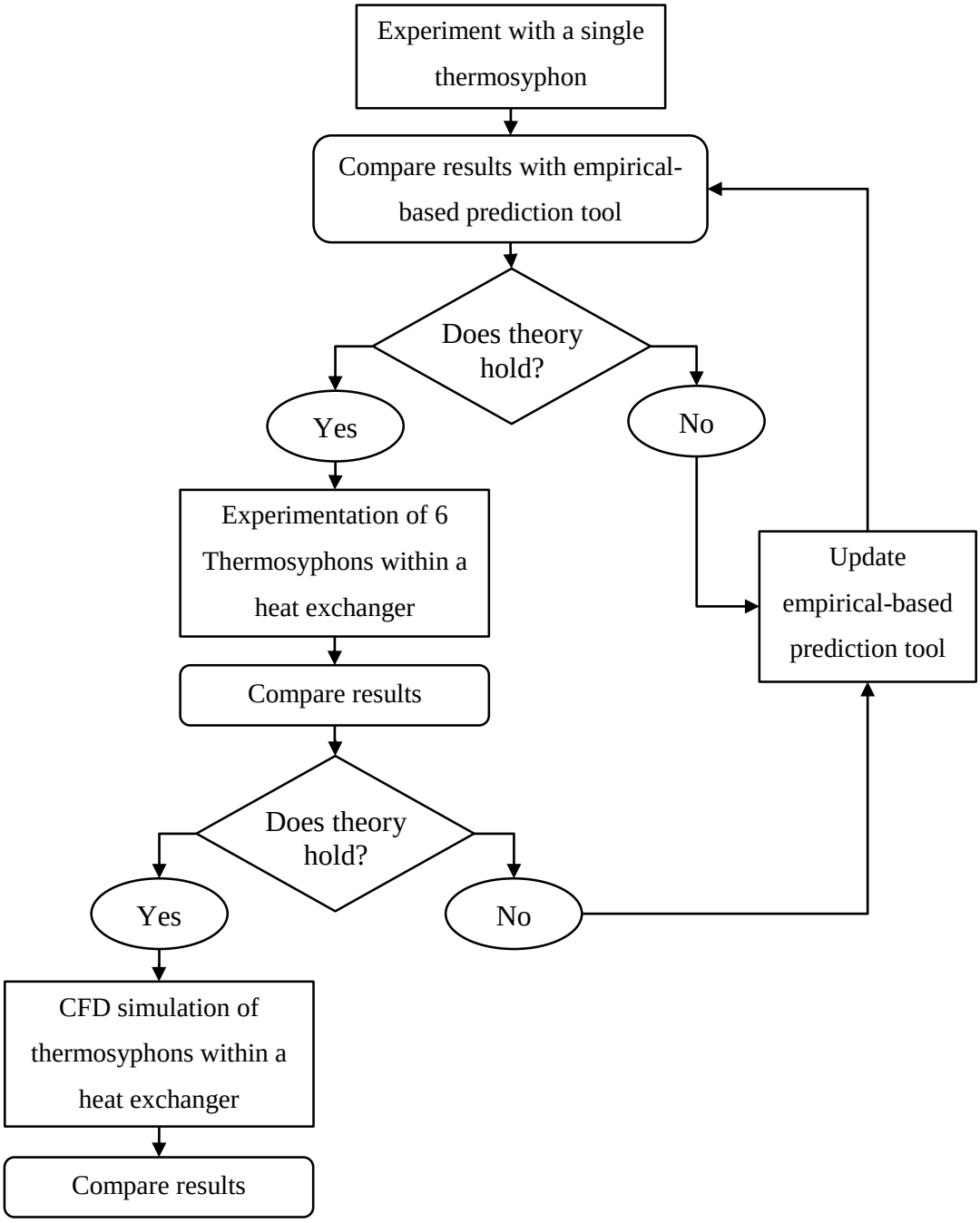

Figure 4-1 – Flow chart of the methodology

The main objective of the last two experiments was to create a relation between the inlet conditions and the internal thermal conductivity of the thermosyphons. The thermosyphons were modelled as superconductors with a thermal conductivity determined analytically, in a hope to simplify the task of predicting the thermal performance of a heat exchanger equipped with thermosyphons. A different thermal conductivity as determined for each inlet condition and was then used as a boundary condition for the thermosyphons in the CFD simulation.

4.1 Single Thermosyphon experiment

The objective of this experiment was to ascertain the correctness of the equations found in the literature and their applicability to the current problem. Two thermosyphons similar to the ones that would be equipping the heat exchanger were individually tested for a variety of conditions.

4.1.1 Design of test rig

The thermosyphons used were made of carbon steel, measured 1,760 mm in length and had a diameter of 28 mm. Both of them were equipped with water as a working fluid filled to 100% of the evaporator section (100% filling ratio). The evaporator section of each thermosyphon measured 1 m and was surrounded by two heating ropes of 500 W, for a maximum of 1 kW of heat energy per thermosyphon. The condenser section measured 200 mm and consisted of a coiled tube surrounding the thermosyphon. Water was used as the shell-side fluid. The experimental apparatus and its schematic representation is presented in Figure 4-2.

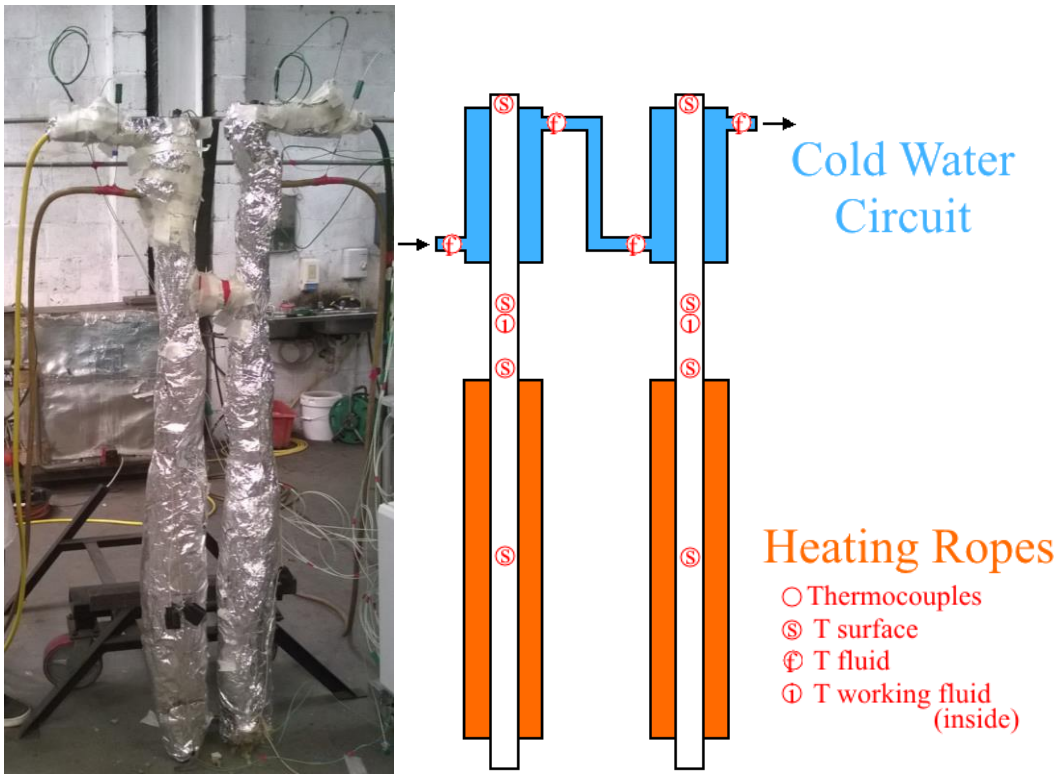

Figure 4-2 – Experimental apparatus of single thermosyphon experiment with thermocouple locations

The orange represents the evaporator section and the blue the condenser section

In terms of instrumentation, type-K thermocouples were used as temperature probes. 7 thermocouples were placed on each thermosyphon. 4 thermocouples on the surface, two located on the evaporator section, one on the middle and one on the top; 1 inside the thermosyphon in the adiabatic section and 2 located in the condenser section, one at the inlet and another at the outlet. The thermocouple positions are graphically represented in the schematic of Figure 4-2.

The purpose of the thermocouples installed in the adiabatic section (inside and outside) was to ascertain if the temperature on the outside of the adiabatic section was the same as in the inside. If there is no variation from the inside to the outside temperature, the working temperature of the thermosyphon may be determined through this thermosyphon located on the outside of the adiabatic section, removing the need for an invasive probe located inside the thermosyphon.

As can be seen in Figure 4-2, both thermosyphons were surrounded with a layer of thermal insulation and wrapped in foil. The white tape seen in the figure was only used to hold some of the thermocouple cables in place.

4.1.2 Experiment design

In total, 12 tests were planned; each of them lasting for approximately 20 minutes at steady state. Two variables were manipulated during the experiment; the power of the heating ropes and the mass flow rate of the water in the condenser section. The Voltage was altered between 150 V, 175 V and 210 V resulting in approximately 485 W, 685 W and 985 W. The mass flow rate varied from 0.01 kg/s to 0.04 kg/s at 0.01 kg/s increments.

4.2 Heat Exchanger equipped with six thermosyphons

The second experimental rig consisted of a heat exchanger equipped with six thermosyphons in a cross-flow arrangement. The design of the rig was based on a scaled-down version of a real working example of a heat exchanger used by Econotherm and can be considered to be a modular design, allowing for future adaptation of different flow configurations. A simple cross flow was investigated in the second experiment.

4.2.1 Design of test rig

The test rig was equipped with six thermosyphons vertically arranged in two staggered rows. The unit was divided into two sections: a hot air circuit and a cold water circuit.

The thermosyphon tube was made of carbon steel, measuring 2 m in length and had a diameter of 28 mm with a surrounding wall with an average thickness of 2.5 mm. The working fluid was distilled water and the filling ratio was 100% (100% of the evaporator section), roughly translated into 0.7 m in height from the bottom of the thermosyphon. All tubes were chemically treated before insertion of water to avoid corrosion.

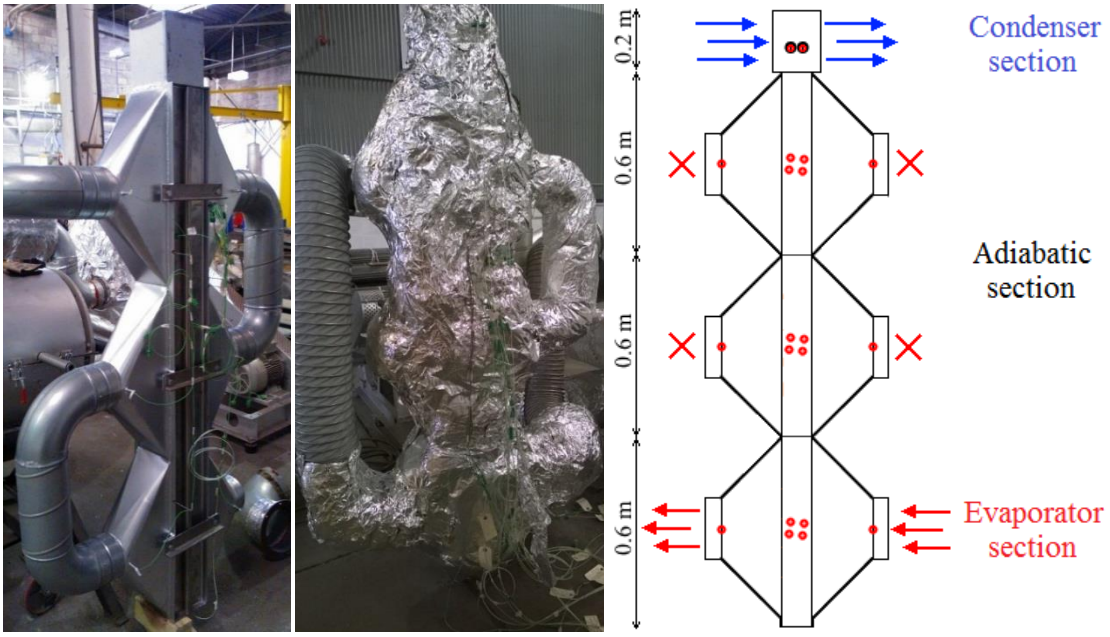

Figure 4-3 – Experimental apparatus of the heat exchanger in cross flow (J Ramos 11/2013)

From left to right: the heat exchanger before installation; the heat exchanger after being thermally insulated; representative schematic of the thermosyphon heat exchanger and the size of its respective sections.

As seen in Figure 4-3, the condenser section occupied the top 0.2 m of the thermosyphons (10% of total length) and the evaporator section the lower 0.6 m (30% of total length). The remaining 1.2 m were fully insulated and served as the adiabatic section (60%). Both the evaporator and the condenser were separated from the adiabatic section by a 10 mm-thick division plate in order to prevent leaks. The difference in size between the evaporator and the condenser is necessary due to different fluids being present in each of the sections.

The thermosyphons were displaced in relation to each other as shown in Figure 4-4 as a diagram and Figure 4-5 (left) in the actual heat exchanger. In the condenser section, a small baffle was placed in order to direct the flow around the thermosyphons one by one, thus improving the local heat transfer coefficient.

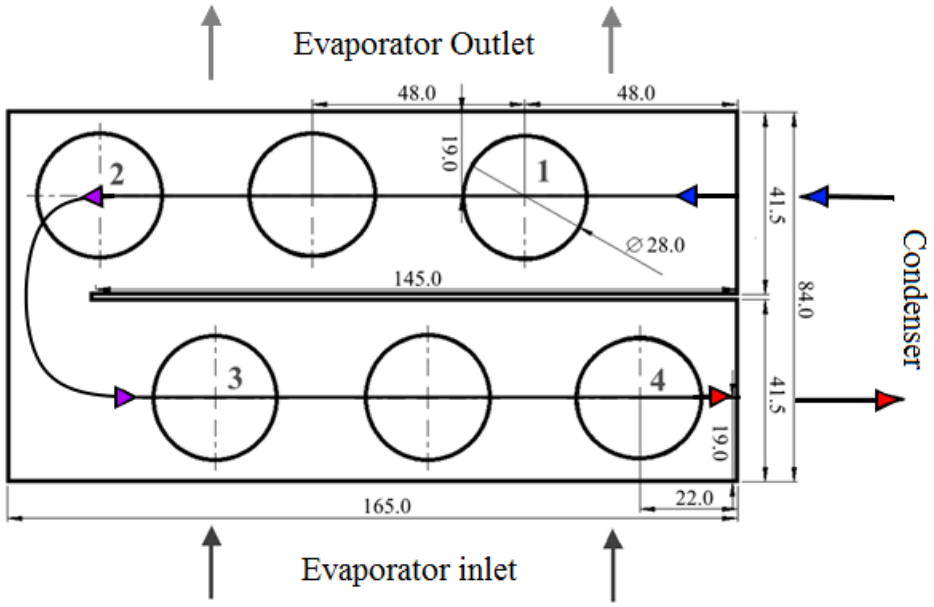

Figure 4-4 – Cross-section of the condenser section of the TSHX under study (all dimensions in mm)

Figure 4-5 – Internal pictures of the heat exchanger

4.2.2 Experiment design

The experimental rig required two circuits; a closed air circuit and an open water circuit, both schematically represented in Figure 4-6.

The hot air circuit consisted of a closed loop equipped with a fan and a heater. The flow was directed to pass through the fan and the heater and then enter the heat exchanger. After leaving the heat exchanger, it was sucked into the fan once again in order to repeat the cycle. The fan frequency was controlled by a leveller and ranged between 10 Hz and 40 Hz in 10 Hz increments. The mass flow rate was read by an analogue pitot tube installed at the inlet of the evaporator section and the frequency translated in a mass flow rate ranging between 0.05 kg/s and 0.14 kg/s by 0.03 increments depending on local pressure and temperature conditions.

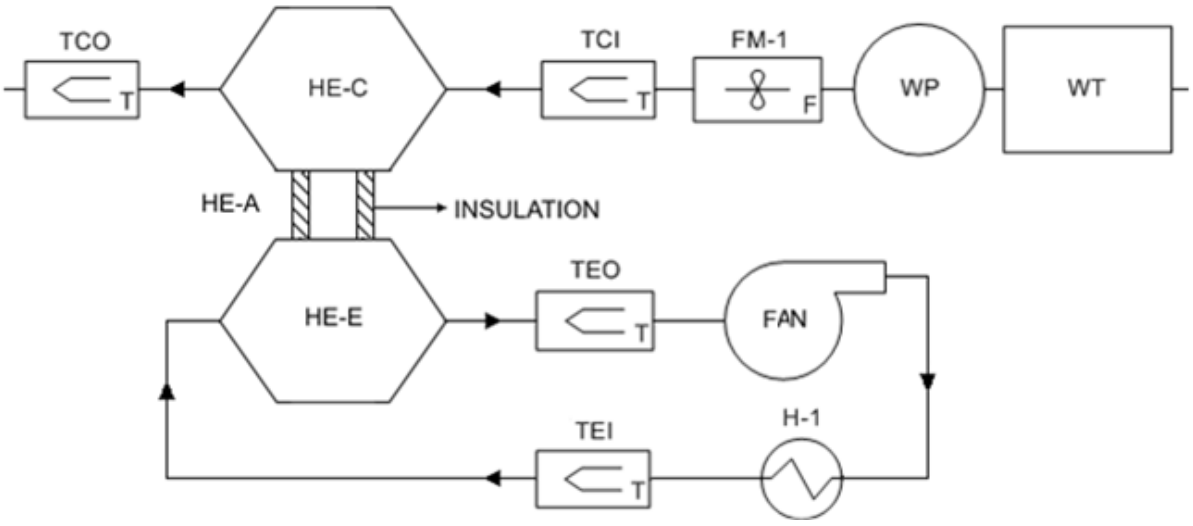

Figure 4-6 – Schematic of the single pass test setup

Description: TCI/TCO – Thermocouples at inlet/outlet of condenser; HE-C/A/E – Thermosyphon heat exchanger Condenser/Adiabatic/Evaporator section; FM-1 – Turbine Flow Meter; WP – Water pump; WT – Water tank; TEI/TEO – Thermocouple at inlet/outlet of evaporator; FAN – Fan; H-1 – Air Heater.

The heater power could be regulated to a desired temperature thanks to a feedback loop connected to a thermocouple located at the outlet of the heat exchanger. The temperature of the air varied between 100 °C and 300 °C in 50 °C increments.

The cold water circuit consisted of an open loop and included a water tank to help regulate the inlet flow rate into the pump. The mass flow rate of water was kept constant throughout the test at 0.08 kg/s and at an average temperature of 10 °C. The water circuit started at the water tank, then the water was sucked into a pump that pumped the water

through the heat exchanger. After flowing through the heat exchanger, the warmed-up water would flow into another process.

The flow inside the condenser section followed a u-shaped path as depicted in Figure 4-4. A bleed valve was also installed on the top of the condenser to allow the removal of air from the section when initiating operation.

4.2.3 Gathering and Processing of Data

There were 20 k-type thermocouples placed in the heat exchanger at specific locations to measure the temperature of the flows and the working temperatures of the thermosyphons. The thermocouples were placed in key sections; namely at the inlet and outlet of both the evaporator and condenser sections, on the surface of each thermosyphon located in a corner (numbered 1 to 4 in Figure 4-4), on the adiabatic section, and within the thermosyphons. The thermocouple placements are marked in red in the simplified schematic of Figure 4-3.

4 thermocouples were placed on the surface of each "corner" thermosyphon: one in the evaporator section, two in the adiabatic section and one in the condenser section. These thermocouples were brazed into the surface of the thermosyphon at 1 mm depth. Figure 4-7 represents the brazed thermocouples already installed in the heat exchanger.

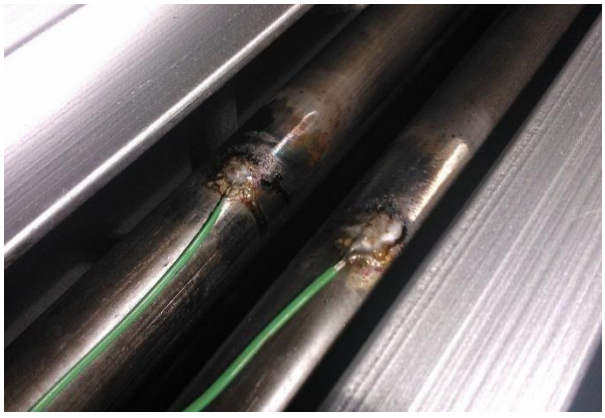

Figure 4-7 – The brazed thermocouples on the surface of the thermosyphon

The experimental procedure was the same in all the tests:

- First the cold water circuit was initiated.
- The air was then bled from the condenser section through the bleed valve located at the top.
- After ensuring the condenser section was filled with water, the heater was turned on and the hot air flow allowed to move through the evaporator section.
- The temperature was set to 300 °C. Data for this temperature setting would be recorded for a fan rate of 10 Hz, 20 Hz, 30 Hz, 40 Hz and 50 Hz. The same flow rates were then tested for 250 °C, 200 °C, 150 °C, 100 °C and 50 °C.
- Data was recorded for each setting for 10 minutes at steady state.

A total of 30 tests were conducted, one for each different inlet condition. The total time at steady state in minutes for each test is shown in Table 4-1.

Table 4-1 – Test matrix for the heat exchanger in single pass (m:s)

		Inlet Temperature of air flow					
Hz	*ṁ (kg/s)*	*50 °C*	*100 °C*	*150 °C*	*200 °C*	*250 °C*	*300 °C*
10 Hz	*0.05*	*09:05*	*08:45*	*08:35*	*10:40*	*08:41*	*09:18*
20 Hz	*0.08*	*09:01*	*08:37*	*08:31*	*08:57*	*09:02*	*08:21*
30 Hz	*0.11*	*10:00*	*08:15*	*08:21*	*09:02*	*08:28*	*10:30*
40 Hz	*0.14*	*09:21*	*10:56*	*10:53*	*11:13*	*14:40*	*08:13*
50 Hz	*0.17*	*10:23*	*16:11*	*11:23*	*10:05*	*09:40*	*07:11*

4.2.4 Details concerning the experiment conducted for double pass

An additional investigation was conducted in the same experimental rig but allowing the air in the evaporator side to return for a second pass, as demonstrated in Figure 4-8 and in the schematic of Figure 4-9. This effectively doubled the evaporator area on the heat exchanger whilst reducing the total length of the adiabatic section.

In this design, two different boiling regimes are present in the thermosyphon. On the lower section a complete pool boiling regime is found. As the air returns for the second pass, it encounters a thin water film that is returning from the condenser to the evaporator. This boiling regime is known as film boiling and the operating conditions of the thermosyphon were made to ensure complete nucleate film boiling in this section.

This dual nature of boiling allows an investigation of the two boiling regimes within the thermosyphon.

On the water side, the mass flow rate was kept constant at 0.08 kg/s and the temperature of the water tank was kept constant at 14°C due to environmental requirements. Due to constraints imposed by the funding body, 50°C, 300°C and 50Hz were also not tested, reducing the total amount of tests to 16.

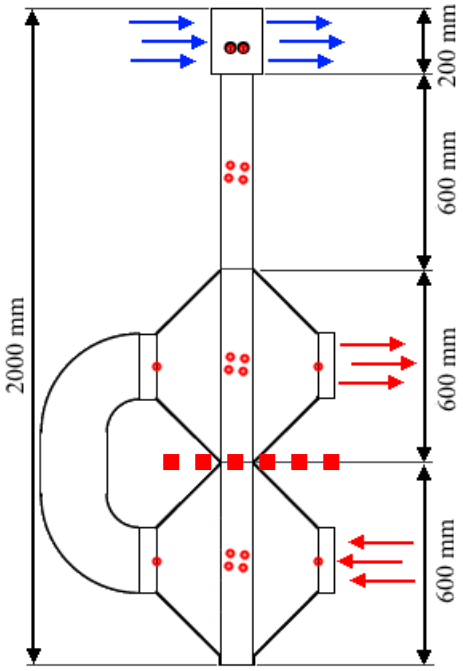

Figure 4-8 – Schematic of the thermosyphon heat exchanger in double pass

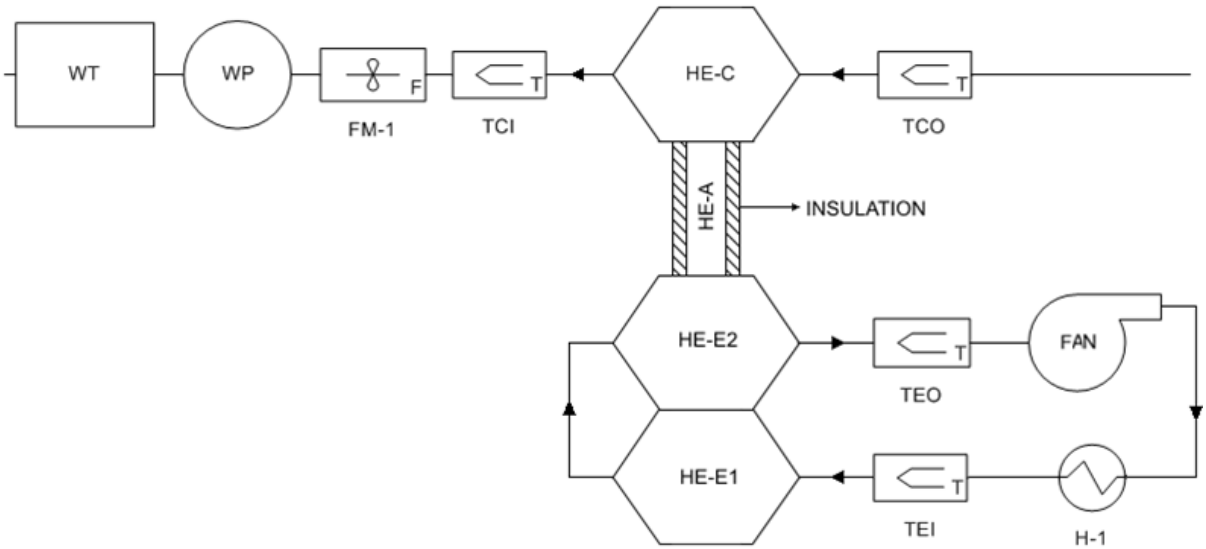

Figure 4-9 – Schematic drawing of the heat exchanger with double pass

WT–Water Tank, WP–Water Pump, FM–Flow Meter, TCI–Thermocouple Condenser Inlet, TCO–Thermocouple Condenser Outlet, FAN–Fan, H–Heater, TEI–Thermocouple Evaporator Inlet, TEO–Thermocouple Evaporator Outlet, HE-Heat Exchanger, A-Adiabatic, C-Condenser, E-Evaporator

4.3 Instrumentation

All of the equipment utilised throughout the experiments are presented in this section. In terms of equipment, a mobile data-logging station incorporating all of the equipment was employed. It was mobile so it could be moved from one experimental rig to the next as they were located in different locations within the factory floor depending on the position of the water mains. The data-logging station included several data loggers arranged in series for a total of 48 channels. The data loggers were connected to a laptop that was exclusively a data-logging device and transferred the data to a format that could be easily processed, in this case Microsoft Excel files.

4.3.1 Temperature logging

For temperature logging, K-type thermocouples were created with a custom length cable in order to better fit the experimental apparatus. All of the thermocouples were connected to the data logger.

4.3.2 Mass flow rate

In all the tests, the mass flow rate of water was controlled by a ball valve but monitored through a turbine flow meter.

In the tests involving air, the mass flow rate was controlled by a custom-made turbine that worked in a closed circuit. It was measured through a pitot tube as the temperature was too high for any of the other electrical equipment to function.

4.3.3 Heat Source

A Variac was also used which could vary the current coming from the mains between 0 and 270 V to a current up to 8 Amps. This Variac powered the heating ropes used in the single thermosyphon experiment. Each heating rope had a maximum rating of 1kW.

4.3.4 Instrumentation Uncertainty Analysis

Errors in experimental measurements can be a combination of many factors including human error, equipment usage and experimental set-up. Manufacturers of lab equipment provide an expected error in the form of a percentage gathered from in-house tests, however this error can propagate through the calculations as more and more variables are taken into consideration.

An uncertainty study was conducted on the results in order to find the error propagation from the measuring instruments used in the experimental rig. The associated error can be found from the following table, adapted from Tayler (1997) and Neuilly (1999):

Table 4-2 – Equations used in error analysis

Mathematical expression	Example	Associated error
Addition/Subtraction	$x = a + b + c + \cdots$	$S_x = \sqrt{{S_a}^2 + {S_b}^2 + {S_c}^2 + \cdots}$
Multiplication/Division	$x = a * b/c \ldots$	$S_x = x\sqrt{\left(\frac{S_a}{a}\right)^2 + \left(\frac{S_b}{a}\right)^2 + \left(\frac{S_c}{a}\right)^2 + \cdots}$
Exponentiation	$x = a^b$	$S_x = x * b * \left(\frac{S_a}{a}\right)$

Where x is the result of the calculation, S_x is the uncertainty associated with the result, a, b, and c are individual numbers used for the calculation of the result, S_a, S_b and S_c are the uncertainties associated with the individual numbers for the calculation of the result.

Taking this into consideration, the error analysis for the heat transfer rate using equation (3-9) would be:

Equation (3-9) $$\dot{Q} = \dot{m} c_p \Delta T \quad (W)$$

Error analysis: $$S_{\dot{Q}_c} = \dot{Q}_c \sqrt{\left(\frac{S_{FR_w}}{FR_w}\right)^2 + \left(\frac{S_{\Delta T_c}}{\Delta T_c}\right)^2} \tag{4-1}$$

Chapter 5

Experimental Results and Discussions

This chapter outlines the main outcomes of the experimental study. The results from the single thermosyphon experiments are presented first followed by the experiments conducted with the heat exchanger equipped with six thermosyphons in single pass and double pass.

5.1 Assumptions

The assumptions made during all the tests are the following:

a) Constant mass flow rate across the heat exchanger in both flow sides
b) Constant specific heat capacity across the fluid side(s) of the heat exchanger
c) Neglectable axial heat transfer from conduction across the thermosyphon wall
d) No heat transfer across the walls of heat exchanger
e) No heat transfer at the adiabatic section of the thermosyphon
f) Steady-state flow
g) Same thermal conductivity for all the thermosyphons

5.2 Single thermosyphon experiment

This experiment investigated the performance of two thermosyphons charged with water at 100% filling ratio. Heat was generated by heating ropes coiled around the evaporator section and absorbed by water on the shell-side of the condenser section as shown in Figure 4-2. The water outlet at the condenser section of one of the

thermosyphons was connected to the water inlet of the other in order to investigate the effect of different inlet temperatures in the performance of the thermosyphon.

A total of twelve tests were conducted for a matrix of different voltages and mass flow rates. The voltages tested were 150 V, 175 V and 210 V resulting in approximately 485 W, 685 W and 985 W. On the condenser side water flowed at different mass flow rates, approximately 0.01 kg/s, 0.02 kg/s, 0.03 kg/s and 0.04 kg/s.

5.2.1 Temperature Comparison

The temperature profile of the two thermosyphons was plotted against the mass flow rate of water on the condenser side. Since the outlet of Thermosyphon #1 is the inlet of Thermosyphon #2, they may be displayed on the same graph (Figure 5-1, Figure 5-2 and Figure 5-3):

$T_{c,in}$ and $T_{c,out}$ represent the inlet and outlet temperatures of the condenser and T_a the temperature in the adiabatic section and simultaneously the saturation temperature of the working fluid. The numbers *(1)* and *(2)* refer to the Thermosyphons #1 and #2. As may be observed in the following figures, the inlet temperature of the water ($T_{c,in}$) was kept constant and by increasing the mass flow rate of water, the outlet temperature decreased as may be observed from the decreasing gap between $T_{c,in}$ and $T_{c,out}$.

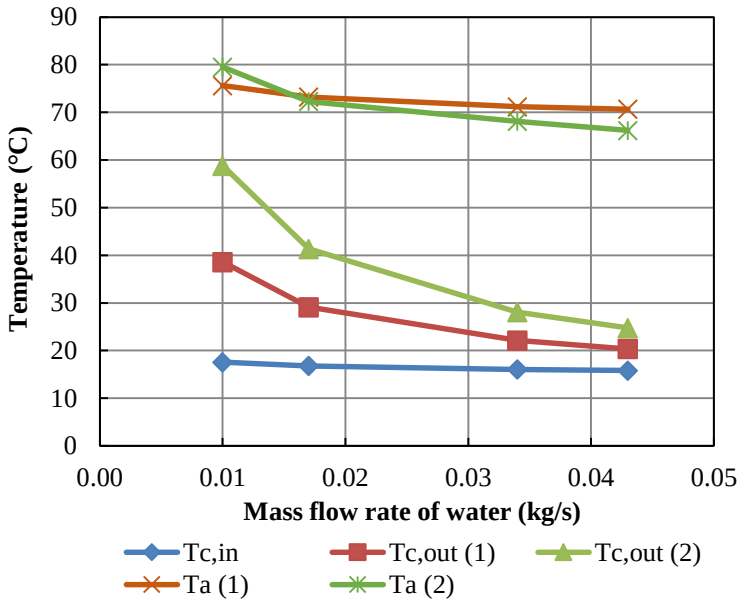

Figure 5-1 – Temperature distribution within the condenser section for 985 W

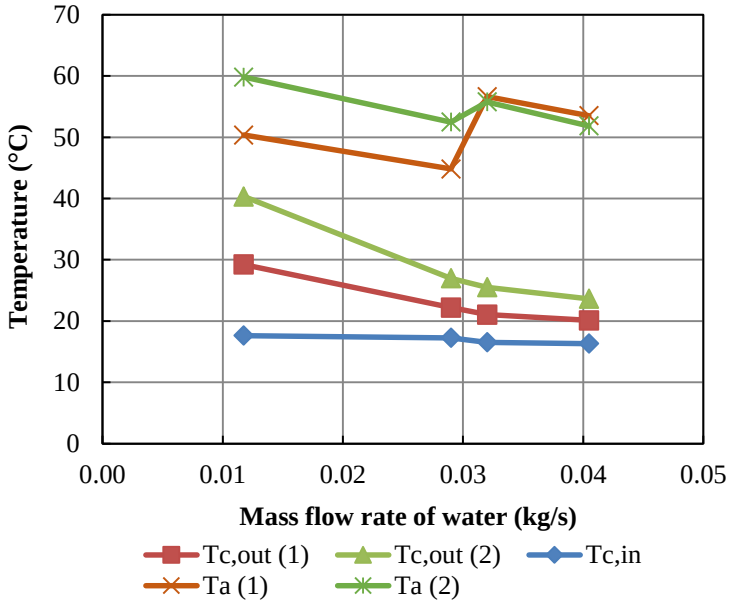

Figure 5-2 – Temperature distribution within the condenser section for 685 W

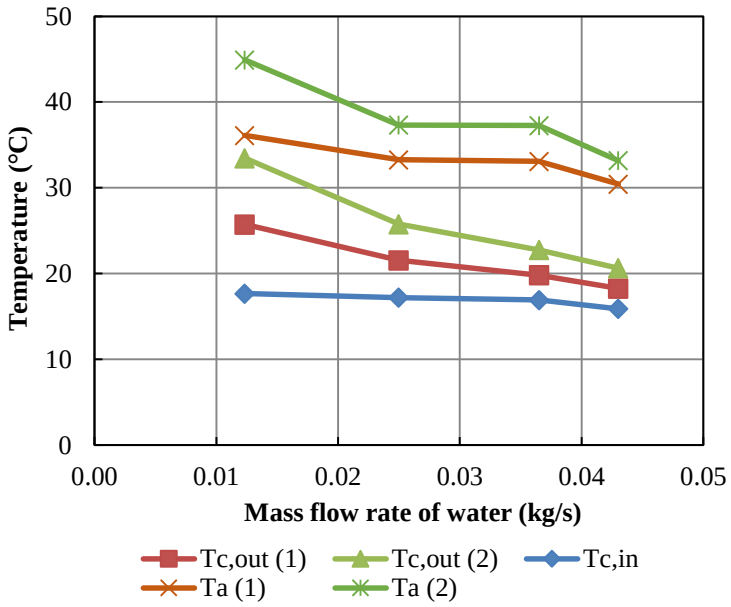

Figure 5-3 – Temperature distribution within the condenser section for 485 W

In the adiabatic region, the saturation temperature of the working fluid is observed to decrease with decreasing outlet temperatures, as expected, since the saturation temperature tends to be located in between the temperatures at the evaporator and the condenser.

The temperature of the evaporator is not available as the thermocouple was found to be in contact with the heater thus giving a reading that was not as accurate as desired.

In order to ensure that the thermosyphons were physically identical, for a number of selected tests they were swapped, the water inlet was fed to thermosyphon #2 before it was fed to thermosyphon #1. Figure 5-4 represents a comparison in the difference in temperature across the condenser (ΔT_c) for both thermosyphons for a normal and swapped (reverse) setup. It was found that the difference in temperature across the condenser was the same regardless of the inlet temperature, as shown by the red marks.

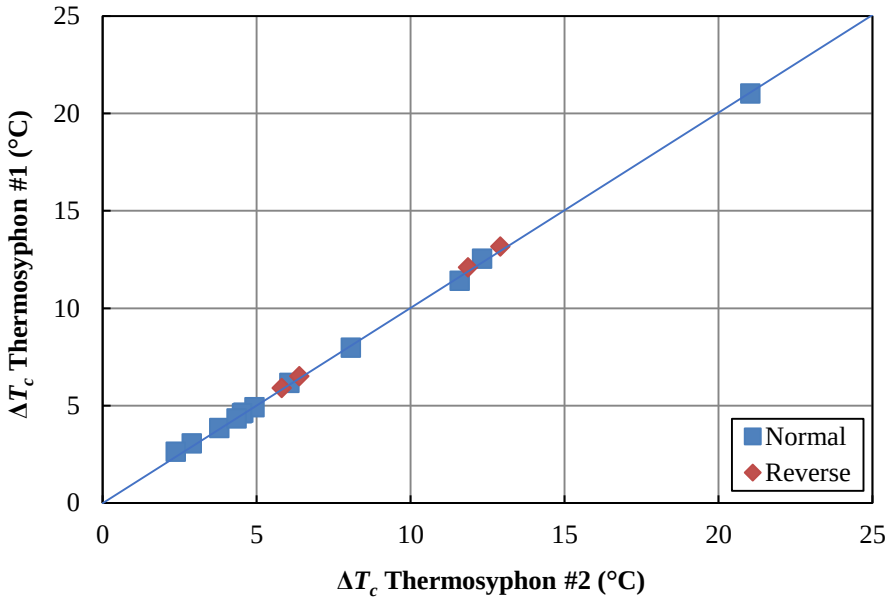

Figure 5-4 – Difference in temperature across the condenser section between both thermosyphons for the same inlet conditions

5.2.2 Heat Transfer

For the heat transfer analysis, the thermosyphons were analysed as a conventional heat exchanger using equation (3-9). The performance of the thermosyphons, represented in Figure 5-5, shows a direct relation between the mean temperature difference (MTD) across the thermosyphon and the heat transfer rate as is to be expected from the formulae used. MTD is used in replacement of the LMTD for this particular example and it is determined arithmetically. Taking a linear trendline and neglecting the thermosyphon working limits, it is possible to have heat transfer even with a really small temperature difference across the thermosyphon.

From Figure 5-5 it can also be seen that Thermosyphon #2 has the highest effectiveness as it requires a smaller difference in temperature across its ends to transport the same amount of heat as Thermosyphon #1.

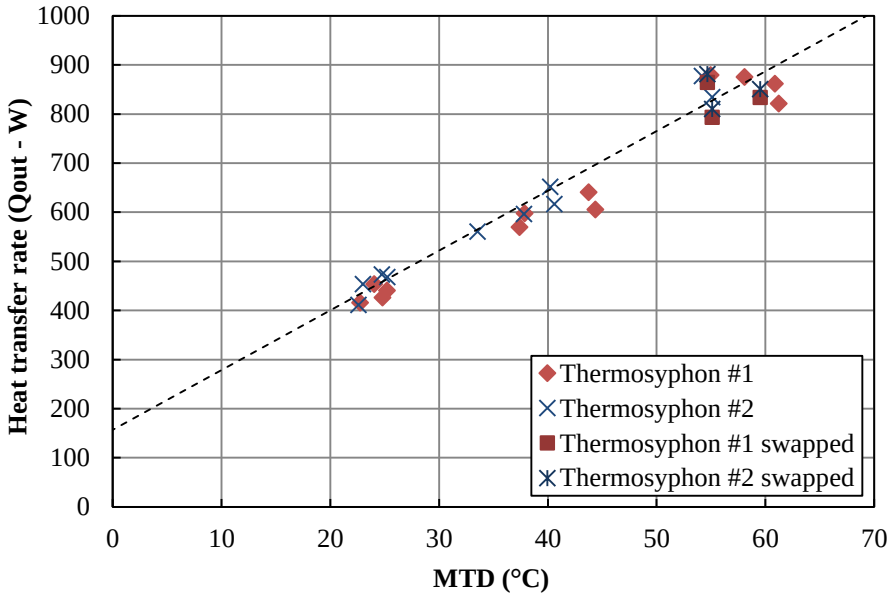

Figure 5-5 – Comparison between Q_{out} and the MTD for the single thermosyphon

A direct comparison was also done between the heat transfer rate of each of the thermosyphons and it was found that overall they fell within the same trendline as shown in Figure 5-6. The trendline tells us that 88.6% of the energy coming into the system in the form of heat is able to leave also in the form of heat through the water.

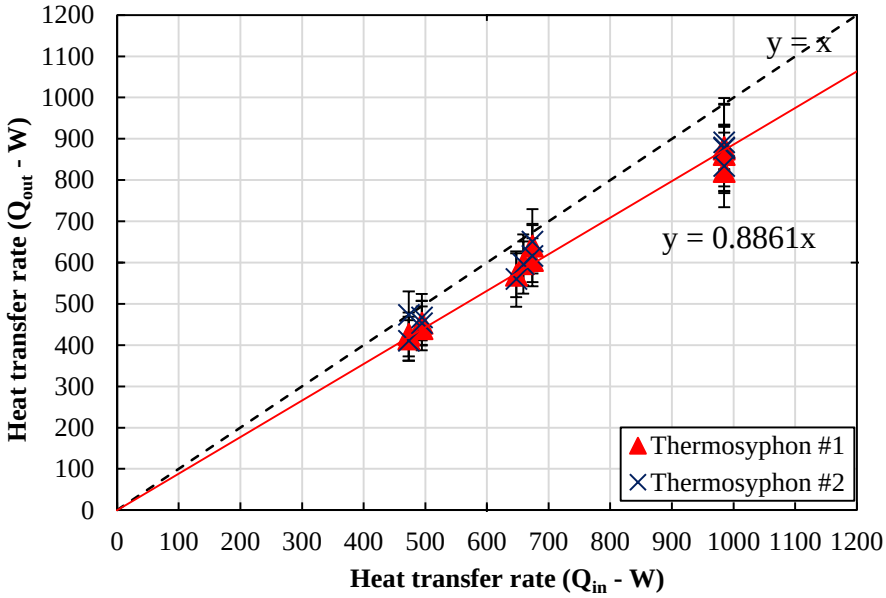

Figure 5-6 – Comparison between Q_{in} and Q_{out} for the single thermosyphon

5.2.3 Thermal Resistance

A study of the thermal resistance across the thermosyphons was also conducted and is displayed in Figure 5-7. It was observed that the thermal resistance of the thermosyphons was effectively constant across all tests.

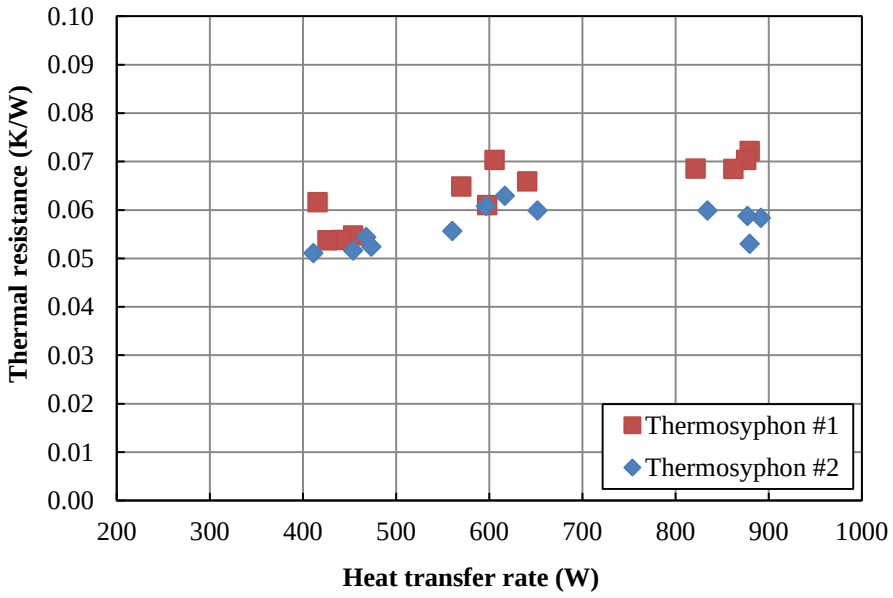

Figure 5-7 – Thermal resistance of the two thermosyphons plotted against the overall heat transfer rate

Thermosyphon #1 registered a higher thermal resistance across all the twelve tests for each respective heat transfer rate. This result is in agreement with Figure 5-5 and it can be said that a lower thermal resistance is directly proportional to a higher effectiveness.

In section 3 – Theoretical Analysis, the total thermal resistance for a single thermosyphon was divided into its different components. The components according to equation (3-11) are convection (mantle to thermosyphon and thermosyphon to water), conduction (through the thermosyphon), and boiling and condensation (within the thermosyphon). An investigation of the relative effect of these resistances when compared to each other was made and is represented for different mass flow rates in Figure 5-8. The thermal resistance from the pressure drop was not included in the graph as its value was negligible.

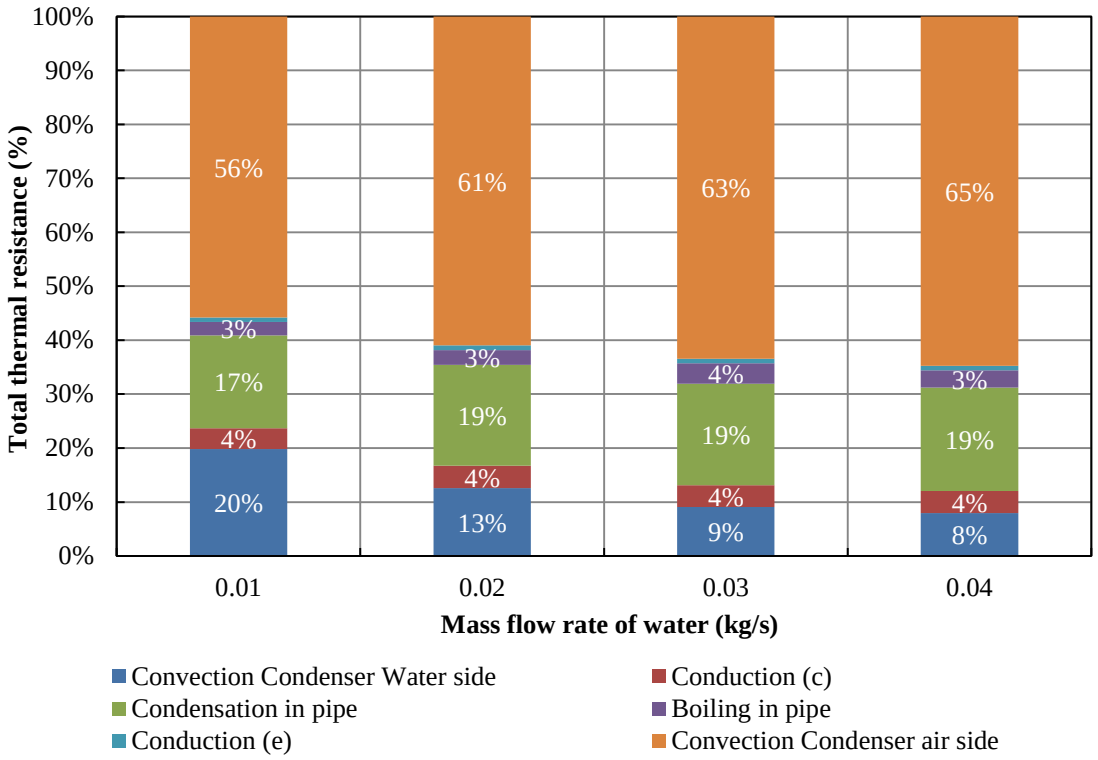

Figure 5-8 – Different components of the thermal network analysis averaged across the twelve experimental tests

As seen in Figure 5-8, the greatest contributor to the total thermal resistance was the convection heat transfer on the evaporator shell-side, responsible for more than half of the total thermal resistance. This is a result of the lower heat transfer coefficient between gas-solid as compared to water-solid. The other great contributors were the convection heat transfer on the shell-side of the condenser section and the condensation heat transfer within the thermosyphon. The heat transfer from condensation of the working fluid was constant as there was very little variation on the temperature of the water on the shell-side.

A slightly larger thermal resistance from conduction on the condenser side when compared to the evaporator side is a result of the thermal conductivity increasing with increasing solid temperature. Overall, the thermal resistance for both pool boiling and conduction through the thermosyphon wall combined contributed to roughly 5% of the total thermal resistance offered by the thermosyphon. This explains why the latter tends to be neglected.

5.2.4 Error Propagation

An instrumentation uncertainty study was conducted in order to locate the error propagation from the measuring instruments used in the experimental rig. The method is described in section 4.3.4. The percentage of uncertainty is displayed in Figure 5-9 for each of the different input heat transfer rates (Q_{in}). The average uncertainty was found to be 13% for both thermosyphons across all experimental tests.

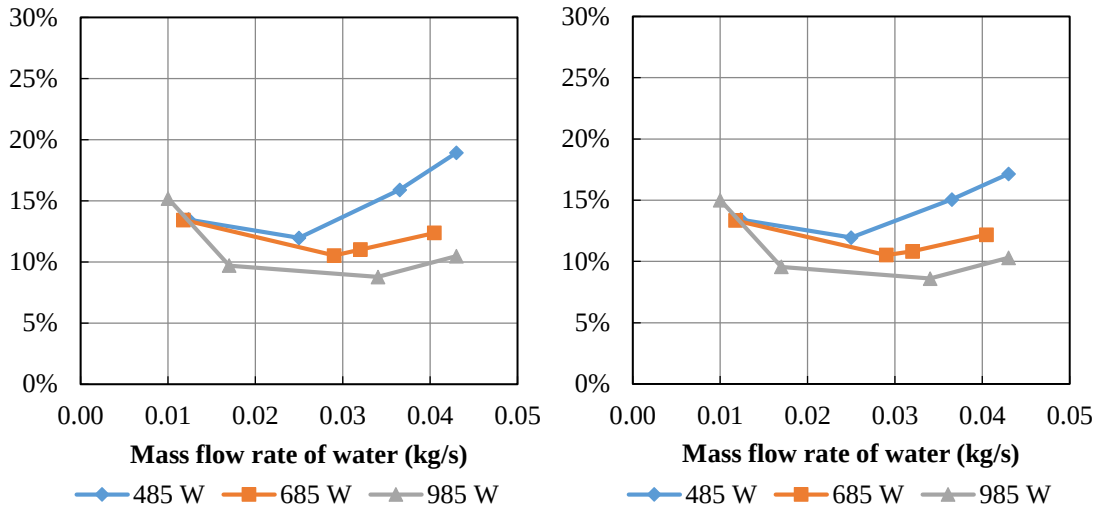

Figure 5-9 – Error propagation as a percentage of the total Q_{out} in the condenser side for Thermosyphon #1 (left) and Thermosyphon #2 (right)

The error propagation study was also compared to the theoretical results. This was done by making a percentile comparison between the total heat transfer rate ($Q_{out,exp}$) and the theoretical heat transfer rate ($Q_{out,theory}$) and plotting it against the results from the uncertainty test. These results are available in Figure 5-10. It was found that the uncertainty is higher than the percentile difference between theoretical and experimental results showing the results are within the error, therefore acceptable.

Figure 5-10 – Comparison between experimental results, theoretical results and the error propagation for the experiment conducted at 985 W (top), 685 W and 485 W (bottom) as a percentage for thermosyphon #1 (left) and thermosyphon #2 (right)

5.2.5 Comparison with Theory

The experimental results for each test using equation (3-11) were compared with the results obtained by doing a thermal network analysis of the thermosyphon and the comparison is displayed in Figure 5-11.

The trend displayed by the theoretical predictions and by the experimental results seem to be in good agreement, especially for a heat input of 685 W, where good agreement is found between the experimental results and the theoretical results. The theoretical results do seem to over-predict the experimental results due to unaccounted heat losses in the experimental rig possibly from the insulation. In the case of the lowest heat input of 485 W, each thermosyphons behaved in a different way; the experimental results for Thermosyphon #1 followed the same trend displayed at 985 W where after 0.02 kg/s a downward trend is seen. On thermosyphon #2, however, a good agreement was found between the theoretical and experimental results.

Overall the results fell within less than 10% of each other as shown from the error bars in Figure 5-11.

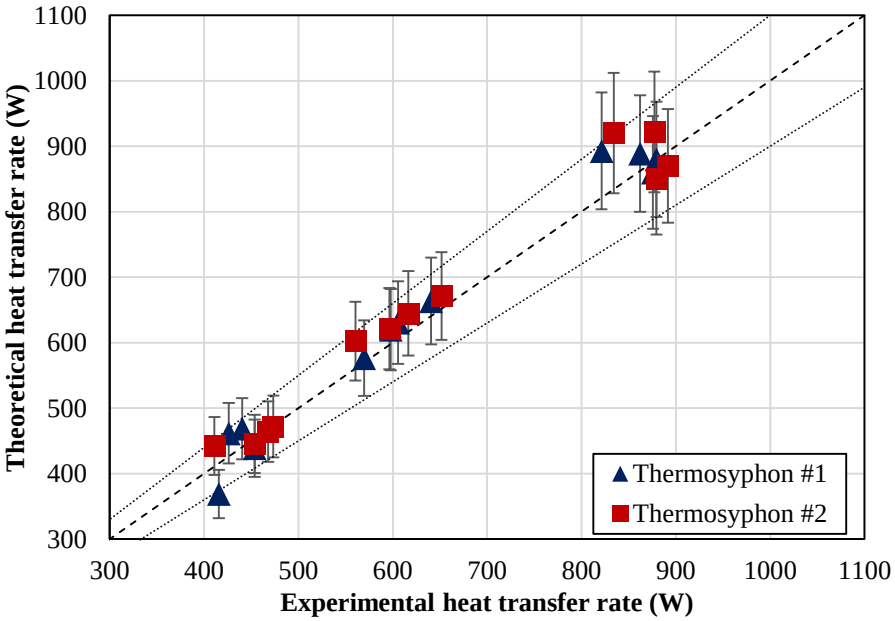

Figure 5-11 – Comparison between theoretical and experimental results

5.3 Heat Exchanger equipped with six thermosyphons – single pass

This section outlines the results for the experiment with six thermosyphons. Air was used as the evaporator-side fluid and water as the condenser-side fluid. The mass flow rate of air varied between 0.05 kg/s and 0.17 kg/s and the inlet air temperature varied between 50 °C and 300 °C. On the condenser side, the inlet temperature and the mass flow rate of water were both kept constant at approximately 7 °C and 0.08 kg/s respectively. A study focussing on this experiment has been published and is available in Appendix A – Published Papers (Ramos, et al., 2014a).

5.3.1 Temperature Comparison

Figure 5-12 displays the temperature distribution within the heat exchanger for inlet temperatures of 50°C, 100°C, 150°C, 200°C, 250°C and 300°C. The temperatures were logged from 5 different locations, namely, at the inlet and outlet of the evaporator (T_{ein}, T_{eout}) at the condenser section (T_{cin}, T_{cout}) and inside the thermosyphons (T_{pipe}). The temperature inside the thermosyphons is an averaged value from the four measured thermosyphons as each thermosyphon has a different working temperature which is a function of the temperatures across its evaporator and condenser section.

It can be seen that the trend is for the difference in temperature across the evaporator section to decrease as the mass flow rate of the hot incoming hot air increases while in the condenser the difference in temperature increases with increasing mass flow rates. From a thermodynamic perspective this is a logical outcome as the increasing mass flow rate of air into the evaporator increases the heat transfer coefficient which in turn increases the heat flow into the thermosyphon thus resulting in more heat being transferred to the water on the condenser section.

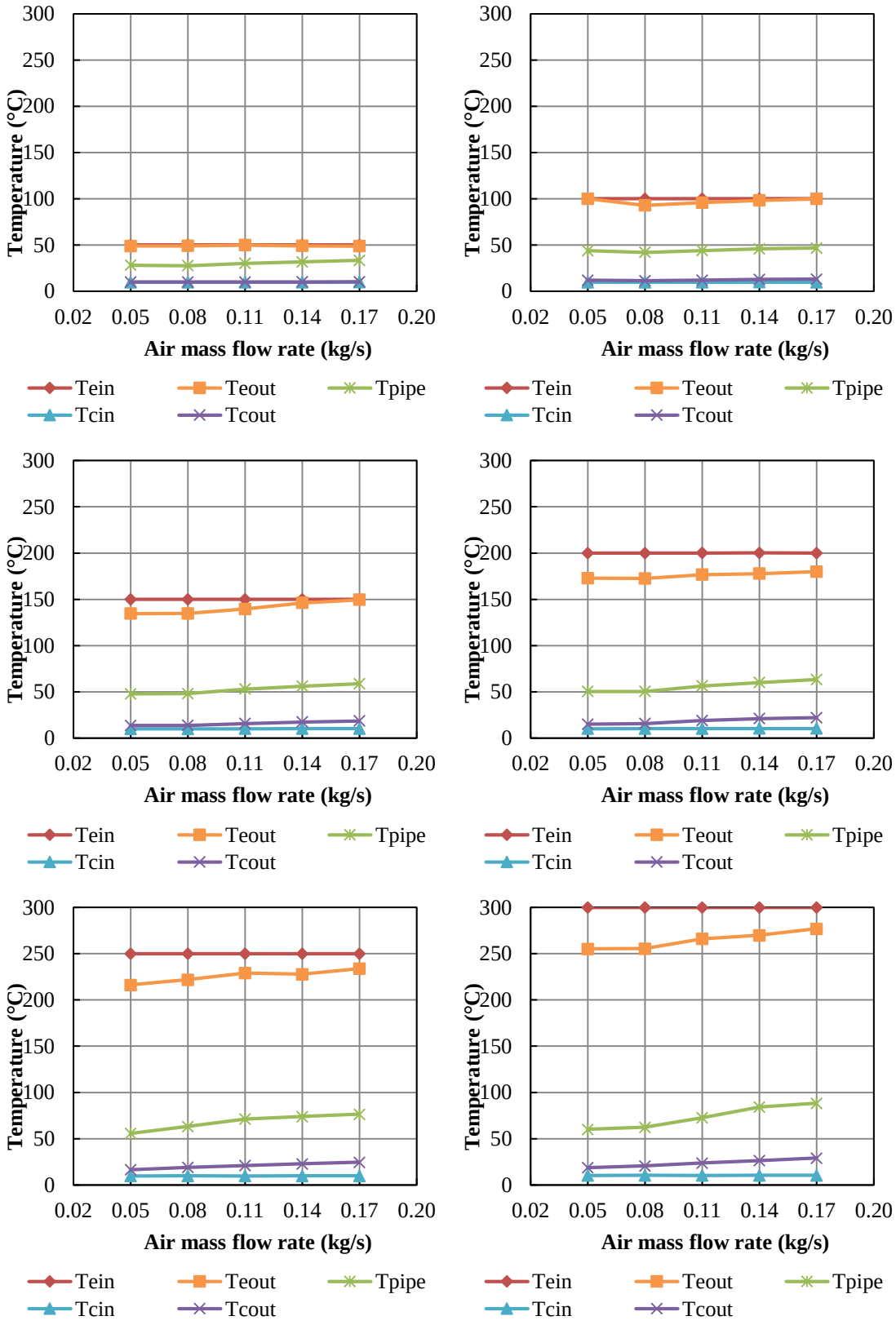

Figure 5-12 – Temperature distribution within the heat exchanger for inlet air temperatures ranging from 50 °C to 300 °C

From the experimental results, a regular pattern emerged between the thermosyphon working temperature and the overall difference in temperature in between the evaporator and the condenser sections ($T_{e,avg} - T_{c,avg}$). The average working temperature of the thermosyphons was plotted against the overall difference in temperature between the evaporator and the condenser section for the range of mass flow rates tested and is displayed in Figure 5-13.

Data from the trend lines, shown in their respective colour, allowed the creation of equation (5-1), an expression able to predict the average working temperature of the thermosyphons for each different set of working conditions.

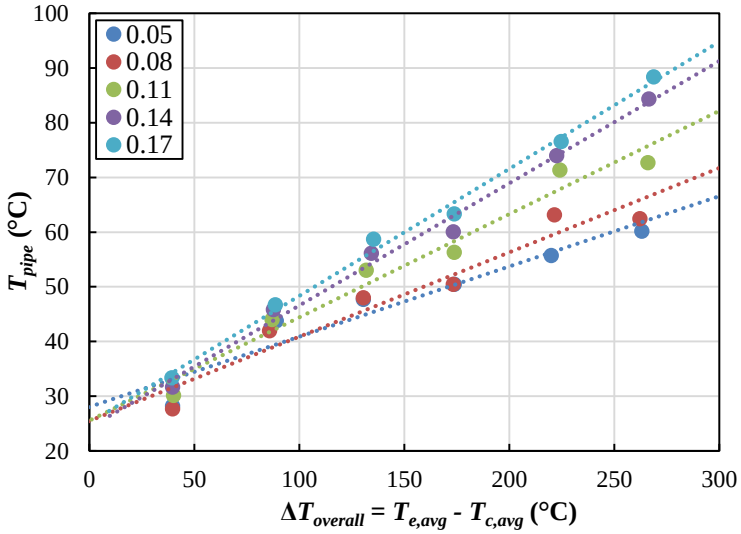

Figure 5-13 – Average working temperature of the thermosyphons for different overall ΔT at different mass flow rates

$$T_{pipe} = 0.589\,\dot{m}^{0.5146}(\Delta T_{overall} - 40) + 32 \quad (°C) \tag{5-1}$$

Equation (5-1) is a correlation that allows the prediction of the average working temperature of the thermosyphons according to the mass flow rate of air on the evaporator side and the difference in temperature across the entire heat exchanger. The expression only applies to the heat exchanger under study with constant temperature and mass flow rate on the condenser side. The output of the applied correlation to the inlet conditions of the heat exchanger is presented in Figure 5-14 which seems to follow the tendency of Figure 5-13 with reasonable accuracy.

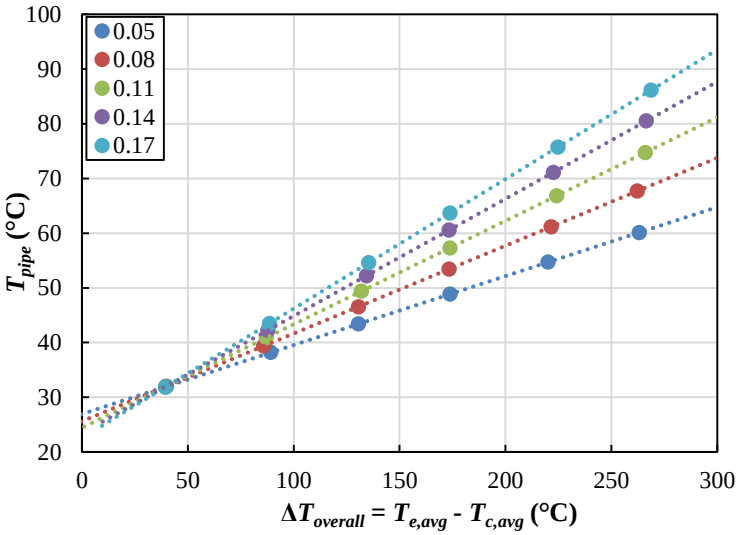

Figure 5-14 – Predicted average working temperature of the thermosyphons for different overall ΔT at different mass flow rates

5.3.2 Heat Transfer

The performance of the heat exchanger was plotted against the mass flow rate for each different inlet temperature and is displayed in Figure 5-15. The results agree with those of El-Baky and Mohamed (2007) as higher exhaust velocities resulted in reduced temperature across the condenser section.

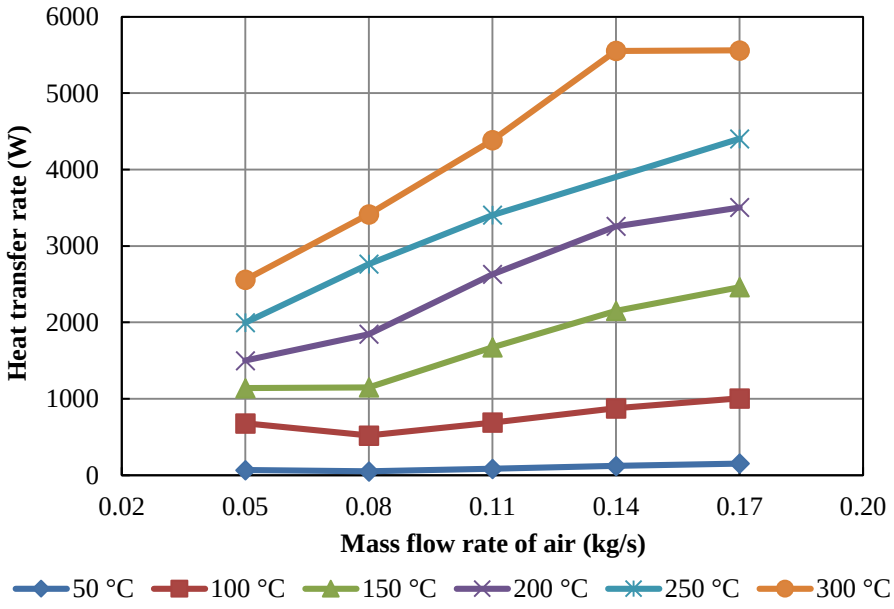

Figure 5-15 – Total heat extraction rate of the heat exchanger according to the experiment results

Higher inlet temperature result in higher heat transfer rate which is in agreement with experimental tests from literature (Yodrak, et al., 2010). A limit was reached after 0.14 kg/s as no substantial increase in the heat transfer rate was found beyond this value for 300°C. This was found to be related to the inability of water on the shell-side of the condenser section to absorb any more thermal energy.

5.3.3 Thermal Resistance

The total thermal resistance of the heat exchanger was also investigated and is displayed in Figure 5-16. It was found that higher inlet temperatures resulted in overall lower thermal resistances across the heat exchanger. The thermal resistance was determined from equation (3-6).

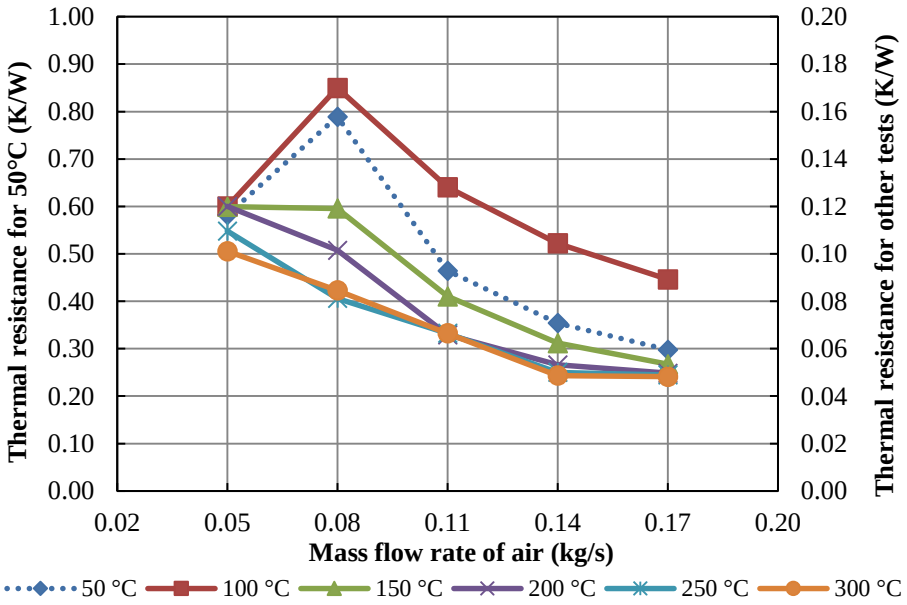

Figure 5-16 – Total thermal resistance of the heat exchanger

The thermal resistance for an inlet temperature of 50°C was found to be higher than the rest and was plotted on a different scale. The high thermal resistance for that test in particular is a combination of two factors; it is a result of the temperature of the air on the evaporation section being almost as low as the saturation temperature of the fluid within and the relatively large length of the thermosyphon when compared to the cross sectional area, which in turn creates what is known as “geyser boiling” if the boiling regime is not stabilised. The other reason is related to experimental uncertainty for low temperature differences, also the case for the lowest mass flow rates for 100°C.

The thermal resistance was also plotted against the overall heat transfer rate as shown in Figure 5-17. A higher difference in temperature produced a lower thermal resistance in the heat exchanger due to the more stable boiling regime inside the thermosyphon. Once again, the results obtained at 50°C are not in agreement with the rest as their thermal resistance is higher than 0.2 K/W. The other results have a lower value ranging between 0.05 and 0.12 K/W. This plot clearly shows the thermal resistance is inversely proportional to the overall heat transfer coefficient.

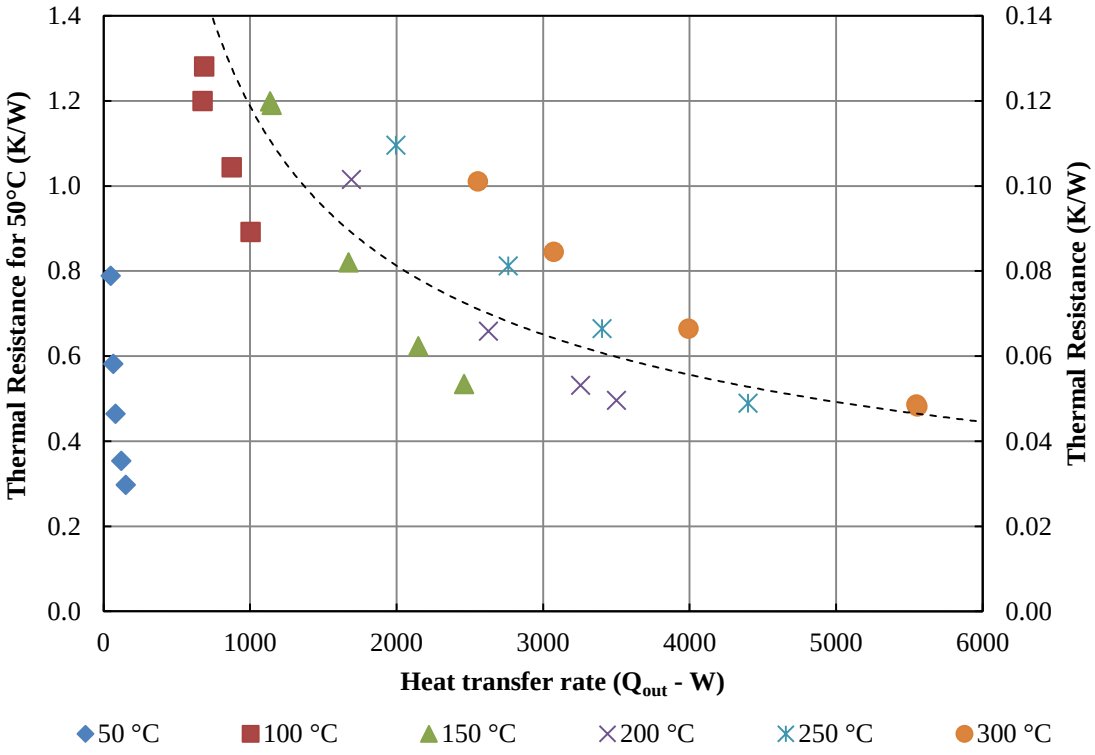

Figure 5-17 – Relation between the Q_{out} and thermal resistance

5.3.4 Effectiveness

Effectiveness is a variable that is an integral part of the Effectiveness-Number of Transfer Units (ε-NTU) method and is a measure of a heat exchanger's heat transfer potential. The effectiveness is a rate of the actual heat transfer of a heat exchanger to the maximum possible heat transfer rate.

Figure 5-18 represents a plot of the effectiveness of the heat exchanger against the mass flow rate of incoming air. A downward trend is observed in all of the results, as with the increased mass flow rate, the temperature difference between the inlet and the outlet of the condenser section is reduced, reducing the overall effectiveness. The plot is in

agreement with Jouhara and Merchant (2012) as higher inlet temperatures result in higher effectiveness.

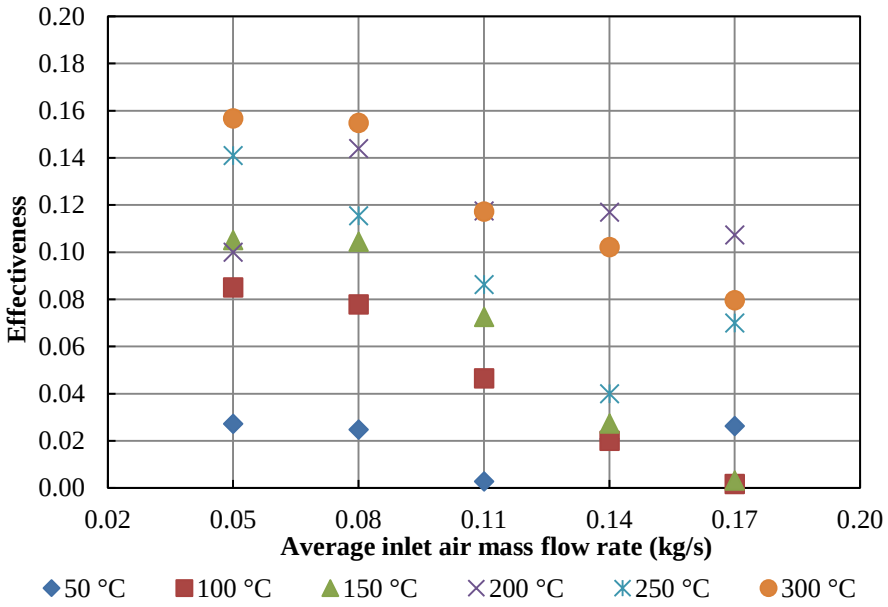

Figure 5-18 – Effectiveness of the heat exchanger

The effectiveness was also plotted against the NTU and it can be concluded that there is a quasi-linear relation in agreement with the literature for this type of plots (Incropera & DeWitt, 1996; Çengel, 2002) as seen in Figure 5-19. Unfortunately, the heat exchanger under study was too small and was incapable of transferring more than 0.2 transfer units.

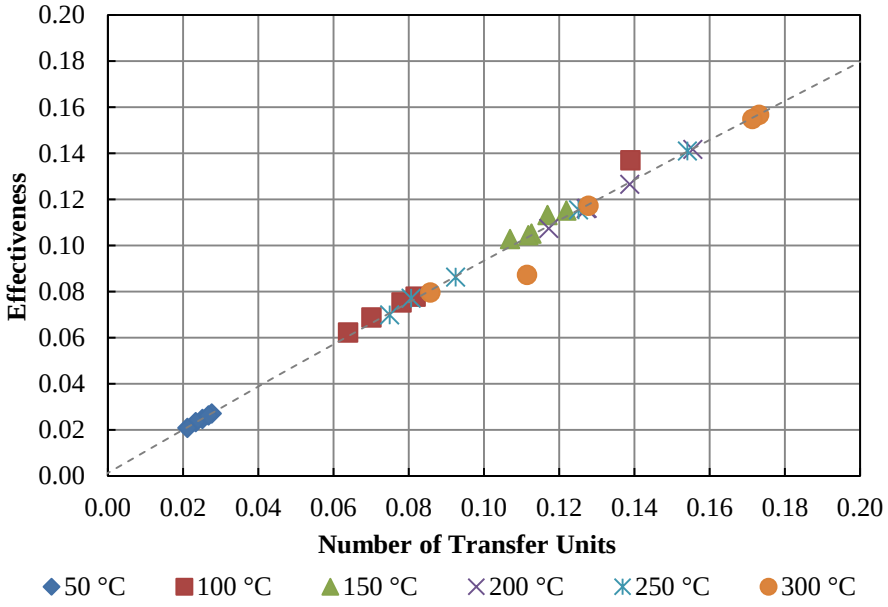

Figure 5-19 – Comparison between ε and the NTU

5.3.5 Error Propagation

An uncertainty study was conducted on the error propagation from the measurement instruments used in the experimental rig and the results are presented in Figure 5-20. The method is explained thoroughly in section 4.3.4.

It was observed that the smaller the difference in temperature between the inlet and the outlet temperatures, the higher the uncertainty. This is particularly striking at 50°C inlet air temperature where the uncertainty hovers the 300% due to the fact that the temperature variation is less than 1°C. At 100 °C the ΔT_c already fluctuates close to 2°C and therefore the uncertainty propagation is reduced. For all the other tests the uncertainty when determining the Q_{out} is lower than 10% and stays within the 5% range, which is a more acceptable range for most engineering applications.

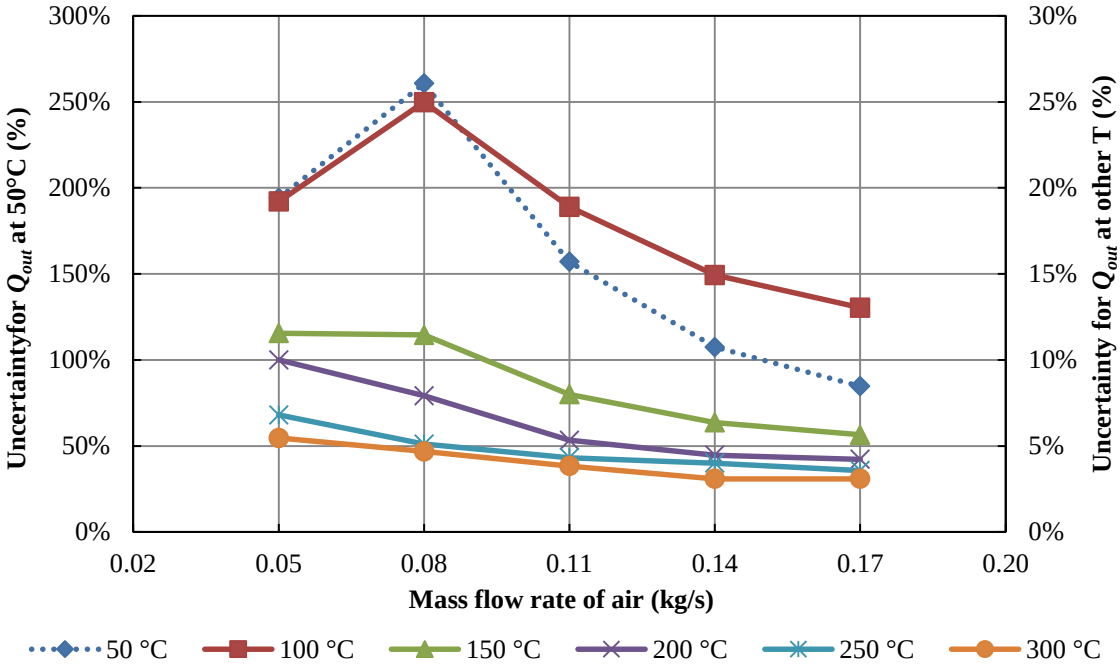

Figure 5-20 – Error propagation for Qout

Overall the trend is for the error propagation to reduce as the mass flow rate and the difference in temperatures increase, a trend seen in all the tests.

5.3.6 Comparison with Theory

Figure 5-21 represents the predicted analytical results using the thermal network analysis for the tested heat exchanger using the same inlet conditions as in the experimental test. The heat transfer rate increases with increasing mass flow rate and inlet temperature on the evaporator side, a trend also displayed in the experimental results.

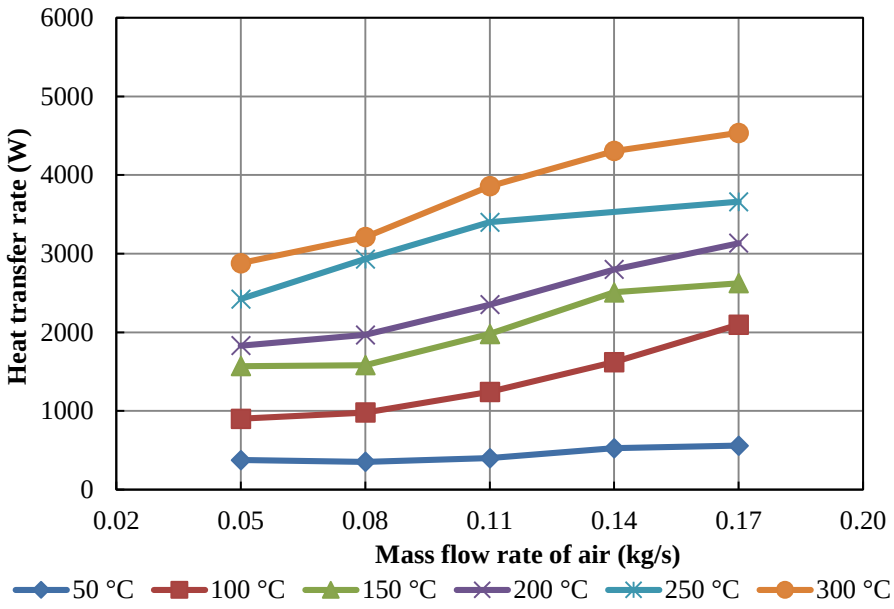

Figure 5-21 – Total heat extraction rate of the TSHX predicted by the theory

Figure 5-22 plots the percentage difference between the two sets of results. The largest percentage of disagreement was at 50 °C inlet temperature with 80%; this is a result of the incomplete boiling regime not taken into account in the correlations used and partly due to the uncertainty. 100 °C inlet temperature had an average disagreement just below 50% partially due to the same reasons but also due to the extremely long thermosyphons when compared to their cross sectional area (Hagens, et al., 2007). On both cases the theoretical results over-predict the experimental values.

All the other values were within a 20% envelope, with lower temperatures over-predicting the experimental results and higher temperatures under-predicting. The same pattern can be identified in Figure 5-23.

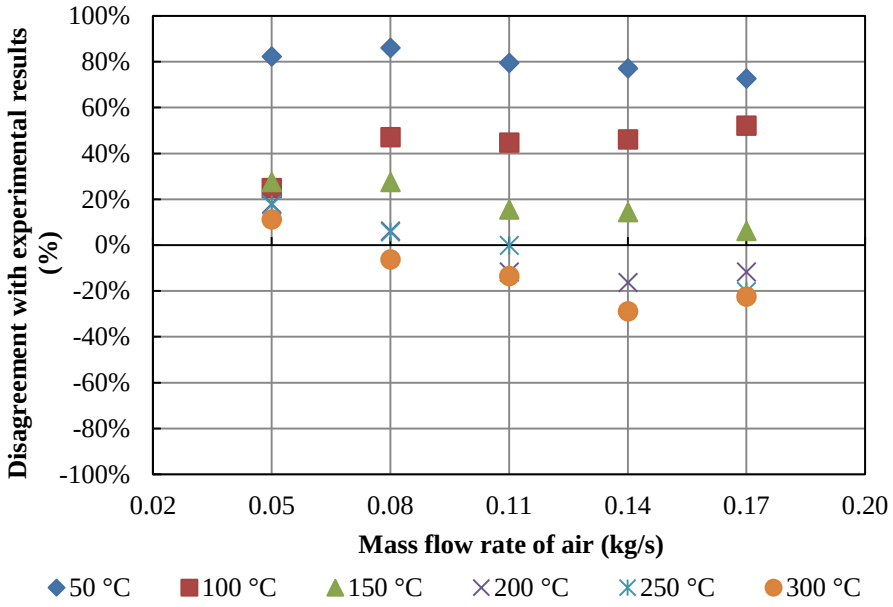

Figure 5-22 – Percentage of disagreement between the theoretical and experimental results

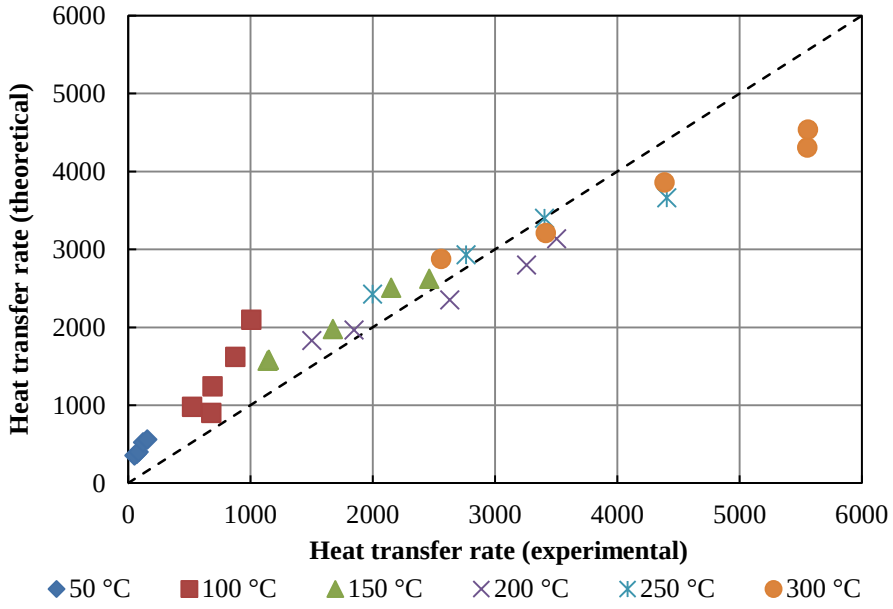

Figure 5-23 – Direct comparison between the experimental and theoretical heat transfer rate

Worth of note is the under-representation of 200°C, 250°C and 300°C which the thermal network analysis seems to under predict. This is a predicted outcome from the expressions used from literature as the inherent chaos from evaporation and condensation have a high degree of inherent chaos that in reality increases the heat transfer coefficient and is often misrepresented in the empirical formulae created.

5.4 Heat Exchanger equipped with six thermosyphons – double pass

This section outlines the results for the experiment with six thermosyphons in double pass as seen in Figure 4-8. The experimental conditions mirrored those used in the single pass test in section 5.3, using air as the evaporator-side fluid and water as the condenser side fluid. The mass flow rate of air varied between 0.05 and 0.14 kg/s and the inlet air temperature varied between 100°C and 250°C. On the condenser side, the inlet temperature and the mass flow rate of water were both kept constant at approximately 14°C and 0.08 kg/s, respectively. The work resulting from this experiment has been published and is available in Appendix A – Published Papers (Mroué, et al., 2015).

5.4.1 Temperature Comparison

Figure 5-25 displays the temperature distribution within the heat exchanger for inlet temperatures of 100°C, 150°C, 200°C and 250°C. The temperatures were determined using thermocouples placed in 5 different locations, namely, at the inlet and outlet of the evaporator (T_{ein}, T_{eout}) and condenser sections (T_{cin}, T_{cout}) and inside the thermosyphons (T_{pipe}).

The trend is for the temperature difference across the evaporator to decrease as the mass flow rate of air increases on the evaporator side. The opposite is true for the water on the condenser side, as the total amount of heat coming into the heat exchanger increases, the more heat is transferred into the water, thus increasing the outlet temperature.

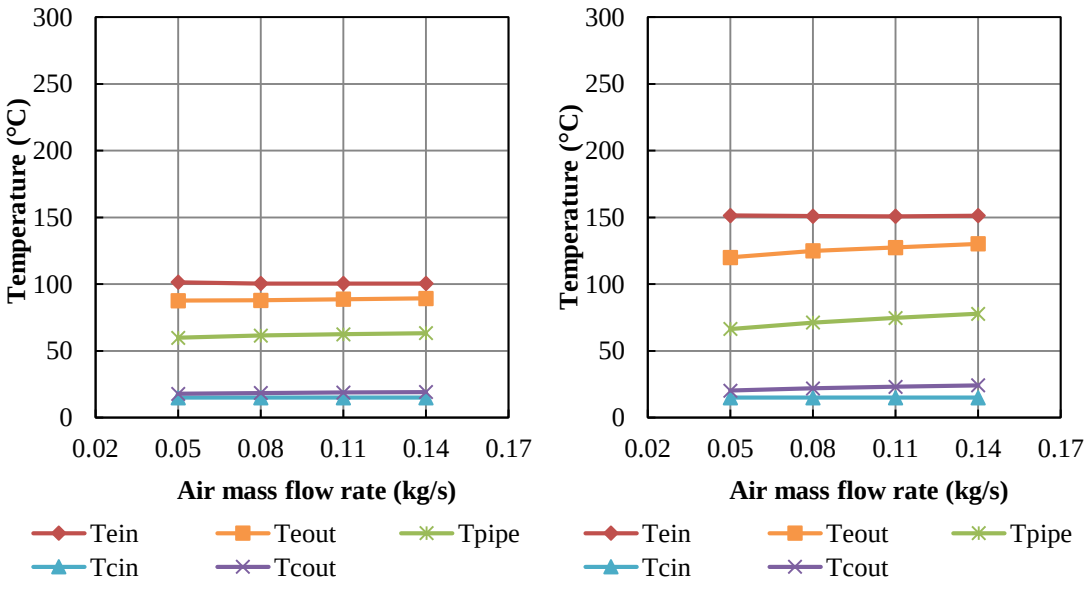

Figure 5-24 – Temperature distribution in the TSHX for air temp 100 °C and 150 °C

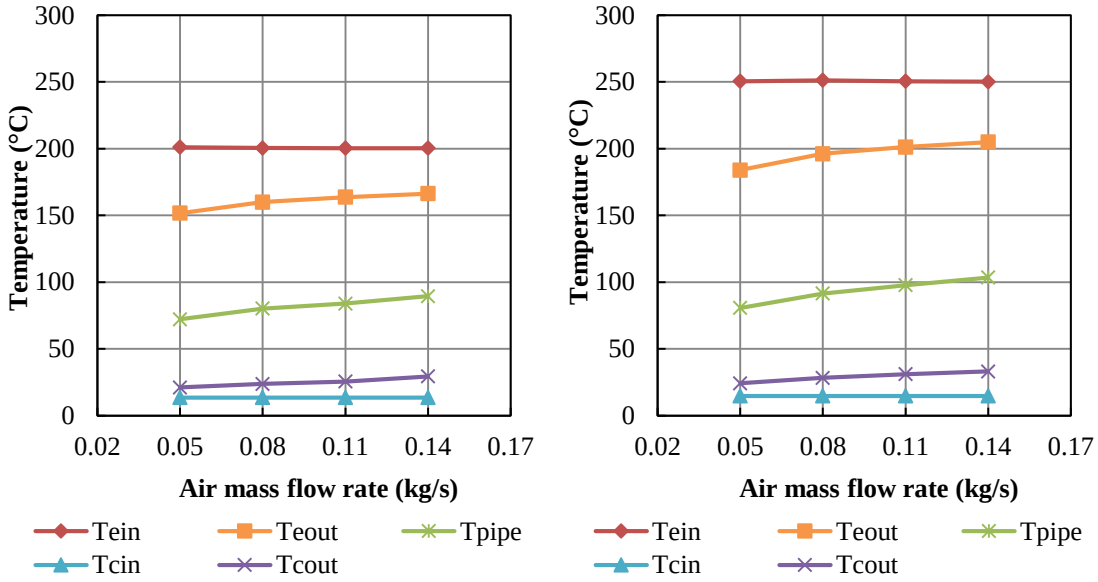

Figure 5-25 – Temperature distribution in the TSHX for air temp 200 °C and 250 °C

A pattern was identified from the experimental results between the overall difference in temperature across the entire heat exchanger and the working temperature of the pipes. This fact is made more evident in Figure 5-26, which plots the two variables against one another for different mass flow rates. This trend was transformed into a correlation, expressed as equation (5-2).

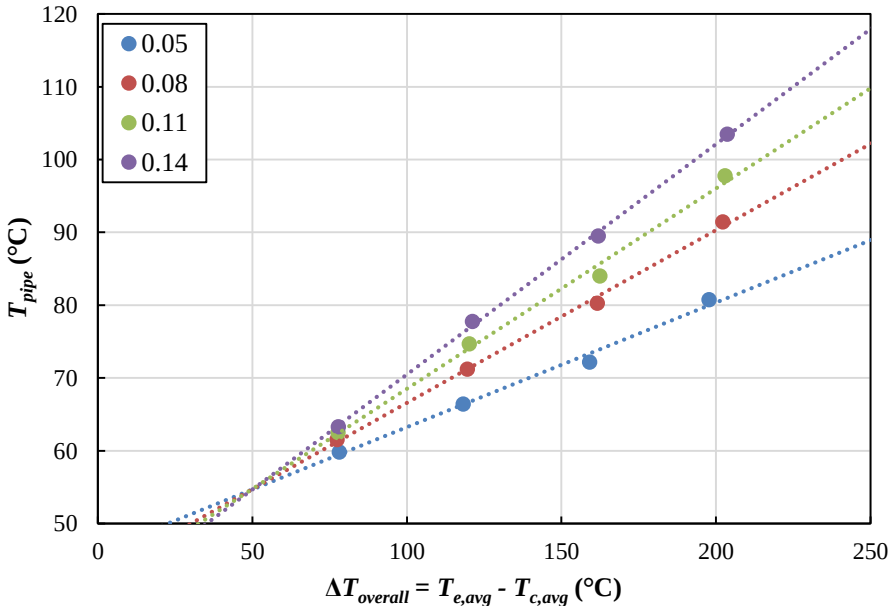

Figure 5-26 – Average working temperature of the thermosyphons for different overall ΔT at different mass flow rates for double pass

Equation (5-2) is a correlation that allows the prediction of the average working temperature of the thermosyphons according to the mass flow rate of air on the

evaporator side and the difference in temperature across the entire heat exchanger. The expression only applies to the heat exchanger under study assuming constant temperature and mass flow rate on the condenser side. The output of the applied correlation was applied to the inlet conditions of the heat exchanger and is presented in Figure 5-27.

$$T_{pipe} = 1.0196\,\dot{m}^{0.5902}(\Delta T_{overall} - 50) + 55 \quad (°C) \tag{5-2}$$

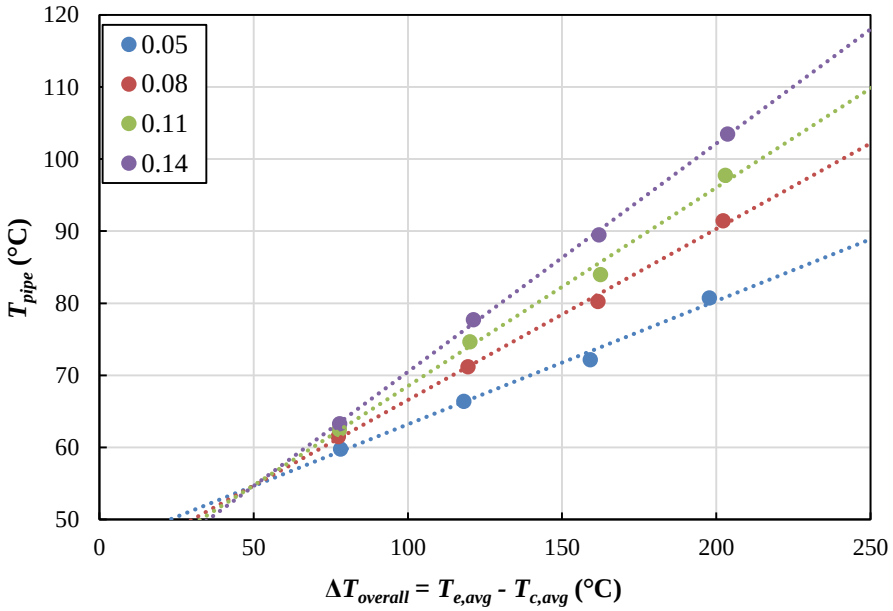

Figure 5-27 – Predicted average working temperature of the thermosyphons for different overall ΔT at different mass flow rates for double pass

5.4.2 Heat Transfer

The heat transfer rate followed the same behaviour as it had in the single pass test albeit a bit more consistently as can be seen in Figure 5-28; increasing inlet temperatures on the evaporator side resulted in higher heat transfer rates. As mentioned in section 0, it was not possible to test the heat exchanger for the same range of inlet conditions as the heat exchanger in single pass due to resource and time constraints by part of the funding body, where the experiments took place.

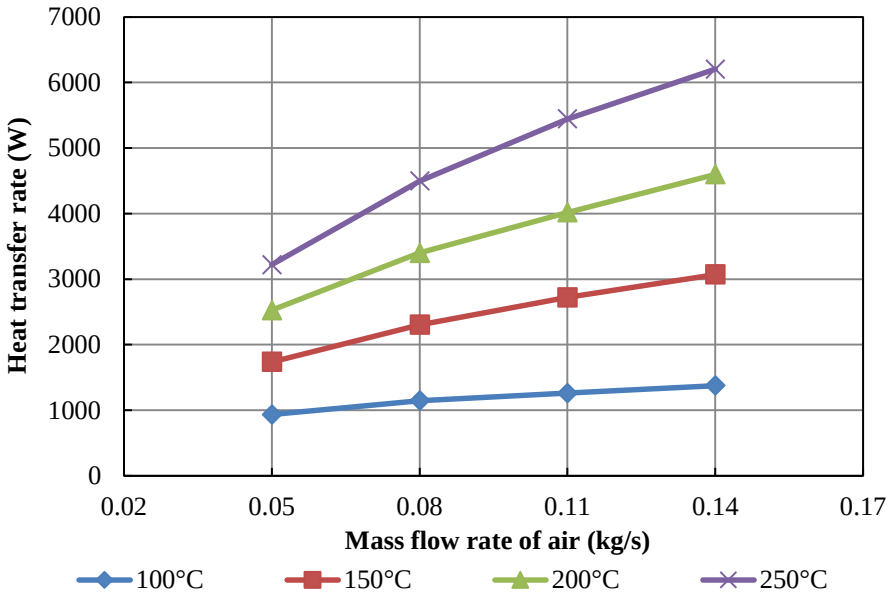

Figure 5-28 – Heat transfer rate of the heat exchanger in double pass according to different inlet conditions

The results for 100°C inlet air temperature appear much more consistent thanks to the double pass which adds additional heat to the evaporator side of the thermosyphons.

The heat transfer rate for each pass was then analysed and compared to the total heat transfer rate and presented in Figure 5-29. The green bar represents the energy lost from the connecting elbow.

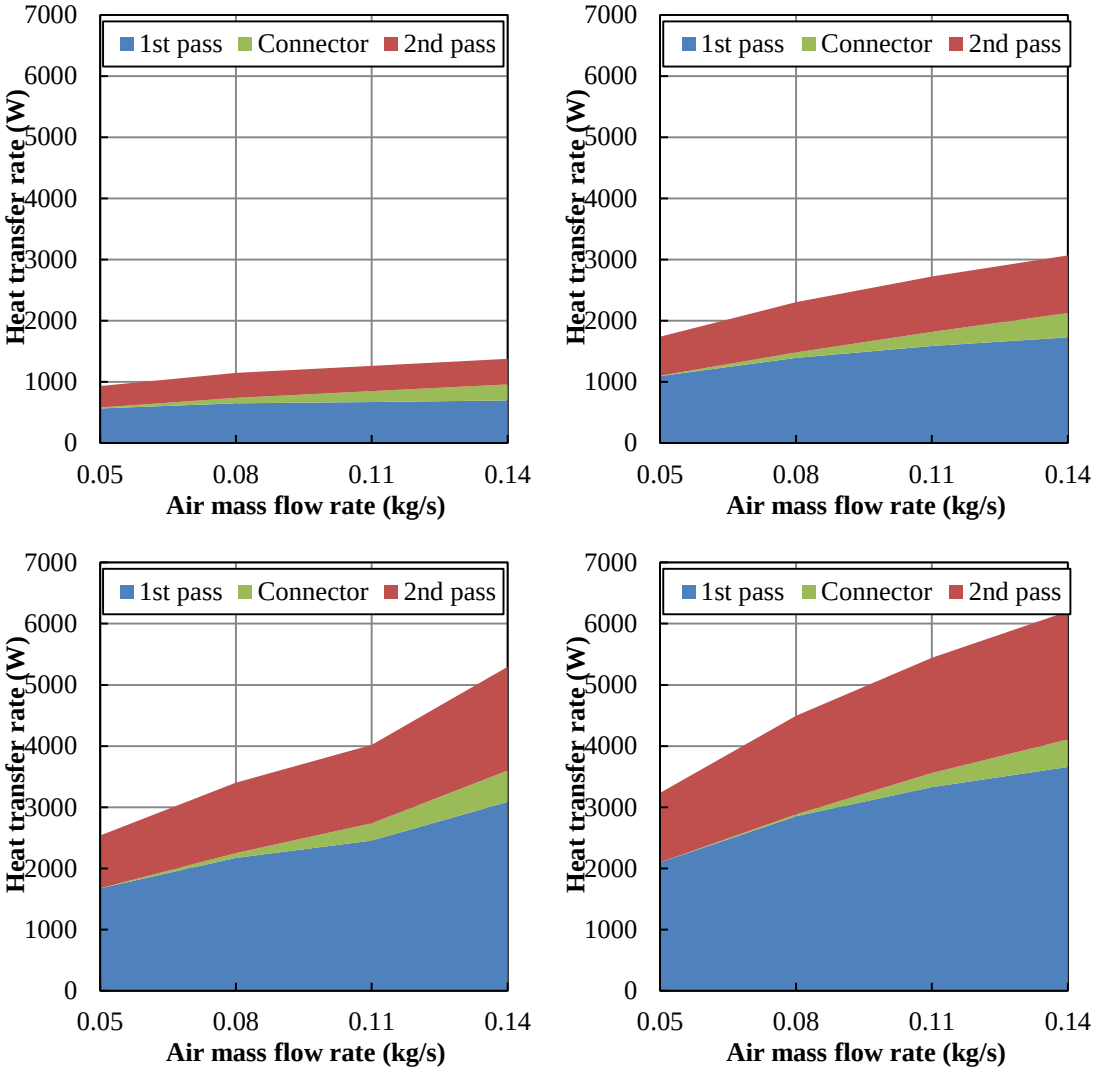

Figure 5-29 – Heat transfer rate of the heat exchanger in double pass for inlet temperatures ranging between 100 °C and 250 °C

Overall the 1st pass had the highest impact on the total heat transfer rate, averaging approximately 60% of the total heat transfer across all of the tests. This is mainly due to the higher temperature difference between the thermosyphons and the incoming flow. The second pass averaged 35% of the total heat transfer across all of the tests. This leads to the conclusion that for this set of thermosyphons, the heat transfer from pool boiling is superior to that from film boiling (the second pass)

5.4.3 Thermal Resistance

The overall thermal resistance for the heat exchanger in double pass is displayed in Figure 5-30. It was found to be lower than that displayed by the heat exchanger in single pass as the evaporator section was effectively twice as large which has a direct influence on the heat transfer rate.

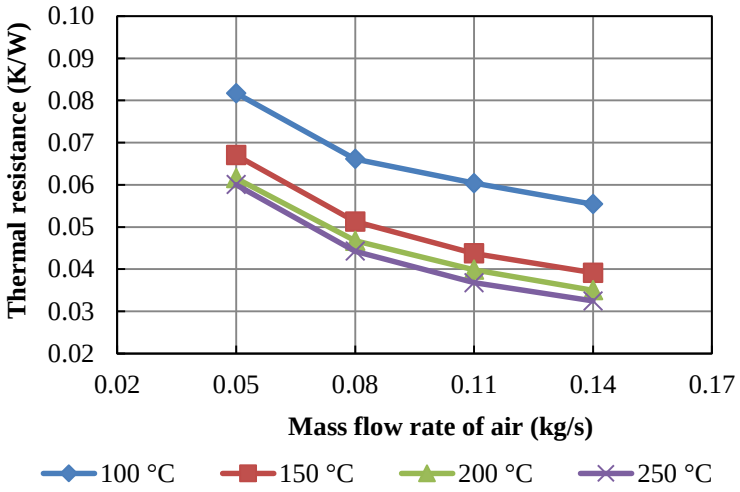

Figure 5-30 – Total thermal resistance of the heat exchanger

The thermal resistance is plotted against the overall heat transfer rate and is shown in Figure 5-31. As in the single pass test, the thermal resistance is inversely proportional to the overall heat transfer coefficient and therefore to the heat transfer rate. It was found to be lower than that of the single test as, once again, the thermal resistance is related to the overall heat transfer area which is larger in the double pass.

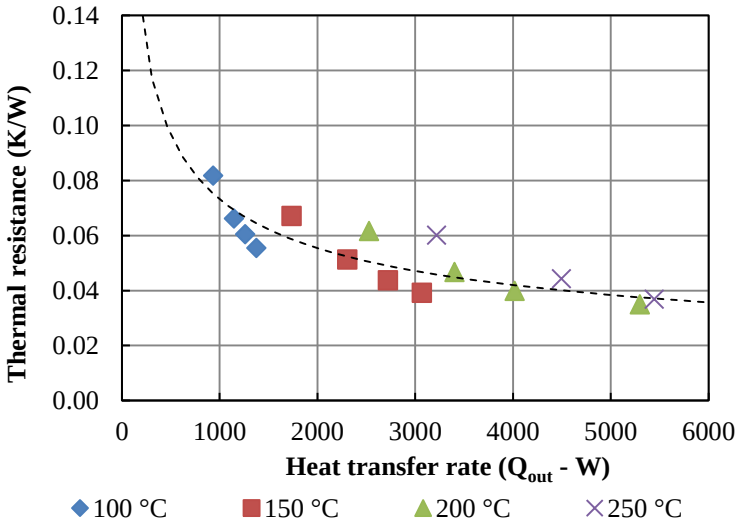

Figure 5-31 – Relation between the Q_{out} and thermal resistance

5.4.4 Effectiveness

The effectiveness of the heat exchanger in double pass followed the same pattern as in the single pass experiment as can be seen from Figure 5-32. Increasing the mass flow rate reduced the effectiveness and increasing the temperature increased the effectiveness. The higher effectiveness was a result of the larger heat transfer area.

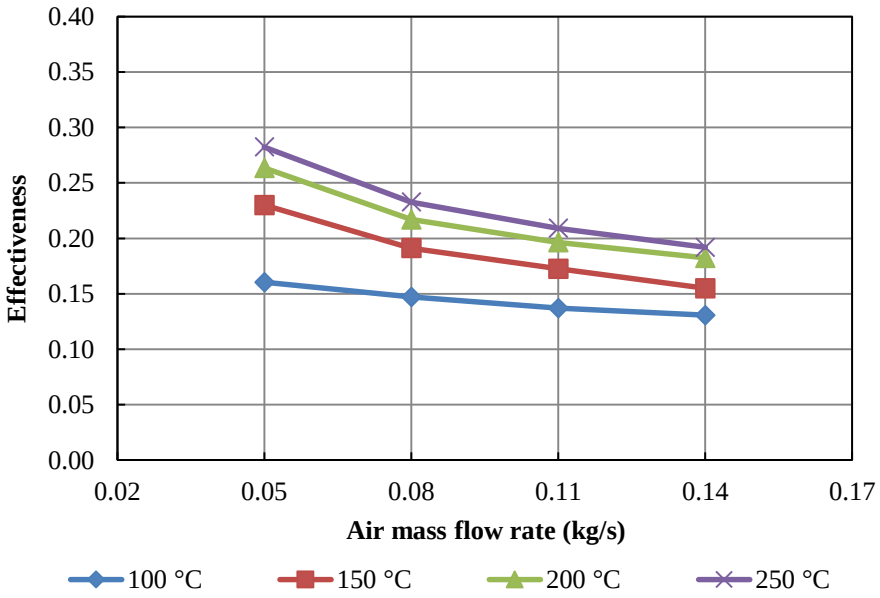

Figure 5-32 – Relation between the effectiveness and the incoming evaporator side conditions

Figure 5-33 plots the effectiveness against the number of transfer units.

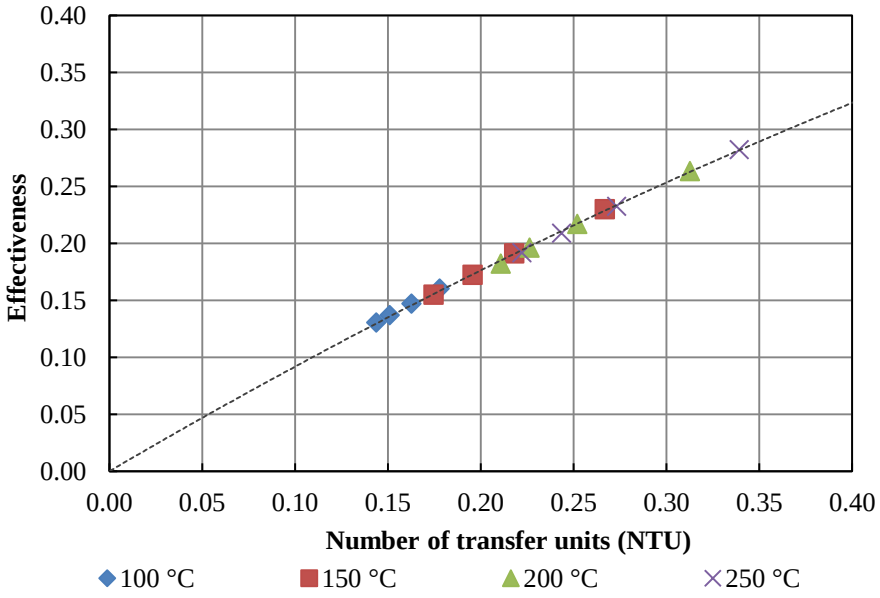

Figure 5-33 – Comparison between ε and the NTU

The results sit on the same trendline as the single pass and due to the enlarged heat transfer area, the NTU achieved is doubled. Further increasing the area of the heat exchanger by adding more thermosyphons would give a more definite view of the potential number of transfer units and its relation to the effectiveness.

5.4.5 Error Propagation

The equipment used to log the temperature and the mass flow rate for the double pass was the same as for the single pass, therefore the error propagation study conducted for the overall heat transfer rate resulted in a plot extremely similar to Figure 5-20. An additional study on the error propagation for the effectiveness was conducted and the results presented in Figure 5-34.

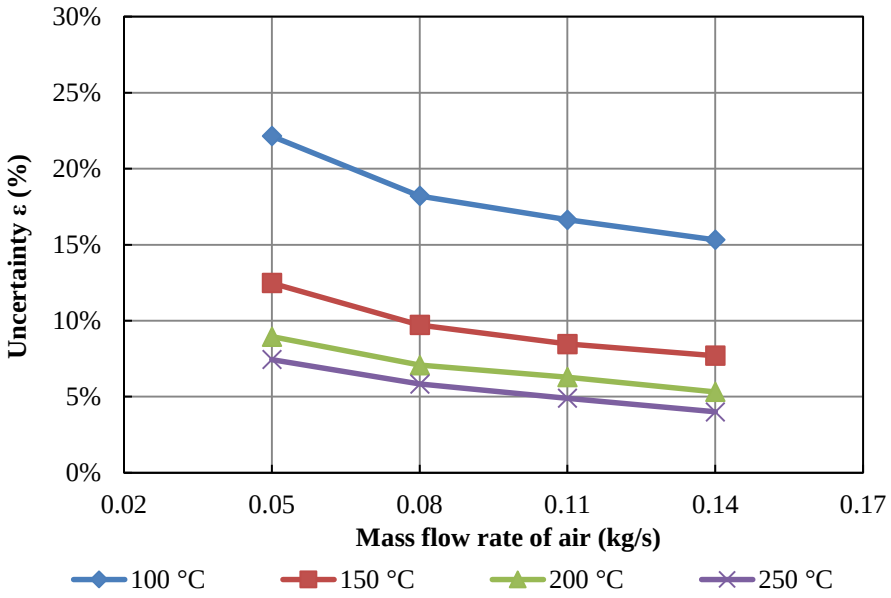

Figure 5-34 – Uncertainty analysis for the effectiveness

The effectiveness relies in additional data compared to the heat transfer rate and the uncertainty associated with the values nears the 10% mark. Once again, the difference in temperature across the evaporator section for 100°C inlet temperature is smaller than the rest, which results in a higher error margin.

5.4.6 Comparison with single pass

A comparison between the heat transfer rate (Q_{out} in W) of the heat exchanger in single pass and the first pass of the double pass heat exchanger was made. The results are presented in Figure 5-35 and seem to suggest that adding a second pass does not greatly affect the performance of the heat exchanger in the first pass as most of the results fall within the same trend line within a 10% envelope. No major reduction or increase in performance were identified.

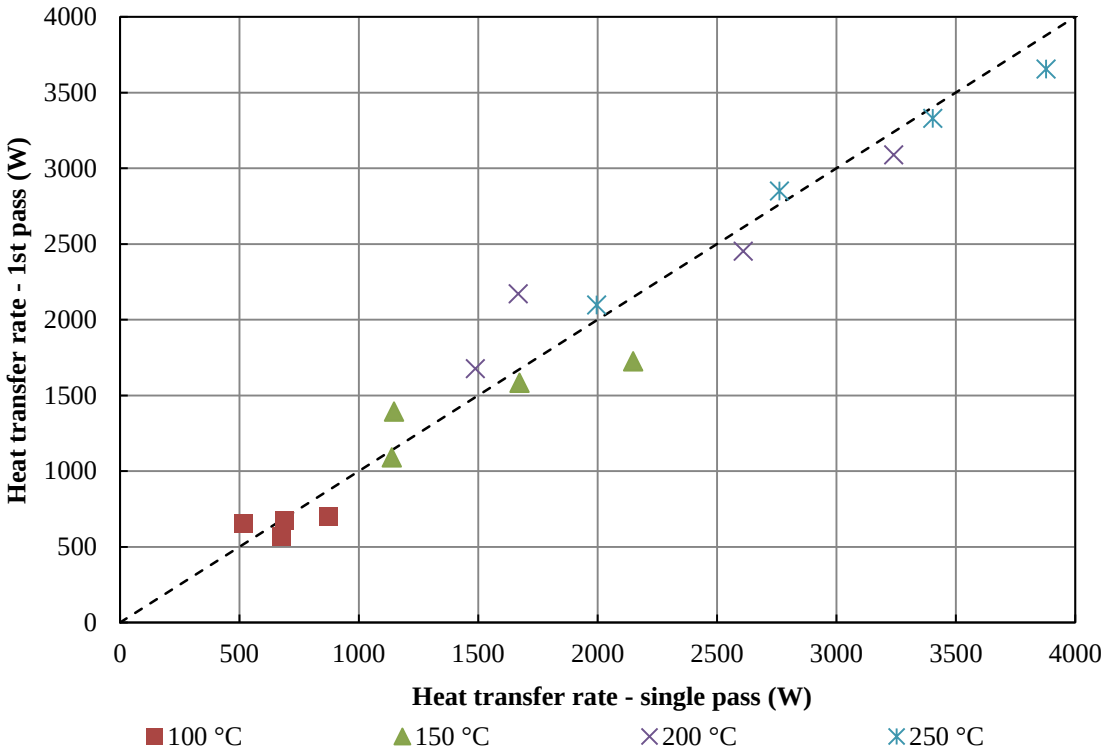

Figure 5-35 – Comparison between the first pass of the double pass heat exchanger and the single pass heat exchanger

A study was conducted on the % of performance increase by comparing the heat transfer rate of the heat exchanger in single pass and in double pass and is presented in Figure 5-36.

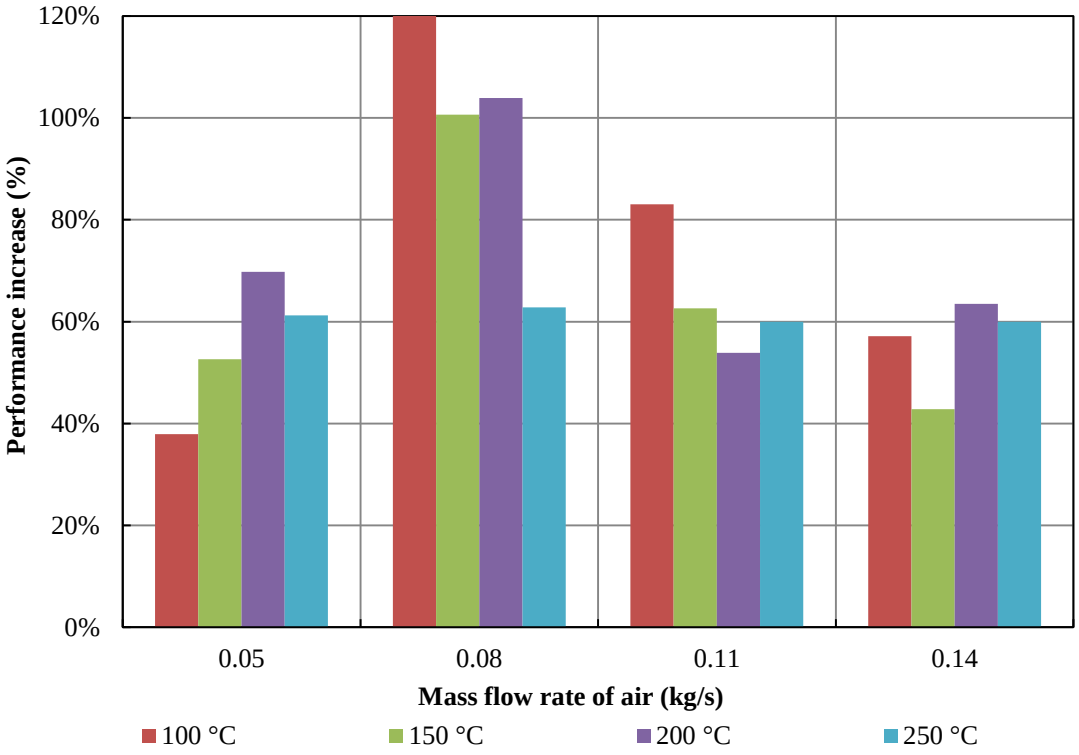

Figure 5-36 – Performance increase by adding the second pass

In average, the second pass increases the performance of the heat exchanger by 50% even though the increase in surface area on the evaporator side had been increased by 100%. One cannot forget that the second pass comes in at a lower temperature and it is basically the recycled air from the first pass. Taking into account this is still the same heat exchanger, this is a considerable increase. The greatest improvement is found at 0.08 kg/s where the heat exchanger in double pass has more than doubled the extracted heat due to the heat exchanger in single pass. This may be possible due to a measuring error at this mass flow rate.

5.5 Discussion

The work aimed at creating a semi-empirical method to predict the behaviour of a thermosyphon-equipped heat exchanger using a combination of current theoretical models. The applicability of the model was tested through various purpose-built experimental rigs. In this section the major decisions and outcomes of the work are presented and discussed.

5.5.1 Single thermosyphon

In total, three experiments were run. The first consisted of two thermosyphons equipped with a heating rope on the evaporator side and a water jacket on the condenser side. Two thermosyphons were used in order to compare the behaviour taking into account different inlet temperatures on the condenser side. Both thermosyphons were identical and were exposed to the same conditions on the evaporator side.

It was found that for the same inlet temperature, the difference in temperature across the condenser (ΔT_c) for both thermosyphons was the same, and this is independent of the order of the thermosyphons. This leads to the conclusion that the thermosyphon performance is not a function of the inlet temperature on the condenser side for low temperature ranges but rather a function of the temperature difference between the evaporator and the condenser sections.

The thermosyphon was also analysed according to the thermal network analysis. The thermal resistances for the thermosyphon were all separated and analysed for different mass flow rates. From Figure 5-8 it was found that the overall heat transfer by convection outside the thermosyphon amounted to 75% of the total thermal resistance. The greatest contributor was the evaporator air side, especially at higher mass flow rates, due to the effect of turbulence causing an increase in the heat transfer coefficient on the condenser side (3-24). The greatest contributor to the thermal resistance within the thermosyphon was the condensation of the working fluid. This value was constant throughout the experiments and amounted to 20% of the total thermal resistance. The heat transfer by conduction, boiling and the small pressure drop across the heat pipe altogether amounted to 7% which is the reason some authors choose the neglect the heat transfer by conduction. Overall the results from the prediction tool were satisfactory and fell close to the experimental results.

5.5.2 Heat exchanger equipped with six thermosyphons

The second study was conducted on a heat exchanger equipped with six thermosyphons for a range of different operating conditions currently encountered in low-grade waste heat recovery. On the condenser section, water was used and kept at constant temperature and mass flow rate, also common in waste heat recovery. Overall it was found that the increased mass flow rate had the effect of decreasing the difference in temperature across the evaporator section but increased the working temperature of the thermosyphons and thus the outlet temperature at the condenser section.

The heat recovery rate was measured at the condenser section by comparing the inlet and outlet temperature of the water. The maximum heat transfer rate was found to be at 5555 W at 300°C and 0.14 to 0.17 kg/s. The limit is found at multiple mass flow rates as the difference in temperature between the thermosyphons and the water reduces, a smaller amount of heat is extracted.

A study of the thermal resistance across the entire heat exchanger was also conducted and it was found that the overall thermal resistance for the heat exchanger at 200°C, 250°C and 300°C fell within the same trendline, which is in agreement with the data found in Figure 5-8 for the single thermosyphon experiments. This leads to the conclusion that at 150°C and lower the thermosyphon was not operating at optimal working conditions possibly due to the long thermosyphon, also reported by Hagens et al. (2007).

An uncertainty propagation study was also conducted and it was found that the difference in temperature across the condenser or evaporator was a major factor affecting this variable. Due to this fact, the experiment conducted at 50°C had a relatively high uncertainty as the difference in temperature across the condenser section was smaller than 1°C. The tests conducted at 150°C and above reported an average uncertainty below 10% which is within acceptable limits.

The average working temperature of the thermosyphons was plotted against the overall difference in temperature across the heat exchanger and a linear relation was found and turned into correlation (5-1). The correlation predicts the average working temperature of the thermosyphons for a set temperature difference across the heat exchanger but it only applies to the heat exchanger under study as the mass flow rate and temperature of the condenser section are kept constant.

The experimental results were then compared to the prediction tool and the theoretical model appeared to over predict the performance of the heat exchanger at lower inlet temperatures and under predict the performance at higher mass flow rates. This could be a result of a number of factors due to the high amount of variables included in the equations used not to mention the unique flow path within the heat exchanger, but the focus should be geared towards Figure 5-8, where the main factors responsible for the skew are identified as the convection heat transfer coefficient outside the thermosyphon and the condensation heat transfer within the thermosyphon. Other factors to take into consideration are the incomplete boiling regime found at 50°C, 100°C and to a certain extent 150°C inlet temperature which could have increased the thermal resistance of boiling thus changing the overall proportion. The under prediction may be a case of peculiar surface-fluid characteristics within the thermosyphon which suggests a creation of a new c_{sf} and n to alter equation (3-29) or even a change in Nusselt's condensation theory which assumes a plain wall and does not take into account the inner circumference of the thermosyphon.

5.5.3 Heat exchanger equipped with six thermosyphons in double pass

The third test consisted of an additional pass being added to the heat exchanger. The major differences are the result of the increased evaporator area, resulting in a higher overall effectiveness and a higher average working temperature of the thermosyphons.

The average working temperature of the thermosyphons was also found to be directly related to the overall difference in temperature across the heat exchanger and incoming mass flow rate thus correlation (5-2) was created. Once again, this expression is only applicable to the heat exchanger under study as the mass flow rate and temperature of the condenser side were kept constant

Comparing with the single pass, it was found that the double pass increase the performance of the heat exchanger by an average of 50%, the greatest increase found at 0.08 kg/s especially at lowest temperatures as can be seen in Figure 5-36. It was also found that the second pass had little to no effect on the performance of the first pass, as can be seen in Figure 5-35, a behaviour only possible due to the isothermal nature of the thermosyphon.

Chapter 6

CFD study, Results and Discussions

A 3 dimensional computational model was run in parallel with the experimental tests conducted on the heat exchanger. In this simplified model the thermosyphons were modelled as super-conductors whose thermal conductivity had been deduced according to the inlet conditions using the theoretical method explained in section 3.3.1. In this section, the set-up procedure of the CFD simulation is explained and the outcome compared with the experimental and theoretical data.

6.1 Assumptions

a) Constant mass flow rate across the heat exchanger in both flow sides
b) Neglectable axial heat transfer from conduction across the thermosyphon wall
c) No heat transfer across the walls of heat exchanger
d) No heat transfer at the adiabatic section of the thermosyphon
e) Constant inlet mass flow rate across inlet area
f) Same thermal conductivity for all the thermosyphons
g) The thermosyphons are assumed to be solid superconductors

6.2 Methodology

ANSYS Fluent was the computational fluid dynamics (CFD) software used to simulate the heat flow within the heat exchanger. A 3 dimensional model was built as the requirement was to investigate the complete flow path and temperature distribution of the flows within the heat exchanger. The realisable k-epsilon turbulence model (k-ε) was used in each of the simulations as it is found to be more accurate at higher Reynolds number and smaller pressure gradients (ANSYS, 2012-2014; Ekambara, et al., 2008), which is the case in the experimental test range. A coupled pressure-based solver is also recommended as it was found to be more efficient in steady-state simulations and offered better results for single-phase fluid flow.

The thermosyphons were modelled as solid objects using the value for thermal conductivity achieved from the method described in section 3.3.1. For the fluid properties, Fluent's own standard tables of substance properties were used to determine the characteristics of the fluids simulated (water in the condenser and air in the evaporator).

6.2.1 Mesh selection

The mesh was selected after running the simulations with different mesh sizes and comparing the accuracy of the results and the time taken to achieve those results. A mesh was deemed "good" if the maximum skewness was lower than 0.7 for hexahedron and tetrahedrons and 0.8 for triangular elements (ANSYS, 2012-2014).

The finest mesh setting was found to take 3 times longer to converge (on average) and the results would not be significantly more accurate (±0.8%); the small difference in the results seen in Table 6-1 also led to the conclusion that the results were grid size independent. Taking into account all of the above, a medium mesh was used for the simulations with Fluent.

Table 6-1 – Mesh Dependency

Level	No of Cells	Type of cells	Skewness	Time per iter.
Coarse	1,408,658	Hex + Tetra	avg: 26%, stdev: 16%	2-10 s
Medium	2,291,364	Hex + Tetra	avg: 21%, stdev: 13%	7-15 s
Fine	3,099,230	Hex + Tetra	avg: 21%, stdev: 13%	25-50 s

Skewness refers to the relative inclination of the elements with respect to each other.

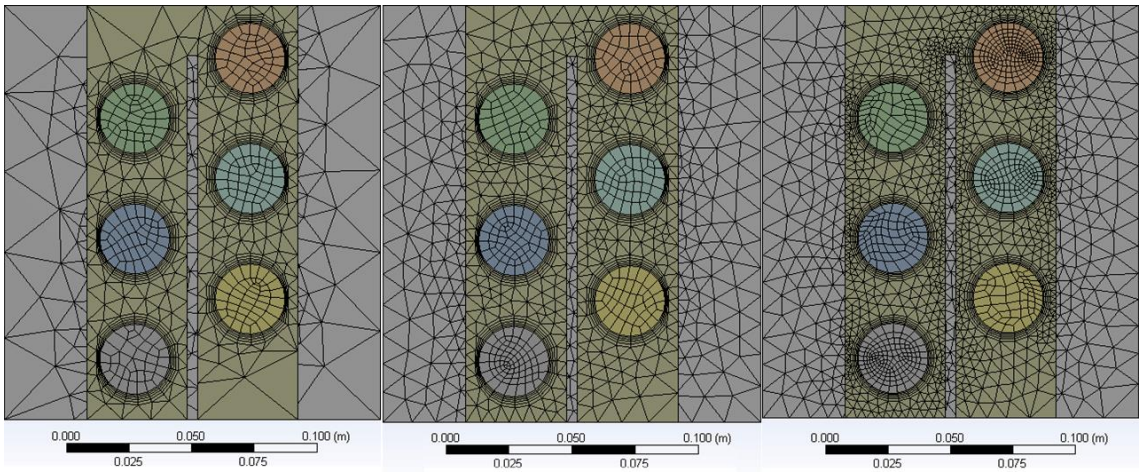

Figure 6-1 – *Comparison between the three different meshes – Coarse, Medium and Fine*

The relaxation factors were set at 1e-6 and the test allowed to run until no change was observed in the scaled residuals.

6.2.2 Boundary Conditions

As can be seen in Table 5-1, the boundary conditions used to simulate the inlets and outlets were of type "mass flow inlet", with the outlets having the opposite direction. This assumption holds remarkably well for both circuits: the air circuit consisted of a closed circuit, so it was in fact being pulled out of the evaporator outlet. The condenser had been completely purged of air prior to starting any test and at normal atmospheric conditions water is incompressible, thus justifying the assumption that the mass flow rate at the exit of the condenser must be the same as the water flowing into the condenser. All the other walls of the heat exchanger were insulated during the experimental test and were thus assumed to be adiabatic in the simulation.

Table 6-2 – Boundary Conditions in the CFD simulation

	Type	**Mass flow rate (kg/s)**	**Temperature (ºC)**
Evaporator Inlet	Mass Flow Inlet	0.05 to 0.17 at 0.03 intervals	50 to 300 at 50 intervals
Evaporator Outlet	Mass Flow Inlet	-	-
Condenser Inlet	Mass Flow Inlet	Constant 0.0715	Constant 10.0 ± 0.3
Condenser Outlet	Mass Flow Inlet	-	-

6.3 CFD Results

A plot of the scaled residuals is shown in Figure 6-2. As can be seen, stability was reached at an average of 800 iterations for each test since the scaled residuals would not reach the relaxation factors of 1e-6. At this point, the total heat flux in the evaporator and the condenser was recorded as well as the outlet temperatures.

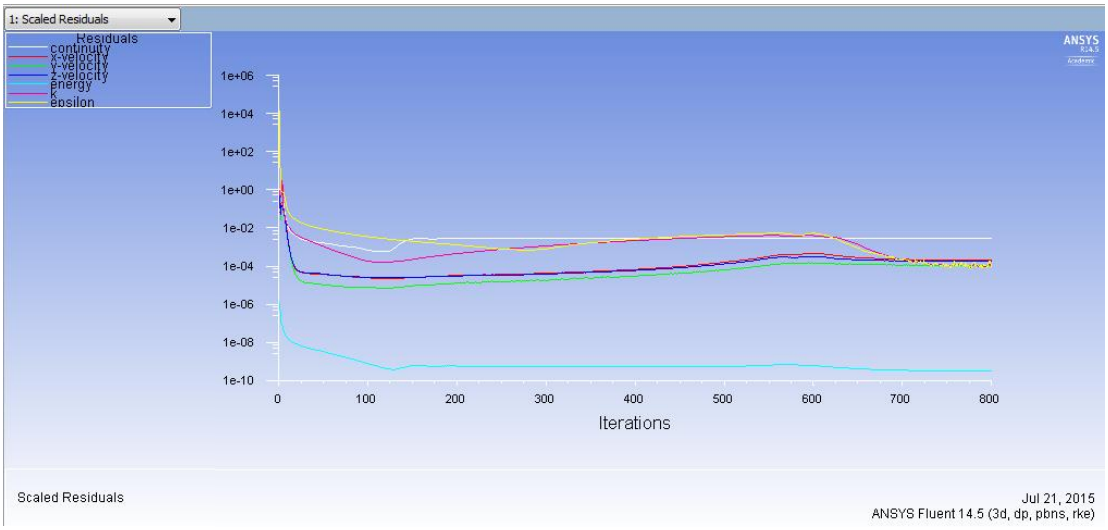

Figure 6-2 – Plot of scaled residuals taken from the simulating software

6.3.1 Heat transfer rate – Single pass

The overall CFD results displayed a similar profile to the experimental results but a steadier progression was observed, as can be seen in Figure 6-3 as each temperature is clearly separated from the next.

The results reflect simulations in which turbulence is always assumed to take place, the thermal resistance of the thermosyphon is constant throughout the test and the adiabatic section of the thermosyphons is completely isolated thus removing any possibility of heat loss – in the experimental test the heat exchanger is also assumed to be isolated, but it is impossible to completely isolate it without a layer of vacuum in between the thermosyphons and the outside.

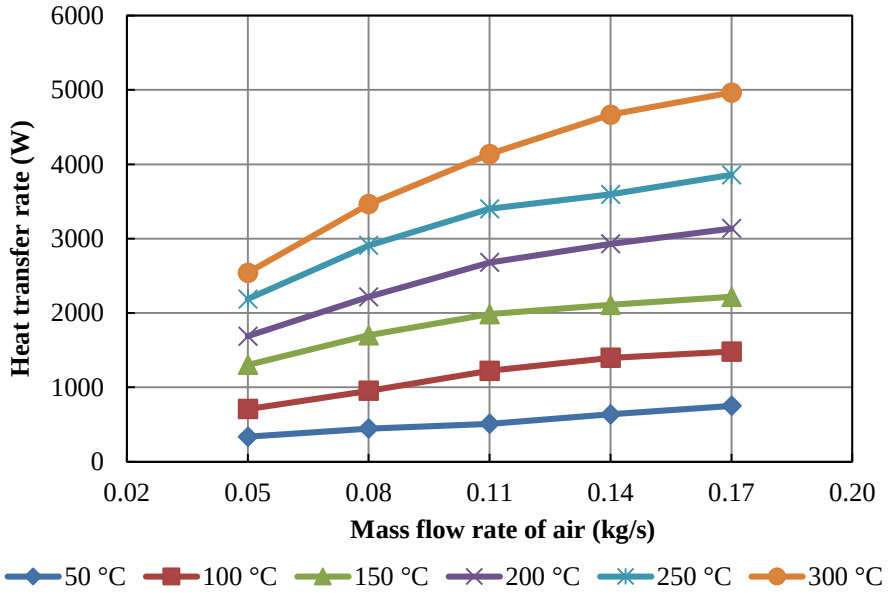

Figure 6-3 – Heat extraction rate in the CFD simulation according to different inlet conditions

Table 6-3 presents the results from the CFD in detail, including the percentage of heat unaccounted for, the difference between the heat transfer rate across the evaporator and the heat transfer rate across the condenser section. This small percentage difference is the source of the error seen in Figure 6-6 and Figure 6-7 where low inlet mass flow rate and temperature conditions result in overestimation by the CFD, simply a result of the percentage of heat missing from the simulation as there is a great percentage of it at lower tests, as seen in Table 6-3. This percentage of heat missing would not fade even through the increase in the number of iterations.

Looking back at Figure 5-8 where the breakdown of the thermal resistance in a thermosyphon was made, the greatest responsible for the heat transfer rate is the convection outside the thermosyphon, which in this case is predicted by Fluent. The overestimation is a result of the k-epsilon turbulence model used in the simulation as the model assumes a fully turbulent flow which may not be the case at lower mass flow rates.

Table 6-3 – Detailed results from the CFD simulation

T (°C)	ṁ (kg/s)	ΔQ (W)	Q_e (W)	Q_c (W)	% Q unaccounted
50	0.05	102	-194	296	41.8%
50	0.08	93	-267	360	29.6%
50	0.11	83	-323	406	22.9%
50	0.14	65	-437	502	13.9%
50	0.17	53	-527	580	9.6%
100	0.05	95	-652	747	13.5%
100	0.08	61	-945	1006	6.3%
100	0.11	-17	-1227	1210	-1.4%
100	0.14	-61	-1429	1368	-4.4%
100	0.17	-67	-1515	1448	-4.5%
150	0.05	-19	-1201	1183	-1.6%
150	0.08	-30	-1620	1590	-1.9%
150	0.11	-167	-1940	1773	-9.0%
150	0.14	-187	-2124	1937	-9.2%
150	0.17	-199	-2250	2051	-9.3%
200	0.05	-57	-1577	1521	-3.7%
200	0.08	-186	-2215	2029	-8.7%
200	0.11	-266	-2681	2415	-10.4%
200	0.14	-319	-2881	2562	-11.7%
200	0.17	-338	-3068	2730	-11.7%
250	0.05	-83	-2011	1928	-4.2%
250	0.08	-196	-2268	2072	-9.0%
250	0.11	-149	-3432	3283	-4.4%
250	0.14	-451	-3748	3298	-12.8%
250	0.17	-469	-3923	3454	-12.7%
300	0.05	-124	-2447	2323	-5.2%
300	0.08	-252	-3405	3154	-7.7%
300	0.11	-469	-4039	3571	-12.3%
300	0.14	-595	-4567	3972	-13.9%
300	0.17	-641	-4978	4337	-13.8%

6.3.2 Comparison between CFD and exp results for single pass

Figure 6-4 presents the percentage difference between the experimental and CFD results and it was found that the difference was below 15% on both the evaporator and condenser sections, and within the instrumentation uncertainty for the experimental test.

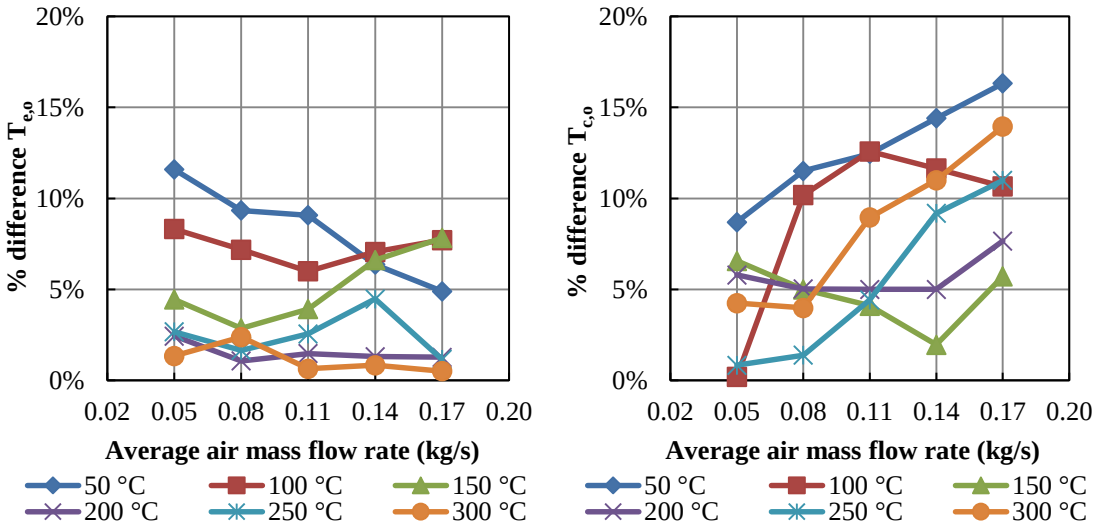

Figure 6-4 – Percentage difference in the outlet temperature of the evaporator (left) and the condenser (right) between the experimental test and the CFD simulation

The outlet temperatures for each section were also compared and are displayed in Figure 6-5 and Figure 6-6. A good agreement was also found between the experimental results and the simulation as the results tend to connect in the middle of the graph.

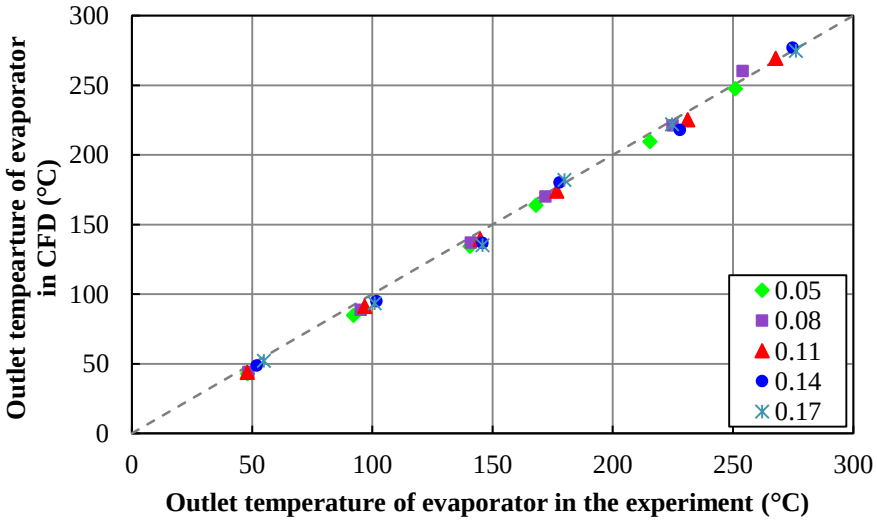

Figure 6-5 – Comparison between experimental and CFD results for the temperature at the outlet of the evaporator for different mass flow rates

Figure 6-6 displays the difference in temperature on the condenser side.

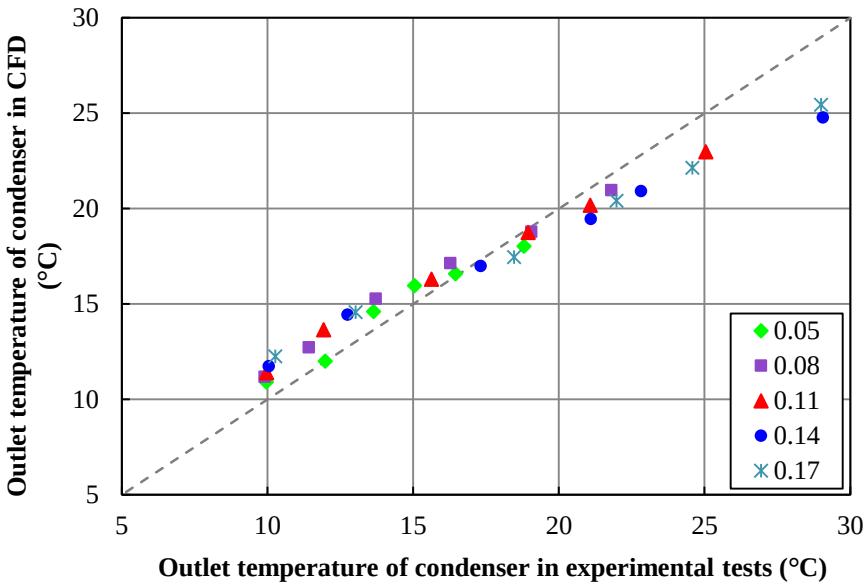

Figure 6-6 – Comparison between experimental and CFD results for the temperature at the outlet of the condenser for different mass flow rates

It is clear on the plot shown in Figure 6-6 that the CFD simulation overestimates the outlet temperature at lower mass flow rates, shown by the results skewing towards the left side of the graph and underestimates at higher mass flow rates as shown by the results tending towards the right side of the line at higher outlet temperatures.

Figure 6-7 includes a direct comparison of the overall heat transfer rate between experimental tests and CFD simulation.

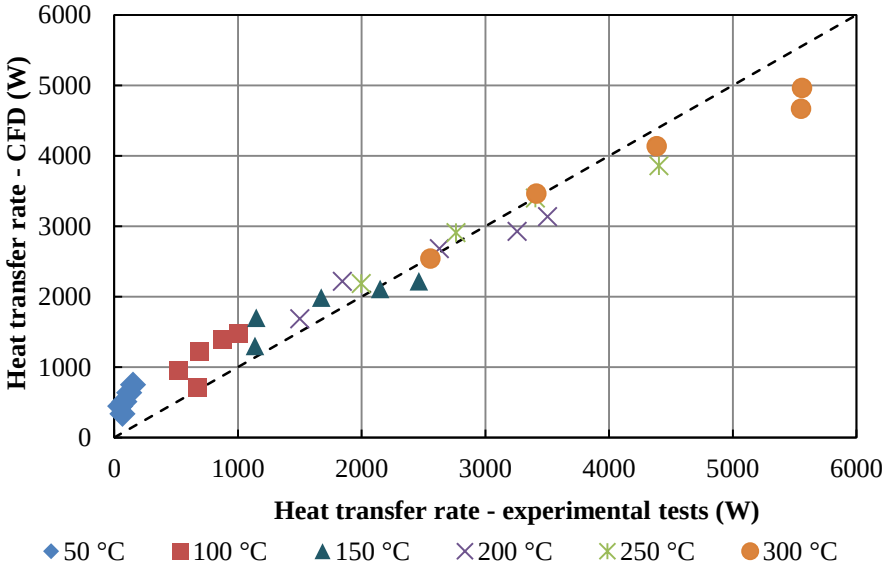

Figure 6-7 – Comparison of the Q_{out} between the experimental test and the CFD model.

Both the experimental and the CFD heat transfer rate found in Figure 6-7 are the average between the heat transfer rate found in the evaporator section and condenser section. All the results are included within a 10% envelope showing good correlation between experimental and simulated data. The CFD results display the same trend as the temperatures in Figure 6-6.

6.3.3 Comparison between CFD and exp results for double pass

Figure 6-8 depicts a direct comparison between the outlet temperature in the experimental rig in double pass and the corresponding CFD simulation. It is observed that the CFD simulation is in good agreement with the experimental results.

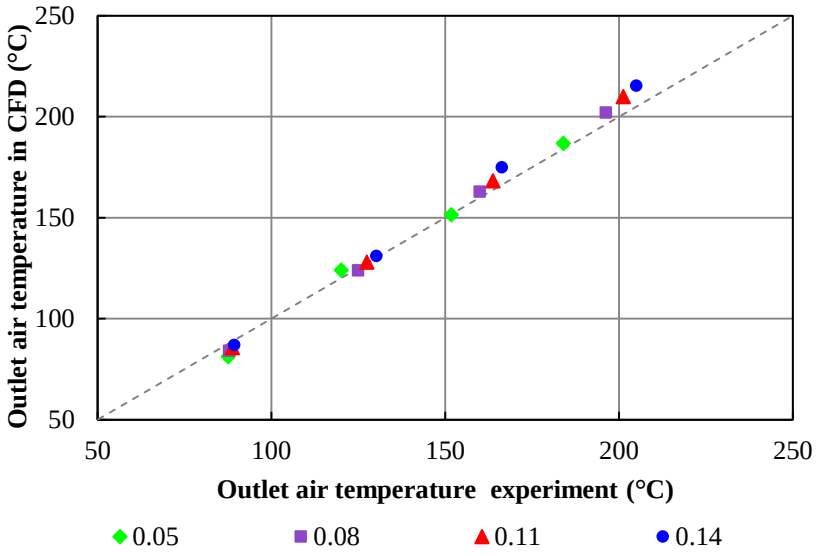

Figure 6-8 – Comparison between the temperatures at the evaporator outlet

Figure 6-9 plots the outlet temperature in the condenser section for the CFD simulation and the experimental results and the same over prediction at lower inlet conditions and under prediction at higher mass flow rates is identified.

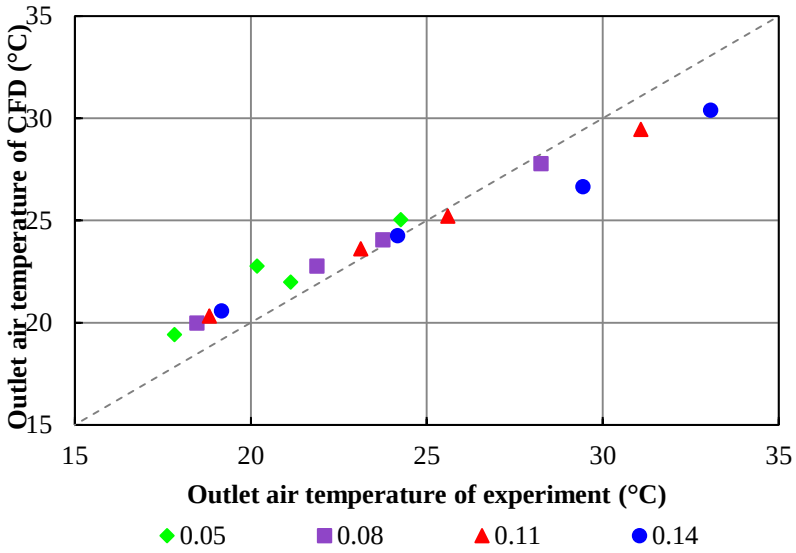

Figure 6-9 – Comparison between the temperatures at the condenser outlet

A more direct comparison between the experimental and CFD simulation results is presented in Figure 6-10 and Figure 6-11 and all the predictions fall into a 5% envelope for the evaporator section and a 10% envelope for the condenser section. This is a sign that good agreement is found between the CFD results and the experimental results, Taking into account the thermal conductivity of the thermosyphons was extracted from an analytical study, a good agreement is found between all of the data presented.

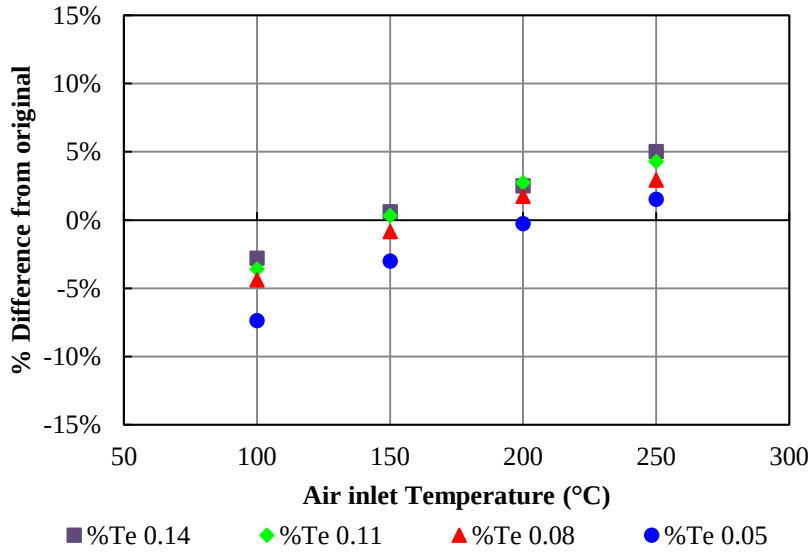

Figure 6-10 – Percentage difference between the CFD and the experimental results for the temperature at the outlet of the evaporator

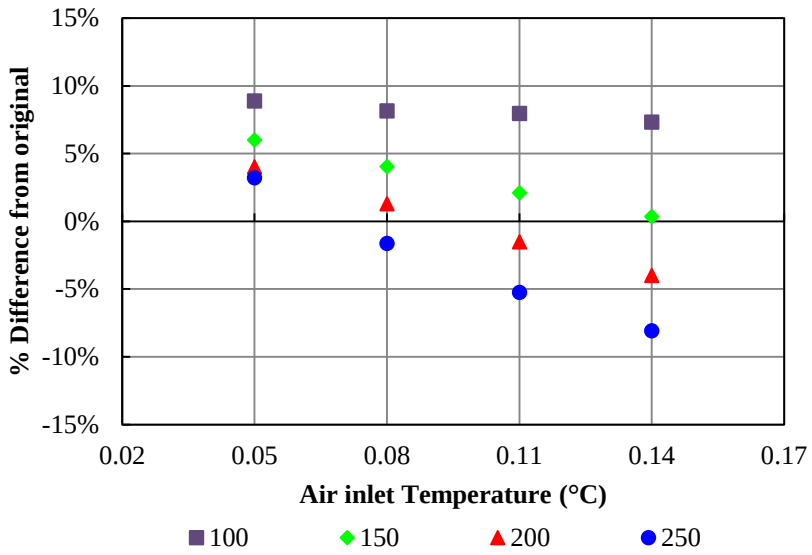

Figure 6-11 – Percentage difference between the CFD and the experimental results for the temperature at the outlet of the condenser

Figure 6-12 represents a direct comparison between the total heat transfer rate obtained for the experimental rig in double pass during testing and the corresponding total heat transfer rate predicted by both the CFD simulation and equations found in literature for the same inlet conditions. The CFD simulation shows the same trend as the experimental results but the simulation seems to over-predict at lower inlet conditions and the results seem to be closer to the experimental ones at medium to high mass flow rate.

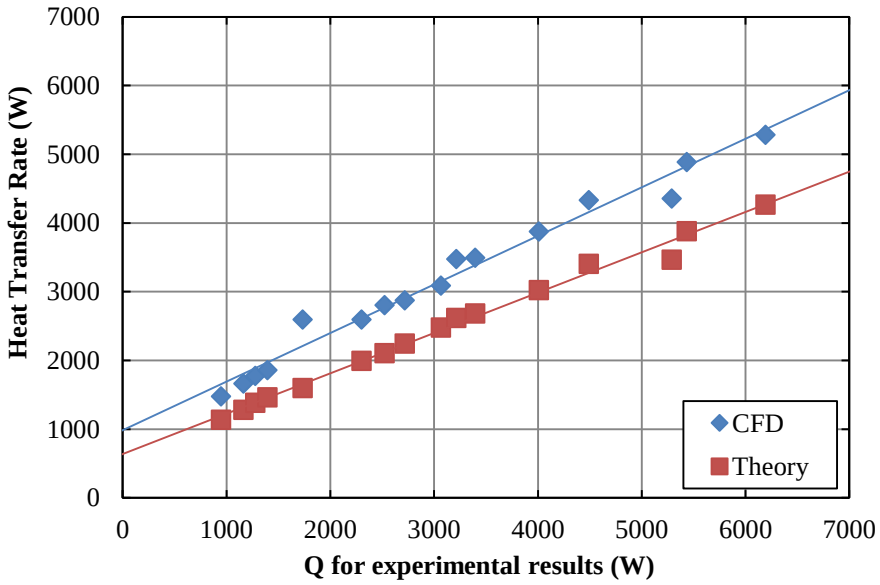

Figure 6-12 – Comparison between the overall heat transfer rate determined by the CFD and the theory

The prediction provided by the empirical correlations was very conservative, as shown by the trend line formed by the red squares; it under-estimates the performance of the heat exchanger at all times. This may be a result of the equations used for convection from the flow to the pipe, as the same inner resistance for the pipes was used for both the CFD and the literature.

6.3.4 CFD vector Plots

One of the greatest advantages of CFD is the visualisation of the flow profile within complex geometries as either vector or area plots which make it very useful for flow pattern investigation. The flow profile within the evaporator section is presented in Figure 6-13 and the fluid particles are represented by vectors located at the intersection of each cell. As assumed, the mass flow rate is constant across the entire inlet and the recirculation zones seem to be on the top and bottom of the evaporator section, particularly before the tube bundle. The areas with higher velocity are found to be between the pipe bundle, where the air particles need to squeeze themselves together in order to pass through.

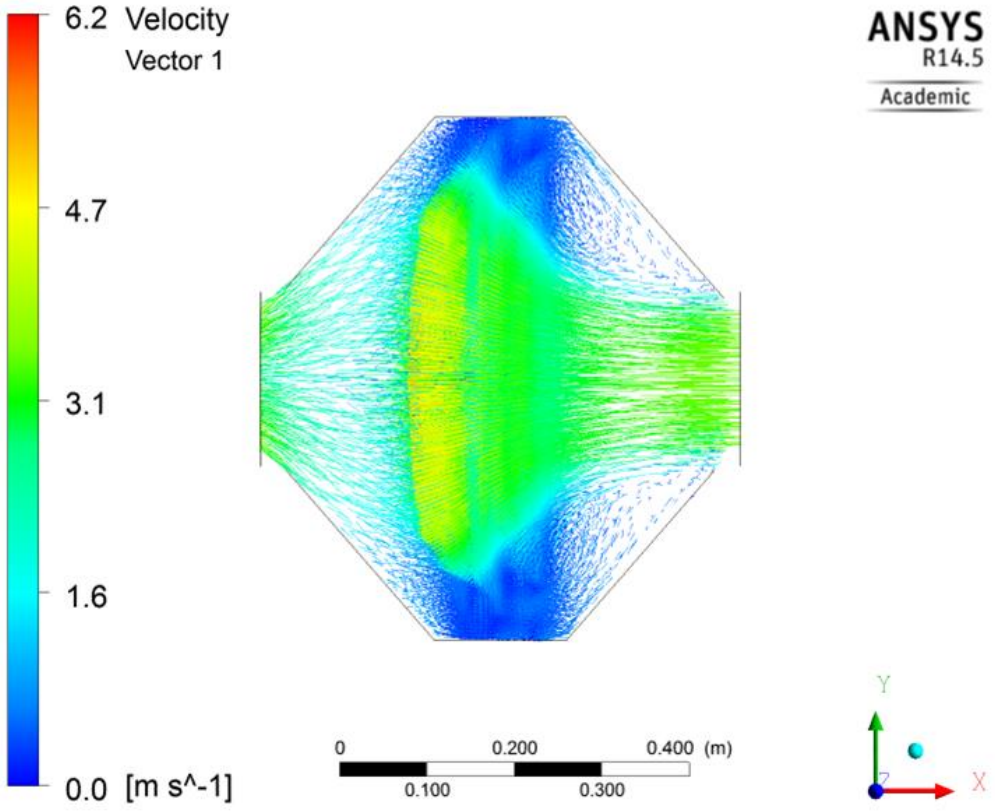

Figure 6-13 – Vector velocity plot in the evaporator section

The vector velocity profile was found to have the same shape but different values as the mass flow rate was reduced across the evaporator section.

Figure 6-14 presents the average velocity profile within the condenser section. The inlet temperature and mass flow rate were kept constant in the condenser section allowing Figure 6-14 to represent the condenser section for all of the conditions tested. The white circles represent the thermosyphons – simulated as solid devices and therefore with no flow movement within. The blue areas represent re-circulation zones, common in between the thermosyphons in parallel arrangements. The higher velocities were found in the vicinity of the thermosyphons particularly on the sides.

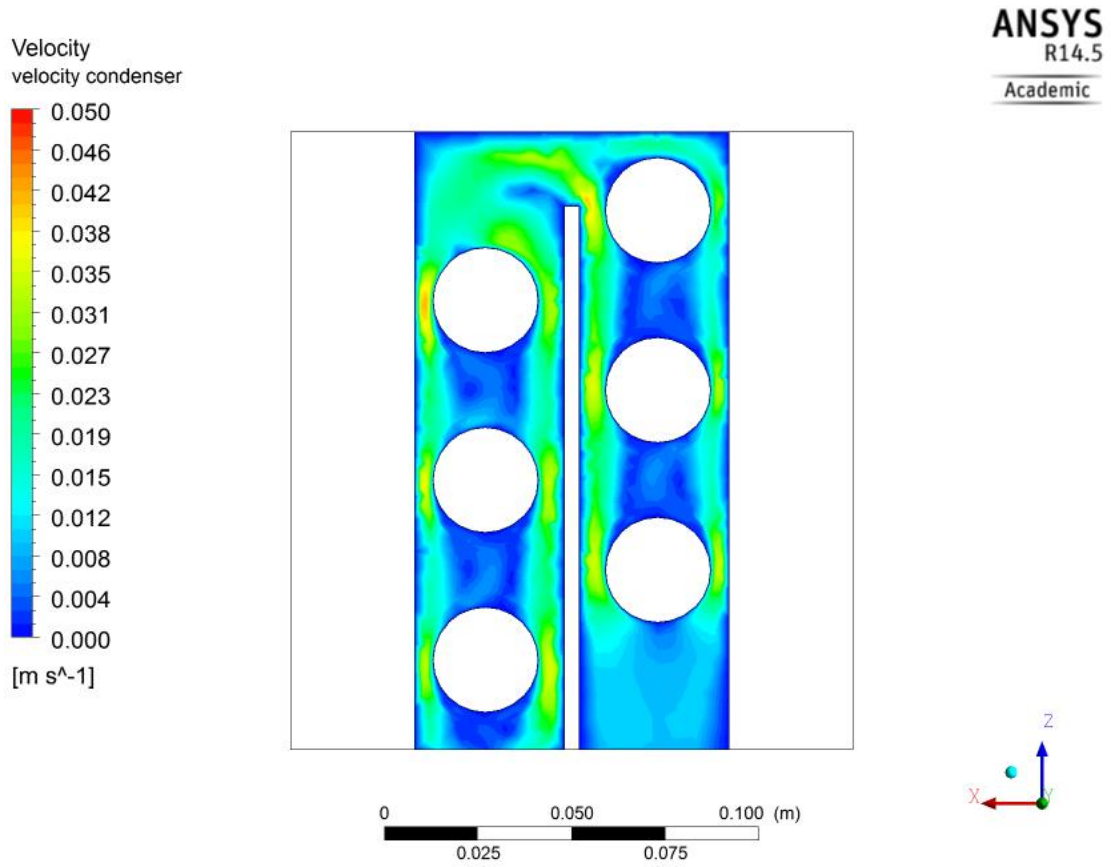

Figure 6-14 – Velocity profile within the condenser section of the heat exchanger

Just after the 180° bend, where the baffle is located, a large green area is identified in the path of the flow. This is assumed to be a result of a somehow normalised flow pattern resulting from the baffle geometry in combination with the flow which circles the last tube in the first sweep.

Figure 6-15 presents a selection of the average velocity flow rate on the evaporator section for different inlet temperatures and it is concluded that the temperature of the flow has no effect on the flow pattern in the CFD simulation of air using the k-epsilon turbulence model. Lower flow velocities are always found after the tubes and higher velocities in between them. The complete list of the velocity profiles is available in Appendix B – CFD results.

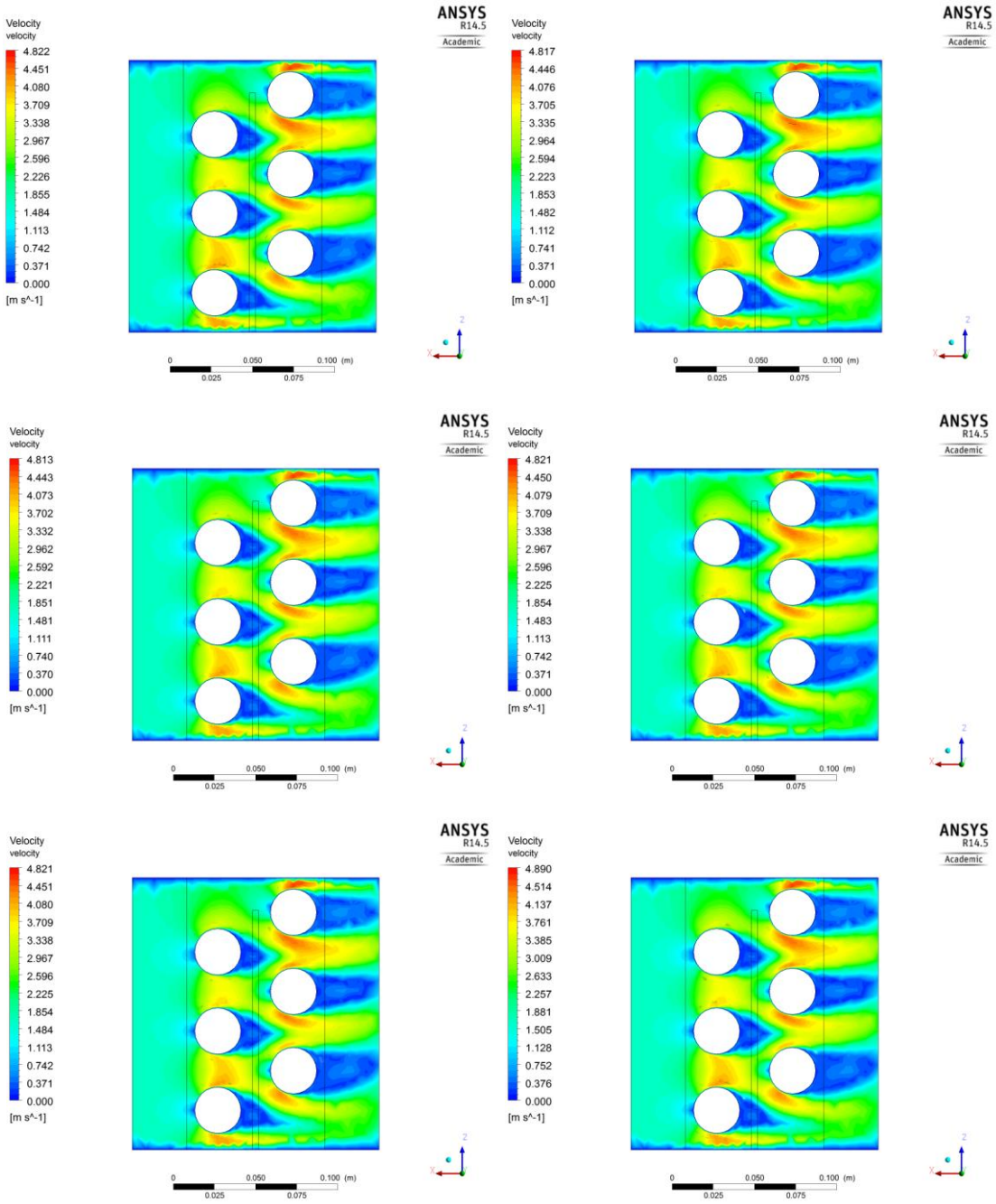

Figure 6-15 – Velocity profile in the evaporator section for different inlet temperatures

Figure 6-16 presents the velocity plot in the evaporator section for 300°C inlet temperature and different inlet mass flow rates. The profile does not suffer any major changes with the increasing mass flow rate but the scale changes as would be expected.

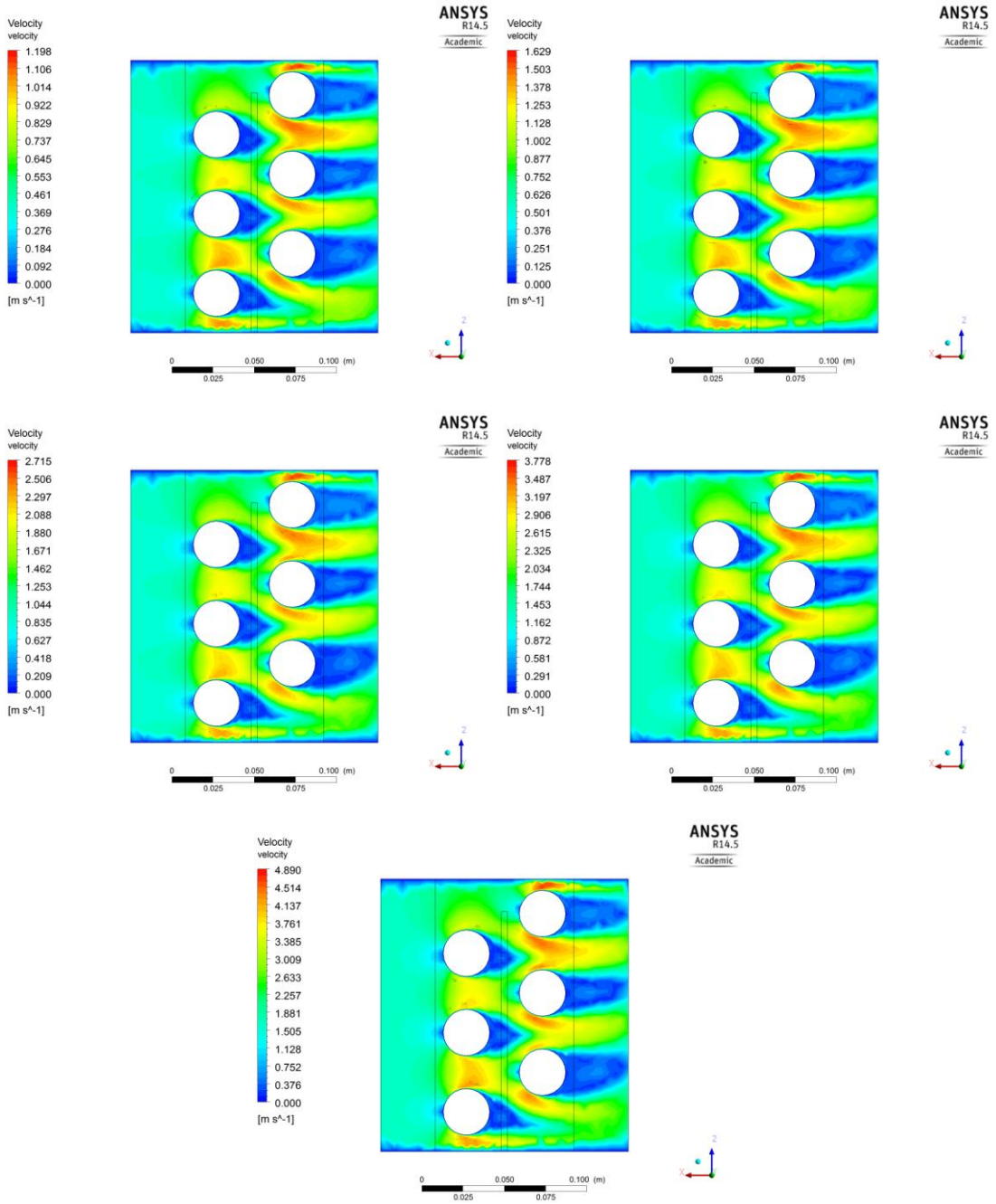

Figure 6-16 – Velocity profile within the evaporator section at 300°C for 0.05 kg/s, 0.08 kg/s, 0.11 kg/s, 0.14 kg/s and 0.17 kg/s

The average temperature profile of the evaporator is presented in Figure 6-17 for a mass flow rate of 0.17 kg/s and varying temperatures ranging from 50°C to 300°C. The blue circles represent the thermosyphons which are at a much lower temperature than the

fluid medium. Once again, the profiles are identical, the only changing parameter is the scale. By comparing with Figure 6-16, it is concluded that for this particular geometry the zones with lower velocities coincide with the zones with lower temperature.

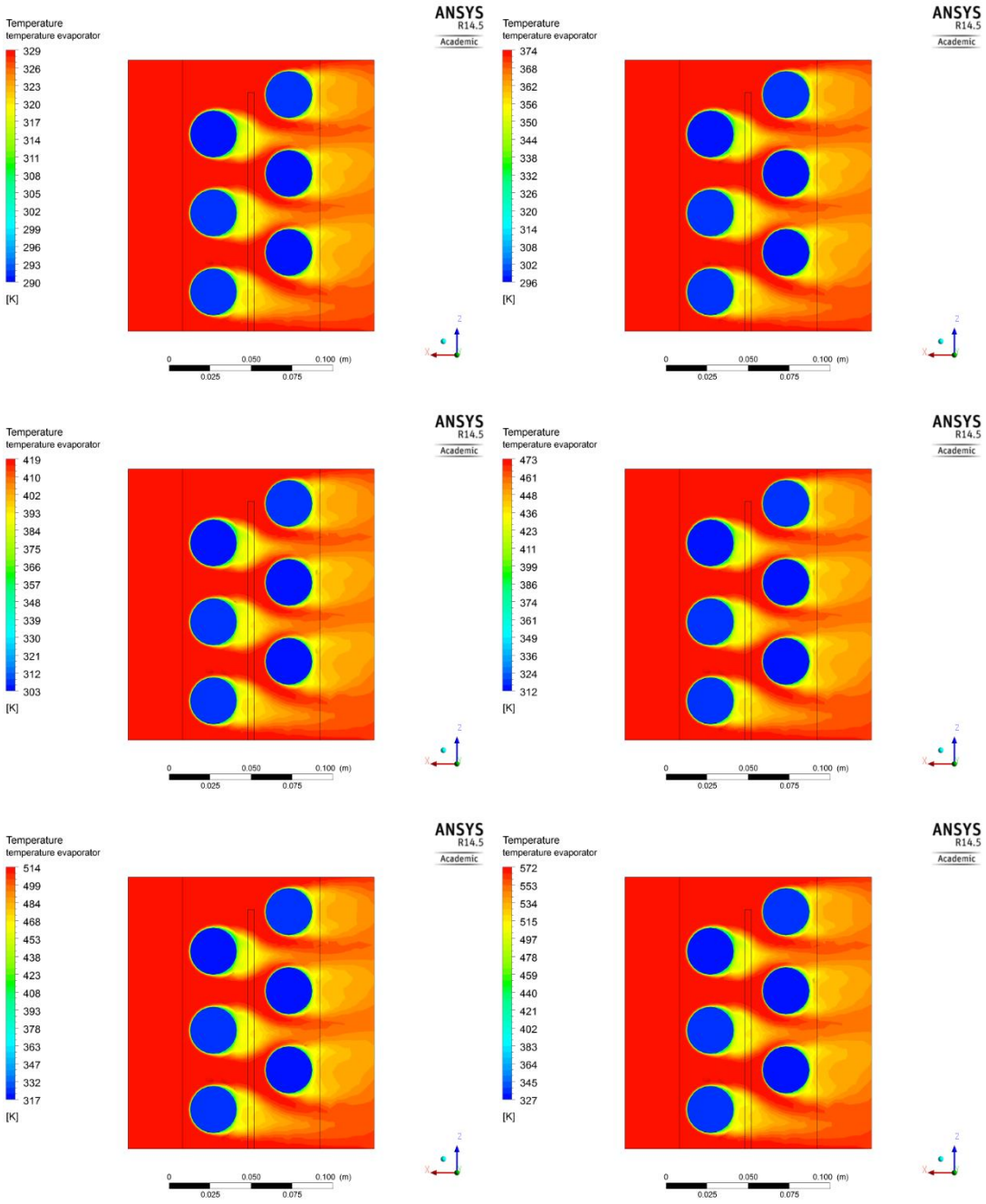

Figure 6-17 – Temperature profile in the evaporator section at 0.17 kg/s for different inlet temperatures

Figure 6-18 presents the different temperature plots for 300°C inlet temperature at different mass flow rates and a difference is clearly visible when comparing to previous plots; the lower mass flow rates leave a longer trail of lower temperature.

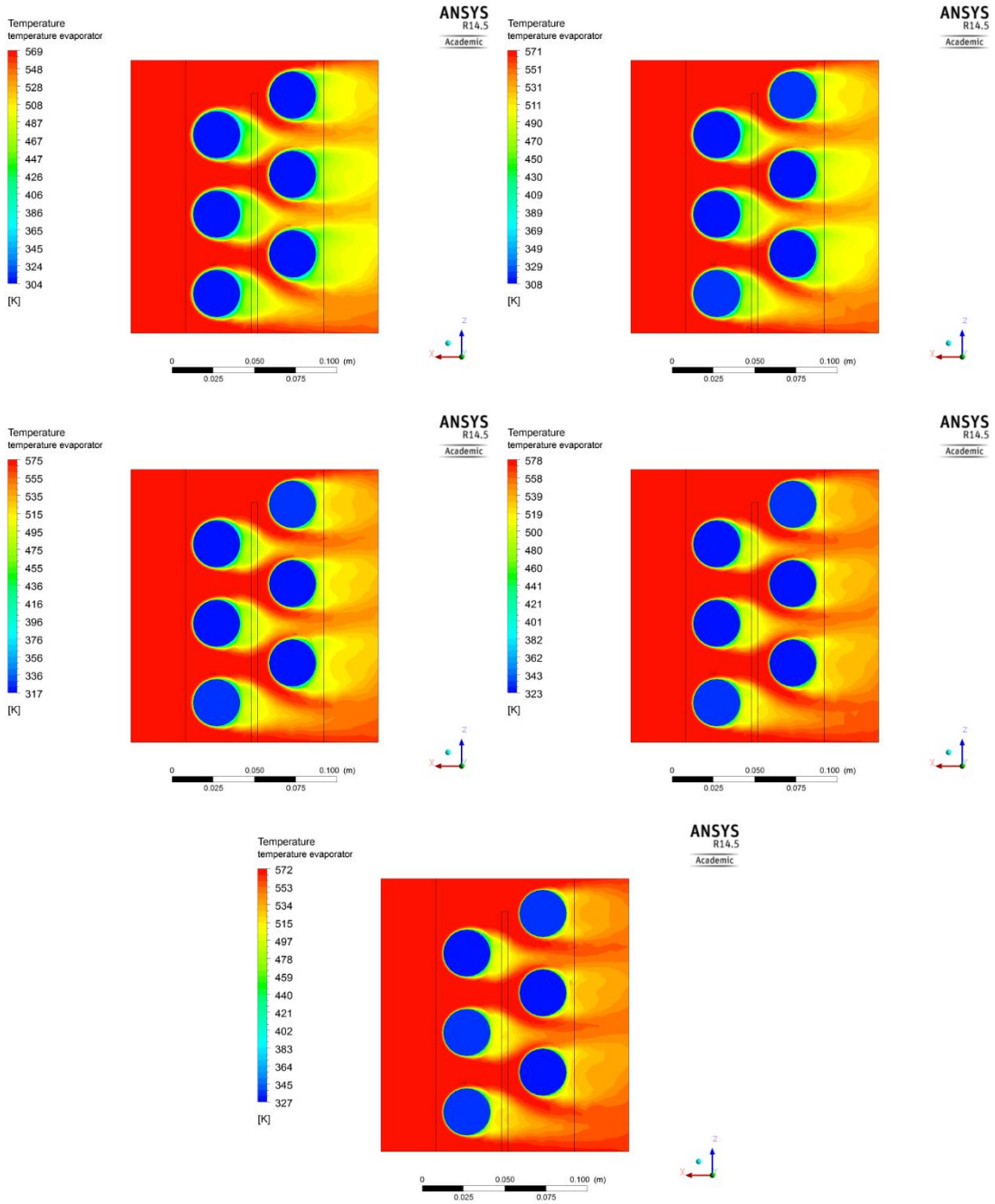

Figure 6-18 – Temperature profile in the evaporator section at 300° for the different inlet temperatures

A detailed contour of the temperature is shown in Figure 6-19 for the test run at 300°C and 0.08 kg/s inlet conditions on the evaporator side. The variation of the temperature

on the hot flow is particularly noticeable in this figure. The temperature of the thermosyphons at that particular height is also shown in its respective location.

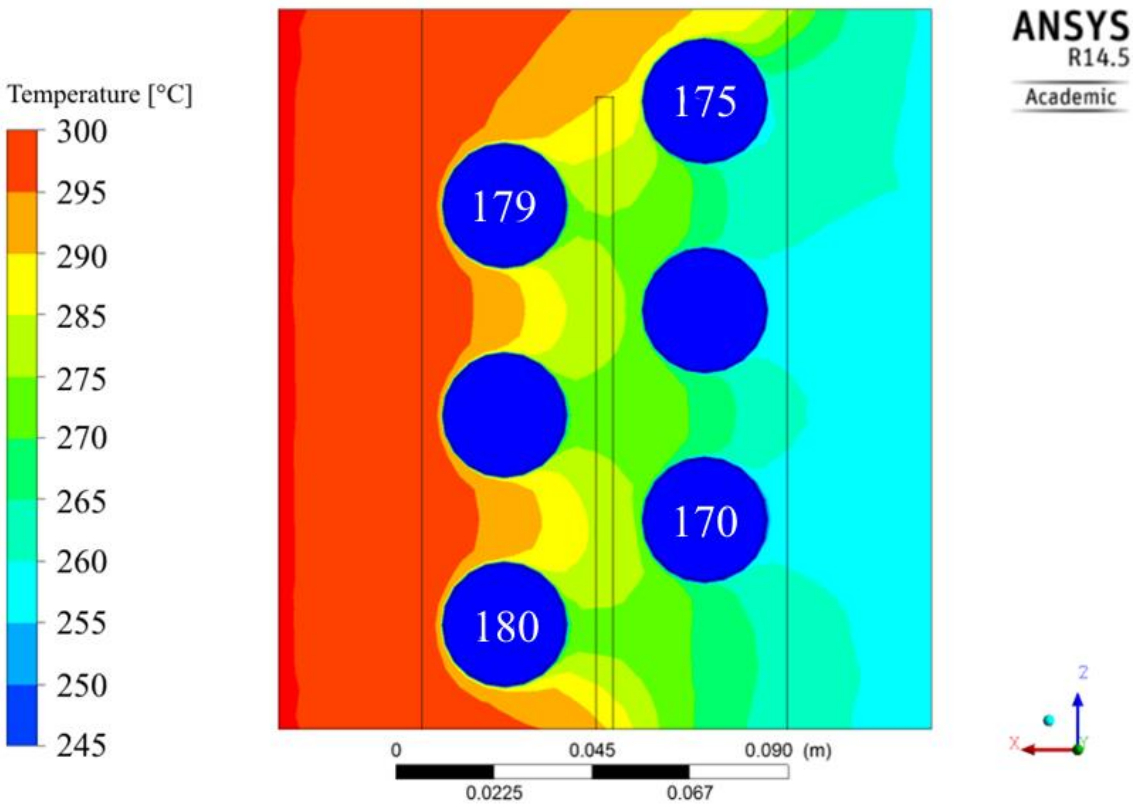

Figure 6-19 – Average temperature contour of the air in the evaporator section at 300 °C and 0.08 kg/s

The internal temperature of the thermosyphons follows the logical progression in which the closer the thermosyphon is to the evaporator inlet and the condenser outlet, the warmer the overall temperature.

The temperature profile of the condenser section is available in Figure 6-20. The average temperature of the thermosyphons in this section is highly influenced by the flow path; numbering thermosyphons from #1 to #6 following the flow path in the condenser section, thermosyphons #2 and #3 are actually at a higher temperature than thermosyphon #4; this is in great part due to the parallel geometry that does now allow proper mixing of the streams and slightly reduces the potential heat transfer rate.

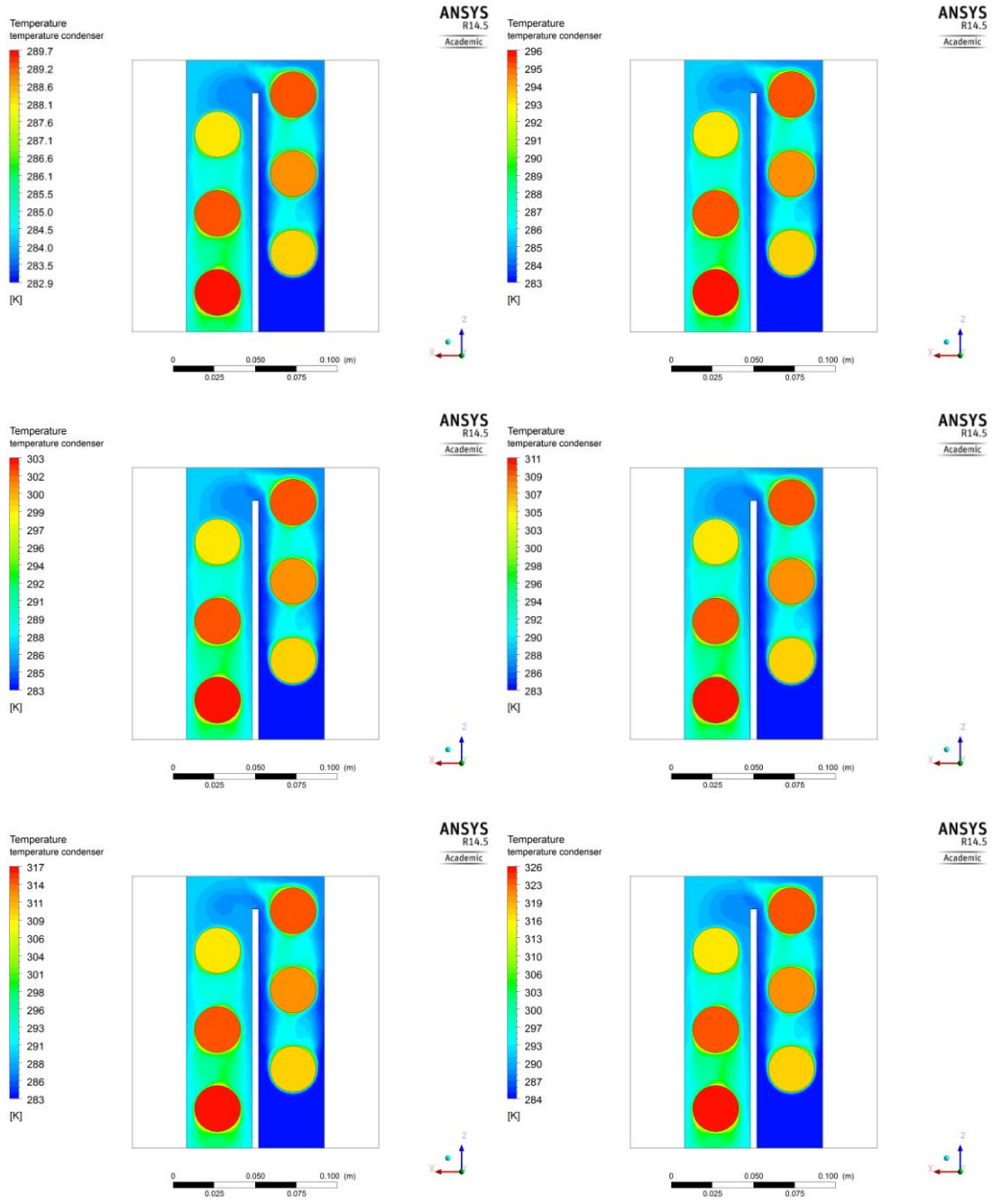

Figure 6-20 – Temperature profile in the condenser section for the same evaporator inlet conditions as Figure 6-17

Figure 6-21 presents a detailed temperature profile with emphasis on the temperatures of the thermosyphons, shown in white digits on the thermosyphons they are measuring. The variation in temperature in the thermosyphons from the evaporator section in Figure 6-19 to the condenser section is clear.

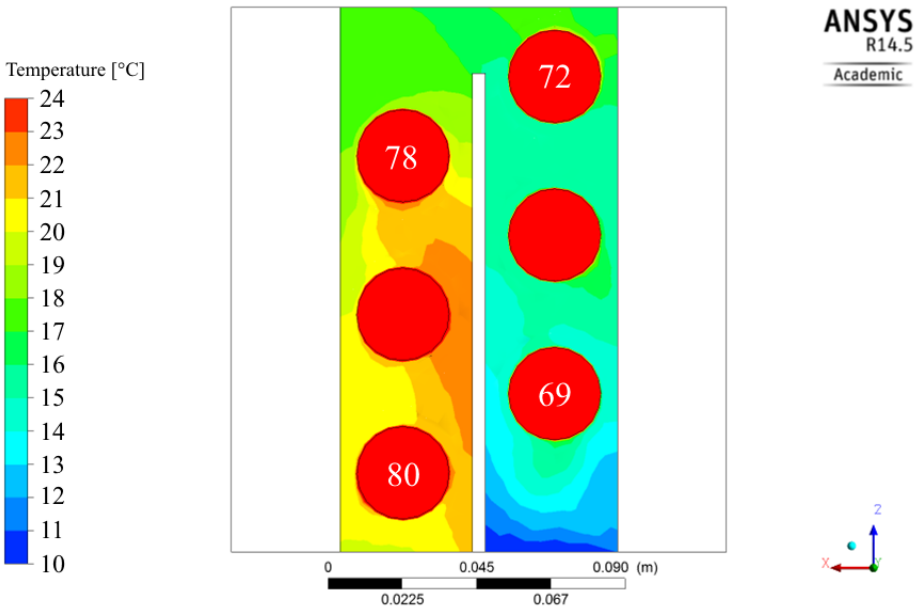

Figure 6-21 – Detailed temperature contour of the water in the condenser for the evaporator conditions of 300 °C and 0.08 kg/s

In a real thermosyphon, the temperature of the working fluid would have a difference of 1-5°C. However, since the thermosyphon has been modelled as a solid superconductor, there will always be a temperature gradient across its length if each end is immersed in a fluid at drastically different temperatures.

6.4 Discussion – CFD simulation

A Computational Fluid Dynamics (CFD) model was created to investigate the flow pattern within the heat exchanger and to apply the use of the thermal conductivity predicted in using the method described in section 3.3.1 in which the thermosyphon is assumed to be a solid tube of constant conductivity, or effectively a superconductor. The results, displayed the same trend identified in the theoretical and experimental results which confirms that this approach could be used in the future to estimate the performance of a heat exchanger equipped with a larger number of thermosyphons.

Chapter 7

Conclusions and Recommendations

In this section the conclusions for the work are presented as well as recommendations for future work. The creation of a prediction model for the characterisation of a heat exchanger equipped with thermosyphons has been developed and tested.

In order to reach the aim of achieving this characterisation, the concept was subdivided into four objectives, as described in Section 1.1, namely:

- To develop a working knowledge of the heat transfer processes inside the tubular thermosyphon, with an emphasis on boiling and condensation heat transfer.
- To create a prediction tool based on empirical formulae that will allow the prediction of the outlet conditions of thermosyphon-equipped heat exchangers.
- To create a CFD model for the performance prediction of a thermosyphon-equipped heat exchanger. The model's boundary conditions are extracted from the prediction tool. The model will help the design of thermosyphon-equipped heat exchangers.
- To validate the theoretical results from the prediction tool and the results from the CFD simulation against experimental results obtained from a purpose-built experimental rig.

7.1 Conclusions

Objective 1:

- **To develop a working knowledge of the heat transfer processes inside the tubular thermosyphon, with an emphasis on boiling and condensation heat transfer**

There are two heat transfer processes contained in the tubular thermosyphon – boiling and condensation. Boiling is separated into different boiling regimes depending on the difference in temperature between the wall of the pipe and the working fluid. The thermosyphons are engineered to work at the nucleate boiling regime, where the greatest heat flux is found. The equation used to describe the heat transfer from boiling takes into account the surface to liquid combination in the form of two variables. The heat transfer from condensation is characterised through an expression describing condensation on a flat plate.

Objective 2:

- **To create a prediction tool based on empirical formulae that will allow the prediction of the outlet conditions of thermosyphon-equipped heat exchangers.**

A prediction tool was created based on the thermal network analysis. The different thermal resistances were deduced from expressions found in the surveyed literature. It was predicted that the greatest contributors to the overall thermal resistance of the heat exchanger would be the convective heat transfer coefficient on the shell-side of the heat exchanger.

Objective 3:

- **To create a CFD model for the performance prediction of a thermosyphon-equipped heat exchanger. The model's boundary conditions are extracted from the prediction tool. The model will help the design of thermosyphon-equipped heat exchangers.**

The thermosyphons were assumed to be super conductors and as such, through the prediction tool, were given a thermal conductivity based on their working conditions. The thermal conductivity was used as a boundary condition in the CFD simulation. The results were satisfactory as it was found that the results from the CFD simulation mirrored those from the theoretical analysis, showing that the approach of modelling the thermosyphon as a super conductor is feasible.

Objective 4:

- **To validate the theoretical results from the prediction tool and the results from the CFD simulation against experimental results obtained from a purpose-built experimental rig.**

In order to verify the correctness of the application, the prediction tool and the CFD results were compared to experimental data gathered from three specifically-built experimental rigs; one consisting of a single thermosyphon and two others consisting of heat exchangers equipped with thermosyphons in single and double pass. The results from the experimental tests were compared to the results from the prediction tool and a good agreement was found, thus concluding that the approach may be used to model heat exchangers equipped with thermosyphons.

7.2 Contribution to knowledge

The main contribution to the area is the creation of a tool capable of predicting the performance of a heat exchanger equipped with thermosyphons for a wide range of evaporator-side conditions. This tool takes advantage of multiple equations currently found in the literature to predict the outlet flow conditions of the heat exchanger.

The prediction model may also be used in parallel with CFD simulation by assuming the thermosyphon is a solid device of constant conductivity and, by predicting the thermal conductivity of the thermosyphon and using it as a boundary condition, the results fell within the predicted margin.

7.3 Recommendations for future work

This work has made a contribution to the field, but as with any body of research there is potential for enhancement and new directions. To this end some future research directions that could provide the next steps are suggested:

- **To look at the possibility of using thermosyphons to produce energy from motion**

At low heat transfer rates, particularly between 50°C and 100°C the thermosyphons were found to oscillate at regular intervals. If it would be possible to quantify this vibration and assess the possibility of recovering energy from the motion this would increase the potential of energy recovery at lower inlet temperatures.

- **Variation of the condenser side conditions**

In the present study the condenser side fluid conditions were kept constant. A suggestion is made to attempt the variation of the inlet conditions on the condenser side in order to allow the creation of new correlations to help predict the behaviour of heat exchangers equipped with thermosyphons.

- **Re-run CFD tests with a k-omega turbulence model**

The use of the k-omega was not included in this study but it is a future direction the results might take as it has been reported by some acquaintances met on conferences that it may be more stable in this particular simulation.

- **Filling ratio**

The effect of filling ratio on the performance of the thermosyphons and its possible impact on their performance of the heat exchanger was not explored in depth in this study.

- **A larger heat exchanger with a greater number of thermosyphons**

The study of a larger heat exchanger with a greater number of thermosyphon or fluid passes is also recommended to size the applicability of the approach in larger heat exchangers.

References

Akbarzadeh, A. & Dube, V., 2001. Industrial waste heat recovery using a loop thermosyphon heat exchnager proofing oven baking oven. *ISES Sol. World Congress,* pp. 851-858.

Alizadehdakhel, A., Rahimi, M. & Alsairafi, A., 2010. CFD modeling of flow and heat transfer in a thermosyphon. *International Communicaitons in Heat and Mass Transfer 37,* pp. 312-318.

Anandan, S. & Bhaskaran, A., 2012. Performance evaluation of thermosyphon integrated heat sink for CPU cooling. *Frontiers in Heat Pipes,* Volume 3, pp. 1-7.

ANSYS, 2012-2014. *Ansys Fluent 14.5 Help.* [Online]
[Accessed 2015].

Aslam Bhutta, M. M.; Hayat, N.; Bashir, M. H.; Khan, A. R.; Ahmad, K. N.; Khan, S., 2012. CFD applications in various heat exchanger design: a review. *Applied Thermal Engineering,* Issue 32, pp. 1-12.

Azad, E. & Geoola, F., 1984. A design procedure for gravity assisted heat pipe heat exchanger. *Heat Recovery System,* 4(2), pp. 101-111.

Bar-Cohen, A., Arik, M. & Ohadi, M., 2006. *Direct liquid cooling of high flux micro and nano electronic components.* s.l., Proceedings IEEE, pp. 1549-1570.

Bayasan, R.M.; Korotchenko, A.G.; Volkov, N.G.; Pustovoit, G.P.; Lobanov, A.D., 2008. Use of two-phase heat pipes with the nelarged heat exchanger surface for thermal stabilization of permafrost soils at the bases of structures. *Applied Thermal Engineering,* Volume 28, pp. 274-277.

BP, 2015. *Statistical Review of World Energy 2015.* [Online]
Available at: http://www.bp.com/en/global/corporate/about-bp/energy-economics/statistical-review-of-world-energy.html
[Accessed 14 07 2015].

Brahic, C., 2007. *Climate myths: the cooling after 1940 shows CO2 does not cause warming.* [Online] Available at: https://www.newscientist.com/article/dn11639-climate-myths-the-cooling-after-1940-shows-co2-does-not-cause-warming/
[Accessed 20 07 2008].

Calautita, J. K., Chaudhrya, H. N., Hughesa, B. R. & Ghanib, S. A., 2013. Comparison between evaporative cooling and a heat pipe assisted thermal loop for a commercial wind tower in hot and dry climatic conditions. *Applied Energy,* Volume 101, pp. 740-755.

Carvajal-Mariscal, I., Sanchez-Silva, F. & Polupan, G., 2012. Development of High Efficiency Two-Phase Thermosyphons for Heat Recovery. In: D. J. Mitrovic, ed. *Heat Exchangers - Basics Design Applications.* s.l.:InTech, pp. 97-116.

Çengel, Y. A., 2002. In: *Heat Transfer: A Practical Approach.* s.l.:McGraw-Hill, pp. 7, 515.

Chan, C.; Siqueiros, E.; Ling-Chin, J.; Royapoor, M.; Roskilly, A.P., 2015. Heat utilisation technologies: A critical review of heat pipes. *Renewable and Sustainable Energy Reviews,* Volume 50, pp. 615-627.

Chen, X.; Ye, Huaiyu; Fan, Xuejun; Ren, Tianling; Zhang, Guoqi, 2016. A review of small heat pipes for electronics. *Applied Thermal Engineering,* Volume 96, pp. 1-17.

Chougule, S. S., Sahu, S. & Pise, A., 2013. Performance enhancement of two phase thermosyphon flat-plate solar collectors by using surfactant and nanofluid. *Frontiers in Heat Pipes,* Volume 4, pp. 1-6.

Claymath, 2015. *Millenium Problems.* [Online]
Available at: http://www.claymath.org/millennium-problems
[Accessed 20 07 2015].

Coal Industry Advisory Board, 2008. *Clean Coal Technologies - Accelerating Commercial and Policy Drivers for Deployment,* Paris: International Energy Agency Publications.

Econotherm, 2012. *Econotherm - Waste Heat Recovery & Recycling Technology.* [Online]
Available at: http://www.econotherm.eu/index.html
[Accessed 1 2012].

Ekambaraa, K., Dhotreb, M. & Joshic, J., 2006. CFD simulation of homogeneous reactions in turbulent pipe flows—Tubular non-catalytic reactors. *Chemical Engineering Journal,* 117(1), pp. 23-23.

Ekambara, K., Sanders, R., Nandakumar, K. & Masliyah, J., 2008. CFD simulation of bubbly two-phase flow in horizontal pipes. *Chemical Engineering Journal,* 144(2), pp. 277-288.

El-Baky, M. A. & Mohamed, M., 2007. Heat pipe heat exchanger for heat recovery in air conditioning. *Applied Thermal Engineering,* Volume 27, pp. 795-801.

EU, 2013. *Decision no 1386/2013/EU of the European Parliament and of the Council of 20 November 2013 on a General Union Environment Action Programme to 2020 'Living Well, within the limits of our planet',* s.l.: The European Parliament and the Council of the European Union.

European Commission, 2014. The EU explained: Environment. *The EU explained,* November.

Fadhl, B., Wrobel, L. C. & Jouhara, H., 2013. Numerical modelling of the temperature distribution in a two-phase closed thermosyphon. *Applied Thermal Engineering,* 60(1-2), pp. 122-131.

Faghri, A., 1995. *Heat Pipe Science and Technology.* s.l.:Taylor & Francis.

Faghri, A., 2012. Review and Advances in Heat Pipe Science and Technology. *Journal of Heat Transfer,* 12 October.134(12).

Faghri, A., 2014. Heat pipes: review, opportunities and challenges.. *Frontiers in Heat Pipes,* Volume 5.

Faghri, A. & Zhang, Y., 2006. *Transport phenomena in Multiphase Systems.* Elsevier: Academic Press.

ForSTEEL Ltd., 2008. *Heat pipe technology.* [Online]
Available at: http://www.forsteel.cz/heat-pipes.html
[Accessed 03 2015].

Gillespie, D., 2015. An Intro to Computational Fluid Dynamics. In: *Fluids Course Work Module.* Oxford: University of Oxford, p. 10.

Grimison, E., 1937. Correlation and utilization of new data on flow resistance and heat transfer for cross flow of gases over tube banks. *Trans. ASME,* Volume 59, pp. 583-594.

Haddad, C.; Périlhon, C.; Danlos, A.; François, M.-X.; Descombes, G., 2014. Some Efficient Solutions to Recover Low and Medium Waste Heat: Competitiveness of the Thermoacoustic Technology. *Energy Procedia,* Volume 50, pp. 1056-1069.

Hagens, H., Ganzevles, F., van der Geld, C. & Grooten, M., 2007. Air heat exchangers with long heat pipes: Experiments and predictions. *Applied Thermal Engineering,* Issue 27, pp. 2646-2434.

Hirt, C. & Nichols, B., 1981. Volume of Fluid (VOF) method for the dynamics of free boundaries. *Journal of Computational Physics,* 39(1), pp. 201-225.

Hughes, B., Chaudhry, H. & Calautit, J., 2014. Passive energy recovery from natural ventilation air streams. *Applied Energy,* Volume 113, pp. 127-140.

Incropera, F. & DeWitt, D., 1996. *Fundamentals of Heat and Mass Transfer.* Fourth Edition ed. New York: John Wiley & Sons.

Jouhara, H., 2009. Economic assessment of the benefits of wraparound heat pipes in ventilation processes for hot and humid climates. *International Journal of Low-Carbon Technology,* Volume 4, pp. 52-60.

Jouhara, H., Anastasov, V. & Khamis, I., 2009. Potential of heat pipe technology in nuclear seawater desalination. *Desalination,* 249(3), pp. 1055-1061.

Jouhara, H., Fadhl, B. & Wrobel, L. C., 2016. Three-dimensional CFD simulation of geyser boiling in a two-phase closed thermosyphon. *International Journal of Hydrogen Energy,* p. In press.

Jouhara, H. & Merchant, H., 2012. Experimental investigation of a thermosyphon based heat exchanger used in energy efficient air handling units. *Energy,* pp. 82-89.

Jouhara, H. & Meskimmon, R., 2014. Heat pipe based thermal management systems for energy-efficient data centres. *Energy,* Volume 77, pp. 265-270.

Jouhara, H.; Milko, J.; Danielewicz, J.; Sayegh, M.A.; Szulgowska-Zgrzywa, M.; Ramos, J.B.; Lester, S.P., 2015. The performance of a novel flat heat pipe based thermal and PV/T (photovoltaic and thermal systems) solar collector that can be used as an energy-active building envelope material. *Energy,* Volume doi:10.1016/j.energy.2015.07.063, p. online.

Jouhara, H. & Robinson, A., 2010. Experimental investigation of small diameter two-phase closed thermosyphons charged with water, FC-84, FC-77 and FC-3283. *Applied Thermal Engineering*, Volume 30, pp. 201-211.

Kays, W. & London, A., 1984. *Compact Heat Exchanger Design.* third ed. ed. New York: McGraw-Hill.

Kearney, S. & Jacobi, A., 1995. *Local and average heat transfer and pressure drop characteristics of annularly finned tube heat exchangers*, s.l.: ACRC TR-69 Report.

Khazaee, I., Hosseini, R. & Noie, S., 2010. Experimental investigation of effective parameters and correlation of geyser boiling in a two-phase closed thermosyphon. *Applied Thermal Engineering*, 30(5), pp. 406-412.

Kim, N. & Kim, S., 2014. Self-convectional three-dimensional integrated circuit cooling system using micro flat heat pipe for portable devices. *Heat Transfer Engineering*, Volume 35, pp. 924-932.

Kim, T., Hyun, B.-S., Lee, J.-J. & Rhree, J., 2013. Numerical study of the spacecraft thermal control hardware combining solid-liquid phase change material and a heat pipe. *Aerospace Science and Technology*, Volume 27, pp. 10-16.

Launder, B. & Spalding, D., 1972. *Lectures in Mathematical Models of Turbulence.* London, England: Academic Press.

Lock, G., 1992. *The Tubular Thermosyphon.* Oxford: Oxford University Press.

Lukitobudi, A., Akbarzadeh, A., Johnson, P. & Hendy, P., 1995. Design, construction and testing of a thermosyphon heat exchanger for medium temperature heat recovery in bakeries. *Heat Recovery Systems and CHP*, 15(5), pp. 481-491.

M. Conde Engineering, 2004. *Thermophysical properties of NH3+H20 solutions for the industrial design of absorption refrigeration equipment.* [Online]
Available at: http://www.mie.uth.gr/ekp_yliko/NH3_H2OProperties_1.pdf
[Accessed June 2015].

Ma, G.; Zhou, F.; Liu, T.; Wang, L.; Liu, Z., 2013. Energy saving evaluation of a thermosyphon heat recovery unit for an air-conditioning system. *Heat Transfer Res.*, Volume 42, pp. 377-388.

McAdams, W., 1954. *Heat Transmission.* New York: McGraw-Hill.

Meyer, A. & Dobson, R., 2006. Thermal performance characterization of R134a and butane charrged two-phase closed thermosyphons. *R&D Journal of the South African Institution of Mechanical Engineering,* 22(3), pp. 26-34.

Mochizuki, M.; Nguyen, T.; Machiko, K.; Saito, Y.; Singh, R.; Nguyen, T.; Wuttijumnong, V., 2013. Prevention possibility of nuclear power reactor meltdown by use of heat pipes for passive cooling of spent fuel. *Frontiers in Heat Pipes,* Volume 4, pp. 1-6.

Mroué, H., Ramos, J., Wrobel, L. & Jouhara, H., 2015. Experimental and numerical investigation of an air-to-water heat pipe-based heat exchanger. *Applied Thermal Engineering,* 78(ISSN 1359-4311), pp. 339-350.

Nair, R. & Balaji, C., 2016. Synergistic analysis of heat transfer characteristics of an internally finned two phase closed thermosyphon. *Applied Thermal Engineering,* p. In Press.

Negishi, K. & Sawada, T., 1983. Heat transfer performance of an inclined two-phase closed thermosyphon. *International Journal of Heat and Mass Transfer,* Volume 26, pp. 1207-1213.

Neuilly, M., 1999. *Modelling and estimation of measurement errors (English).* Paris: s.n.

Noie-Baghban, S. & Majideian, G., 2000. Waste heat recovery using heat pipe heat exchanger (HPHE) for surgery rooms in hospitals. *Applied Thermal Engineering,* Volume 20, pp. 1271-1282.

Noie, S., 2005. Heat transfer characteristics of a two-phase closed thermosyphon. *Applied Thermal Engineering 25,* pp. 495-506.

Noie, S., 2006. Investigation of thermal performance of an air-to-air thermosyphon heat exchanger using ε-NTU method. *Applied Thermal Engineering,* 26(5-6), pp. 559-567.

Nuntaphan, A., Tiansuwan, J. & Kiatsiriroat, T., 2001. *Heat Transfer Coefficients of Thermosyphon Heat Pipe at Medium Operating Temperature,* Thailand: s.n.

Nusselt, W., 1916. *Die Oberflacchenkondensation des wasserdamfes.* s.l.:VDI.

Ozden, E. & Tari, I., 2010. Shell side CFD analysis of a small shell-and-tube heat exchanger. *Energy Converstion and Management,* pp. 1004-1014.

Peng, H., Ling, X. & Li, J., 2012. Numerical simulation and experimental verification on thermal performance of a novel fin-plate thermosyphon. *Applied Thermal Engineering,* Volume 40, pp. 181-188.

Peterson, G., 1994. *An Introduction to Heat Pipes.* Canada: John Wiley & Sons.

Piasecka, M., 2015. Correlations for flow boiling heat transfer in minichannels with various orientations. *International Journal of Heat and Mass Transfer,* Volume 81, pp. 114-121.

PISCO, 2010. *Ocean Currents and Climate Change.* [Online]
Available at: http://www.piscoweb.org/research/science-by-discipline/coastal-oceanography/ocean-currents
[Accessed 15 07 2015].

Ramos, J., Chong, A. & Jouhara, H., 2015. *Numerical investigation of a cross flow air-to-water heat pipe-based heat exchanger used in waste heat recovery,* Newcastle: SusTEM 2015.

Ramos, J.; Chong, A.; Tan, Chee K.; Matthews, J.; Boocock, M.A.; Jouhara, H., 2014a. *Experimental Analysis of gas to water two phase closed thermosyphon based heat exchanger,* Orlando, USA: 10th International Conference on Heat Transfer, Fluid Mechanics and Thermodynamics.

Ramos, J.; Chong, A.; Tan, C.; Matthews, J.; Boocock, M.; Jouhara, H., 2014b. *CFD Simulation and Analysis of a gas-to-water two-phase closed thermosyphon-based heat exchanger,* A Coruña, Spain: WIT Press.

Rassamakin, B.; Khairkov, S.; Zaripov, V.; Rassamakin, A.; Alforova, O., 2013. Aluminum heat pipes applied in solar collectors. *Solar Energy,* Volume 94, pp. 145-154.

Reay, D. A. & Kew, P. A., 2006. Heat Pipes - Theory, Design and Applications. In: Oxford: Elsevier, p. I.

Revellin, R. & Thome, J., 2008. A theoretical model for the prediction of the critical heat flux in heated microchannels. *International Journal of Heat and Mass Transfer,* Volume 51, pp. 1216-1225.

Robertson, A. & Cady, E., 1980. Development and operational testing of a heat pipe dry cooling tower. *American Society Mechanical Engineering,* Volume 80, p. 22.

Rohsenow, W. M., 1952. A method of correlating heat-transfer data for surface boiling of liquids. *Trans. ASME,* Volume 74, pp. 969-976.

Rosenfeld, J.; Ernst, D.M.; Lindemuth, J.E.; Sanzi, J.L.; Geng, S.M.; Zuo, J., 2003. An overview of long duration sodium heat pipe tests. *New Front. Future Concepts,* Volume 699, pp. 1-10.

Sawyer, R., 2004. *Calculating total power requirements for data centres (White Paper #3),* s.l.: American Power Conversion.

Schmidt, T., 1963. Der warmeubergang an rippenrohre und due berechnung von ruhrbundel-warmeaustaschern. *Kaltetechnik,* Volume 15, pp. 98-102.

Selma, B., Désilets, M. & Proulx, P., 2014. Optimization of an industrial heat exchanger using an open-source CFD code. *Applied Thermal Engineering,* 69(1-2), pp. 241-250.

Shabgard, H.; Allen, M. J.; Sharifi, N.; Benn, S. P.; Faghri, A.; Bergman, T. L., 2015. Heat pipe heat exchangers and heat sinks: Opportunities, challenges, applications, analysis, and state of the art. *International Journal of Heat and Mass Transfer,* Volume 89, pp. 138-158.

Shabgard, H., Bergman, T., Sharifi, N. & Faghri, A., 2010. High temperature latent heat thermal energy storage using heat pipes. *International Journal of Heat and Mass Transfer,* 53(15-16), pp. 2979-2988.

Shabgard, H.; Xiao, B.; Faghri, A.; Gupta, R.; Weissman, W., 2014. Thermal characteristics of a closed thermosyphon under various filling conditions. *International Journal of Heat and Mass Transfer,* Volume 70, pp. 91-102.

Shah, R. & Sekulić, D., 2003. Fundamentals of Heat Exchanger Design. In: New Jersey: John Wiley & Sons, pp. 1-2.

Sharifi, N., Bergman, T., Allen, M. & Faghri, A., 2014. Melting and solidification enhancement using a combined heat pipe, foil approachh. *International Journal of Heat and Mass Transfer,* Volume 78, pp. 930-941.

Smith, R., 2008. *Origins of the Commercial CFD Industry.* [Online]
Available at: http://www.symscape.com/blog/origins-of-the-commercial-cfd-industry
[Accessed 7 12 2012].

Sobhan, C., Rag, R. & Peterson, G., 2007. A review and comparative study of the investigations on micro heat pipes. *International Journal of Energy Research,* 2 January, Volume 31, pp. 664-688.

Srimuang, W. & Amatachaya, P., 2012. A review of the applications of heat pipe heat exchangers for heat recovery. *Renewable and Sustainable Energy Reviews,* Volume 16(Issue 6), pp. 4303-4315.

Taylor, J., 1997. *An Introduction to Error Analysis: The Study of Uncertainties in Physical Measurements.* Sausalito: University Science Books.

Temam, R., 2012. *Navier-Stokes Equations, Theory and Numerical Analysis.* s.l.:AMS Chelsea.

Terpstra, M. & Veen, J. V., 1987. Application of heat pipes, heat pipe equipped heat exchangers. In: *Heat Pipes: Construction and Application.* s.l.:Springer, pp. 83-363.

The Engineering Toolbox, 2012. *Heat Exchangers - Arithmetic and Logarithmic Mean Temperature Difference.* [Online]
Available at: http://www.engineeringtoolbox.com/arithmetic-logarithmic-mean-temperature-d_436.html
[Accessed June 2012].

Thermacore, 2016. *High-Temperature Thermal Management.* [Online]
Available at: http://www.thermacore.com/applications/high-temperature-heat-pipes.aspx
[Accessed 20 06 2015].

Valliappan, P., 2015. *Unpublished thesis: Detecting burner instabilities using joint-time frequency methods and artificial neural networks whilst co-firing coal and biomass.* Pontypridd: University of South Wales.

Vandermeersch, T., Alvarenga, P., Ragaert, P. & Dewulf, J., 2014. Environmental sustainability assessment of food waste valorization options. *Resources, Conservation and Recycling,* Volume 87, pp. 57-64.

Vasiliev, L., 2005. *Heat Pipes in modern heat exchangers*, Belarus Minsk, Russia: Elsevier.

Wang, J., 2008. Novel thermal resistance network analysis of heat sink with embedded heat pipes. *Jordan Journal of Mechanical and Industrial Engineering*, Volume 2, pp. 23-30.

Wilcox, D., 1998. *Turbulence Modeling for CFD*, La Canada, California: DCW Industries, Inc..

Wu, X. P.; Mochizuki, M.; Mashiko, K.; Nguyen, T.; Nguyen, T.; Wuttijumnong, V.; Cabusao, G.; Singh, R.; Akbarzadeh, A., 2011. Cold energy storage systems using heat pipe technology for cooling data centres. *Frontiers in Heat Pipes*, Volume 2, pp. 1-7.

Yau, Y., 2007. Application of a heat pipe heat exchanger to dehumidification enhancement in a HVAC system for tropical climates - a baseline performance characteristics study. *International Journal of Thermal Science*, Volume 46, pp. 164-171.

Yau, Y., 2008b. The heat pipe heat exchanger: a review of its status and its potential for coolness recovery in tropical buildings. *Building Services Engineering Research Technology*, Volume 29, pp. 291-310.

Yau, Y., 2010. Analyses of heat recovery devices in the HVAC system in an operating theatre in the tropics. *Building Services Engineering Research Technology*, Volume 31, pp. 341-355.

Yau, Y. & Ahmadzadehtalatapeh, M., 2010. A review on the application of horizontal heat pipe heat exchangers in air conditioning systems in the tropics. *Applied Thermal Engineering*, Volume 30, pp. 77-84.

Yau, Y. H., 2008. The use of a double heat pipe heat exchanger system for reducing energy consumption of treating ventilation air in an operating theatre-A full year energy consumption model simulation. *Energy and Buildings*, 40(5), pp. 917-925.

Yau, Y. & Ng, W., 2011. A comparison study on energy savings and fungus growht control using heat recovery devices in a modern tropical operating theatre. *Energy Conversion Management*, Volume 52, pp. 1850-1860.

Yau, Y. & Tucker, A., 2003. The performance study of a wet six-row heat-pipe heat exchanger operating in tropical buildings. *International Journal of Energy Research,* Volume 27, pp. 187-202.

Yodrak, L., Rittidech, S., Poomsa-ad, N. & Meena, P., 2010. Waste heat recovery by heat pipe air-preheater to energy thrift from the furnace in a hot forging process. *American Journal of Applied Sciences,* Volume 7, pp. 675-681.

Zhang, M.; Lai, Y.; Dong, Y.; Jin, L.; Pei, W.; Harbor, J., 2013. Laboratory investigation of the heat transfer characteristics of a two-phase closed thermosyphon. *Cold Reg. Sci. Technology,* Volume 95, pp. 67-73.

Zhang, Y. & Faghri, A., 2008. Advances and unsolved issues in pulsating heat pipes. *Heat Transfer Engineering,* Volume 29, pp. 20-44.

Zhi, W.; Yu, S.; Wei, M.; Jilin, Q.; Wu, J., 2005. Analysis on effect of permafrost protection by two-phase closed thermosyphon and insulation jointly in permafrost regions. *Cold Reg. Sci. Technology,* Volume 45, pp. 150-163.

Zhou, F., Chen, J., Ma, G. & Liu, Z., 2013. Energy-saving analysis of telecommunication base station with thermosyphon heat exchanger. *Energy Build,* Volume 66, pp. 537-544.

Zhukauskas, A., 1972. Heat Transfer from Tubes in Cross Flow. In: J. H. a. T. Irvine, ed. *Advances in Heat Transfer.* New York: Academic Press.

Zhukauskas, A. & Ulinskas, R., 1988. *Heat transfer in Tube Banks in Crossflow*. New York: Hemisphere.

Zumbrunnen, D., Viskanta, R. & Incropera, F., 1989. The Effect of Surface Motion on Forced Convection Film Boiling Heat Transfer. *Journal of Heat Transfer,* 111(3), pp. 760-766.

Appendix A – Published Papers

[Page 137] J.B. Ramos, A.Z. Chong, C. Tan, J. Matthews, M.A. Boocock, H. Jouhara (2014) Simulation and Analysis of gas to water two phase closed thermosyphon heat exchanger *Heat Transfer XIII: Simulation and Experiments in Heat and Mass Transfer* 217 – 228. 2-4 July 2014, A Coruña, Spain.

[Page 147] J.B. Ramos, A.Z. Chong, C. Tan, J. Matthews, M.A. Boocock, H. Jouhara (2014) Experimental Analysis of gas to water two phase closed thermosyphon based heat exchanger *The 10th International Conference on Heat Transfer, Fluid Mechanics and Thermodynamics*, 14 – 16 July 2014, Florida, USA.

[Page 154] H. Mroue, **J.B. Ramos**, L. Wrobel, H. Jouhara (2015) Experimental and Numerical Investigation of an Air-to-water Heat pipe-based heat exchanger, *Applied Thermal Engineering*. 78, 339-350.

[Page 178] J. Ramos, A. Chong, H. Jouhara (2015) Numerical investigation of a cross flow air-to-water heat pipe-based heat exchanger used in waste heat recovery *SusTEM – Sustainable Thermal Energy Management Conference*, 7-8 July 2015, Newcastle, UK.

[Page 190] J.B. Ramos, A Chong, H. Jouhara (2016) Experimental and Numerical investigation of a cross flow air-to-water heat pipe-based heat exchanger used in waste heat recovery, *International Journal of Heat and Mass Transfer*. 102, November 2016, 1267-1281,

CFD Simulation and Analysis of gas to water two phase closed thermosyphon based heat exchanger

J.B. Ramos[1], A.Z. Chong[1], C. Tan[1], J. Matthews[1],
M.A. Boocock[2] & H. Jouhara[2]
[1]*Faculty of Advanced Technology, University of South Wales, Wales, UK*
[2]*Econotherm (UK) Ltd, an associate company of Spirax-Sarco Engineering plc, Wales, UK*

Abstract

Wickless heat pipes are devices with high reliability and heat transfer potential per unit area. Owed to that fact, their application range has been widened in the past 20 years. In the process industry, they are usually coupled to waste heat recovery devices, namely heat exchangers. Heat-pipe-based heat exchangers offer many advantages when compared to conventional waste heat recovery systems, such as increased reliability and reduced cost of production. The design of such devices, however, is not a straightforward process due to the complex modes of heat transfer mechanisms involved. In this paper, the characterisation of a cross-flow heat pipe based heat exchanger is made via the use of ANSYS Fluent, a CFD solver. A design tool with the purpose of predicting the performance of the test unit is also developed and validated through comparison between the CFD model and previous experimental results.
Keywords: heat recovery, heat exchangers, heat pipes, thermosyphons, CFD, effectiveness.

Introduction

The heat pipe is a heat transfer device with a high heat transfer potential. It consists of a sealed evacuated tube partially filled with a working fluid. The working fluid is responsible for the high heat transfer rates, as a large amount of energy can be transferred via the latent heat in the fluid through phase change.

Heat pipes have a proven track record in many areas, including space applications [1], computer and electronics [2], ventilation and air conditioning [3,4], including dehumidification devices [5] heating systems [6,7], solar energy systems [8], water desalination [9] and nuclear energy [10]; however, waste heat recovery seems to be the preferred application for heat-pipe-equipped heat exchangers [3], partly due to some specific characteristics, namely, the simple structure, high efficiency, compact build, reversibility and the lack of energy input requirement.

Heat pipes are physically divided in three sections: the evaporator, located on the lower section of the pipe, where heat is added to the system; the condenser, located on the upper section of the pipe, where heat is removed from it; and the adiabatic section, located between the two. Theoretically, no heat transfer takes place in the adiabatic section. Logically, a heat exchanger equipped with heat pipes can be divided in the same way, the hotter flow used in the lower part (evaporator) and the colder flow used in the upper part (condenser).

The basic working principle of a heat pipe consists of a continuous cycle of evaporation/condensation of the working fluid (the name given to the fluid inside the pipe) triggered by a difference in temperature. In the evaporator, the heat supplied to the pipe is absorbed by the working fluid; this triggers the evaporation of the fluid and forces the phase change process, flowing up to the condenser section in a gas form. The wall of the heat pipe is cooler in the condenser section, due to the colder fluid flowing on the shell side. Upon making contact with the cooler surface, the working fluid condenses, giving up its latent heat to the wall of the heat pipe and, due to the force of gravity, flowing back down in a liquid form to the evaporator.

There is one characteristic that ought to be mentioned and that is one that substantially alters the behaviour of a heat pipe: the existence (or lack) of a wick structure. The wick usually consists of a sintered structure located on the inside wall of the heat pipe. It applies a capillary pressure to the fluid, allowing it to flow towards the evaporator even when turned upside down and against the force of gravity. Wickless heat pipes are technically named two-phase closed thermosyphons or gravity-assisted heat pipes and are the type used in this paper.

1.1 Literature

Heat pipes have been thoroughly investigated in the past decade [11]. However, due to the intricacies in simulating the phase change process inside the pipe, there are only a handful of Computational Fluid Dynamics (CFD) simulation studies available on the topic and most of them two dimensional. More so, most of the studies were done at temperatures below 50 ºC, as the researchers often aim at studying the application of heat pipes in refrigeration or air conditioner units. For the sake of comparison, in industrial waste heat recovery, the temperature of an exhaust can rise to 300 ºC and the pipes usually have more than 2 metres length.

The closest simulation of the two-phase flow within a heat pipe has been developed by Fadhl *et al* [12]. In his two dimensional study, he was able to accurately simulate the actual boiling and condensation processes inside the pipe

through user-defined functions using the Volume of Fluid (VoF) method in ANSYS FLUENT.

However, simulating the phase change process, even in a two-dimensional study is not an easy matter, and that is the main reason the VoF method is not yet widely used to simulate bundles of pipes or heat pipe-equipped heat exchangers. Instead, most recent papers treat the heat pipe as a single entity, as Annamalai and Ramalingam [13] did when investigating a wicked heat pipe; in an effort to create a better correlation, Annamalai *et al* chose not to simulate the evaporation and boiling processes inside the pipe, assuming the inner side of the pipe to be composed of a single phase of vapour and the wick structure to be a liquid phase throughout the inner wall of the pipe. Good agreement was found between the predicted surface temperature and the experimental results.

Legierski *et al* [14] also conducted a study in a horizontal wicked heat pipe in a low temperature environment (<100 ºC). The variation of thermal conductivity through time was investigated, and the simulation, once again, proved to be very close to the experimental results. The thermal conductivity of the pipe was estimated to range between 15,000 and 30,000 W/m K, a value achieved after 20-30 seconds of operation.

So it is possible to have good agreement between a CFD study and experimental data without simulating the two-phase flow. There are even applications within the CFD solver that allow the user to simulate the heat exchanger; in fact, Drosatos *et al* [15] have used this macro heat exchanger approach in their heat pipe based heat exchanger experiments and achieved very accurate sets of data. The working fluid outlet temperatures and the conjugated heat flux deviated by less than 3.6% and 5.7%, respectively.

In addition, CFD simulation can also be used in order to increase the performance of an existing heat exchanger, even when equipped with heat pipes, as has been proven by Selma *et al* [17]. The improvement in performance resulting from changes in the pipe diameter and the angle between the pipes was investigated within the CFD simulation and then applied to the heat exchanger under investigation. The limitations seem to always be the same, a limited temperature range that does not take into account waste heat applications (0 – 40 ºC).

The present paper produces a CFD simulation predicting the heat transfer performance of a heat exchanger equipped with heat pipes, assuming the heat pipes are solid materials with a constant thermal conductivity. The advantage of this method is a lower simulation time and high adaptability, with possibility of being used in other heat exchanger designs equipped with heat pipes.

The numerical model presented in this paper is a replica of a real heat exchanger used in an experimental rig that was built with the purpose of investigating the behaviour of an actual air-to-water heat exchanger equipped with heat pipes. The model predictions are then compared to the experimental results in an effort to prove the new method (using a constant conductivity) has the potential to size heat pipe based heat exchangers operating at higher temperatures.

2. Physical problem description

The heat exchanger being simulated in this paper is based on an experimental rig that aimed at characterising an air-to-water heat pipe based heat exchanger. In Figure 1 the heat exchanger can be seen rotated 90º to the right. As can be observed, the three sections are clearly shown, the evaporator (0.6 m on the left), the condenser (0.2 m on the right) and the adiabatic section composing the sections in the middle. The thermocouples were placed in key locations, namely in all the inlets and outlets and on the surface of the pipes at 0.6 m intervals.

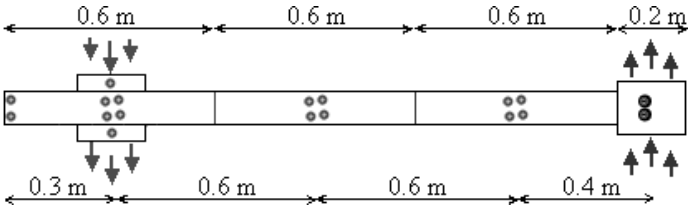

Figure 1: Representative schematic of the heat pipe heat exchanger and respective thermocouple locations (represented by the circles). The evaporator is located on the left and the evaporator on the right.

The heat exchanger is equipped with a set of 6 vertical heat pipes in a staggered arrangement. The pipes are two-phase closed thermosyphons measuring 2.0 m and having a diameter of 28.0 mm. The pipes are made of carbon steel, filled with distilled water to about a third of their total length. The surrounding wall of the heat pipes has an average thickness of 2.5 mm.

In the evaporator section, the pipes are swept 3 at a time by the hot air (looking at Figure 2, the hot air flows from the bottom to the top of the picture). In the condenser, the pipes are swept as shown in Figure 2. Following the arrows, the flow takes a u-turn, sweeping the pipes in order.

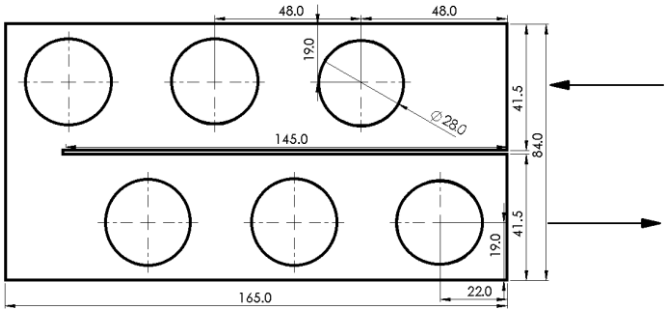

Figure 2: Cross-section of the Condenser part of the Heat Exchanger (Top view all dimensions in mm).

The principal purpose of this simulation is to prove that by equating the heat pipe to a solid rod of constant conductivity, the other modes of heat transfer inside the heat pipe can be neglected.

The temperature and mass flow rate of hot incoming air varied from 50 ºC to 300 ºC and 0.05 kg/s to 0.2 kg/s, respectively. The water inlet was kept at a constant mass flow rate of 0.07 kg/s and constant temperature at 10 ºC.

2.1 Numerical model

ANSYS Fluent was used to develop a numerical model to simulate the external heat flow over the pipes on both the air side (evaporator) and water side (condenser). The model was developed in order to access the possibility of using constant conductivity as a boundary condition in heat pipe simulation for future heat exchanger modelling.

The mesh was first built and sized. Afterwards, the full range of simulations attempted the repetition of the experimental results and finally the results were compared with the experimental results.

The standard k-epsilon (k-ε) turbulence model was used for all the tested results. It is the most used model in practical engineering flow calculations due to its robustness and reasonable accuracy for a wide range of turbulent flows. It is a semi-empirical model based on model transport equations for the turbulence kinetic energy (k) and its dissipation rate (ε). In order to use the standard k-ε, the flow has to be fully turbulent. The pressure-velocity scheme used was coupled as it offers a better result for a single-phase flow, more consistent and efficient at steady-state [16]. This is due to the fact that the algorithm solves the pressure-based continuity and momentum equations simultaneously.

2.2 Mesh selection

There were three meshing levels generated: coarse, medium and fine. In the case of hexahedrons or tetrahedrons meshes, the maximum skewness should be lower than 0.7, while in triangular elements, it must be inferior to 0.8 [17].

Table 1: Mesh Dependency.

Level	No of Cells	Type of cells	Max. Skewness	Time/iter (s)
Coarse	191,299	Hex + Tetra	0.68	0.5-1
Medium	825,904	Hex + Tetra	0.70	10-12
Fine	1,518,970	Hex + Tetra	0.57	24-26

Two evaporator inlet conditions were considered to which the experimental results were compared to the simulated results. The results provided by the fine mesh were the most acceptable in the end and the limit guaranteed for grid independency. The medium mesh gave unexpected results, less accurate than the experimental.

Table 2: Mesh comparison, the percentage error is shown in brackets.

Inlet Conditions:	$T_{h,out}$ Exp.	$T_{h,out}$ Fine Mesh	$T_{h,out}$ Medium Mesh
$T_{h,in}$ = 300 ºC $\dot{m}_{h,in}$ = 0.20 kg/s	276.1 ºC	275.0 ºC (*-0.4%*)	277.9 ºC (*0.7%*)
$T_{c,in}$ = 10 ºC $\dot{m}_{c,in}$ = 0.07 kg/s	29.0 ºC	28.0 ºC (*-3.4%*)	27.6 ºC (*-4.8%*)
$T_{h,in}$ = 300 ºC $\dot{m}_{h,in}$ = 0.17 kg/s	274.8 ºC	271.7 ºC (*-1.1%*)	275.8 ºC (*0.4%*)
$T_{c,in}$ = 10 ºC $\dot{m}_{c,in}$ = 0.07 kg/s	29.1 ºC	27.6 ºC (*-5.2%*)	26.6 ºC (*-8.6%*)

The finer mesh was used for all the tests, and not only was the percentage error smaller, but the flows appeared to extract more heat than in the experimental test, which is to be expected taking into account the walls of the heat exchanger are 100% adiabatic (Q = 0).

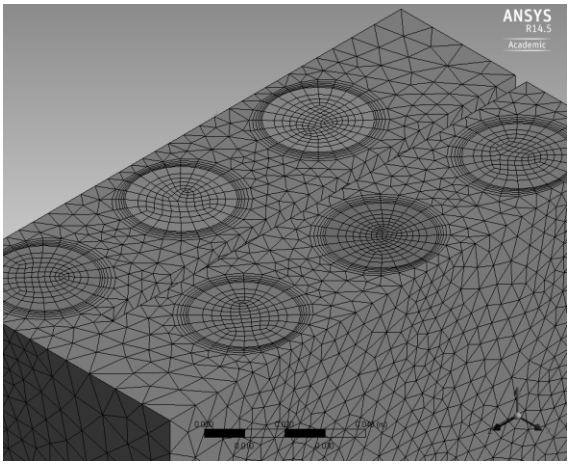

Figure 3: Detailed view of the Mesh used in the model.

2.3 Boundary conditions

When starting the solver, the boundary conditions need to be specified. First the characteristics of the fluids in question (water and air) were set, based on the default values given by Fluent (included in the nomenclature). Then the conductivity of the pipes was set to be 200,000 W/(m.K). The inlet and outlet conditions for the flows can be seen in Table 3. Note that beyond the inlets and outlets, all the other walls were considered to be adiabatic as they were insulated in the experimental rig.

Table 3: Boundary Conditions.

	Mass flow rate (kg/s)	Temperature (ºC)
Evaporator Inlet Conditions	0.05 to 0.2	50 to 300
Evaporator Outlet Conditions	0.05 to 0.2	*Desired Output*
Condenser Inlet Conditions	constant 0.07	10
Condenser Outlet Conditions	constant 0.07	*Desired Output*

The value for conductivity used in this paper is a co-relation between several expressions. The first required value is the thermal conductivity. In axial conduction through a solid, Fourier's Law states that thermal conductivity is represented by the letter *k* and can be used in equation (1) [18]:

$$\dot{Q}_c = \frac{kA\Delta T}{\delta} \tag{1}$$

Applied to a heat pipe, $\dot{Q}_c$ represents the axial heat transfer rate by conduction from the bottom to the top of the pipe (W), *k* represents the overall thermal conductivity (W/m.K), ΔT represents the difference in temperature between each end of the pipe (K) and δ the axial distance (m), which in our case is the length of the adiabatic section. The thermal conductivity, *k*, has to be related to the thermal resistance of the heat pipe and that is done through eqn. (2):

$$R_{hp} = \frac{\Delta T}{\dot{Q}} \ , \ \dot{Q} = \frac{\Delta T}{R_{hp}} \tag{2}$$

Thermal resistance is the ability of resisting the flow of heat [18]. Where $\dot{Q}$ denotes the heat transfer rate through the pipe (W), ΔT the difference in temperature between each end of the pipe (K) and R_{hp} the thermal resistance of the heat pipe (K/W). The equation is re-arranged in order to set $\dot{Q}$ as the variable under study. Equating both, eqn. (1) and (2), we are left with eqn. (3):

$$\frac{\Delta T}{R_{hp}} = \frac{kA\Delta T}{\delta} \tag{3}$$

Leading to the conclusion that:

$$k = \frac{\delta}{A \cdot R_{hp}} \tag{4}$$

The thermal resistance of a heat pipe, R_{hp} (K/W), is determined from the conditions of the flow in the vicinity of the pipe, a re-iteration of eqn. (2) that looks like the following:

$$R_{hp} = \frac{\bar{T}_h - \bar{T}_c}{Q_{hp}} \quad (5)$$

$\bar{T}_c$ and $\bar{T}_h$ represent the average temperature in both the evaporator and the condenser sections (K) and Q_{hp} is the heat flow through the heat pipe (W). Since the heat exchanger is equipped with 6 heat pipes, the use of the Total Resistance, R_T (K/W), is advised. Following the electric circuit analogy, the heat pipes are assumed to be thermal resistances arranged in parallel and the Total Thermal Resistance becomes the following:

$$R_T = \frac{1}{\frac{1}{R_{hp1}} + \frac{1}{R_{hp2}} + \frac{1}{R_{hp3}} + \frac{1}{R_{hp4}} + \frac{1}{R_{hp5}} + \frac{1}{R_{hp6}}} \quad (6)$$

Assuming all the heat pipes offer the same resistance to heat transfer:

$$R_T = \frac{R_{hp}}{n} \quad (7)$$

Where n represents the number of heat pipes in the heat exchanger. The total resistance is related to the heat flow of the entire heat exchanger through equation (2), which leads to the determination of R_{hp} which in turn allows the calculation of k as a boundary condition in the CFD simulation.

3. Results and discussion

Using 4 processors operating in parallel, the simulation was conducted smoothly, following the trend shown in Table 1. The reported results were mainly the outlet temperatures as they are directly related to the heat transfer rate. The simulation was repeated for each experimental test and the value for the conductivity used was extracted from an average R_{hp} from eqn. (7).

Figures 4 and 5 are a visualisation of the results from the CFD simulation. The inlet data for the results presented was the highest temperature difference at the highest mass flow rate (T = 300 ºC and $\dot{m}$ = 0.2 kg/s). The temperature profile of the heat pipe is plotted in Figure 4 according to the tube's length. The average temperature inside the pipe is 55 ºC (328 K), a 7% difference to the experimental values. The temperature profile of the flow within the heat exchanger is presented in Figure 5 for the same inlet conditions.

Figure 6, on the left, shows the difference in temperature between the inlet and outlet of the evaporator section. It compares the experimental values to the values obtained in the CFD simulation. The lines represent the experimental values and the markers the CFD values. Good agreement is found from the results in the evaporator side, an average difference of 3%, according to Figure 7. The figure on the right compares the values obtained in the condenser section between the CFD simulation and the experimental test. The difference is more visible here and can go up to 40%, but the average is about 25% difference. Coincidentally, it was the area of the heat exchanger with the highest uncertainty rate during the

experimental tests. The main reason for the high deviation was the inability to create a perfect adiabatic section; there were losses registered in the adiabatic section during the experimental test that the simulation did not take into consideration. Additionally, the low accuracy identified at lower temperatures was a result of the reduced thermal conductivity of the heat pipe at those temperatures [19]. The lower thermal conductivity is due to the partial evaporation and condensation processes which were not taken into consideration in the equations used.

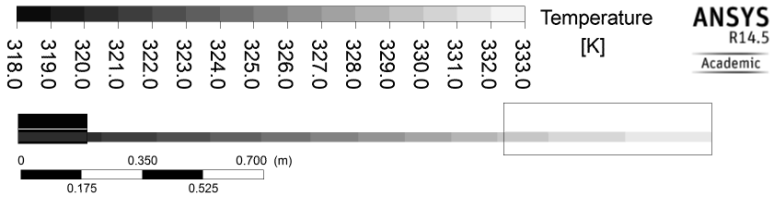

Figure 4: Temperature profile of the heat pipe ($T_{h,in}$ = 300 ºC $\dot{m}_{h,in}$ = 0.2 m/s, $T_{c,in}$ = 10 ºC $\dot{m}_{c,in}$ = 0.07 m/s).

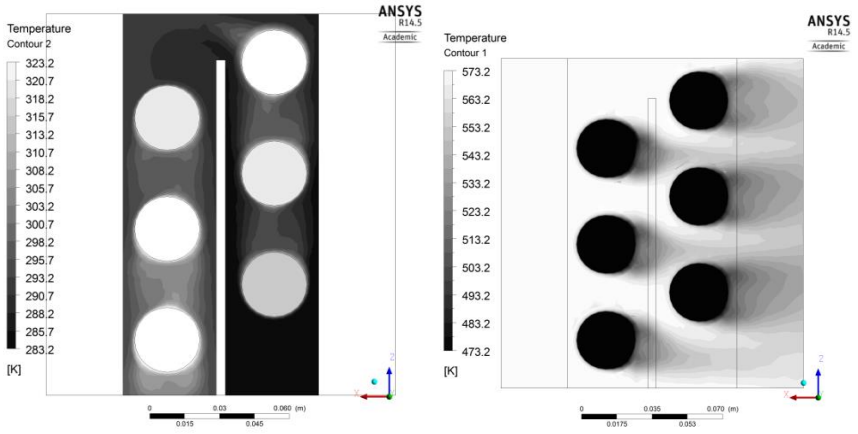

Figure 5: Visualisation of CFD results. Condenser (left) and evaporator (right) ($T_{h,in}$ = 300 ºC $\dot{m}_{h,in}$ = 0.2 m/s, $T_{c,in}$ = 10 ºC $\dot{m}_{c,in}$ = 0.07 m/s). Conversion Kelvin – Centigrade: 10 ºC (283 K), 50 ºC (323.2 K); 200 ºC (473.2 K), 300 ºC (573.2 K).

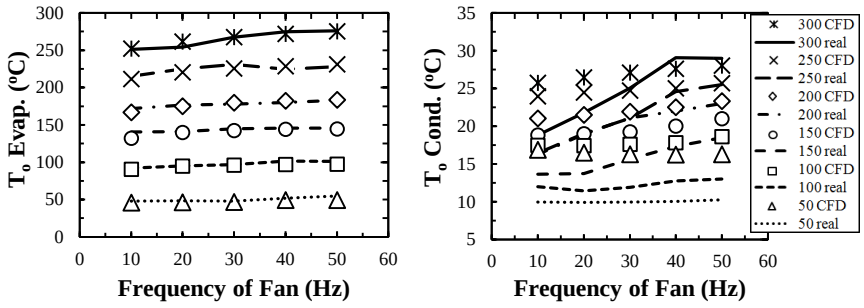

Figure 6: Difference in temperature in the evaporator and condenser sections.

Overall, the CFD results show a higher outlet temperature in the cold section, a result of the lack of heat transfer in the adiabatic section, which is not physically possible in the existing experimental rig.

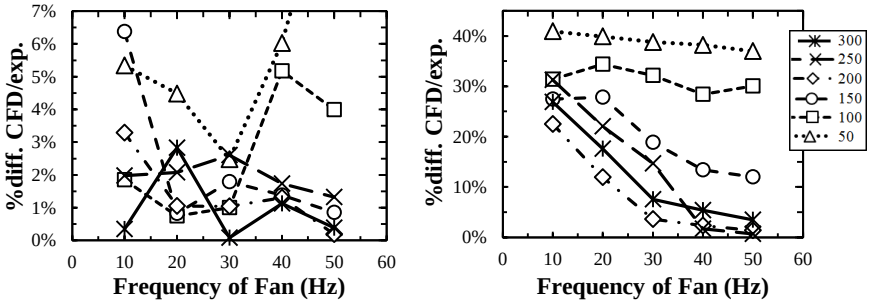

Figure 7: Percentage difference between outlet temperatures in the condenser section.

4. Conclusion

CFD has been used to simulate the behaviour of a heat pipe based heat exchanger through the assumption that the heat pipes are solid devices of constant conductivity. The model results proved to be within an average of 20% of the experimental results assuming a constant conductivity for all the results. The creation of a relation between thermal resistance of the heat pipe and inlet conditions is suggested in order to perfect the model.

4. Acknowledgements

Special thanks are due to the staff at Econotherm, specifically Mr Stefan Munteanu, Mr Viorel Munteanu and Mr Peter Blackwell for the fast and flawless way the experimental rig was prepared. Thanks are also due to Mr David Jenkins, Mr Hassan Mroue and Mr Michael Jones for their overall helpfulness.

Nomenclature

A	(m^2)	Heat Transfer Area
k	(W/(m.K))	Constant of Thermal Conductivity
$\dot{m}$	(kg/s)	Mass Flow Rate
$\dot{Q}$	(W)	Heat Transfer Rate
R	(K/W)	Thermal Resistance
T	(^oC)	Temperature
$\bar{T}$	(^oC)	Average Temperature
ΔT	(^oC)	Difference in Temperature
U	(W/(m^2.K))	Overall Heat Transfer Coefficient
δ	(m)	Distance (used in Conduction)
ε	(-)	Effectiveness

Subscripts

c	Condenser side / Cold side
h / e	Hot side / Evaporator side
hp	Heat pipe / Thermosyphon
i	Inlet
n	Number of pipes
o	Outlet
T	Total
w	Water

Abbreviations

CFD	Computational Fluid Dynamics
HPHE	Heat pipe Heat Exchanger
k-ε	k-epsilon turbulence method
NTU	Number of Transfer Units
VoF	Volume of Fraction

References

[1] Dong, S.J., Li, Y.Z. & Wang, J., Fuzzy incremental control algorithm of loop heat pipe cooling system for spacecraft applications, *Computers & Mathematics with Applications*, 64 (2012) 877-886.

[2] Wang, J.C., 3-D numerical and experimental models for flat and embedded heat pipes applied in high-end VGA card cooling system, *International Communications in Heat and Mass Transfer*, 39 (2012) 1360-1366.

[3] Jouhara, H. & Robinson, A.J., An experimental study of small-diameter wickless heat pipes operating in the temperature range 200C to 450C., *Applied Thermal Engineering*, 30 (2011) 1041-1048.

[4] Chaudhry, H.N., Hughes, B.R. & Ghani S.A., A review of heat pipe systems for heat recovery and renewable energy applications, *Renewable and Sustainable Energy Reviews*, 16 (2012) 2249-2259.

[5] Yau, Y.H. & Ahmadzadehtalatapeh, M., A review on the application of horizontal heat pipe heat exchangers in air conditioning systems in the tropics, *Applied Thermal Engineering*, 30 (2010) 77-84.
[6] Wang, Z., Duan, Z., Zhao, X., & Chen, M., Dynamic performance of a façade-based solar loop heat pipe water heating system, *Solar Energy*, 86 (2012) 1632-1647.
[7] Zhang, X., Zhao, X., Xu, J. & Yu, X., Characterization of a solar photovoltaic/loop-heat-pipe heat pump water heating system, *Applied Energy*, 102 (2013) 1229-1245.
[8] Nithyanandam K. & Pitchumani, R., Computational studies on a latent thermal energy storage system with integral heat pipes for concentrating solar power, *Applied Energy*, 103 (2013) 400-415.
[9] Jouhara, H., Anastasov, V. & Khamis, I., Potential of heat pipe technology in nuclear seawater desalination, *Desalination*, 249 (2009) 1055-1061.
[10] Laubscher, R. & Dobson, R.T., Theoretical and experimental modelling of a heat pipe heat exchanger for high temperature nuclear reactor technology, *Applied Thermal Engineering*, 61 (2013) 259-267.
[11] Vasiliev, L.L., Heat pipes in modern heat exchangers, *Applied Thermal Engineering*, 25 (2005) 1-19.
[12] Fadhl, B., Wrobel, L.C. & Jouhara, H., Numerical modelling of the temperature distribution in a two-phase closed thermosyphon, *Applied Thermal Engineering*, 60 (2013) 122-131.
[13] Annamalai, A. & Ramalingam, V., Experimental Investigation and Computational Fluid Dynamics of a Air Cooled Condenser Heat Pipe, *Thermal Science*, 15 (2011) 759-772.
[14] Legierski, J., Wieçek, B. & de Mey, G., Measurements and simulations of transient characteristics of heat pipes, *Microelectronics Reliability*, 46 (2006) 109-115.
[15] Drosatos, P., Nikolopoulos, N., Agraniotis, M., Itskos, G., Grammelis, P. & Kakaras, E., Decoupled CFD simulation of furnace and heat exchangers in a lignite utility boiler, *Fuel*, 117, Part A (2014) 633-648.
[16] FLUENT 6.3 User's Guide, Fluent Inc. Online http://aerojet.engr.ucdavis.edu/fluenthelp/html/ug/node998.htm
[17] Selma, B., Désilets, M. & Proulx, P., Optimization of an industrial heat exchanger using an open-source CFD code, *Applied Thermal Engineering*, (2013).
[18] Incropera, F. & Dewitt, D., *Fundamentals Of Heat And Mass Transfer*, 4th Ed, John Wiley & Sons, 1996.
[19] Khazaee, I, Hosseini, R. & Noie, S.H., Experimental investigation of effective parameters and correlation of geyser boiling in a two-phase closed thermosyphon, *Applied Thermal Engineering*, (2010)

HEFAT2014
10th International Conference on Heat Transfer, Fluid Mechanics and Thermodynamics
14 – 16 July 2014
Orlando, Florida

EXPERIMENTAL ANALYSIS OF GAS TO WATER TWO PHASE CLOSED THERMOSYPHON BASED HEAT EXCHANGER

Ramos, J.B.[1], Chong, A.[1], Tan, C.[1], Matthews, J.[1], Boocock, M.A.[2], Jouhara, H.[2]
[1]University of South Wales, Faculty of Advanced Technology,
Trefforest, CF37 1DL, UK, E-mail:
joao.ramos@southwales.ac.uk
[2]Econotherm (UK) Ltd, an associate company of Spirax-Sarco Engineering plc,
Waterton Rd, Bridgend, CF31 3YY, UK, E-mail:
hussam.jouhara@econotherm.eu

ABSTRACT

Wickless heat pipes have been attracting increased attention in the last two decades due to their reliability and high heat transfer potential per unit area. Their most common application is in the process industry, when coupled to waste heat recovery devices. Heat pipe based heat exchangers offer many advantages when compared with conventional waste heat recovery systems; advantages that are detailed in the current work. The design of such devices, however, is not a straightforward process due to the complex modes of heat transfer mechanisms involved. In this paper, the characterisation of a cross-flow heat pipe based heat exchanger is studied experimentally, using correlations currently available in literature. A design tool with the purpose of predicting the performance of the test unit was also developed and validated through comparison with the experimental results. The design tool was validated with the use of a purpose-built experimental facility.

Keywords: *heat recovery, heat exchangers, heat pipes, thermosyphons, effectiveness*

INTRODUCTION

Waste heat recovery is a growing area in industry. This recent growth is a direct result of tighter environmental policies instigated by the Kyoto Protocol [1,2]. Present heat recovery systems have to be safe, efficient and economical in order to be justifiable in today's competitive market. Of all the ideas and designs available, heat pipe based systems are desirable due to their increased reliability, ease of operation, system efficiency and reduced manufacturing cost. The reliability is provided by their passive operation and flow separation, and the reduction in cost is a result of recent advances in manufacturing methods. Due to their mode of operation through evaporation and condensation of an internal fluid, heat pipes have been described as super thermal conductors [3,4], as the phase change process is able to transport heat energy at a much higher rate than pure conduction through a solid.

Heat pipes are known for their adaptability, having a proven track record in a wide range of different areas, namely space applications [5], computer and electronics [6], ventilation and air conditioning [7-9], heating systems [10,11], solar energy systems [12], water desalination [13] and nuclear energy [14]; but perhaps the most promising incorporation of heat pipe technology is in waste heat recovery for industrial applications.

An extensive amount of literature is available on heat pipes being used in air handling units at low temperatures (<100 ^{o}C), but it is quite scarce for higher temperatures, (100 ^{o}C < T < 300 ^{o}C). Waste heat recovery units can have multiple uses: pre-heating incoming air, maintaining a fluid at a high temperature, generating steam, or space heating.

NOMENCLATURE

A	[m^2]	Heat Transfer Area
c_p	[J/(kg.K)]	Specific heat capacity
C	[W/K]	Heat Capacity Rate
C_r	[-]	Heat Capacity Ratio
FR	[m^3/s]	Flow Rate
h	[W/m^2.K]	Heat Transfer Coefficient
$\dot{m}$	[kg/s]	Mass Flow Rate
$\dot{Q}$	[W]	Heat Transfer Rate
R	[K/W]	Thermal Resistance
T	[^{o}C]	Temperature
ΔT	[^{o}C]	Difference in Temperature
U	[W/m^2.K]	Overall Heat Transfer Coefficient
ε	[-]	Effectiveness

Subscripts

a	Air
av	Average
c	Condenser side / Cold side
e / h	Evaporator side / Hot side
hp	Heat pipe / Thermosyphon
i	Inlet
n	Number of pipes
o	Outlet
w	Water

Abbreviations

NTU	Number of Transfer Units
HPHE	Heat pipe Heat Exchanger

A heat pipe heat exchanger can be described as an indirect-transfer heat exchanger relying solely on the evaporation and condensation of the working fluid to transfer heat [4]. It usually consists of an array of straight heat pipes arranged vertically; the pipes are swept by a hot flow in their lower section and a cold flow in the upper section. They will passively absorb heat from the hotter medium and release it in the colder stream through the constant evaporation and condensation of the working fluid inside the pipe. One of the requirements of a working heat pipe is a temperature difference between the streams that the heat pipe is exposed to at each of its ends [15].

The heat extraction behaviour of a heat pipe based heat exchanger is highly dependent on the flow configuration and conditions. Therefore, a detailed experimental study is required in order to characterise the performance of the system [16].

Due to the complex nature of the heat transfer mechanisms in the pipes and their interaction with their fluid environments, an experimental investigation is proposed for a specific heat exchanger configuration.

The thermal resistance analogy is a well-known method for characterisation of a heat exchanger using experimental data. It consists of comparing the heat exchanger to an electrical circuit and turning all modes of heat transfer into resistances. This method is further complemented by the use of the Effectiveness [17,18], a variable often used in the characterisation of heat exchangers and a great tool when generating numerical prediction models.

This paper describes the characterisation of an air-to-water heat pipe-equipped heat exchanger. The evaporator inlet conditions, such as temperature and mass flow rate, are manipulated, and the heat extraction profile is investigated, assuming the heat pipes have a constant thermal resistance. The resistance to heat transfer offered by the heat pipes is then related to the Effectiveness of the heat exchanger.

TEST FACILITY DESIGN

The experimental rig consisted of a heat exchanger equipped with six heat pipes in a cross-flow arrangement. The design of the rig was based on a real working example of a larger heat exchanger. The test facility was composed of two parts: a hot air circuit and a cold water circuit. The hot air circuit was a closed loop propelled by a fan. The cold water circuit was controlled by a simple ball valve, as can be seen in Figure 1.

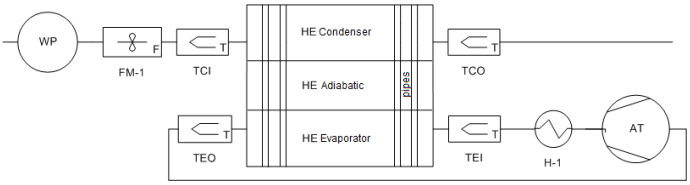

Figure 1 Schematic of the test setup. Description: WP – Water pump; FM-1 – Turbine Flow Meter; TCI/TCO – Thermocouple at inlet/outlet of condenser; HE-C/E – Heat pipe heat exchanger Condenser/Evaporator; TEI/TEO – Thermocouple at inlet/outlet of evaporator; H-1 – Air Heater; AT – Air Turbine

The hot air flow consisted of a single pass sweeping all 6 pipes at a time. The mass flow rate was controlled by a fan. The temperature was measured by a K-type thermocouple located at the inlet of the evaporator section which also controlled the power of the air heater. The data was gathered using a 32-channel data logging device connected to an array of K-type thermocouples. These thermocouples were placed in specific locations within the heat exchanger in order to provide information on the flow, and the heat pipe's surface and interior temperature.

TEST PIECE DESIGN

In order to have a better working understanding of the heat pipe heat exchanger, it is customary to divide it in three sections. The bottom section is in contact with the hot air stream and is named Evaporator; here the heat energy supplied to the heat pipes causes the internal working fluid to evaporate. The top section where the cold water stream flows is termed Condenser; here the heat is removed from the heat pipes, causing the working fluid within the pipes to condense and flow back to the bottom, aided by the force of gravity. The middle section is termed Adiabatic since there is no heat transfer taking place.

The condenser section occupied the top 0.2 m of the pipes, and the evaporator section covered the lower 0.6 m. Both sections were separated from the adiabatic section by a 10 mm-thick division plate in order to prevent leaks. The flow inside the condenser consisted of a u-shaped path (please see Figure 2) and a bleeding valve was installed on the top of the condenser to remove all the air from the section when initiating operation.

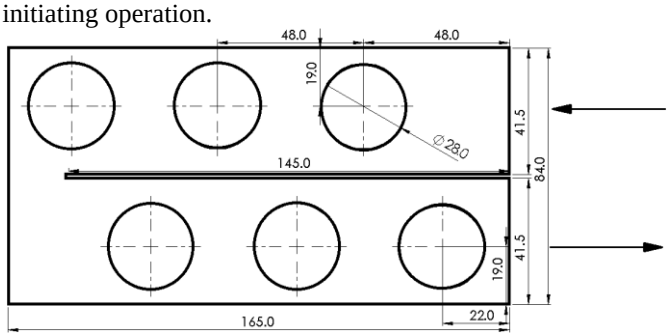

Figure 2 Cross-section of the Condenser part of the Heat Exchanger (all dimensions in mm)

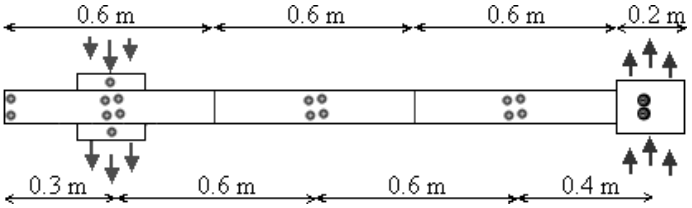

Figure 3 Representative schematic of the heat pipe heat exchanger and thermocouple placements (represented by the circles)

The thermocouples were placed in key sections; namely at each inlet and outlet of both the hot flow and the cold flow, on the surface of each pipe, in the adiabatic section, and within the heat pipes. The thermocouple placements can be seen in Figure 3, represented by the circles. The thermocouples in the pipes were located in the base of the heat pipes.

The six heat pipes were all made of carbon steel, measured 2 meters in length and had a diameter of 28 mm. The surrounding wall of the heat pipes had an average thickness of 2.5 mm. The working fluid was distilled water, filled to a third of the total volume. All the pipes were chemically treated before insertion of water in order to avoid corrosion.

HEAT EXCHANGER EFFECTIVENESS MODEL

Through the data gathered, a numerical effectiveness model can be developed in order to predict the effectiveness of the heat exchanger. In order to develop the model, the entire system is divided into two separate heat exchangers with the working fluid as the division between them. The effectiveness is the ratio of the actual heat transfer rate to the maximum theoretical heat transfer rate and if the results are available, it is determined from the following expression:

$$\varepsilon = \frac{\dot{Q}_{actual}}{\dot{Q}_{max}} = \frac{C_w(T_{c,o}-T_{c,i})}{C_{min}(T_{max}-T_{min})} = \frac{C_w(T_{c,o}-T_{c,i})}{C_{min}(T_{h,i}-T_{c,i})} \quad (1)$$

Where $\dot{Q}$ represents the heat transfer rate, C_w refers to the heat capacity rate for water (w) and C_{min} represents the minimum heat capacity rate between the water side and the air side. T_c refers to the cold side and T_h to the hot side. The heat transfer rate is usually determined through the equation:

$$\dot{Q} = \dot{m} c_p \Delta T \quad (2)$$

In this equation $\dot{m}$ represents the mass flow rate (kg/s), c_p the specific heat capacity (J/(Kg.K)) for the fluid in question and ΔT (ºC or K) the difference in temperature between the inlet and the outlet of a given section.

However, the effectiveness can also be related to the Number of Transfer Units. The general formula for the effectiveness in each side of the heat exchanger is the following [18]:

$$\varepsilon = \frac{1-e^{[-\mathrm{NTU}(1-C_r)]}}{1-C_r \cdot e^{[-\mathrm{NTU}(1-C_r)]}} \quad (3)$$

The expression above refers to either the heat being transferred from the hot flow to the working fluid inside the heat pipe or to the heat transfer from the working fluid to the cold flow. C_r is the ratio between the heat capacity rates of the shell-side fluid and the working fluid inside the pipe (C_{min}/C_{max}). The working fluid inside the pipe, however, is in a constant state of evaporation on the hot side and of condensation on the cold side, which results in an incredibly high value of the heat capacity rate (C). Since the heat capacity rate for the fluid in phase change is far superior to the fluid on the shell side, the ratio of heat capacity rates (C_r) is assumed to be zero. Assuming $C_{min}/C_{max} \approx 0$ we are left with an expression of effectiveness for each side of the heat exchanger:

$$\varepsilon_h = 1 - e^{(-\mathrm{NTU}_h)} \quad (4)$$

$$\varepsilon_c = 1 - e^{(-\mathrm{NTU}_c)} \quad (5)$$

The Number of Transfer Units (NTU) is a method of presenting mean temperature differences, and it is the relation between the overall heat transfer coefficient (U), the total heat transfer area (A) and the minimum Heat Capacity Rate (C_{min}) like so:

$$\mathrm{NTU}_h = \frac{U_h A_h}{C_h} \quad (6)$$

$$\mathrm{NTU}_c = \frac{U_c A_c}{C_c} \quad (7)$$

The heat transfer coefficient is then related to the local heat transfer coefficients (h_x), the Area of exposure to the flow and the heat pipe's inner resistance to temperature change.

$$\frac{1}{U_h A_h} = \frac{1}{h_h A_{hp}} + R_{hp,h} \quad (8)$$

$$\frac{1}{U_c A_c} = \frac{1}{h_c A_{hp,c}} + R_{hp,c} \quad (9)$$

The method to determine the internal resistances of the thermosyphon is made available by the Engineering Sciences Data Unit (ESDU) [19].

Additionally, the effectiveness of a single heat pipe can be found from the following equation by Faghri [20]:

$$\varepsilon_p = \left(\frac{1}{\varepsilon_{min}} + \frac{C_r}{\varepsilon_{max}}\right) \quad (10)$$

C_r is the ratio of Heat Capacity rates (C_{min}/C_{max}) within the heat pipe and ε_x are the maximum and minimum values of effectiveness for each of the sides (evaporator and condenser). The expression below is required in order to determine the effectiveness of the entire heat exchanger [18]:

$$\varepsilon = \frac{\left(\frac{1-\varepsilon_p C_r}{1-\varepsilon_p}\right)^n - 1}{\left(\frac{1-\varepsilon_p C_r}{1-\varepsilon_p}\right)^n - C_r} \quad (11)$$

This is, coincidentally, the equation used on a shell and tube heat exchanger with n passes. In the original equation, ε_p represents the effectiveness for a single pass; it is only logical that in order to incorporate heat pipes the effectiveness of a single pipe is used. In this case, however, the superscript n represents the number of rows of heat pipes in the direction of air flow. The ratio of heat capacity rates (C_r) in the equation above refers to the different heat capacity rates in the shell side fluid of the evaporator and the condenser [21]. The effectiveness determined through equation (11) can then be used to determine the heat transfer rate through the following expression:

$$\dot{Q} = \varepsilon \cdot \dot{Q}_{max} \quad (12)$$

Going back to equation (1), the maximum heat extraction rate can be found by multiplying the minimum heat capacity rate by the maximum difference in temperature, which in this case is the difference between the inlet temperatures:

$$\dot{Q}_{max} = C_{min}(t_{h,i} - t_{c,i}) \quad (13)$$

Through manipulation of the equation above, the outlet temperatures can be predicted through equations (14) and (15) below:

$$T_{h,o} = T_{h,i} - \frac{\dot{Q}}{C_h} \quad (14)$$

$$T_{c,o} = T_{c,i} + \frac{\dot{Q}}{C_c} \quad (15)$$

The iterative thermal balancing technique used in the empirical model makes use of the known parameters of inlet temperatures and air flow rates. The main assumption is that all the thermosyphons have the same value of overall thermal resistance: an average value derived from the experimental data. This iteration is based on the law of conservation of

energy, and only possible if it is assumed that there are no losses in the adiabatic section. Therefore the thermal resistance offered by a single heat pipe is the inverse of the heat transfer rate:

$$R_{hp} = \frac{T_{e,av} - T_{c,av}}{Q_{hp}} \quad (16)$$

OPERATIONAL PROCEDURE

In order to investigate the thermal performance of the heat exchanger, a number of tests were performed. The temperature in the hot air stream ranged from 50 °C to 300 °C at 50 °C increments, and the mass flow rate varied between 0.05 kg/s and 0.2 kg/s at approximately 0.035 m^3/s increments, a result of the fan setting from 10 Hz to 50 Hz. In the cold section, the mass flow rate was a constant 7.16×10^{-2} m^3/s at an average temperature of 10 °C. All the tests were run for a minimum of 9 minutes at steady state, as can be seen in Table 1.

Table 1 Testing time for each variable (at s.s., in minutes)

Hz\°C	50 °C	100 °C	150 °C	200 °C	250 °C	300 °C
10 Hz	09:05	08:45	08:35	10:40	08:41	09:18
20 Hz	09:01	08:37	08:31	08:57	09:02	08:21
30 Hz	10:00	08:15	08:21	09:02	08:28	10:30
40 Hz	09:21	10:56	10:53	11:13	14:40	08:13
50 Hz	10:23	16:11	11:23	10:05	09:40	07:11

The cold flow was kept at essentially constant temperature and its variation is presented in Table 2. The mass flow rate was also kept at a constant rate of 7.16×10^{-2} m^3/s throughout all the experiments.

Table 2 Comparison between inlet temperatures

Average inlet temperature of Evaporator (air)	Average inlet temperature of Condenser (water)
300 °C	10.3 °C
250 °C	9.8 °C
200 °C	10.2 °C
150 °C	10.0 °C
100 °C	9.7 °C
50 °C	9.7 °C

RESULTS AND DISCUSSION

The total heat extraction duty of the system was determined with the equation $\dot{Q} = \dot{m} c_p \Delta T$. To determine the heat transfer rate, the characteristics of the water side were used in the calculation.

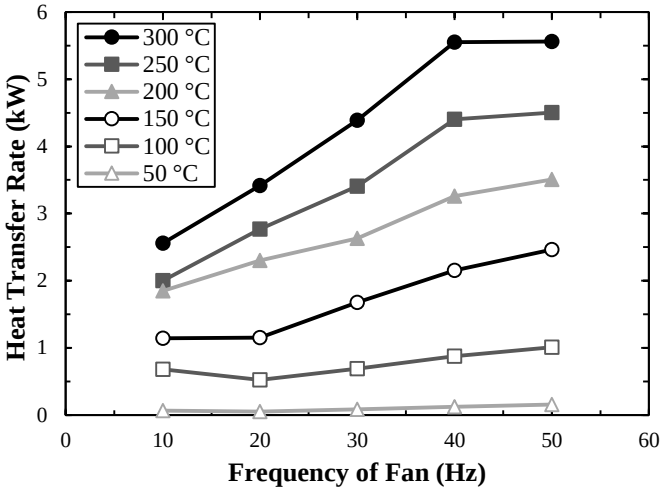

Figure 4 Power output according to Inlet temperature and mass flow rate

The value of the heat transfer rate (Q) was found for every temperature and frequency of fan combination, as can be seen in Figure 4. A pattern occurs for all inlet temperatures: the heat transfer rate increases steadily with an increasing flow rate, and then a "plateau" is reached from 40 Hz to 50 Hz. The "plateau" is a result of the constant mass flow rate on the cold side having reached its saturation point and not being able to absorb any more heat energy. At higher temperatures (200 – 300 °C), the power output seems to be quite similar, following a steady trend.

The temperature distribution profiles can be seen in Figure 5. Here, higher mass flow rates on the hot air side seem to result in smaller temperature differences between the inlet and the outlet of the evaporator, and also higher temperature differences between the inlet and the outlet of the condenser, which is to be expected. According to the charts, the temperature of the adiabatic section suffers a slight fluctuation. This fluctuation is explained by the thermocouples' placements; the adiabatic section is a hollow box and the thermocouples are in contact with the air contained inside this box. Due to the insulation covering the adiabatic section, whenever the temperature or the mass flow rates of the shell-side fluids are changed, the heat energy is kept within, delaying the response of the thermocouples.

The resistance to heat transfer offered by the heat pipe bundle has also been plotted for each different set of data and is presented in Figure 6. A pattern seems to emerge in which higher inlet temperatures have a comparatively lower value of resistance. The resistance is very high at inlet temperatures of 50 °C, (0.3 – 0.8) and that is due to reduced performance of the heat pipe at lower temperature differences between the two streams.

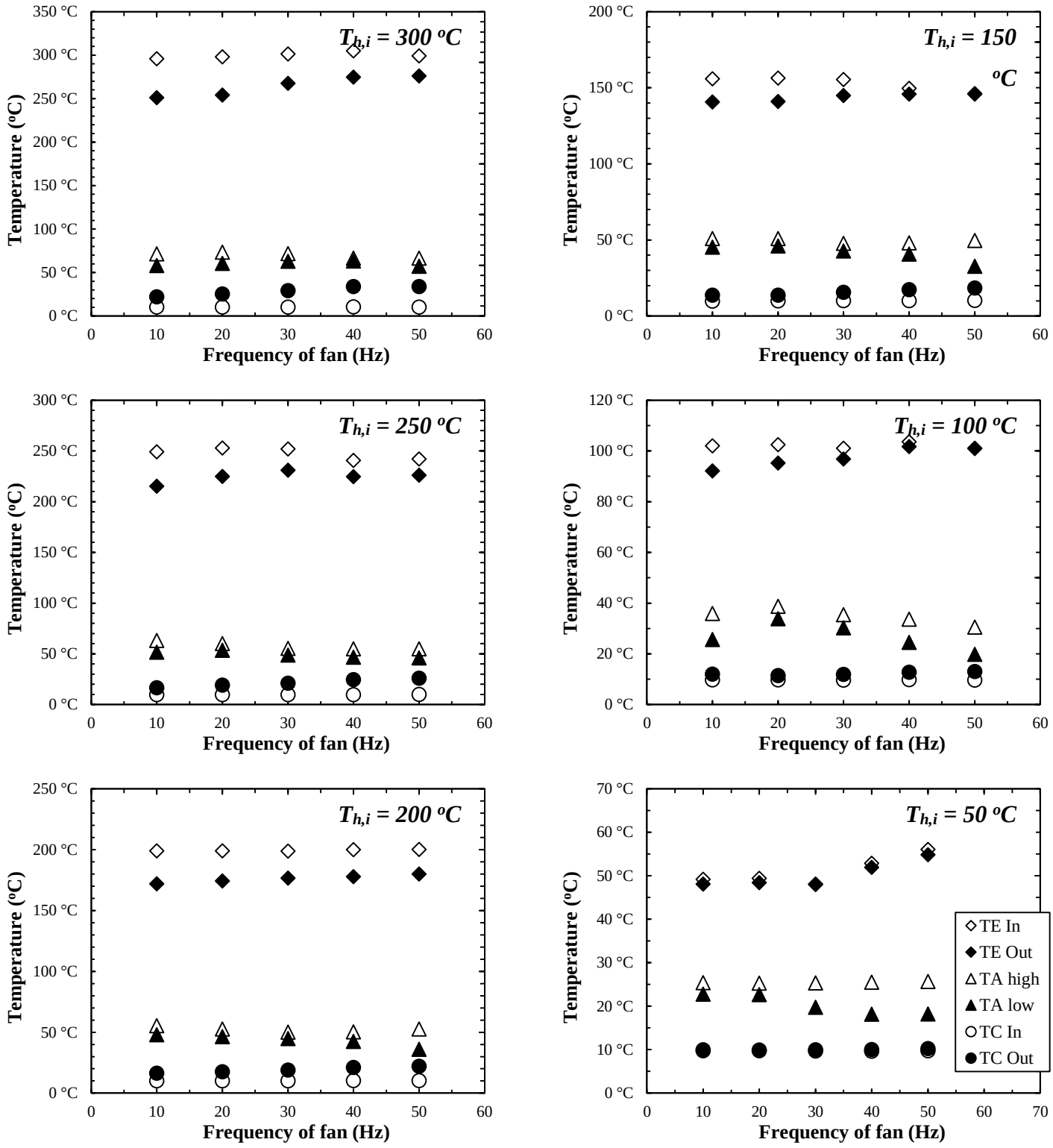

Figure 5 *Temperature distribution profiles through the HPHE at various power throughputs. TE – Temperature in the Evaporator Section; TA – Temperature in the Adiabatic Section; TC – Temperature in the Condenser Section*

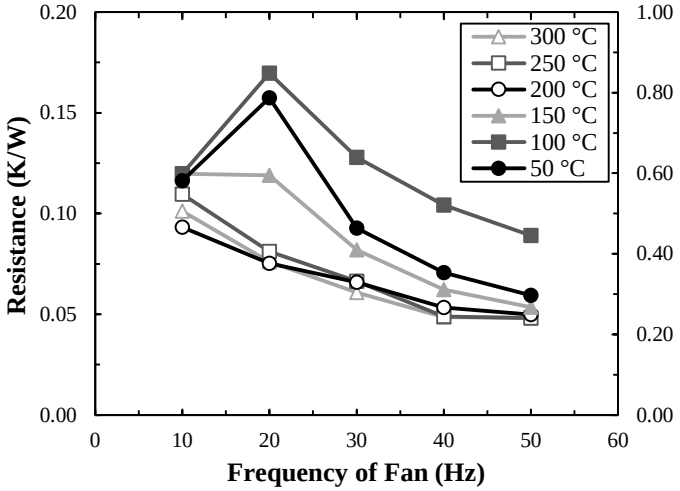

Figure 6 Thermal Resistance of the heat exchanger in relation to the flow conditions at the inlet of the hot air flow (The results for 50 ºC are represented in a different scale)

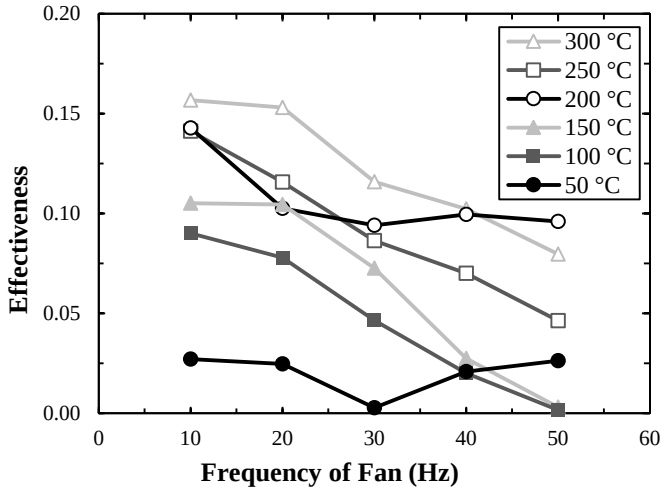

Figure 7 Effectiveness of Heat Exchanger according to different fan frequencies and temperatures

The effectiveness of the heat exchanger exhibits a constant downward trend as the mass flow rate of the hot air increases. This is a direct result of the reduction in the time spent by the hot air within the proximity of the heat pipes.

A constant downward slope can be seen for the effectiveness of all the temperature profiles, which is the result of having a constant mass flow rate in the cold side, limiting the heat absorption potential of the condenser. The tests done at 50 ºC and 200 ºC do not follow the normal downward trend. The irregularity in 50 ºC tests does not come as a surprise as the uncertainty values are relatively high for this test (please refer to Table 3) and the Thermal Resistance (Figure 6) is the highest among all the tested mass flow rates. As for the experiments made at 200 ºC a possible explanation could be that a sudden increase in the mass flow rate of the cold side was not reflected in the experimental data.

ERROR ANALYSIS

The main source of uncertainty for the calculated effectiveness values in Equation (12) came from the temperature measurements of $T_{c,i}$ and $T_{c,o}$, obtained using K-type thermocouples (NiCr/NiAl) and a data logger (DataScan). The uncertainties for K-type thermocouples are estimated to be ±0.05% rdg + 0.3 ºC.

The propagation of uncertainties associated with the calculated effectiveness values can be calculated from:

$$S_\varepsilon = \varepsilon \cdot \sqrt{\left(\frac{S_{Q_c}}{Q_c}\right)^2 + \left(\frac{S_{C_a}}{C_a}\right)^2 + \left(\frac{S_{\Delta T_{max}}}{\Delta T_{max}}\right)^2} \quad (17)$$

Where,

$$S_{Q_c} = Q_c \cdot \sqrt{\left(\frac{S_{FR_w}}{FR_w}\right)^2 + \left(\frac{S_{\Delta T_c}}{\Delta T_c}\right)^2} \quad (18)$$

$$S_{\Delta T_{max}} = \sqrt{\left(S_{T_{h,i}}\right)^2 + \left(S_{T_{c,i}}\right)^2} \quad (19)$$

$$S_{\Delta T_c} = \sqrt{\left(S_{T_{c,o}}\right)^2 + \left(S_{T_{c,i}}\right)^2} \quad (20)$$

Table 3 presents the maximum experimental uncertainty which was more prominent at lower temperatures and mass flow rates.

Frequency	300 ºC	250 ºC	200 ºC	150 ºC	100 ºC	50 ºC
10 Hz	8.11%	9.98%	10.74%	16.83%	*38.29%*	*277.74%*
20 Hz	6.57%	7.80%	8.21%	16.69%	*36.05%*	*371.65%*
30 Hz	5.77%	7.03%	7.11%	12.56%	*29.22%*	*496.06%*
40 Hz	5.25%	6.56%	6.88%	16.65%	*33.95%*	*160.39%*
50 Hz	5.54%	6.27%	5.99%	*125.52%*	*317.47%*	*125.64%*

Table 3 Maximum Uncertainty for Effectiveness (%)

In engineering applications, 10% is usually considered an acceptable value of uncertainty [22]. As can be seen in Table 3, there is a high degree of uncertainty related to the experiments carried out at lower temperatures (represented in Italics); however this is to be expected, as the heat capacity rate of the air side was deduced from the data gathered in the cold side. Furthermore, heat pipes with water as a working fluid are known to perform less efficiently at lower temperatures.

CONCLUSION

An air-to-water heat exchanger equipped with heat pipes was investigated experimentally for a range of inlet flow conditions in the evaporator side. The effectiveness and its relation to the heat transfer rate and the temperature profile have also been determined within the constraints imposed by the experimental rig. The heat transfer rate for the heat exchanger exhibits a constant upward trend as the mass flow rate of the hot air increases. It is only limited at its maximum value by a combination of the inability of the cold water to absorb more heat and the hot air not being allowed enough time in the vicinity of the pipes to transfer the heat conserved within. Although the heat transfer rate increases with increasing mass flow rates, the effectiveness of the heat exchanger exhibits a constant downward trend, as explained before, a result of the hot air not being having enough time to transfer its heat to the pipes. There is lower uncertainty at higher temperatures, which also reveal a higher overall effectiveness and heat transfer rate as well as lower resistance

to heat transfer. The experimental results were in accordance with the numerical approach for shell-and-tube heat exchangers based on current literature, demonstrating that heat pipe equipped heat exchangers may be characterised through the same methods as shell-and-tube heat exchangers by considering the heat pipes as solid objects of constant thermal resistance. It is advised that the tests should be repeated in a more controlled environment in order to reduce the level of uncertainty. Additionally, the effect of the manipulation of the flow characteristics on the water side could be further explored as it was not on the scope of the experiment.

ACKNOWLEDGEMENTS

Special thanks are due to Mr Stefan Munteanu and Mr Peter Blackwell for the fast and flawless way they got the rig ready for experimentation. Thanks are also due to Mr Michael Jones for having helped with the maintenance and technical support.

REFERENCES

[1] United Nations. Kyoto Protocol. 11-12-1997.
[2] Hansen J., Sato M., Ruedy R., Lo K., Lea D.W., and Medina-Elizade M., Global temperature change, *Proceedings of the National Academy of Sciences*, 103 (2006) 14288-14293.
[3] Yang X., Yan Y.Y., and Mullen D., Recent developments of lightweight, high performance heat pipes, *Applied Thermal Engineering*, 33-34 (2012) 1-14.
[4] Jouhara H., and Ezzuddin H., Thermal performance characteristics of a wraparound loop heat pipe (WLHP) charged with R134A, *Energy*, 61 (2013) 128-138.
[5] Dong S.J., Li Y.Z., and J. Wang, Fuzzy incremental control algorithm of loop heat pipe cooling system for spacecraft applications, *Computers & Mathematics with Applications*, 64 (2012) 877-886.
[6] Wang J.C., 3-D numerical and experimental models for flat and embedded heat pipes applied in high-end VGA card cooling system, *International Communications in Heat and Mass Transfer*, 39 (2012) 1360-1366.
[7] Jouhara H., and Robinson A.J., An experimental study of small-diameter wickless heat pipes operating in the temperature range 200C to 450C., *Applied Thermal Engineering*, 30 (2011) 1041-1048.
[8] Chaudhry H.N., Hughes B.R., and Ghani S.A., A review of heat pipe systems for heat recovery and renewable energy applications, *Renewable and Sustainable Energy Reviews*, 16 (2012) 2249-2259.
[9] Akbarzadeh A., Johnson P., Nguyen T., Mochizuki M., Mashiko M., Sauciuc I., Kusaba S., and Suzuki H., Formulation and analysis of the heat pipe turbine for production of power from renewable sources, *Applied Thermal Engineering*, 21 (2001) 1551-1563.
[10] Wang Z., Duan Z., Zhao X., and Chen M., Dynamic performance of a façade-based solar loop heat pipe water heating system, *Solar Energy*, 86 (2012) 1632-1647.
[11] Zhang X., Zhao X., Xu J., and Yu X., Characterization of a solar photovoltaic/loop-heat-pipe heat pump water heating system, *Applied Energy*, 102 (2013) 1229-1245.
[12] Nithyanandam K., and Pitchumani R., Computational studies on a latent thermal energy storage system with integral heat pipes for concentrating solar power, *Applied Energy*, 103 (2013) 400-415.
[13] Jouhara H., Anastasov V., and Khamis I., Potential of heat pipe technology in nuclear seawater desalination, *Desalination*, 249 (2009) 1055-1061.
[14] Laubscher R., and Dobson R.T., Theoretical and experimental modelling of a heat pipe heat exchanger for high temperature nuclear reactor technology, *Applied Thermal Engineering*, 61 (2013) 259-267.
[15] Wadowski T., Akbarzadeh A., and Johnson P., Characteristics of a gravity-assisted heat pipe-based heat exchanger, *Heat Recovery Systems and CHP*, 11 (1991) 69-77.
[16] Hagens H., Ganzevles F.L.A., van der Geld C.W.M., and Grooten M.H.M., Air heat exchangers with long heat pipes: Experiments and predictions, *Applied Thermal Engineering*, 27 (2007) 2426-2434.
[17] Noie, S.H. Investigation of thermal performance of an air-to-air thermosyphon heat exchanger using e-NTU method, *Applied Thermal Engineering*, 26 (2006) 559-567.
[18] Incropera F., and Dewitt D., Fundamentals Of Heat And Mass Transfer, 4th Ed, John Wiley & Sons, 1996.
[19] ESDU 81038. Heat pipes - performance of two-phase closed thermosyphon, *Engineering Sciences Data Unit*, 1983.
[20] Faghri A. Heat pipe science and technology, Taylor & Francis, 1995.
[21] Jouhara H., and Merchant H., Experimental investigation of a thermosyphon based heat exchanger used in energy efficient air handling units, *Energy*, 39 (2012) 82-89.
[22] Taylor, JR. An introduction to error analysis: the study of uncertainties in physical measurements, University Science Books, 1997.

EXPERIMENTAL AND NUMERICAL INVESTIGATION OF AN AIR-TO-WATER HEAT PIPE-BASED HEAT EXCHANGER

H. Mroue[1,2], J.B. Ramos[1], L.C. Wrobel[2], H. Jouhara[*,1]
[1]Institute of Energy Futures, RCUK Centre for Sustainable Energy Use in Food Chains (CSEF),
[2]Institute of Materials and Manufacturing

College of Engineering, Design and Physical Sciences, Brunel University London, Uxbridge UB8 3PH, UK
[*]Corresponding author: hussam.jouhara@brunel.ac.uk

Abstract

An experimental and analytical investigation was conducted on an air-to-water heat exchanger equipped with six wickless heat pipes charged with water as the working fluid. The flow pattern consisted of a double pass on the evaporator section and simple cross flow in the condenser. The six heat pipes were all made from carbon steel, measured 2m in length and were installed in a staggered arrangement.

The objectives of the reported experimental investigation were to analyse the effect of multiple air passes at different air inlet temperatures (100 to 250°C) and air mass flow rates (0.05 to 0.14kg/s) on the thermal performance of the heat exchanger unit including the heat pipes. The results were compared with a CFD model that assumed the heat pipes were solid rods with a constant conductivity. The conductivity of the pipes was extracted from modifications of correlations available in the literature based around the theory of Thermal Resistance. The results proved to be very accurate within 10% of the experimental values.

keywords: *heat pipe, thermosyphon, heat exchanger, CFD, Effectiveness*

1. Introduction

Heat pipe-based heat exchangers are finding increased usage in a variety of applications due to new environmental policies to reduce exhaust temperatures and the carbon footprint of many industries [1,2]. These devices uniqueness derives from the use of heat pipes, responsible for increasing the heat exchanger's reliability, flow separation, ease of operation, system efficiency and reducing the overall manufacturing and maintenance cost. A heat pipe is essentially a superconductor [3], consisting of a sealed and evacuated tube partially filled with a working fluid. The working fluid is responsible for the device's high heat transfer capabilities as when faced with a temperature difference it enters a state of evaporation/condensation, allowing large quantities of heat to be transferred at an essentially constant temperature.

Heat pipe-based heat exchangers find use in a wide variety of industries, such as space [4], computing and electronics [5], ventilation and air conditioning (including dehumidification devices) [6], solar energy systems [7], water desalination [8], and nuclear systems [8,9], from temperatures below zero degrees [10], to as high as 950°C [11], depending on the materials composing the pipe and the working fluid used.

The basic operation of a wickless heat pipe relies upon a difference in temperature between both ends of the pipe. Upon coming into contact with a heat source, the working fluid inside the pipe evaporates, transporting the heat to the top of the pipe. When this vapour makes contact with the cooler wall of the pipe at the top, it condenses, releasing its latent heat and changing phase, the change in density causing it to flow back to the evaporator in liquid form to complete the working cycle [12].

There is a particular characteristic that can change a heat pipe's working principle and that is the existence or lack of a wick structure. Heat pipes found in electronic components have a built-in wick structure that allows them to work against the force of gravity, due to capillary pressure being exerted on the fluid. Heat pipes applied in industrial heat exchangers are devoid of a wick in order to keep costs in check without suffering from reduced heat transfer performance. A schematic of a wickless heat pipe can be seen in Figure 1. Wickless heat pipes are technically named two-phase closed thermosyphons or gravity-assisted heat pipes and are the ones used in the experiment described in this paper.

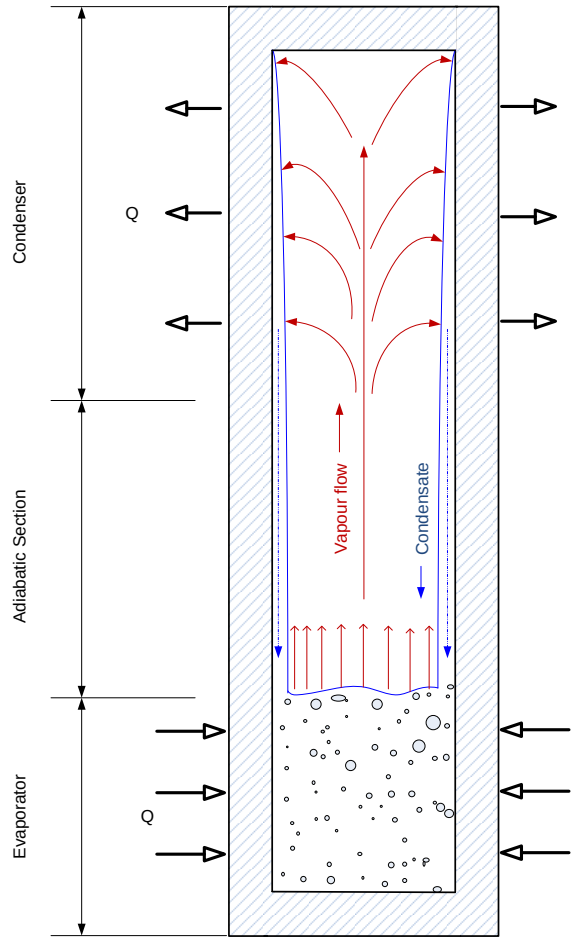

Figure 1 – Schematic of a working two-phase closed thermosyphon.

A heat pipe-heat exchanger is usually divided in three parts: evaporator, adiabatic section and condenser, which coincide with the parts of the heat pipe as can be seen in Figure 1. In the evaporator of the heat exchanger under investigation, the air passes through the pipes twice in what is effectively called "two passes", as can be seen in Figure 2Figure . The purpose of having two passes in the evaporator section is to balance the temperature field.

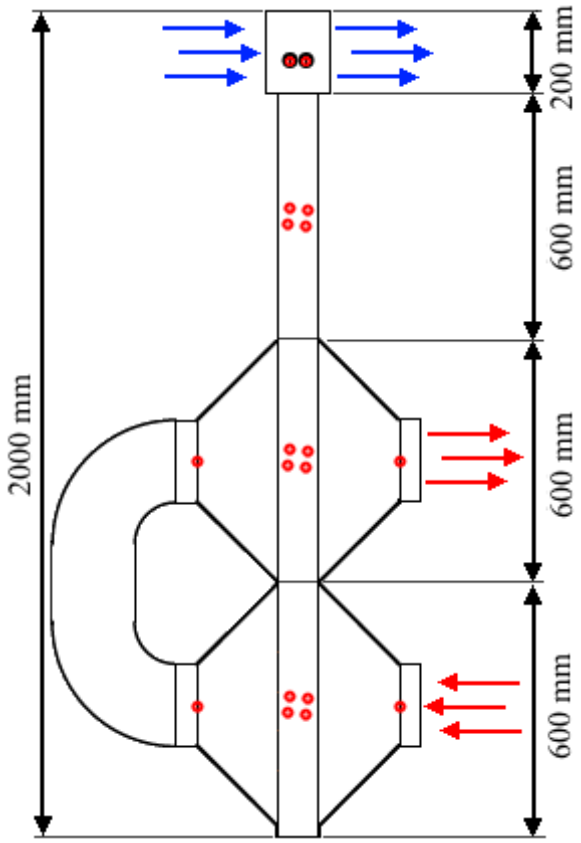

Figure 2 – Schematic representation of the heat pipe heat exchanger thermocouple locations (each red dot represents a K-type thermocouple) and dimensions (all in mm).

The temperature of the working fluid inside each thermosyphon is effectively the same throughout the length of the pipe (±1 °C) due to the constant phase change process, but depending on the flows in contact with the pipe, this temperature will differ depending on the position of the pipe within the heat exchanger. This means that the pipes in the front row will be subjected to a higher temperature when compared to the ones in the latter rows. According to the basic laws of heat transfer, heat energy is a function of the flow rate, the specific heat of the fluid in question and the difference in temperature between the flow and the surface of the object in question [13]. A higher difference in temperature results in a higher amount of heat transferred, and that is where the double pass comes into play to increase the heat transfer potential of the pipes on the back rows. By having the flow double back and pass through the pipes again, the pipes in the back row are given more heat, normalising the working temperatures of the heat pipes in the heat exchanger. The main purpose of the design is the normalisation of the working temperatures, but there are other advantages to be had from the inclusion of a baffle in the evaporator, such as an increase in the fluid velocity in the vicinity of the pipes resulting in an increase in turbulence. The Nusselt number is directly proportional to the Reynolds number (turbulence) which results in higher heat transfer coefficients. In order to determine the heat transfer coefficient on the shell sides, there are widely accepted correlations derived from empirical studies, as noted by Incropera & DeWitt [14]. The flow in the condenser section makes contact with the pipes linearly and according to the numbering of the pipes, as seen in Figure 3.

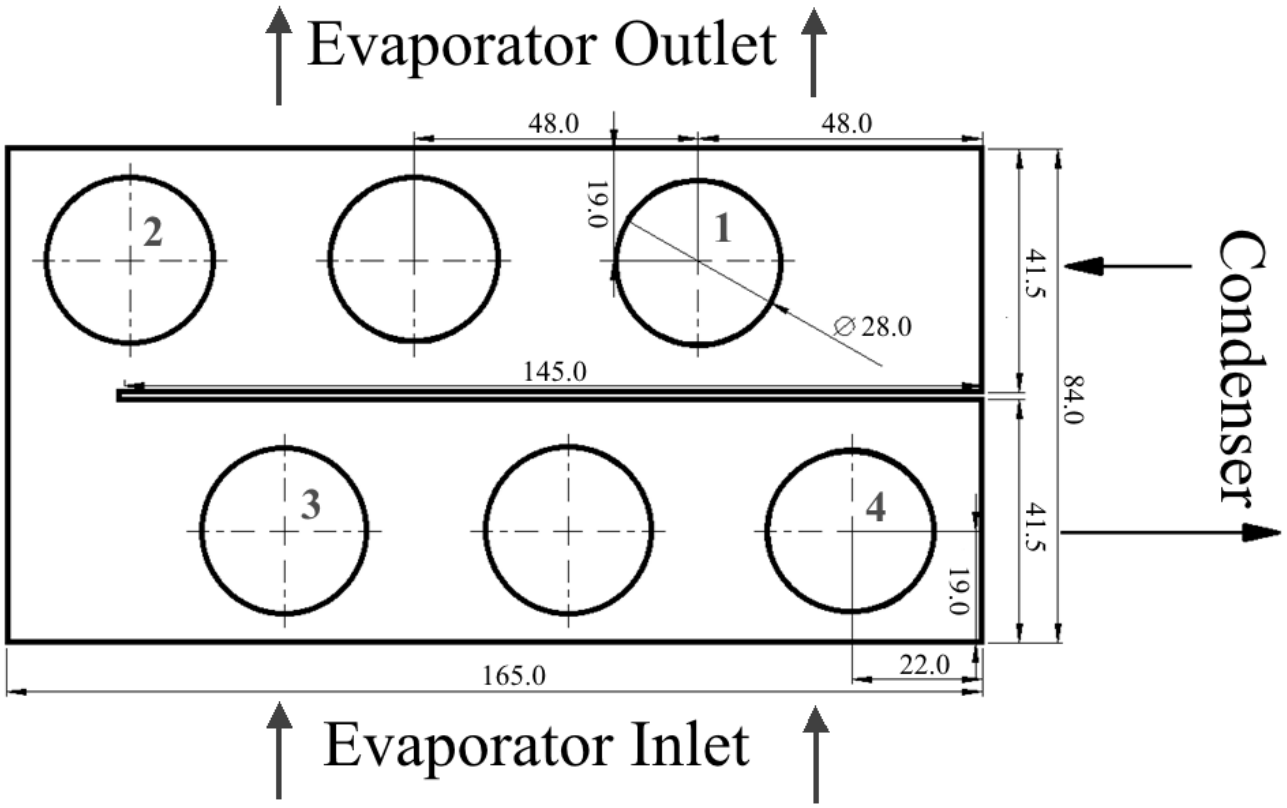

Figure 3 – Top down view of a cross section of the condenser section. The pipes numbered are the pipes with thermocouples on their surface.

Danielewicz et al. [15] have conducted an investigation of an air-to-air heat exchanger with a similar geometry and produced a correlation which allowed the prediction of multiple variables related to heat exchanger performance based on the inlet conditions. A similar principle was used in this investigation; the experimental results were compared and validated through Computational Fluid Dynamics. Jouhara and Merchant [16] have also conducted an experimental study of a gas-to-air heat pipe-based heat exchanger of similar design, demonstrating the effect of different flow rates on the effectiveness of the heat exchanger.

In this paper, a two-pass heat pipe-based heat exchanger is investigated with the objective of balancing the working temperatures inside the heat pipes. There are multiple correlations available in the literature for multi pass shell and tube heat exchangers [17]. The addition of heat pipes to the geometry adds some further complexity to the correlations due to the boiling and condensation processes constantly taking place inside the pipe.

2. Test facility design

The design of the test unit under study (shown in Figure 4) was based on a real heat exchanger unit currently in use albeit at a smaller scale. The model was equipped with six heat pipes arranged vertically in two rows of three pipes each. The experimental rig was divided in two circuits: the heat source consisted of a closed air circuit located in the lower part of the heat exchanger whereas the heat sink was an open-ended water circuit located at the top of the heat exchanger, as can be seen in Figure 5.

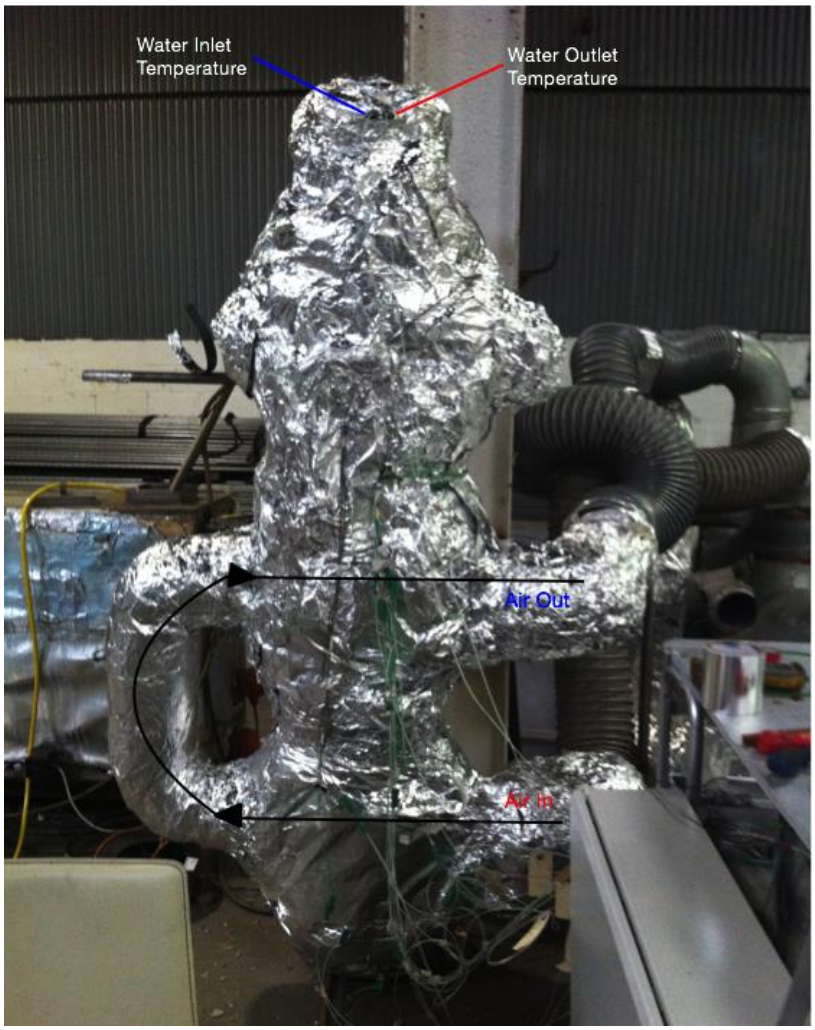

Figure 4 – Actual test rig used for testing.

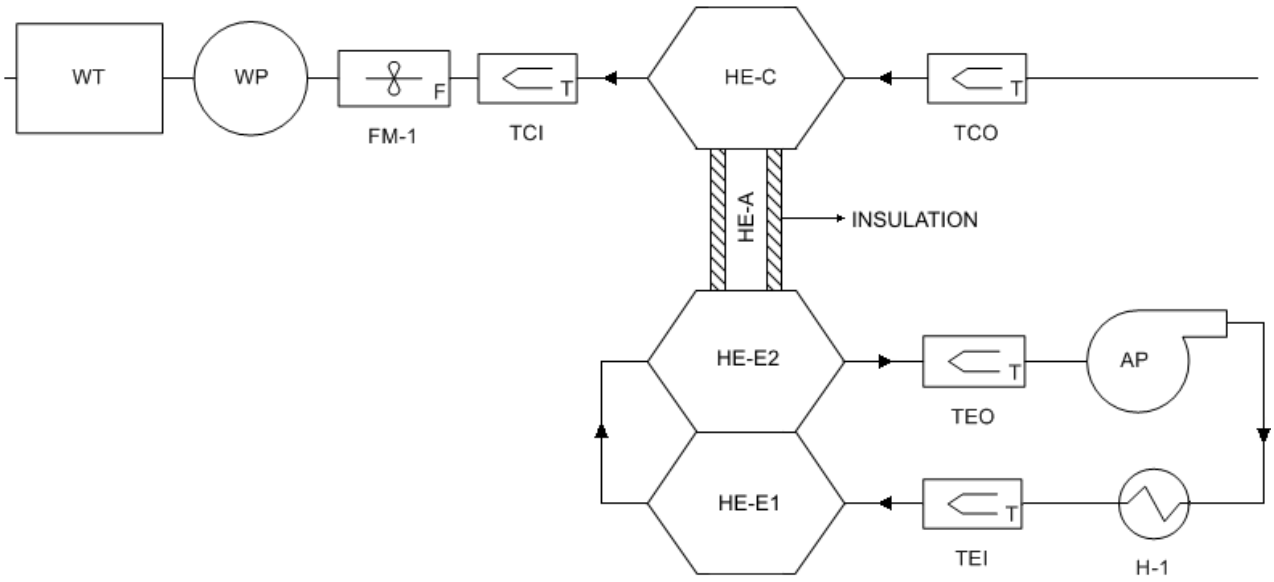

Figure 5 – Schematic drawing of the Heat Exchanger: WT–Water Tank, WP–Water Pump, FM–Flow Meter, TCI–Thermocouple Condenser Inlet, TCO–Thermocouple Condenser Outlet, AP–Air Pump, H–Heater, TEI–Thermocouple Evaporator Inlet, TEO–Thermocouple Evaporator Outlet, HE-Heat Exchanger, A-Adiabatic, C-Condenser, E-Evaporator.

The mass flow rate of the air circuit was controlled by a centrifugal fan, which forced the air through a heater and into the heat exchanger. The heater's power was controlled by a feedback system receiving data from a thermocouple placed at the inlet of the first evaporator section. The hot air then travelled through both evaporator sections and was then led back into the fan, closing the cycle.

The cold water circuit was kept at a constant flow rate and temperature, controlled by a constant water head on the water tank and the temperature by a small cooler located within the tank.

K-type thermocouples were placed at the inlet and outlet of each air pass and water pass to measure the temperature of the fluid. A total of 22 thermocouples were placed in specific locations within the evaporator, adiabatic and condenser sections (see figure 2). The thermocouples were connected to a data-logging device to gather information of the flow temperature behaviour within the heat exchanger unit.

There was a thermocouple installed at the inlet and outlet of each section, four in the evaporator section as two were needed for each "pass". In addition, there were two thermocouples on the surface of each pipe at the evaporator section, one in the adiabatic section and one in the condenser section.

3. Test piece design

When characterising heat pipes and consequently heat pipe heat exchangers, it is customary to divide them into three separate sections: evaporator, adiabatic section and condenser. The evaporator section comprises the hot air circuit where heat is added to the system, the condenser section includes the water circuit and serves as the heat sink, and the adiabatic section is simply the insulated area in the middle of both where, theoretically, no heat transfer takes place.

The unit under investigation was equipped with six thermosyphons arranged vertically. The heat pipes were made of carbon steel and each measured 2 m with a diameter of 28 mm. The average wall thickness of the pipes was 2.5 mm giving them an average inner diameter of 23 mm. The heat pipes were chemically treated from inside to prevent corrosion from the working fluid and then filled with distilled water to half the volume of the evaporator section.

The evaporator part of the heat exchanger was divided into two sections each spanning 0.6 m of the pipe's length. As the hot air entered the heat exchanger, it flowed over the lower 0.6 m of the pipes. Then it was led through two 90 degree bends to come back in between 0.6 m and 1.2 m of the bottom of the heat exchanger, making contact with the surface of the pipes in that location. Taking into account the pipes were filled to 50% of the total evaporator length, the double hot air pass allows the investigation of the heat transfer performance on the pool boiling and on the film condensate at the inner walls of the heat pipe. Each "pass" measured 0.6 m, the first physically displayed under the second, as can be seen in Figure 2.

The condenser section was located on the top of the heat exchanger, occupying exactly 0.2 m and sweeping the 6 heat pipes one by one.

It was observed that the temperature measured at the adiabatic section of the heat pipe coincided with the value for the saturation temperature of the working fluid. The thermocouples located on the outer surface of the adiabatic section of selected heat pipes allowed the reading of the saturation temperature of that particular heat pipe. They were placed at exactly 1.5 m from the bottom of the unit (Figure 2).

4. Operational procedure

The performance of the test rig was monitored for an average of one hour of steady state per combination of mass flow rate and temperature. Only two parameters were varied during the experiment: the inlet air

temperature and the mass flow rate. In the evaporator side, the air inlet temperature was controlled by the heater and varied between 100°C and 250°C at 50°C increments while the mass flow rate was controlled by the fan frequency which varied between 0.05 kg/s and 0.14 kg/s at 0.03 kg/s increments.

In the condenser side, the water inlet temperature and flow rate were kept constant throughout the experiments. The water was kept at an average temperature of 14°C and the mass flow rate was kept at an average of 0.08 kg/s.

5. CFD Boundary Conditions

ANSYS Fluent was used to develop a numerical model to simulate the external heat flow over the pipes on both the air side (evaporator) and the water side (condenser). The model was developed in order to assess the efficiency of simulating the pipes as solid rods of constant conductivity for future heat exchanger modelling. For the model, the standard k-epsilon (k- ε) turbulence model was used for all the tested results. The pressure-based coupled solver is the recommended choice as it offers a better result for a single-phase fluid flow, and is more consistent and efficient at steady-state [18].

The characteristics of the fluids in question (water and air) were based on standard tables of material properties [18]. The heat pipes were modelled as solid rods of conductivity k, a value derived from equations adapted from literature and described in detail in the next section. The inlet and outlet conditions for the heat exchanger can be seen in Table 1; boundary conditions of type "mass flow inlet" were used for both flows, with the outflow being in the opposite direction. For the air, the assumption was valid as it consisted of a closed circuit, so the air was being pulled out of the evaporator section at the outlet. Water is incompressible at normal atmospheric conditions and since the condenser had been completely purged of air, the flow at the outlet was safely assumed to be the same at the inlet, thus justifying the assumption. All the walls of the heat exchanger were considered to be adiabatic as they were well insulated in the experimental rig.

The CFD was run multiple times for each range of inlet conditions used in the experimental test.

Table 1 – Boundary Conditions.

	Type	Mass flow rate (kg/s)	Temperature (ºC)
Evaporator Inlet	Mass Flow Inlet	0.05 to 0.14 at 0.03 intervals	100 to 300 at 50 intervals
Evaporator Outlet	Outflow	-	*Desired Output*
Condenser Inlet	Mass Flow Inlet	constant 0.08	Varied between 13 and 14
Condenser Outlet	Outflow	-	*Desired Output*

6. Governing Equations

The conductivity of the heat pipe k, as mentioned before, was derived from equations found in the literature; more specifically, from the resistance to heat transfer offered by the heat pipes within the heat exchanger (K/W). This total resistance to heat transfer may be represented by [19]:

$$R_T = \frac{\Delta T_{LM}}{\dot{Q}_t} \tag{3}$$

ΔT_{LM} represents the logarithmic mean temperature difference and $\dot{Q}_T$ the heat transfer rate (W). Equation (2) clearly shows that the total thermal resistance is an inverse to the total rate of heat transfer in a heat exchanger, represented below:

$$\dot{Q}_T = U A_T \Delta T_{LM} \tag{4}$$

U represents the overall heat transfer coefficient (W/m^{2}K), A_T the total heat surface area and ΔT_{LM} the Logarithmic Mean Temperature Difference.

In order to break down the total thermal resistance (R_T) into all its constituent parts, an analogy to an electrical resistance ought to be done. The total resistance for a single heat pipe is a sum of the resistances for each mode of heat transfer:

$$R_{hp} = \left(\frac{1}{R_{k,e}+R_{h,film\,b}} + \frac{1}{R_{k,e}+R_{h,pool\,b}}\right)^{-1} + R_{hp,inner} + R_{h,condensation} + R_{k,c} \qquad (5)$$

The subscript *h* represents convection, *k* conduction, *b* boiling, *e* evaporator and *c* condenser. Nucleate film boiling and pool boiling take place in parallel while the other modes of heat transfer take place in series. The method to determine the internal resistances of the thermosyphon is made available by the Engineering Sciences Data Unit (ESDU) [20]. Considering that all the pipes in this particular configuration are 6 resistances in parallel, the total resistance will be:

$$\frac{1}{R_{6hp}} = \frac{1}{R_1} + \frac{1}{R_2} + \frac{1}{R_3} + \frac{1}{R_4} + \frac{1}{R_5} + \frac{1}{R_6} \qquad (6)$$

Assuming all the heat pipes have the same thermal resistance (R_{hp}), the total thermal resistance offered by the six heat pipes can be determined from:

$$R_{6hp} = \frac{R_{hp}}{6} \qquad (7)$$

and the total thermal resistance of the heat exchanger becomes:

$$R_T = R_{6hp} + R_{h,e} + R_{c,e} \qquad (8)$$

Moving back to equation 3, in order to find the different values of resistance to complete the equation, the heat pipe is divided in at least 3 parts; the evaporator section, the condenser section and the adiabatic section. The evaporator section is further divided into a lower half and an upper half.

Inside the heat pipe, there are at least three different heat transfer mechanisms at work: pool boiling, nucleate film boiling and film condensation; pool boiling takes place in the first pass of the heat exchanger, film boiling on the second and film condensation on the condenser section. There are expressions available in the literature for each of these heat transfer mechanisms and some of them were adapted in order to better suit this application.

Looking at the evaporator section, the first heat transfer mode from the fluid to the pipe is made through convection and given by the general equation below, displaying the following resistances to heat transfer:

$$\dot{Q}_h = hA\Delta T \quad \therefore \quad R_{h,e} = \frac{1}{h_e A_e} \quad and \quad R_{h,c} = \frac{1}{h_c A_c} \qquad (9)$$

where *h* refers to the heat transfer coefficient (W/m^{2}K) between the fluid and the solid surface, which in our case is air-carbon steel and water-carbon steel. The subscript *h* refers to convection heat transfer. *A* is the surface area or exposure (m^2) and ΔT the difference in temperature between the two.

Moving with the flow of heat the next barrier is the pipe wall, and heat is transferred by conduction, to which the general equation is the following:

$$\dot{Q}_k = \frac{2\pi k l \Delta T}{\ln(r_{out} - r_{in})} \quad \therefore \quad R_k = \frac{\ln(r_{out} - r_{in})}{2\pi k l} \tag{10}$$

where k is the thermal conductivity, L is the length of the pipe subjected to the two different flows, $r_{out} - r_{in}$ represent the tube thickness and ΔT is the difference in temperature between the inside and the outside of the pipe. This equation will be applied to the two evaporator sections and the condenser section. It is mainly affected by the area of exposure and the conductivity of the material.

The next heat transfer process is boiling, in which the heat travels from the pipe wall to the working fluid. This process essentially consists of pool boiling, whose correlation is given by Rohsenow [21]:

$$\frac{\dot{q}}{A} = \mu \times h_{fg} \times \sqrt{\frac{g(\rho_L - \rho_v)}{\sigma}} \times \left(\frac{c_p \Delta T_b}{h_{fg} C_{sf}}\right)^{1/m} \times Pr^{-n/m} \tag{11}$$

C_{sf} is a constant for boiling, which changes in accordance to different surface materials and fluids. All thermophysical properties of the fluid are evaluated at the saturation temperature. m and n are constants, m is generally 1/3, n is 1.0 for water and 1.7 for other fluids.

Looking at the second pass, there is also evaporation on the condensate flowing down to the evaporator. The heat transfer coefficient for nucleate film boiling is the following [22]:

$$\frac{\dot{q}}{A} = 1.155 \times 10^{-3}\, Nu_{\mu f}^{0.33}\, Pr_l^{0.35}\, K_p^{0.7} \left(q_e l_m / \left(\rho_V h_{fg} \upsilon_l\right)\right)^{0.7} \times \Delta T_b k / l_l \tag{12}$$

where K_p is a dimensionless parameter inverse to surface tension, l_m the bubble length scale and l_l the film thickness scale. Each equation is applied for each different surface area and the heat transfer to the top of the heat exchanger can be determined, assuming there are no heat losses at the adiabatic section as the fluid travels up and down the pipe. After getting to the top section, where the walls are cooler the fluid will condense, giving its latent energy to the wall. For this heat transfer, the laminar condensation from Nusselt is used [23]:

$$h_m = 0.943 \times \left(\frac{{k_L}^3 \rho_L (\rho_L - \rho_V) g\, h_{fg}}{\mu_l\, \theta\, l}\right)^{1/4} \tag{13}$$

McAdams [24] suggests that experimental values are often 20% larger than theoretical values, and we can also assume that $\rho_l \gg \rho_v$ which simplifies our equation into:

$$h_m = 1.13 \times \left(\frac{{k_L}^3 {\rho_L}^2 g\, h_{fg}}{\mu_l\, \theta\, l}\right)^{1/4} \tag{14}$$

7. Heat Exchanger Effectiveness Model

A numerical effectiveness model was developed based on the data gathered in order to predict the effectiveness of the heat exchanger. The effectiveness is the ratio of the actual heat transfer rate to the maximum theoretical heat transfer rate and it is determined from the following expression after the outlet conditions are known [25]:

$$\varepsilon = \frac{\dot{Q}_{actual}}{\dot{Q}_{max}} = \frac{C_w(T_{c,o} - T_{c,i})}{C_{min}(T_{max} - T_{min})} = \frac{C_w(T_{c,o} - T_{c,i})}{C_{min}(T_{h,i} - T_{c,i})} \tag{15}$$

where $\dot{Q}$ represents the heat transfer rate, C_w refers to the heat capacity rate for water (subscript w) and C_{min} represents the minimum heat capacity rate between the water side and the air side. T_c refers to the condenser side and T_h to the evaporator side.

The effectiveness determined through equation (12) can then be used to determine the heat transfer rate of the heat exchanger through the following expression:

$$\dot{Q} = \varepsilon \cdot \dot{Q}_{max} \tag{16}$$

Going back to equation (12), the maximum heat extraction rate can be found by multiplying the minimum heat capacity rate by the maximum difference in temperature, which in this case is the difference between the inlet temperatures:

$$\dot{Q}_{max} = C_{min}\left(T_{h,in} - T_{c,in}\right) \tag{17}$$

Through manipulation of the above equation, the outlet temperatures can be predicted as follow:

$$T_{h,out} = T_{h,in} - \frac{\dot{Q}}{C_h} \tag{18}$$

$$T_{c,out} = T_{c,in} + \frac{\dot{Q}}{C_c} \tag{19}$$

8. Mesh selection

Three meshing levels were generated: coarse, medium and fine. In the case of hexahedron or tetrahedron meshes, the maximum skewness should be lower than 0.7, while in triangular elements, it must be less than 0.8 [18]. There was also inflation included around the pipes in order to better simulate the heat transfer between the pipes and the other volumes.

Table 2 – Mesh Dependency.

Level	No of Cells	Type of cells	Skewness	Time per iter.
Coarse	798,852	Hex + Tetra	av: 28%, stdev: 20%	5-10 s
Medium	1,299,435	Hex + Tetra	av: 22%, stdev: 13%	7-15 s
Fine	2,948,489	Hex + Tetra	av: 22%, stdev: 13%	30-50 s

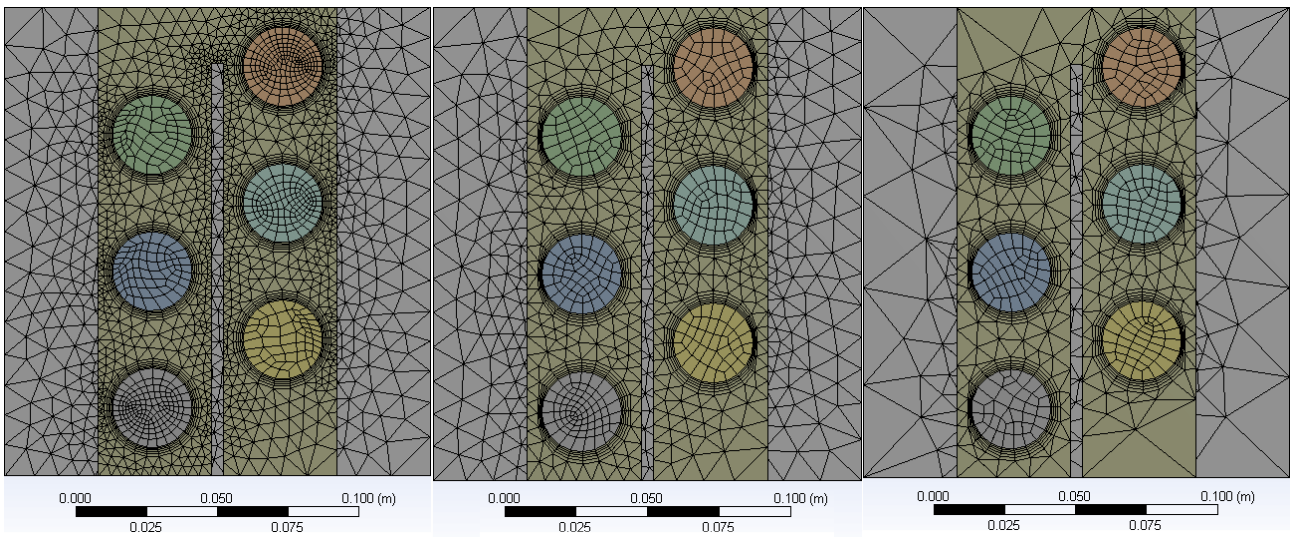

Figure 6 – Comparison between the three different meshes – Fine, Medium and Coarse, respectfully.

Two evaporator inlet conditions were considered for which the experimental results were compared to the simulated results. The results provided by the medium mesh were the most acceptable in the end taking into account the time taken until convergence is observed.

Table 3 – Mesh comparison (the percentage error is shown in brackets).

Inlet Conditions:	T_{out} Exp.	T_{out} Fine Mesh	T_{out} Medium Mesh	T_{out} Coarse Mesh
$T_{h,in}$ = 250 ºC, $\dot{m}_{h,in}$ = 0.14 kg/s	205.0 °C	214.4 °C (*+4.6%*)	215.2 °C (*+5.0%*)	225.4 °C (*+9.9%*)
$T_{c,in}$ = 14.8 ºC, $\dot{m}_{c,in}$ = 0.08 kg/s	33.1 ºC	30.6 °C (*-7.6%*)	30.4 °C (*-8.1%*)	27.8 °C (*-16.0%*)
$T_{h,in}$ = 150 ºC, $\dot{m}_{h,in}$ = 0.08 kg/s	124.9 °C	124.0 °C (*-0.7%*)	123.9 °C (*-0.9%*)	117.8 °C (*-5.6%*)
$T_{c,in}$ = 14.8 ºC, $\dot{m}_{c,in}$ = 0.08 kg/s	21.9 °C	22.6 °C (*+3.1%*)	22.8 °C (*+4.1%*)	24.8 °C (*+13.5%*)

The comparison between the meshes is laid out in Table 3 for two different inlet conditions. The first three rows represent the air inlet conditions at 250 °C and 0.14 kg/s, and the last three rows represent the air inlet conditions at 150 °C and 0.08 kg/s, the water inlet conditions are the same for both (14.8°C and 0.08 kg/s). The first column shows part of the inlet boundary conditions, the second column displays the outlet temperatures of the experimental test and the next three columns show the predicted CFD results for each different element sizing method.

The medium mesh was selected as the best alternative for all the CFD simulations due to the fact that the results were not much improved by refining the mesh. Regardless of this fact, it can be observed that all the flows appeared to extract more heat than in the experimental test. This is to be expected, taking into account the walls of the pipes in the adiabatic section of the CFD simulation were 100% adiabatic (Q = 0) whereas in real life there are always some differences in temperature even with the best possible insulation as was the case.

9. Results and discussion

A plot of the temperatures versus the mass flow rates was created to ensure the results were consistent. Figure 7-11 show the temperature of the flow at the inlets and outlets of the evaporator and condenser sections of the heat exchanger. It can be observed that the duty of the heat exchanger increases at higher mass flow rates and higher temperatures, shown by the greater difference in temperature in the water side at higher temperatures and mass flow rates.

At lower flow rates, the pipe is given more time to absorb the heat and that is reflected in an increase of the temperature difference across the evaporator, but as has been mentioned before, this does not reflect an increase in the duty or total heat transfer rate, shown in Figure 11.

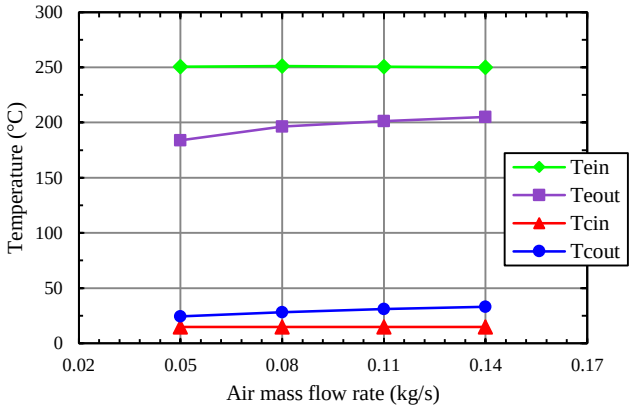

Figure 7 – Temperature distribution along the heat exchanger for 250 °C inlet temperature.

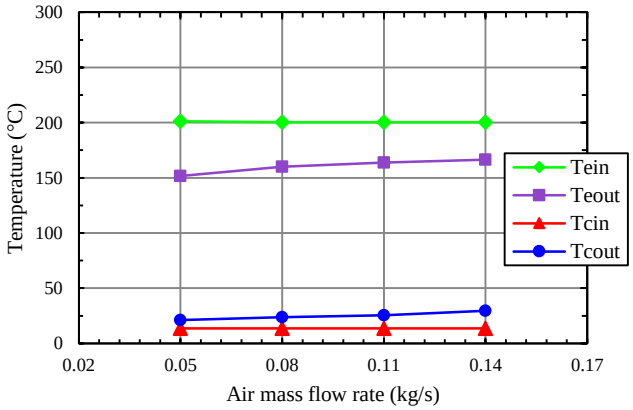

Figure 8 – Temperature distribution along the heat exchanger for 200 °C inlet temperature.

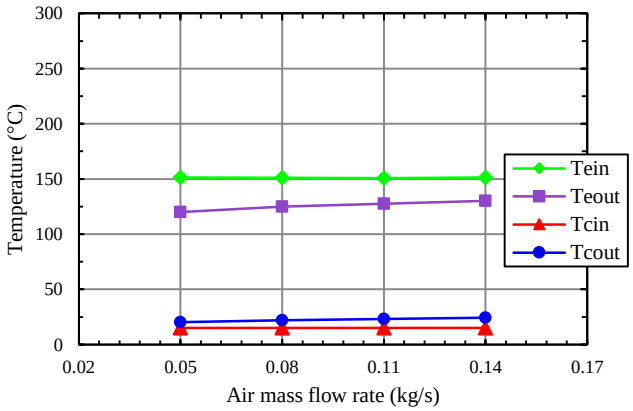

Figure 9 – Temperature distribution along the heat exchanger for 150 °C inlet temperature.

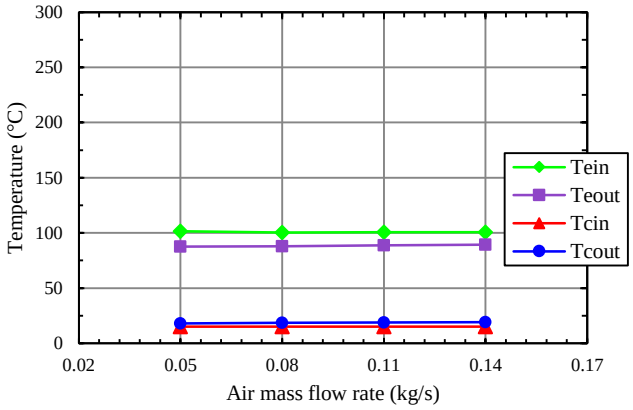

Figure 10 – Temperature distribution along the heat exchanger for 100 °C inlet temperature.

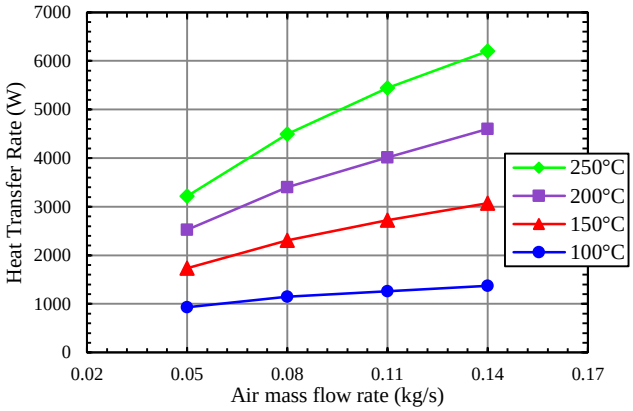

Figure 11 – Heat Transfer Rate of the Heat Exchanger according to the inlet conditions.

Figure 12 to Figure 15 compare the working temperature of the heat pipes for each inlet condition. The working temperature increases with the increase in mass flow rate and inlet temperature at the evaporator section, as expected. However, there is a difference in temperature between each individual pipe. The pipes were numbered in accordance to the diagram in Figure 5.

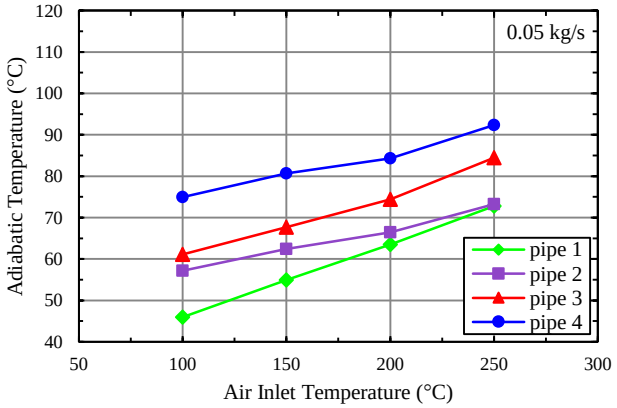

Figure 12 – Working temperature of each pipe for different inlet temperatures (ṁ = 0.05 kg/s).

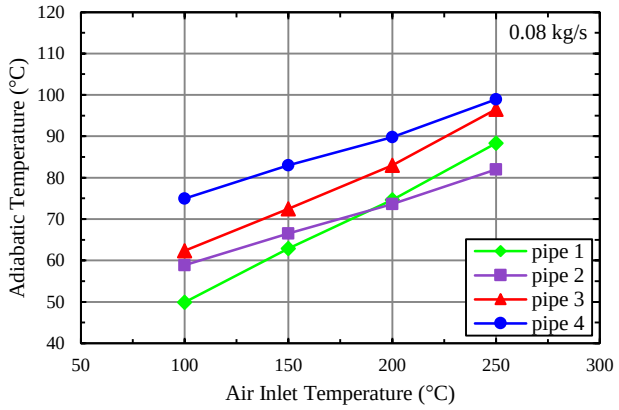

Figure 13 – Working temperature of each pipe for different inlet temperatures (ṁ = 0.08 kg/s).

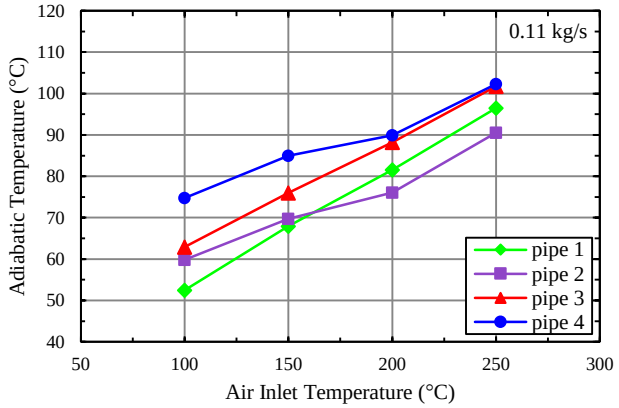

Figure 14 – Working temperature of each pipe for different inlet temperatures (ṁ = 0.11 kg/s).

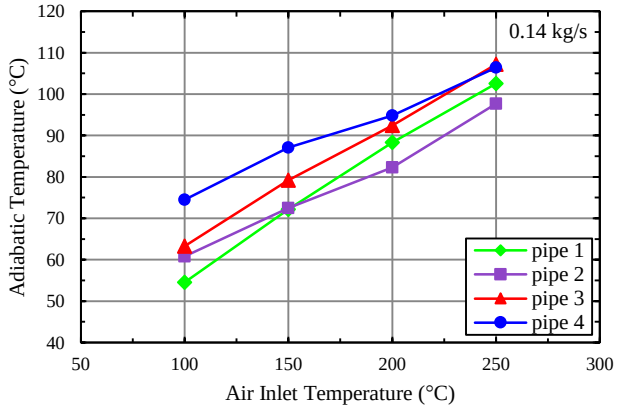

Figure 15 – Working temperature of each pipe for different inlet temperatures (ṁ = 0.14 kg/s).

It can be observed that the heat pipe with the highest average working temperature is pipe 4; it is located on the row of pipes that first make contact with the hot flow at the first pass and it is the heat pipe furthest away from the condenser inlet. After pipe 4, all the pipes follow in the inverse order to the condenser section, therefore 3 has the next highest average temperature, followed by 2 and 1, the closest to the condenser inlet. Pipes 1 and 2 are located on the first row of the second pass in the evaporator section.

With the increase in mass flow rate, the temperatures become more similar to one another but it can still be observed that the average working temperature of pipes 3 and 4 is higher at lower air inlet temperatures. This is due to a combination of factors. Firstly, as can be observed in Figure 5 and has been mentioned before, pipes 3 and 4 are on the first row that comes into contact with the evaporator inlet. Secondly, they are also located the farthest away to the condenser inlet, receiving warmer water at the condenser side, which results in a lower difference in temperature between the bottom and the top of the heat pipe.

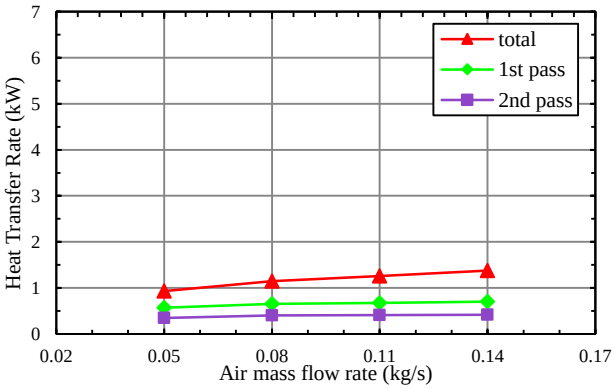

Figure 16 – Heat transfer rate for different flow rates at 100°C air inlet temperature

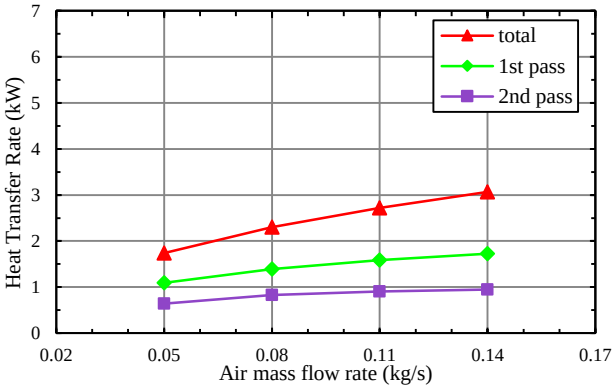

Figure 17 – Heat transfer rate for different flow rates at 150°C air inlet temperature

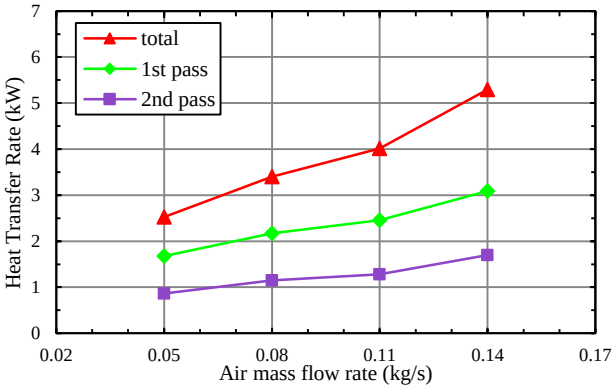

Figure 18 – Heat transfer rate for different flow rates at 200°C air inlet temperature

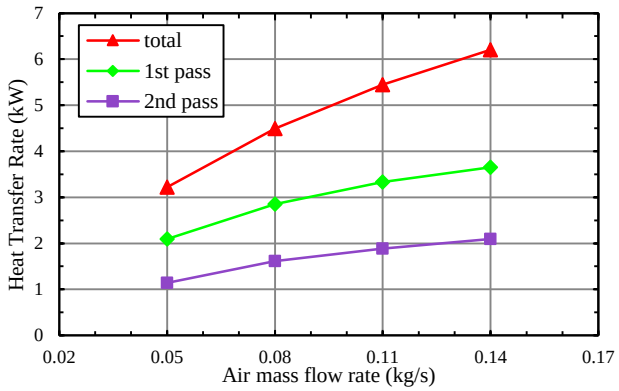

Figure 19 – Heat transfer rate for different flow rates at 250°C air inlet temperature

Figures 16 to 19 show the heat transfer rate (Q) across each air pass of the heat exchanger unit for each different inlet condition. Total represents the total heat transfer rate taking into account both air passes. The trend is for the temperature difference across the first pass to be larger than the second pass due to a higher difference in temperature between the incoming flow and the working temperature of the pipes, therefore higher heat transfer. Increasing the inlet air temperature results in a higher temperature difference across each pass and therefore an increase in the heat transfer rate. Likewise, increasing the mass flow rate increases the overall turbulence, also having the effect of increasing the overall heat transfer rate.

The effectiveness of the test unit (given by the variable ε and in equation 12) was also determined according to the different inlet conditions and is displayed in Figure 20. The graph shows a good downward trend for different flow rates and temperatures except for 100°C. This is caused by a lack of heat being absorbed by the pipe, causing irregularities in the boiling regime which results in poor performance. At lower mass flow rates the effectiveness is higher as the pipe has more time to absorb the heat in the flow.

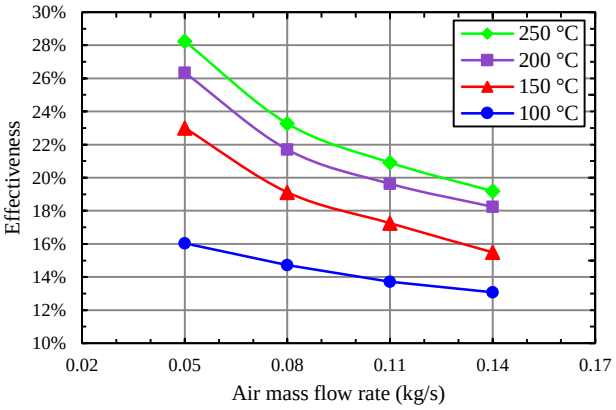

Figure 20 – Relation between the effectiveness of the heat exchanger and the incoming evaporator side conditions.

Figure 20 also illustrates how the effectiveness increases with the increase in the air inlet temperature. Increasing the air inlet temperature results in an increase in the temperature change in the cold side and therefore an increase in the effectiveness of the exchanger. The maximum effectiveness achieved was 28.24% at 0.05 kg/s, 250°C which means that higher temperatures result in higher effectiveness but higher mass flow rates result in lower effectiveness.

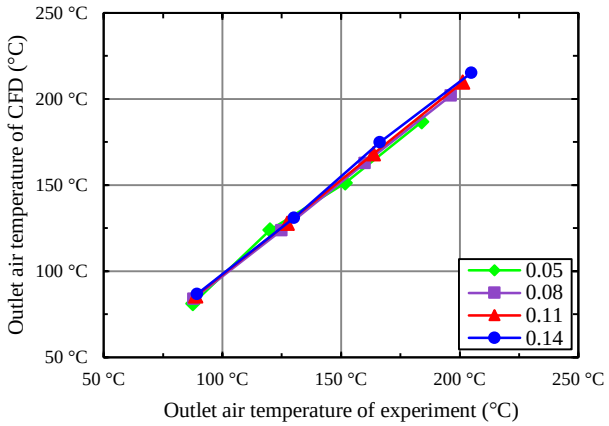

Figure 21 – Comparison between experimental and CFD results for the temperature at the outlet of the evaporator.

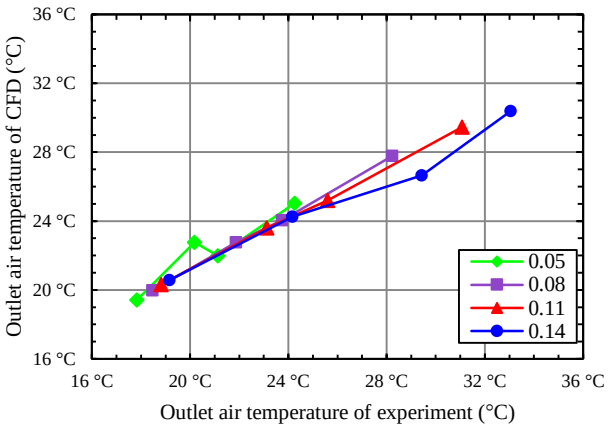

Figure 22 – Comparison between experimental and CFD results for the temperature at the outlet of the condenser.

Figure 23 shows a direct comparison between the results of the experiment and the CFD for both the evaporator section and the condenser section, respectively. It is observed that the CFD simulation under-predicts the performance of the heat pipes at higher mass flow rates but over-predicts it at lower mass flow rates. This could possibly be improved by a minor update on the equation governing the conductivity of the pipe, especially in the boiling region.

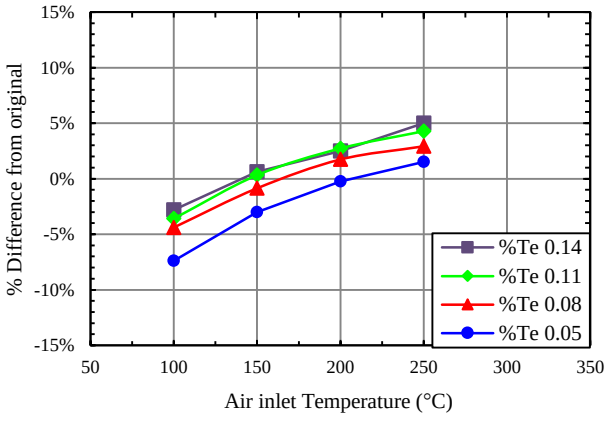

Figure 23 – Percentage difference between the experimental and the CFD results for the evaporator section for different inlet conditions.

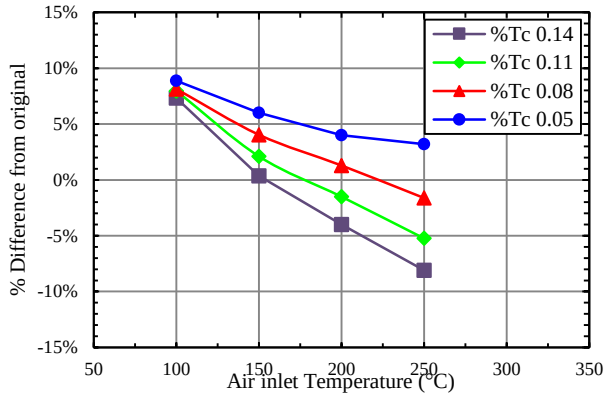

Figure 24 – Percentage difference between the experimental and the CFD results for the condenser section for different inlet conditions.

A more direct comparison between the experimental and CFD simulation results is presented in Figure 18. All the predictions fall into a 10% envelope, the most accurate ones being the test done at more average conditions. The evaporator side shows an upward trend, where the governing equation for the heat pipe's conductivity over predicts the conductivity at lower air inlet temperatures, but as the inlet temperature increases, it starts under-predicting it. The condenser section has a similar behaviour, but inverted. Overall, there is a very good agreement between the CFD, the empirical correlations and the experimental data (10%).

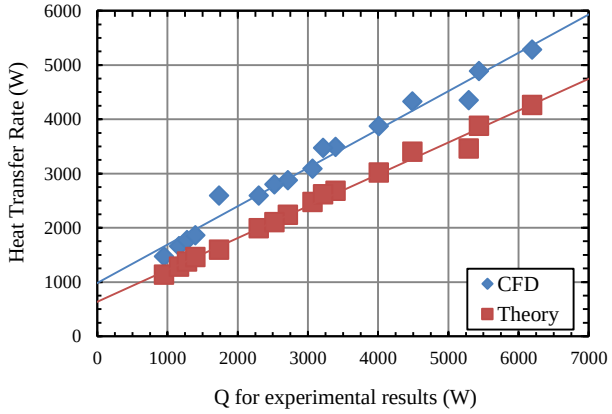

Figure 25 – Comparison of the total heat transfer rate value for the CFD results, the empirical correlations and the experimental data.

Figure 25 represents a direct comparison between the total heat transfer rate (Q) obtained for the experimental rig during testing (through $Q = \dot{m}c_p\Delta T$) and the corresponding total heat transfer rate predicted by both the CFD simulation and equations found in literature for the same inlet conditions. Looking at the figure, the CFD software seems to over-estimate the performance of the heat exchanger at lower heat transfer rates (given by at lower inlet mass flow rate and temperatures) and under-estimating as the inlet conditions improve, as can be seen from the blue trend line created by the rhombuses. This pattern is in agreement with Figure 18. Overall there is good agreement between the experimental results and the CFD.

The prediction provided by the empirical correlations is very conservative, as is shown by the trend line formed by the red squares; it under-estimates the performance of the heat exchanger at all times. This may be a result of the equations used for convection from the flow to the pipe, as the same inner resistance for the pipes was used for both the CFD and the literature.

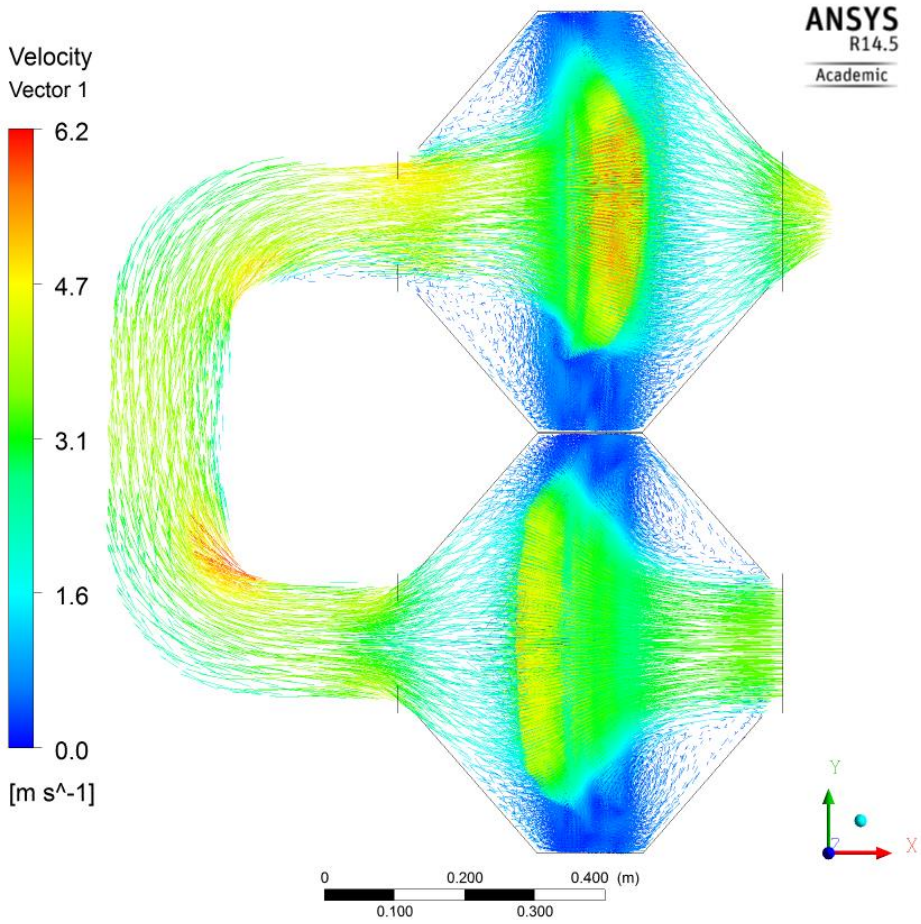

Figure 26 – Vector velocity plot of the evaporator section.

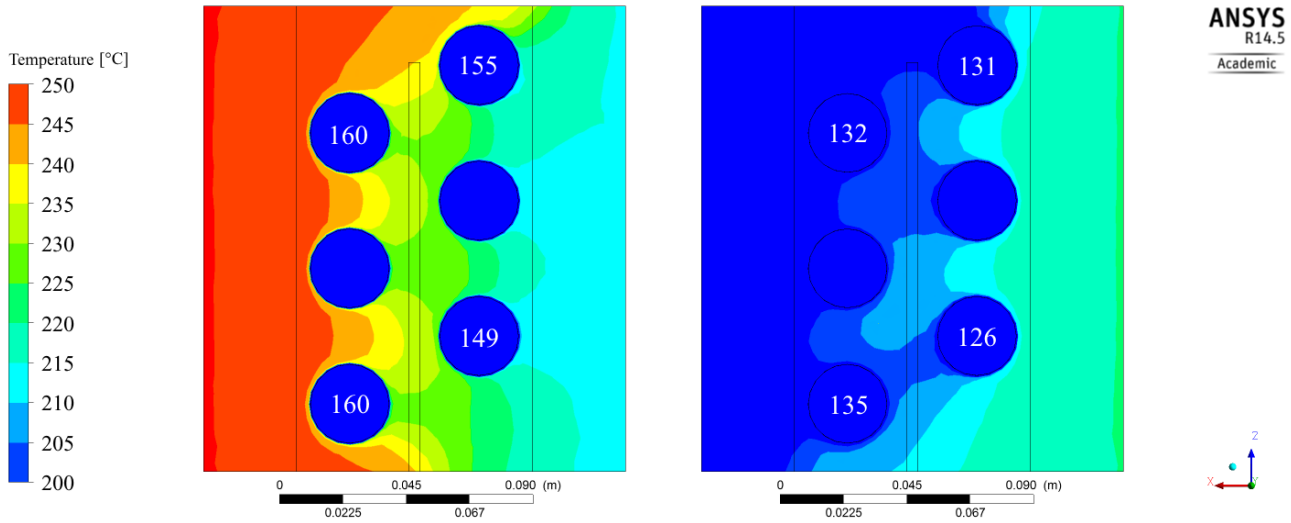

Figure 27 – Temperature contour of the evaporator section in the first (y = 0.3 m) and second (y = 0.9 m) air pass at 250°C and 0.14kg/s.

Figure 26 illustrates a vector plot of the velocity inside the evaporator section of the heat exchanger showing the higher velocity zones at the bends. Figure 27 illustrates the temperature contours of the evaporator section in the first and second air passes. The air enters the heat exchanger at 250 °C from the left of the first pass and

then flows through a u-shaped bend (at 220 °C) that leads it to the second air-pass, represented on the right side of the figure, leaving the evaporator at 200 °C. The numbers inside the pipes represent the temperatures of the solid rods at the specified height (in °C). As it can be easily discerned, the solid rods are not isothermal throughout their length as a thermosyphon would be; their temperature varies with the height due to the different fluid temperatures surrounding the pipes. However, their average temperature closely matches the saturation temperature of the pipes.

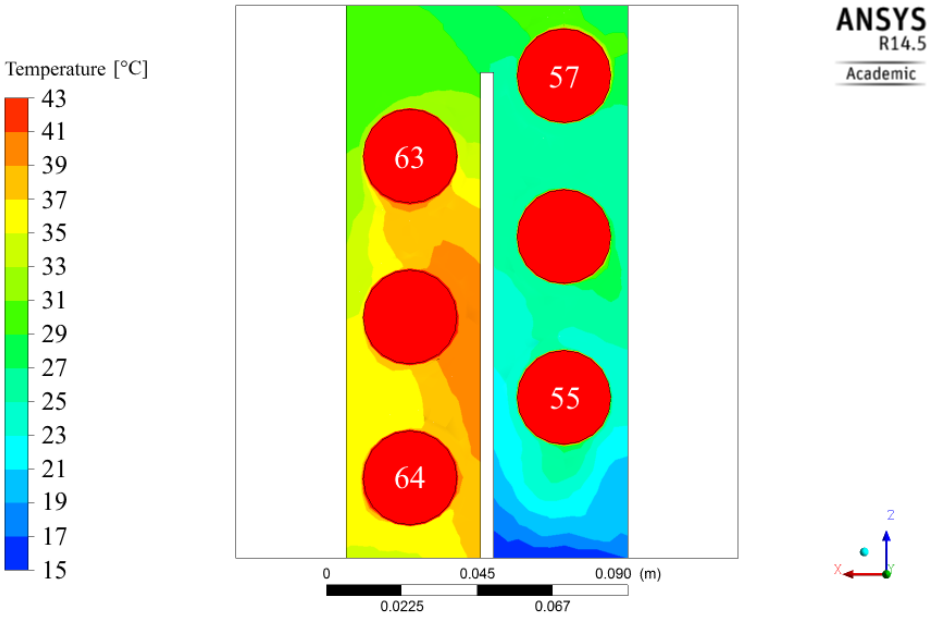

Figure 28 – Temperature contour of the condenser (y = 1.9 m) at 250°C and 0.14kg/s.

A temperature profile of the condenser is displayed in Figure 28. The water enters the condenser at a temperature of 15 °C and reaches a temperature of approximately 35 °C at the condenser outlet. The numbers in the pipes represent the temperature of the solid rods at that height. The temperatures keep the consistency shown in Figure 27 where the pipe closer to the inlet of the condenser displays the lower temperature.

10. Error Analysis

No physical quantity can be measured with certainty and measurements always contain errors. Errors can propagate through an experimental procedure due to many factors mainly human error, equipment usage and inaccurate experiment set-up. Effectiveness (ε) was studied to investigate the error analysis. The uncertainty analysis of the effectiveness was calculated using the following equations [26]:

$$S_{\dot{Q}_c} = \dot{Q}_c \sqrt{\left(\frac{S_{FR_w}}{FR_w}\right)^2 + \left(\frac{S_{\Delta T_c}}{\Delta T_c}\right)^2} \tag{20}$$

$$S_{\Delta T_{max}} = \sqrt{\left(S_{T_{h,i}}\right)^2 + \left(S_{T_{c,i}}\right)^2} \tag{21}$$

$$S_{\Delta T_c} = \sqrt{\left(S_{T_{c,o}}\right)^2 + \left(S_{T_{c,i}}\right)^2} \tag{22}$$

Figure 29 shows how the percentage error of the effectiveness varies with the change in the inlet air mass flow rate for different inlet temperatures. It is obvious from the graph that the propagated error associated with the calculated effectiveness is inversely proportional to both mass flow rate and the inlet temperature. The greatest error came from the reading of the thermocouples at lower temperatures, more specifically at 10Hz. Figure 29 shows an inversely proportional relationship between the uncertainty for the effectiveness and temperature change, which explains why the maximum uncertainties were achieved at low inlet temperature because the temperature change is very small. For most engineering applications, a 10% error is often considered acceptable [26].

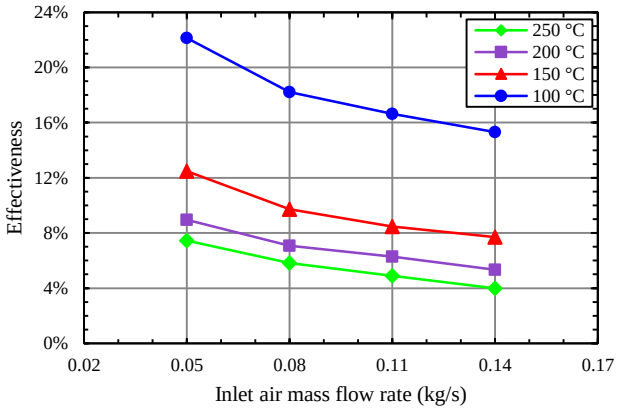

Figure 29 – Uncertainty analysis for the effectiveness.

11. Conclusion

An experimental and analytical investigation of a heat pipe-based heat exchanger with two air-passes was successfully carried out, its thermal performance analysed by a combination of several techniques including effectiveness and heat transfer rate. The results were analysed using expressions from recent literature and verified through modified correlations to ensure the heat balance had been achieved. Inlet conditions used in the experiment such as mass flow rate, inlet temperature and thermal conductivity have been converted into boundary conditions that were then used in the numerical modelling of the heat exchanger. The following conclusions were drawn from the experimental and numerical results:

- Higher heat transfer rate was achieved at higher inlet temperatures and mass flow rates;
- Effectiveness was found to be proportional to the air inlet temperature and inversely proportional to the inlet air mass flow rate;
- A maximum effectiveness of 29% was achieved at the lowest air flow rate and maximum inlet temperature;
- A higher heat transfer rate was achieved in the first pass than in the second pass, a fact demonstrated both experimentally and numerically;
- Good agreement has been found between the experimental and numerical results for all the outlet temperatures;
- An average temperature difference of 3% was observed between the experimental and numerical results in the evaporator section and an average difference of 5% in the condenser side.

Acknowledgements

The authors would like to acknowledge Econotherm UK Ltd. for their in kind contribution.

Nomenclature

A	(m^2)	Heat transfer area
C	(W/K)	Heat capacity rate
C_r	(-)	Ratio of heat capacities
c_p	(J/(kg.K))	Specific heat capacity
C_{sf}	(-)	Coefficient of liquid/surface combination
h	($W/(m^2.K$)	Heat transfer coefficient
h_{fg}	(J/kg)	Specific enthalpy of evaporation / latent heat of vaporisation
K_p	(-)	Dimensionless parameter
k	(W/(m.K))	Constant of thermal conductivity
l	(m)	Length
$\dot{m}$	(kg/s)	Mass flow rate
Nu	(-)	Nusselt number
Pr	(-)	Prandtl number
$\dot{Q}$	(W)	Heat transfer rate
$\dot{q}$	(W)	Local heat transfer rate
R	(K/W)	Thermal resistance
r	(m)	Radius of cylinder
Re	(-)	Reynolds number
T	(^oC)	Temperature
$\overline{T}$	(^oC)	Average temperature
ΔT	(^oC)	Difference in temperature
U	($W/(m^2.K)$)	Overall heat transfer coefficient
ε	(-)	Effectiveness
μ	(Pa.s)	Dynamic viscosity
ρ	(kg/m^3)	Density
σ	(N/m)	Surface tension

Subscripts

b	Boiling
c	Condenser side
h	Convection
e	Evaporator side
hp	Heat pipe / thermosyphon
i	Inlet
k	Conduction
L	Liquid phase
LM	Logarithmic mean
n	Number of pipes
o	Outlet
r	Rate
T	Total
V	Vapour phase
w	Water
6hp	For 6 heat pipes

Abbreviations

CFD	Computational Fluid Dynamics
k-ε	k-epsilon turbulence method
NTU	Number of Transfer Units
TPCT	Two-phase closed thermosyphons

References

[1] M. Grubb, C. Vrolijk, D. Brack, and Energy and Environmental Programme (Royal Institute of International Affairs), The Kyoto Protocol: A Guide and Assessment, Energy and Environmental Programme, Royal Institute of International Affairs, 1999.

[2] W. Steffen, I. Noble, J. Canadell, M. Apps, E.D. Schulze, and P.G. Jarvis, The terrestrial carbon cycle: implications for the Kyoto Protocol, Science, 280 (1998) 1393-1394.

[3] D. Reay and A. Harvey, The role of heat pipes in intensified unit operations, Applied Thermal Engineering, 57 (2013) 147-153.

[4] D.A. Reay, P.A. Kew, and R.J. McGlen, Chapter 6 - Special types of heat pipe, in: D.A. Reay, P.A. Kew, and R.J. McGlen (eds.), Heat Pipes (Sixth Edition), Butterworth-Heinemann, Oxford, 2014, pp. 135-173.

[5] F.L. Chang and Y.M. Hung, The coupled effects of working fluid and solid wall on thermal performance of micro heat pipes, International Journal of Heat and Mass Transfer, 73 (2014) 76-87.

[6] A. Teke and O. Timur, Assessing the energy efficiency improvement potentials of HVAC systems considering economic and environmental aspects at the hospitals, Renewable and Sustainable Energy Reviews, 33 (2014) 224-235.

[7] Z. Wang and W. Yang, A review on loop heat pipe for use in solar water heating, Energy and Buildings, 79 (2014) 143-154.

[8] H. Jouhara, V. Anastasov, and I. Khamis, Potential of heat pipe technology in nuclear seawater desalination, Desalination, 249 (2009) 1055-1061.

[9] D.A. Reay, P.A. Kew, and R.J. McGlen, Chapter 7 - Applications of the heat pipe, in: D.A. Reay, P.A. Kew, and R.J. McGlen (eds.), Heat Pipes (Sixth Edition), Butterworth-Heinemann, Oxford, 2014, pp. 175-206.

[10] L. Bai, G. Lin, H. Zhang, J. Miao, and D. Wen, Operating characteristics of a miniature cryogenic loop heat pipe, International Journal of Heat and Mass Transfer, 55 (2012) 8093-8099.

[11] R. Laubscher and R.T. Dobson, Theoretical and experimental modelling of a heat pipe heat exchanger for high temperature nuclear reactor technology, Applied Thermal Engineering, 61 (2013) 259-267.

[12] H. Jouhara and A.J. Robinson, Experimental investigation of small diameter two-phase closed thermosyphons charged with water, FC-84, FC-77 and FC-3283, Applied Thermal Engineering, 30 (2010) 201-211.

[13] M.S. Kim, K.S. Lee, and S. Song, Effects of pass arrangement and optimization of design parameters on the thermal performance of a multi-pass heat exchanger, International Journal of Heat and Fluid Flow, 29 (2008) 352-363.

[14] F.P. Incropera and P.D. David, Chapter 7 - External Flow, Fundamentals of Heat and Mass Transfer, John Wiley & Sons, New York, 1996, pp. 377-386.

[15] J. Danielewicz, M.A. Sayegh, B. Üniechowska, M. Szulgowska-Zgrzywa, and H. Jouhara, Experimental and analytical performance investigation of air to air two phase closed thermosyphon based heat exchangers, Energy, 77 (2014) 82-87.

[16] H. Jouhara and H. Merchant, Experimental investigation of a thermosyphon based heat exchanger used in energy efficient air handling units, Energy, 39 (2012) 82-89.

[17] F.P. Incropera and P.D. David, Chapter 11 - Heat Exchangers, Fundamentals of Heat and Mass Transfer, John Wiley & Sons, New York, 1996, pp. 581-632.

[18] Fluent Inc. FLUENT 6.3 User's Guide. 2014.

Ref Type: Online Source

[19] M.Thirumaleshwar, Fundamentals of Heat and Mass Transfer, Pearson Education, 2009.

[20] ESDU 81038, Heat pipes - performance of two-phase closed thermosyphon, 1983.

[21] W.M. Rohsenow and J.P. Hartnett, Chapter 13 - Boiling, Handbook of heat transfer, McGraw-Hill, New York, 1973.

[22] M.S. El-Genk and H.H. Saber, Heat transfer correlations for small, uniformly heated liquid pools, International Journal of Heat and Mass Transfer, 41 (1998) 261-274.

[23] F.P. Incropera and P.D. David, Chapter 10 - Boiling and Condensation, Fundamentals of Heat and Mass Transfer, John Wiley & Sons, New York, 1996, pp. 535-580.

[24] W.H. McAdams, Heat Transmission, McGraw-Hill, New York, 1954.

[25] H. Jouhara and R. Meskimmon, Experimental investigation of wraparound loop heat pipe heat exchanger used in energy efficient air handling units, Energy, 35 (2010) 4592-4599.

[26] J.R. Taylor, An Introduction to Error Analysis: The Study of Uncertainties in Physical Measurements, University Science Books, 1997.

Numerical investigation of a cross flow air-to-water heat pipe-based heat exchanger used in waste heat recovery

Joao Ramos [a], Alex Chong [a], Hussam Jouhara [b*]

[a] Faculty of Computing, Engineering and Science, University of South Wales, Pontypridd, CF37 1DL, United Kingdom
[b] Institute of Energy Futures, RCUK Centre for Sustainable Energy Use in Food Chains, Brunel University London, Uxbridge, UB8 3PH, United Kingdom

* Corresponding author. Email: hussam.jouhara@brunel.ac.uk; Tel. +44(0) 1895267806

Abstract
This paper presents the application of CFD modelling to predict the thermal performance of a cross flow heat pipe based air to water heat exchanger. The investigated heat exchanger is equipped with six wickless water-charged heat pipes with a single pass flow pattern on the air side and two flow passes on the water side. For the purpose of CFD modelling, the heat pipes were considered as solid devices of a known thermal conductivity, which is estimated from comprehensive experimental investigation on these heat pipes under the whole testing range. The CFD results were validated using a full scale system and it was found that the modelling predictions are within 10% of the experimental results.

Keywords heat pipe, heat exchanger, CFD modelling, heat recovery.

1 Introduction

With the launch of new environmental policies (Anon., November 2008) and the increased globalisation of the term Sustainability (Vandermeersch, et al., June 2014), pressure is being exerted on several governments to reduce the energy wastage on their territories. Heat is a major contributor to this wasted energy (Haddad, et al., 2014) and so heat exchangers are employed to recover the wasted heat energy from exhaust outlets so it may be reused or stored for a later use.

The greatest heat energy waste in industry seems to be found at low to medium-grade heat (Haddad, et al., 2014) (temperatures from 100 °C to 300 °C). It is in this environment that heat pipe-equipped heat exchangers are finding increased use due to an array of advantages ranging from a complete flow separation, great redundancy and ease of maintenance. All of the advantages are a direct result of the mechanism of phase change happening within the heat pipe (Yau, 2008).

Heat pipes were initially developed by NASA as effective heat sinks to cool down small-scale electronic equipment in space (Swanson & Birur, June 2003), and it is for cooling electronic equipment that small heat pipes are being mass manufactured in the present day, being found everywhere from mobile phones to CPUs (Choi, et al., November 2012; Jouhara & Meskimmon, December 2014). A heat pipe consists of a hermetically-sealed tube that is with filled with a small mass of saturated working fluid that exists in liquid and vapour form and occupies the whole of the internal volume of the tube. Applying heat to one end of the heat pipe will cause the working fluid inside the pipe to boil and, due to the lower density travel in vapour form to the cooler end of the pipe, where it condenses and gives away the absorbed latent heat that was collected in the evaporator section (Reay & Kew, 2006) thus completing the thermal cycle. A representation of the heat pipe working cycle can be seen in Figure 1. Due to the high effective thermal conductivity of these devices, heat pipes have been termed superconductors, and their effective conductivity can easily be several orders of magnitude greater than pure conduction through a solid metal (Jouhara & Meskimmon, December 2014; Jouhara & Meskimmon, December 2010).

The small heat pipes used in electronics applications are equipped with a porous wick structure, which allows them to function in any orientation, provided there is a difference in temperature between both sides of the pipe (Reay & Kew, 2006). However, the heat pipe does not require a wick in order to

function properly; as long as the evaporator section is located under the condenser section, the condensate is pushed back to the evaporator through the force of gravity. Wickless heat pipes are also known as gravity-assisted heat pipes or two-phase closed thermosyphons and are employed in this study.

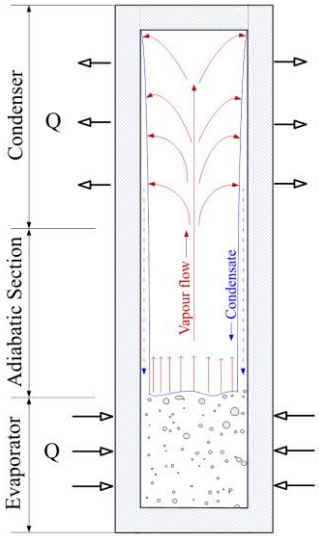

Figure 1: *Schematic of a working heat pipe*

There is much literature available in heat exchangers equipped with heat pipes (HPHE) used in Heating, Ventilation and Air-conditioning applications (HVAC) (Jouhara & Meskimmon, December 2014; Jouhara & Meskimmon, December 2010; Yau & Ahmadzadehtalatapeh, February 2010; Ahmadzadehtalatapeh, April 2013), as well as heat recovery (Yang, et al., February 2003; Wang, et al., March 2015; Sriumang & Amatachaya, August 2012). For low to medium grade heat, consisting of temperatures above 150°C, Noie (Noie, April 2006) presents an analytical method of characterising the HPHE using the Effectiveness (ε-NTU method) to predict the performance of the heat exchanger. The same approach is taken by Danielewicz et al. (Danielewicz, et al., December 2014), and Jouhara (Jouhara & Merchant, 2012) with the aid of a computer code that makes slightly changes to the effectiveness depending on the inlet conditions. All the papers refer to air-to-air HPHE and it is mentioned by Noie that the theory applies even for different fluids on the shell side.

The simulation of heat pipes through CFD is a fairly novel area, made possible due to the increase in computational power of modern machines. Alizadehdakhel et al. (Alizadehdakhel, et al., March 2010) and Fadhl et al. (Fadhl, et al., October 2013) have both successfully modelled the thermosyphon using a custom volume of fraction (VOF) code in Fluent, a popular CFD release. Both simulations were done in 2 dimensions and proved that the software is capable of simulating the phase change process within a single heat pipe during the evaporation and condensation processes albeit after a long processing time.

In terms of simulations involving heat pipes and heat exchangers, Selma et al. (Selma, et al., August 2014) have designed a working model of a heat exchanger equipped with heat pipes using OpenFOAM, an open-access CFD release, in order to improve the energy efficiency of an existing model. A 2-dimensional simulation of the external flow surrounding the pipes was created and used the outer wall of the pipes as a constant temperature boundary condition gathered from industrial practice. The results proved very satisfactory and correlated very well with both experimental data and a commercial CFD release.

The objective of this paper is to fuse the analytical background to the CFD simulation, by assuming that the pipes are solid devices of a constant conductivity. The conductivity is predicted using adapted versions of equations found in literature. The results shall prove that the thermal resistance analogy within the heat pipe can be extended to CFD simulations.

2.1 Boundary conditions

ANSYS Fluent was the computational fluid dynamics (CFD) software used to simulate the heat flow within the heat exchanger. The model was created with the purpose of assessing the potential of simulating heat pipes as solids rods of constant conductivity for the modelling of future heat exchangers. The standard k-epsilon turbulence model (k-ε) was used in each of the simulations. A coupled pressure-based solver is also recommended as it is more efficient in steady-state simulations and offers better results for single-phase fluid flow [20].

Standard tables of material properties were used to determine the characteristics of the fluids simulated (water in the condenser and air in the evaporator) [20]. The pipes were modelled as solid objects and were given a value of conductivity (k) which had been derived from equations found in literature (described in detail in 2.2 Governing Equations).

The inlet and outlet conditions used in the CFD model are displayed in Table 1. The CFD model was run several times for each different inlet condition to reduce the variance of the results.

Table 1: Boundary Conditions

	Type	***Mass flow rate (kg/s)***	***Temperature (ºC)***
Evaporator Inlet	*Mass Flow Inlet*	*0.05 to 0.19 at 0.035 intervals*	*50 to 300 at 50 intervals*
Evaporator Outlet	*Outflow*	-	*Desired Output*
Condenser Inlet	*Mass Flow Inlet*	*Constant 0.0715*	*Constant 10.0 ± 0.3*
Condenser Outlet	*Outflow*	-	*Desired Output*

As can be seen in Table 1, the boundary conditions used to simulate the inlets and outlets were of type "mass flow inlet", with the outlets having the opposite direction. This assumption holds true for both circuits: the air circuit consisted of a closed circuit, so it was in fact being pulled out of the evaporator outlet. The condenser had been completely purged of air prior to starting any test and at normal atmospheric conditions water is incompressible, thus justifying the assumption that the mass flow rate at the exit of the condenser must be the same as the water flowing into the condenser. All the other walls of the heat exchanger were insulated during the experimental test and were thus assumed to be adiabatic.

2.2 Governing Equations

The average effective conductivity of the heat pipes, in W/mK, is given by the variable *k*, and it was derived from adapted versions of equations found in the literature. It is inversely related to the thermal resistance (K/W) offered by the heat pipes. The total thermal resistance of a system is also inversely proportional to the total rate of heat transfer:

$$R_T = \frac{\Delta T_{LM}}{\dot{Q}_t} \qquad (23)$$

ΔT_{LM} represents the logarithmic mean temperature difference and $\dot{Q}_T$ the heat transfer rate (W). The overall heat transfer rate may be found using the following expression:

$$\dot{Q}_T = U A_T \Delta T_{LM} \qquad (24)$$

U represents the overall heat transfer coefficient (W/m^{2}K), A_T the total heat surface area and ΔT_{LM} the logarithmic mean temperature difference.

The total resistance to heat transfer, however, is divided mainly in three different terms: the resistance offered by convection in the evaporator, in the condenser and the resistance offered by the heat pipes from the evaporator to the condenser:

$$R_T = R_{6hp} + R_{h,e} + R_{h,c} \qquad (25)$$

Focusing on the first term of the equation, the 6 heat pipes are all in parallel from a thermal energy perspective. Therefore, the total resistance to heat transfer may be found through:

$$\frac{1}{R_{6hp}} = \frac{1}{R_{p1}} + \frac{1}{R_{p2}} + \frac{1}{R_{p3}} + \frac{1}{R_{p4}} + \frac{1}{R_{p5}} + \frac{1}{R_{p6}} \qquad (26)$$

R_{pn} represents the thermal resistance of each individual heat pipe. In the heat exchanger the pipes are all subjected to different flow temperatures at the evaporator and at the condenser section. The average effective conductivity *k* of the heat pipes is determined after the assumption that the thermal resistance of all the heat pipes is the same. Assuming all the resistances are equal:

$$R_{6hp} = \frac{R_p}{6} \qquad (27)$$

Each of these heat pipes has different heat transfer mechanisms active within, including conduction through the wall, evaporation, condensation and the movement of the encased fluid from the evaporator to the condenser. Putting the unknowns in the same expression, the thermal resistance of a single heat pipe may be found from:

$$R_p = R_{k,e} + R_{h,pool\ b} + R_{hp,inner} + R_{h,condensation} + R_{k,c} \qquad (28)$$

The subscript k represents conduction (W/mK), h represents convection (W/m2K), e evaporator and c condenser. The method to determine the internal resistances of the thermosyphon is made available by the Engineering Sciences Data Unit (ESDU) (ESDU 81038, 1983).

Following the same logic as equation 6, the flow of heat transfer starts with heat entering the heat pipe through the evaporator wall. The thermal resistance at the evaporator wall is deducted from conduction through a hollow pipe wall:

$$\dot{Q}_k = \frac{2\pi k l \Delta T}{ln(r_{out} - r_{in})} \quad \therefore \quad R_k = \frac{ln(r_{out} - r_{in})}{2\pi k l} \qquad (29)$$

Where k is the thermal conductivity of the encasing material (W/mK), l is the length of the pipe in contact with the hot air flow (m), $r_{out} - r_{in}$ represent the tube thickness (m) and ΔT is the difference in temperature between the inside and the outside of the pipe (°C). This applies to the evaporator and to the condenser section equally but with different values for the inner and outer temperatures. It is mainly affected by the area of exposure and the conductivity of the material.

The next heat transfer process is pool boiling, where the heat travels from the pipe wall to the working fluid. The correlation for pool boiling is given by Rohsenow (Rohsenow & Hartnett, 1973):

$$\frac{\dot{q}}{A} = \mu \times h_{fg} \times \sqrt{\frac{g(\rho_L - \rho_v)}{\sigma}} \times \left(\frac{c_p \Delta T_b}{h_{fg} C_{sf}}\right)^{1/m} \times Pr^{-n/m} \qquad (30)$$

C_{sf} is a constant for boiling, which changes in accordance to different surface materials and fluids, m and n are constants dependent upon the two substances; m is generally 1/3, n is 1.0 for water and 1.7 for other fluids. All the properties of the working fluid are evaluated at the saturation temperature

Condensation is found to take place in the condenser section, where the working fluid, upon coming into contact with the cooler walls, condenses, giving up its latent energy. For this heat transfer mechanism, the laminar condensation from Nusselt is used (Incropera & David, 1996):

$$h_m = 0.943 \times \left(\frac{{k_L}^3 \rho_L (\rho_L - \rho_V) g\, h_{fg}}{\mu_l\, \theta\, l}\right)^{1/4} \qquad (31)$$

Assuming that ρ_l≫ρ_v further simplifies the equation. McAdams (McAdams, 1954) also suggests a 20% increase to theoretical expressions due to the fact that experimental values are often larger, changing equation 9 into:

$$h_m = 1.13 \times \left(\frac{{k_L}^3 {\rho_L}^2 g\, h_{fg}}{\mu_l\, \theta\, l}\right)^{1/4} \quad (32)$$

All of the variables displayed in the previous equations are extracted from the initial conditions after some degree of iteration. In order to find the output values in advance and to create a relation between the inner temperature of the heat pipes with the temperature of the flow, the convection heat transfer from the outside to the inside of the pipe needs to be determined. Looking at the evaporator section, the first heat transfer mode from the fluid to the pipe is made through convection and given by equation 9 where the manipulation in order to find the thermal resistance is also shown:

$$\dot{Q}_h = hA\Delta T \quad \therefore \quad R_{h,e} = \frac{1}{h_e A_e} \quad and \quad R_{h,c} = \frac{1}{h_c A_c} \quad (33)$$

h refers to the heat transfer coefficient (W/m^{2}K) between the fluid and the solid surface, which in our case is air-carbon steel for h_e and water-carbon steel for h_c. A is the surface area or exposure (m^2) and ΔT the difference in temperature between the flow and the surface area.

2.3 Mesh selection

The mesh selection was done by running the same simulation with different mesh sizes and comparing the accuracy of the results. A mesh is deemed "good" if the maximum skewness is lower than 0.7 for hexahedron and tetrahedrons and 0.8 for triangular elements [20].

Table 2 Mesh Dependency.

Level	*No of Cells*	*Type of cells*	*Skewness*	*Time per iter.*
Coarse	*1,408,658*	*Hex + Tetra*	*avg: 26%, stdev: 16%*	*2-10 s*
Medium	*2,291,364*	*Hex + Tetra*	*avg: 21%, stdev: 13%*	*7-15 s*
Fine	*3,099,230*	*Hex + Tetra*	*avg: 21%, stdev: 13%*	*25-50 s*

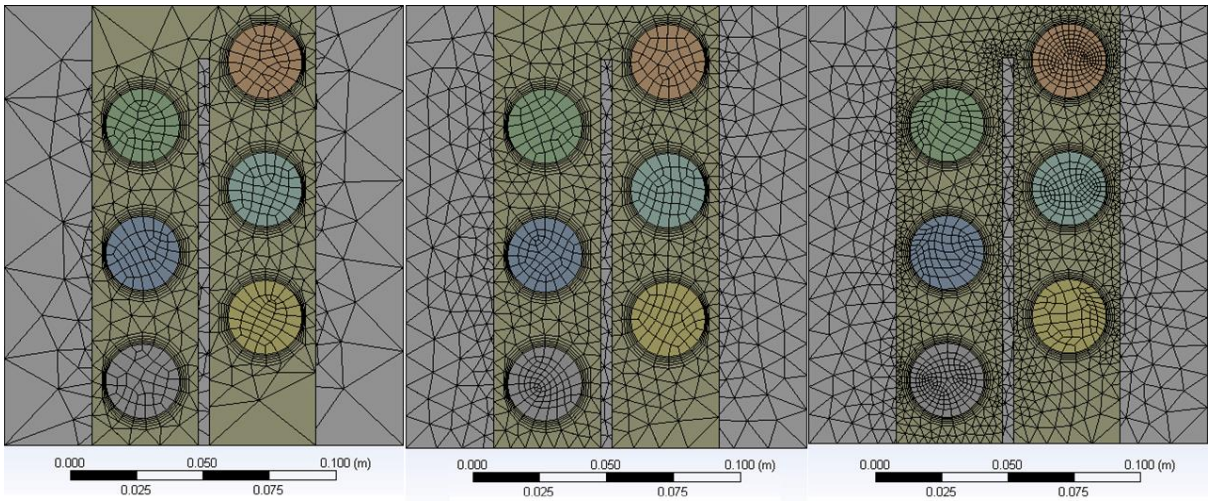

Figure 2: *Comparison between the three different meshes – Coarse, Medium and Fine*

It was found that a fine mesh would take 3 times longer to converge (on average) and the results would not be significantly more accurate (±0.8%); therefore the medium mesh was used in all the tests ran in Fluent.

3. Results and discussion

The heat transfer rate was found to be directly proportional to the inlet air mass flow rate and to the temperature of the flow at the inlet, as can be seen in Figure 3. The profile of the lines indicate that if a higher mass flow rate was provided, the heat exchanger would be capable of transporting that much more heat, however, the lines also start to become more flat as the mass flow rate increases. The average maximum duty according to the data gathered was 900 W maximum heat flux per heat pipe.

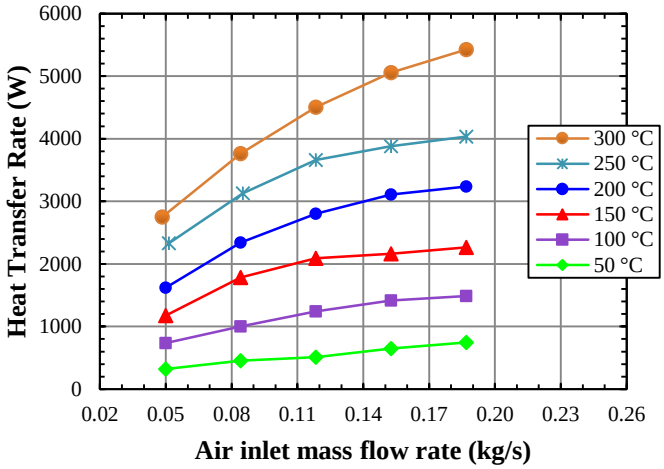

Figure 3: *Total heat transfer rate of the heat exchanger according to different inlet conditions on the simulation*

Figure 6 illustrates a vector plot of the velocity within the evaporator section of the heat exchanger. The higher velocities were found in the vicinity of the heat pipes. A temperature contour of the evaporator is shown in 5; the air is entering the evaporator at 300 °C from the left and leaves the evaporator at approximately 255 °C. Temperatures lower than 250 °C are shown within the pipes.

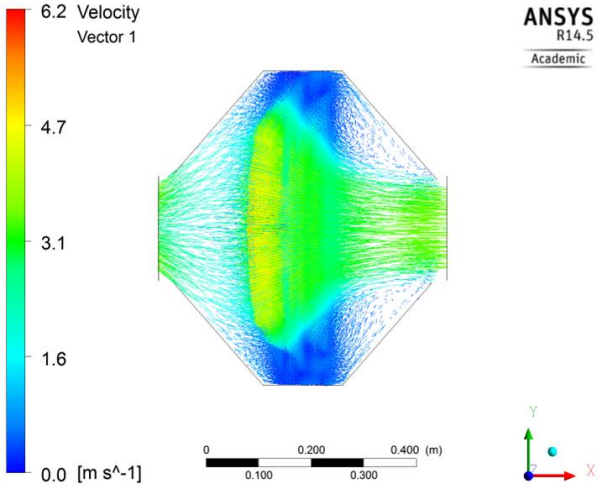

Figure 4: *Vector velocity plot of the evaporator section*

Figure 6 illustrates the temperature contour of the condenser section for the same inlet conditions as Figure 5. The water enters the condenser at 10 °C and leaves the condenser at approximately 20 °C. The numbers in the pipes represent the temperatures of the pipes at the condenser section. It can be observed that they diverge from the temperatures shown in Figure 5 and that is because the pipes are not isothermal within as a normal thermosyphon would be; their temperature varies along the y-axis due to the different fluid temperatures surrounding the pipes. The overall average temperature of the pipes, however, coincided with the saturation temperature of the pipes.

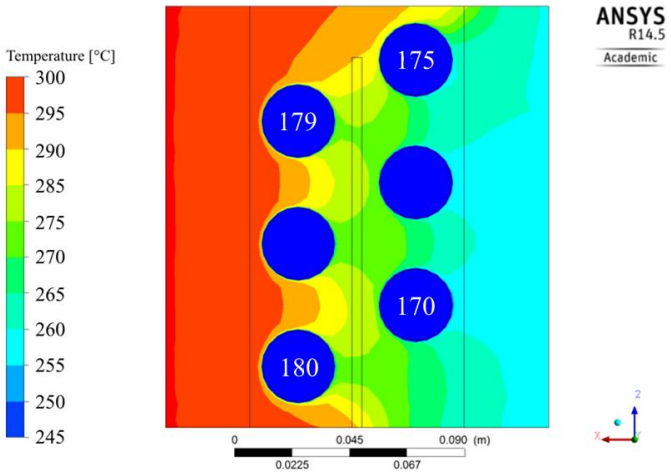

Figure 5: *Average temperature contour of the air in the evaporator section at 300 °C and 0.08 m/s.*

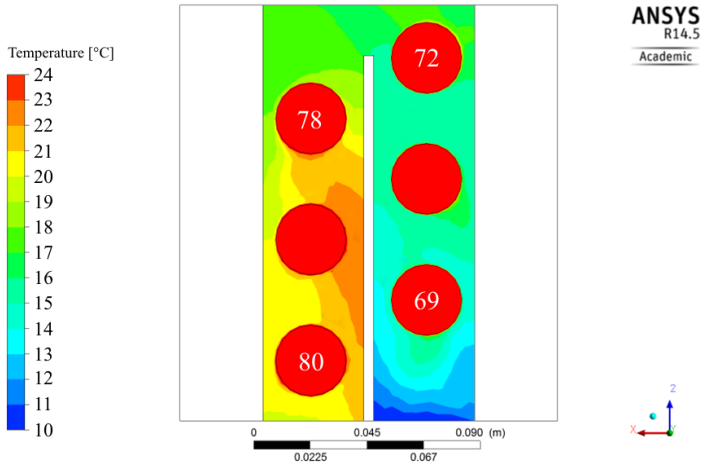

Figure 6: *Average temperature contour of the water in the condenser for the evaporator conditions of 300 °C and 0.08 m/s*

3.1 Validation of results

Regarding the temperature at the outlets, the CFD results compared well to the experimental results, with a maximum difference of 10% at the evaporator section and 15% at the condenser section as can be seen in Figure 7.

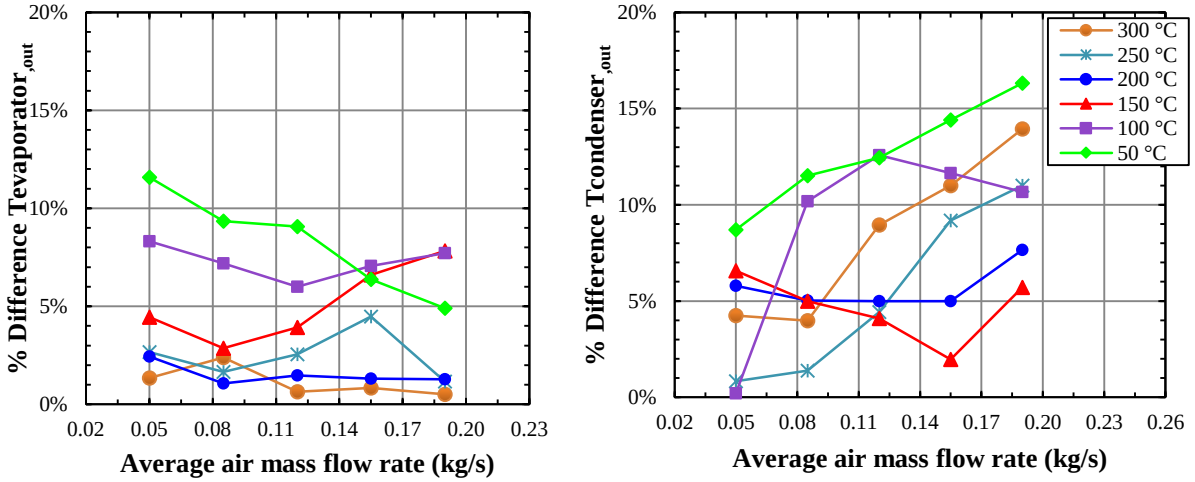

Figure 7: *Percentage temperature difference at the outlets between the experimental test and the CFD simulation*

Figure 8 and Figure 9 show a more detailed comparison between the outlet temperature of the evaporator section and the condenser section, and a good agreement is found on both as they tend towards the centre of the graph. According to Figure 9, it is found that the CFD simulation is slightly over-estimating the temperature at the outlet at low evaporator mass flow rates and under-estimating them as the mass flow rates increase.

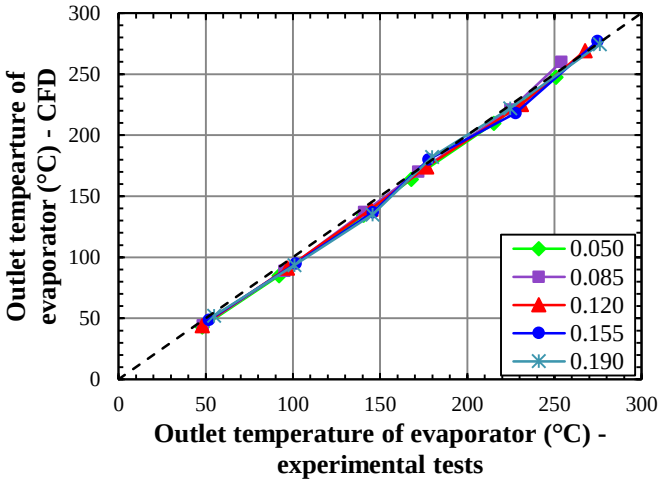

Figure 8: *Comparison between experimental and CFD results for the temperature at the outlet of the evaporator at different mass flow rates.*

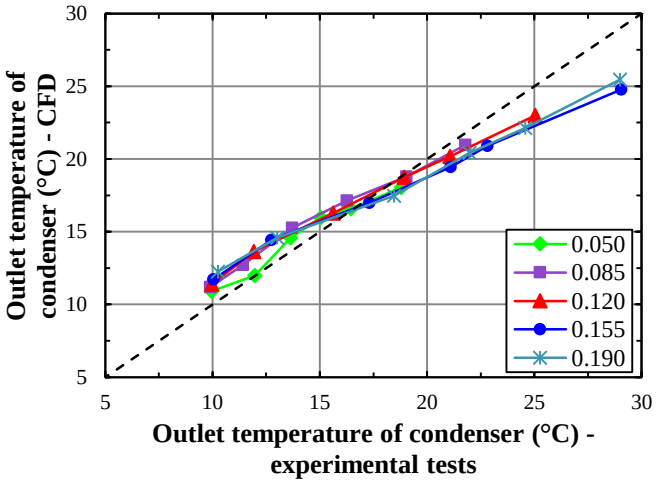

Figure 9: *Comparison between experimental and CFD results for the temperature at the outlet of the condenser at different mass flow rates.*

The heat transfer rate achieved in the CFD was compared with that found from the experimental results and is plotted in Figure 10. Following the same behaviour as Figure 9, the CFD simulation over-estimates the performance of the heat exchanger. However, this is to be expected as in reality it is impossible to have an insulation that is completely adiabatic; particularly with the geometry of the heat exchanger under study. The CFD simulation also appears to be slightly under-estimating the performance of the heat exchanger at higher mass flow rates (10%); this may be due to higher inlet turbulence in the experimental rig as a result of an increased mass flow rate which is impossible to predict as an inlet boundary condition for the CFD model.

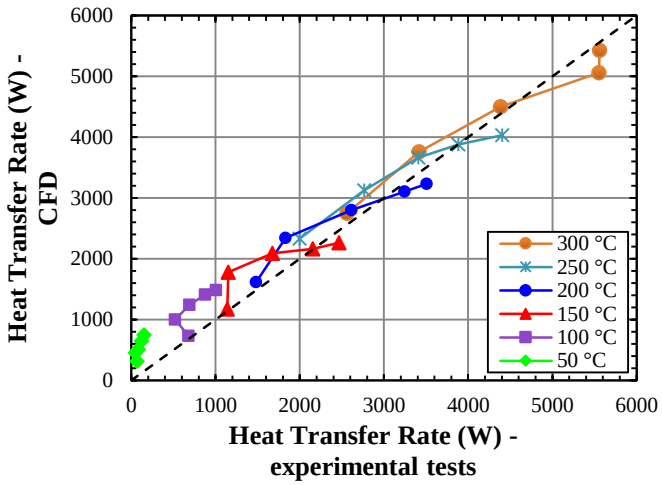

Figure 10: *Comparison of the heat transfer rate between the experimental test and the CFD model for different operating temperatures.*

4. Conclusions

A numerical investigation of a heat pipe-based heat exchanger was successfully carried out and verified through comparison with a real-world test experiment. The following was concluded from the results:

- Higher temperatures and mass flow rates result in higher heat transfer rates up to a limit of 900 W/pipe.
- Equations found in the literature seem to over-predict the results at low evaporator temperatures and under-predict at higher evaporator temperatures.
- Good agreement between the experimental and numerical results for all temperatures; an average 5% temperature difference was observed between the numerical and experimental results in the evaporator section and 7% in the condenser section.

Acknowledgements

The authors would like to thank the funding bodies, the European Development Fund, and Econotherm UK Ltd. for their in kind contribution.

References

[1] "European Commission Directive (2008/98/EC) of the European parliament and of the council of 19 November 2008 on waste and repealing certain Directives," Official Journal of the European Union, November 2008.

[2] T. Vandermeersch, P. Alvarenga, P. Ragaert and J. Dewulf, "Environmental sustainability assessment of food waste valorization options," Resources, Conservation and Recycling, vol. 87, pp. 57-64, June 2014.

[3] C. Haddad, C. Périlhon, A. Danlos, M.-X. François and G. Descombes, "Some Efficient Solutions to Recover Low and Medium Waste Heat: Competitiveness of the Thermoacoustic Technology," Energy Procedia, vol. 50, pp. 1056-1069, 2014.

[4] Y. H. Yau, "The use of a double heat pipe heat exchanger system for reducing energy consumption of treating ventilation air in an operating theatre-A full year energy consumption model simulation," Energy and Buildings, vol. 40, no. 5, pp. 917-925, 2008.

[5] T. D. Swanson and G. C. Birur, "NASA thermal control technologies for robotic spacecraft," Applied Thermal Engineering, vol. 23, no. 9, pp. 1055-1065, June 2003.

[6] J. Choi, M. Jeong, J. Yoo and M. Seo, "A new CPU cooler design based on an active cooling heatsink combined with heat pipes," Applied Thermal Engineering, vol. 44, pp. 50-56, November 2012.

[7] H. Jouhara and R. Meskimmon, "Heat pipe based thermal management systems for energy-efficient data centres," Energy, vol. 77, pp. 265-270, December 2014.

[8] D. Reay and P. Kew, Heat pipes: Theory, Design and Applications, Elsevier Limited, 2006.

[9] H. Jouhara and R. Meskimmon, "Experimental investigation of wraparound loop heat pipe heat exchanger used in energy efficient air handling units," Energy, vol. 35, no. 12, pp. 4592-4599, December 2010.
[10] Y. Yau and M. Ahmadzadehtalatapeh, "A review on the application of horizontal heat pipe heat exchangers in air conditioning systems in the tropics," Applied Thermal Engineering, vol. 30, no. 2-3, pp. 77-84, February 2010.
[11] M. Ahmadzadehtalatapeh, "An air-conditioning system performance enhancement by using heat pipe based heat recovery technology," Scientia Iranica, vol. 20, no. 2, pp. 329-336, April 2013.
[12] F. Yang, X. Yuan and G. Lin, "Waste heat recovery using heat pipe heat exchanger for heating automobile using exhaust gas," Applied Thermal Engineering, vol. 23, no. 3, pp. 367-372, February 2003.
[13] Y. Wang, X. Han, Q. Liang, W. He and Z. Lang, "Experimental investigation of the thermal performance of a novel concentric condenser heat pipe array," International Journal of Heat and Mass Transfer, vol. 82, pp. 170-178, March 2015.
[14] W. Sriumang and P. Amatachaya, "A review of the applications of heat pipe heat exchangers for heat recovery," Renewable and Sustainable Energy Reviews, vol. 16, no. 6, pp. 4303-4315, August 2012.
[15] S. H. Noie, "Investigation of thermal performance of an air-to-air thermosyphon heat exchanger using ε-NTU method," Applied Thermal Engineering, vol. 26, no. 5-6, pp. 559-567, April 2006.
[16] J. Danielewicz, M. A. Sayegh, B. Sniechowska, M. Szulgowska-Zgrzywa and H. Jouhara, "Experimental and analytical performance investigation of air to air two phase closed themrosyphon based heat exchangers," Energy, vol. 77, pp. 82-87, December 2014.
[17] H. Jouhara and H. Merchant, "Experimental investigation of a thermosyphon based heat exchanger used in energy efficient air handling units," Energy, vol. 39, pp. 82-89, 2012.
[18] A. Alizadehdakhel, M. Rahimi and A. A. Alsairafi, "CFD modeling of flow and heat transfer in a thermosyphon," International Communications in Heat and Mass Transfer, vol. 37, no. 3, pp. 312-318, March 2010.
[19] B. Fadhl, L. C. Wrobel and H. Jouhara, "Numerical modelling of the temperature distribution in a two-phase closed thermosyphon," Applied Thermal Engineering, vol. 60, no. 1-2, pp. 122-131, October 2013.
[20] B. Selma, M. Désilets and P. Proulx, "Optimization of an industrial heat exchanger using an open-source CFD code," Applied Thermal Engineering, vol. 69, no. 1-2, pp. 241-250, August 2014.
[21] ESDU 81038, "Heat pipes - performance of two-phase closed thermosyphon," 1983.
[22] W. M. Rohsenow and J. P. Hartnett, "Chapter 13 - Boiling," in Handbook of heat transfer, New York, McGraw-Hill, 1973.
[23] F. P. Incropera and P. D. David, "Chapter 10 - Boiling and Condensation," in Fundamentals of Heat and Mass Transfer, New York, John Wiley & Sons, 1996, pp. 535-580.
[24] W. H. McAdams, Heat Transmission, New York: McGraw-Hill, 1954.
[25] Fluent Inc., "FLUENT 6.3 User's Guide," 2014.

Experimental and numerical investigation of a cross flow air-to-water heat pipe-based heat exchanger used in waste heat recovery

Joao Ramos[a], Alex Chong[a], Hussma Jouhara[b,*]

[A] Faculty of Computing, Engineering and Science, University of South Wales, Pontypridd CF37 1DL, United Kingdom
[B] Institute of Energy Futures, College of Engineering, Design and Physical Sciences, RCUK Centre for Sustainable Energy Use in Food Chains, Brunel University London, Uxbridge UB8 3PH, United Kingdom

Submitted to the International Journal of Heat and Mass Transfer
Received 10 February 2016
Received in revised form 14 June 2016
Accepted 29 June 2016

Abstract

This paper applies CFD modelling and numerical calculations to predict the thermal performance of a cross flow heat pipe based heat exchanger. The heat exchanger under study transfers heat from air to water and it is equipped with six water-charged wickless heat pipes, with a single-pass flow pattern on the air side (evaporator) and two flow passes on the water side (condenser). For the purpose of CFD modelling, the heat pipes were considered as solid devices of a known thermal conductivity which was estimated by experiments conducted on the exact same heat pipe configuration under an entire testing range. The CFD results were compared with the experimental and the numerical results and it was found that the modelling predictions are within 10% of the experimental results.

Keywords heat pipe; heat exchanger; CFD modelling; heat recovery.

Nomenclature

Abbreviations

HPHX	Heat pipe-equipped heat exchanger
HVAC	Heating, Ventilation and Air Conditioning
NTU	Number of Transfer Units
TSHX	Thermosyphon-equipped heat exchanger
VOF	Volume of Fraction (CFD method)
Pr	Prandtl number
Nu	Nusselt number
Re	Reynolds number

Symbols

A	Area
C	Heat Capacity Rate (m ̇×c_p)
cp	Specific heat at constant pressure
Cr	Heat Capacity Ratio(C_e⁄C_c)
csf	Constant/coefficient dependent on surface-liquid combination
d	Characteristic dimension
g	Acceleration of gravity
h	Heat transfer coefficient
hfg	Latent heat
k	Thermal Conductivity
Q	Heat Transfer Rate
q"	Heat flux
r	Radius
T	Temperature
U	Overall Heat Transfer Coefficient
Δ	Difference
ΔTLM	LMTD – Logarithmic Mean Temperature Difference
ε	Effectiveness
μ	Static viscosity of the liquid phase
π	Pi

ρ	Density
σ	Surface tension

Subscripts

act	Actual
b	Boiling
c	Condenser
cd/cond	Condensation
e	Evaporator
h	Heat transfer coefficient
i	Inside
in	inner
k	Conduction
l	Liquid phase
min	Minimum
n	Number of pipes
o	Outside
s	Surface
sat	Saturation
t	Total
ts	thermosyphon

1 Introduction

Heat exchangers are commonly employed as heat recovery devices to reuse the wasted heat energy from exhaust outlets so it may be furtherly reused or stored for a later use. According to the research of Haddad et al. [1] 90% of the wasted heat energy is found at low to medium-grade heat applications (temperatures from 100 to 400°C), as can be seen in Figure 1. It is in this environment that heat pipe-equipped heat exchangers are finding wide use due to an array of advantages ranging from a complete flow separation, great redundancy and ease of maintenance. All of the advantages are a direct result of the mechanism of phase change happening within the heat pipe [2].

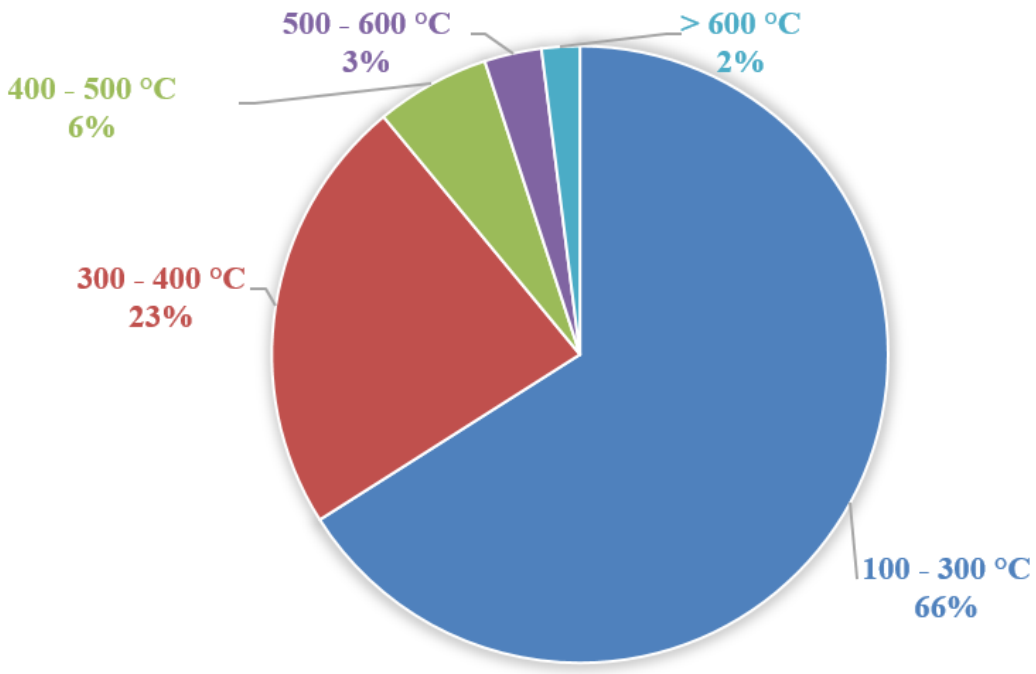

Figure 1: Waste heat energy by temperature range (adapted from [1])

1.1 Literature Review

Heat pipes were initially developed by NASA as effective heat sinks to cool down small-scale electronic equipment in space[3], while nowadays they are commonly used for cooling purposes of electronic equipment from mobile phones to CPUs[4, 5, 6]. A heat pipe consists of a hermetically-sealed tube filled with a small mass of saturated working fluid that exists in liquid and vapour form and occupies the whole of the internal volume of the tube. Applying heat to one end of the heat pipe will cause the working fluid inside the pipe to boil and, due to the lower density, to travel in vapour form towards the cooler end of the pipe, where it condenses and gives away the absorbed latent heat that was collected in the evaporator section; thus completing the thermal cycle [7]. A representation of the heat pipe working cycle can be seen in Figure 2. Due to the high effective thermal conductivity of these devices at essentially constant temperature throughout its length [8, 9, 10], heat pipes have been referred as superconductors. Their effective conductivity can easily be several orders of magnitude greater than pure conduction through a solid metal [5, 10, 11].

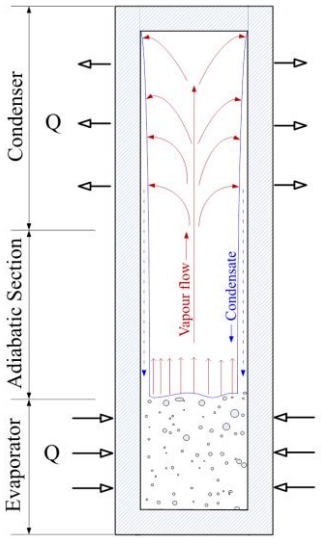

Figure 2: Schematic of a working heat pipe

The small heat pipes used in electronic applications are equipped with a porous wick structure, which allows them to function in any orientation, provided there is a difference in temperature between both sides of the pipe [7, 9]. However, the heat pipe does not require a wick in order to function properly; as long as the evaporator section is located below the condenser section, the condensate working fluid is pushed back to the evaporator through the force of gravity. For that reason, wickless heat pipes are also known as gravity-assisted heat pipes or two-phase closed thermosyphons [9]. The term "thermosyphon" is used throughout the paper and refer to the devices employed in this study.

Thermosyphon-equipped heat exchangers (TSHE) offer many advantages when used as waste heat recovery devices, such as an increased redundancy and reliability, ease of cleaning, no additional power input to the system, reduced risk of cross-contamination and no moving parts; all advantages widely highlighted in the literature surveyed [12, 13, 14, 15, 16, 17]. There is much literature available in heat exchangers equipped with heat pipes (HPHX) used in Heating, Ventilation and Air-conditioning applications (HVAC) [5, 10, 18, 19, 20], as well as heat recovery [21, 22, 23]. For low to medium grade heat, consisting of temperatures above 150°C, Noie [24] presents an analytical method of characterising the HPHX using the Effectiveness (ε-NTU method) to predict the performance of the heat exchanger. The same approach is taken by Danielewicz et al. [25], Jouhara & Merchant [26] and Han & Zou [8] with the aid of a computer coding that predicts the effectiveness depending on different inlet conditions. All the surveyed papers refer to air-to-air HPHX even if it is mentioned by Noie that the ε-NTU method theory applies even if different fluids are used on the shell side.

The development of CFD codes for simulation of heat pipes and heat pipe heat exchangers is a relatively new field of research. It has been receiving renewed interest due to recent advances in computing which allow the simulation of the phase change within the thermosyphon. However, a divide seems to exist in the reviewed literature; the authors either focus solely into the CFD simulation of the phase change process in the thermosyphon or on the behaviour of the fluid on the shell side of a HPHX.

The simulation of heat pipes through CFD is a fairly novel field of research, made possible due to the increase in computational power of modern computers. Alizadehdakhel et al. [27] and Fadhl et al. [28] have both successfully modelled the thermosyphon using a custom volume of fraction (VOF) code in Fluent, a popular CFD release. Both works depicted a 2 dimensional study and proved that the software is capable of simulating the phase change process within a single heat pipe during the evaporation and condensation processes albeit after a long processing time. More recently, the same method has been successfully applied to a 3D model to simulate Geyser boiling in the heat pipe [29]. Geyser boiling usually takes place at low heat input, when a large amount of evaporated fluid bubbles starts to form below the liquid bulk. When the pressure difference between the bubble and the liquid bulk becomes too great, the liquid is projected into the top of the thermosyphon [30, 31].

CFD has also been used to calculate the optimum filling ratio for a thermosyphon by calculating the quantity that will allow the shortest response time and lowest thermal resistance [32]. According to Shabgard et al. [32], it is recommended that an extra 5-10% of fluid is inserted in the pipe to prevent breakdown of the liquid film from the thermosyphon wall. A three-dimensional numerical study simulating multi-phase flow inside horizontally oriented heat pipes was conducted by Hughes et al. [33] for steady-state conditions. In this study, a multiphase flow with coupled heat and mass transfer was used. In order to predict the performance of the heat pipes, the effectiveness of the heat exchanger was determined through an experimental study. A good correlation was found between the results from the CFD model and the experimental results for the same operating conditions.

As mentioned previously, a progression is being observed in the application of CFD to the simulation of thermosyphons, however there is not much literature on the study of the entire HPHX or TSHX. Selma et al. [34] have designed a working model of a heat exchanger equipped with heat pipes using OpenFOAM, an open-access CFD release, in order to improve the energy efficiency of an existing model. A 3-dimensional simulation of the external flow surrounding the pipes was created and used the outer wall of the pipes as a constant temperature boundary condition gathered from industrial practice. The results proved very satisfactory and correlated very well with both experimental data and a commercial CFD release. Peng et al. [35] conducted a CFD study on the effect of fin shape on the air-side heat transfer performance of a fin-plate thermosyphon used in electronics cooling. The simulation focused solely on the air side and results from the CFD model were within 15% error of the experimental results. CFD has also been employed to simulate the feasibility of installing heat pipes within a wind tower. In a study by Calautita et al. [36], the heat pipes were modelled as having a constant surface temperature, a reasonable assumption taking into account there is little difference in the temperature of the working fluid inside the pipe. The results showed that the incorporation of heat pipes in this application is capable of improving the reduction in inlet air temperature.

It appears that there is a gap in the form of o attempt made at simulating the thermosyphons and the heat exchanger in the same simulation. Other than the VOF method, there were no other recommendations in terms of alternative methods of simulating the thermosyphons using, for example, the thermal network analogy. The author therefore recommends the application of the thermal network analogy in order to predict the thermal conductivity of the thermosyphons and feeding that value as a boundary condition into the CFD model of the TSHX. Mroué et al. [37] conducted a study similar to the one present in this work, in which the flow on the hot side of the TSHX was allowed to return in order to make contact with the tubes where film boiling takes place. The thermal network analysis is also used in conjunction with the ε-NTU method in order to accurately predict the behaviour of the TSHX.

The objective of this paper is to implement the analytical and theoretical background analysis of thermosyphons with CFD simulations, by assuming that the heat pipes are solid devices of a constant conductivity. The conductivity is predicted using adapted versions of equations found in literature. The results shall prove that the thermal resistance analogy within the heat pipe can be extended to 3-dimensional CFD simulations.

At first the theoretical modelling of thermosyphons is presented in detail. It is followed by the experimental set up and the designing conditions of the CFD model. The results are then presented and compared.

2 Theoretical Analysis

In terms of predicting the performance of a heat exchanger equipped with thermosyphons, there are quite a few examples in the literature; Azad & Geoola [38] and Kays & London [39] were some of the first to report the use of the effectiveness-Number of Transfer Units (ε-NTU) method to predict the performance of a heat exchanger equipped with thermosyphons to great effect. Even to this day authors continue using the same approach as it has provided satisfactory results; Lukitobudi et al. [40] used it in an approach to recovering waste heat in bakeries, Noie [24] used it in an investigation of an air-to-air heat exchanger used in heat recovery, and Jouhara & Merchant [26] reported the same in their multi-use apparatus.

2.1 Predicting the performance of a single thermosyphon

A thermosyphon is, in many ways, a miniature heat exchanger; so it is only natural to approach it the same way a heat exchanger is approached. The most reported method of predicting the performance of a thermosyphon is through the thermal network analogy [7, 9, 13, 37], also approached in this study. In this analogy, the thermosyphon is broken down into its inner thermal resistances, conduction, boiling, condensation, etc.

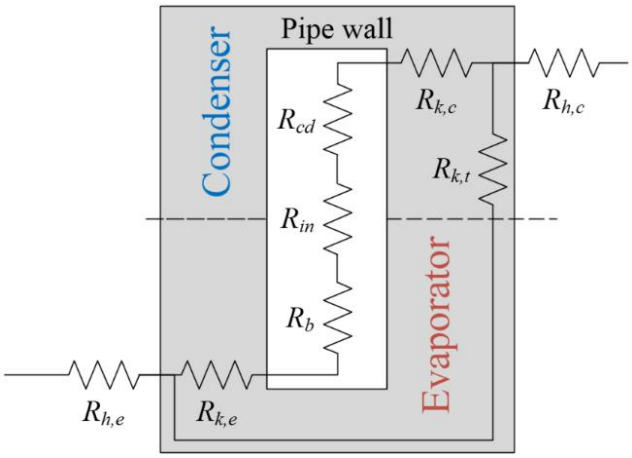

$R_{h,e}$	Thermal resistance from convection on outside of evaporator section
$R_{k,e}$	Thermal resistance from conduction across wall of evaporator section
R_b	Thermal resistance from boiling on TS wall
R_{in}	Thermal resistance from change in pressure between top and bottom
R_{cd}	Thermal resistance from condensation on TS wall
$R_{k,c}$	Thermal resistance from conduction across wall of condenser section
$R_{h,c}$	Thermal resistance from convection on outside of condenser section
$R_{k,t}$	Thermal resistance from Axial conduction across thermosyphon

Figure 3: Schematic of the thermal resistances within the thermosyphon

Treating the circuit displayed in Figure 3 as an electrical circuit; and neglecting the axial thermal conductivity, the total thermal resistance for the thermosyphon is found through equation (1).

$$R_T = R_{h,e} + R_{k,e} + R_b + R_{in} + R_{cd} + R_{k,c} + R_{h,c} \quad (1)$$

The axial thermal conductivity along thin-walled thermosyphons with long adiabatic sections may be considered negligible [7, 13] therefore simplifying the expression to a simple addition. In the case of a heat pipe, which is equipped with a wick structure, an additional parallel network of thermal resistances is added which includes the convection to enter the wick and the axial conductivity along the length of the device.

2.2 Conduction through the thermosyphon walls

The flow of heat through the thermosyphon starts with heat entering the heat pipe through the evaporator wall. The thermal resistance at the evaporator wall is deducted from conduction through a hollow pipe wall:

$$\dot{Q}_k = \frac{2\pi k l \Delta T}{ln(r_{out} - r_{in})} \quad \therefore \quad R_k = \frac{ln(r_{out} - r_{in})}{2\pi k l} \tag{2}$$

Where k is the thermal conductivity of the encasing material (*W/mK*), l is the length of the pipe in contact with the hot air flow (*m*), $r_{out} - r_{in}$ represent the tube thickness (*m*) and ΔT is the difference in temperature between the inside and the outside of the pipe (°*C*). This applies to the evaporator and to the condenser section equally but with different values for the inner and outer temperatures. It is mainly affected by the area of exposure and the conductivity of the material.

2.3 Convection outside the thermosyphon

Looking at either section, heat transfer through convection from the surrounding medium to the pipe is given by the following equations for the evaporator section and the condenser section, respectfully:

$$\dot{Q}_h = hA\Delta T \quad \therefore \quad R_{h,e} = \frac{1}{h_e A_e} \quad and \quad R_{h,c} = \frac{1}{h_c A_c} \tag{3}$$

h refers to the heat transfer coefficient (W/m^2K) between the fluid and the solid surface, which in this case is air-carbon steel for h_e and water-carbon steel for h_c. *A* is the exposed surface area (m^2) and ΔT the difference in temperature between the flow and the surface area.

The heat transfer coefficient is derived from the Nusselt number through the expression:

$$Nu = \frac{hd}{k} \tag{4}$$

Where *h* represents the heat transfer coefficient (W/m^2K), *d* the characteristic dimension (*m*) and *k* the thermal conductivity (*W/mK*) of the surrounding fluid. The Nusselt number is a function of the flow conditions, in particular the turbulence and will therefore be different in the evaporator section and in the condenser section.

2.3.1 Convection outside the thermosyphon's condenser section

A cut-section of the condenser section of the heat exchanger under study is schematically represented in Figure 4.

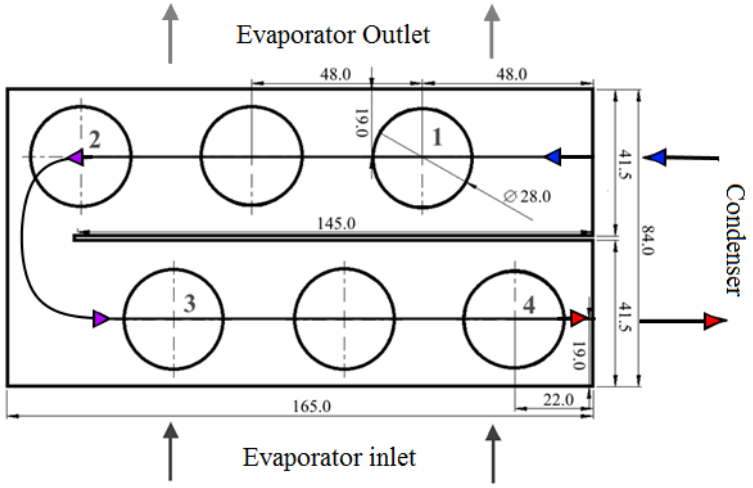

Figure 4: Cross-section of the condenser section of the heat exchanger under study (all dimensions in mm)

Water flows through each thermosyphon one by one following a u-shaped path. The heat transfer by convection over a vertical cylinder in cross-flow has been extensively studied in literature and it applies to the case at hand. The correlation used for external flow over a single cylinder is that of Zhukauskas [41]:

$$Nu = C\ Re^m\ Pr^n \left(\frac{Pr}{Pr_s}\right)^{1/4} \quad (5)$$
$$[0.7 < Pr < 500]$$
$$[1 < Re < 1 \times 10^6]$$

The constants C and m are functions of the turbulence in the vicinity of the cylinder and are available in Table 1. All fluid properties are evaluated at the arithmetic mean of the fluid inlet and outlet temperatures except for the properties marked with an s, which are evaluated at the boundary between the solid and the fluid.

Table 1: Constants of equation (5) for a circular cylinder in cross flow [41] – excerpt

Re	C	m
1 – 40	0.75	0.4
40 – 1000	0.51	0.5
10^3 – 2×10^5	0.26	0.6

2.3.2 Convection outside the thermosyphon's evaporator section

In the evaporator section the thermosyphons are organised into two lines of three thermosyphons each as seen in Figure 4. Equation (5) is not applicable to the evaporator section due to the higher volume of pipes, and Zhukauskas' [41] correlation for a range of vertical tubes in a staggered arrangement is preferred. The expression has the form:

$$Nu = C_1\ C_2\ Re_{max}^m\ Pr^{0.36} \left(\frac{Pr}{Pr_s}\right)^{1/4} \quad (6)$$
$$[N_L \geq 20]$$
$$[2000 < Re_{max} < 40{,}000]$$
$$[Pr \geq 0.7]$$

All properties of the fluids used in equation (6) are evaluated at the mean film temperature except the properties marked with an s, which are evaluated at the boundary temperature. C1 and m depend on the geometry of the tube bundle and are taken from Table 2, C2 is the correction factor used in case fewer than 20 rows of tubes (N_L<20) are present and is available in Table 3.

This expression also takes into account the maximum turbulence and therefore Remax is used, a variable based on the maximum fluid velocity. The maximum velocity occurs at the smallest area; transversally or diagonally between the tubes, according to Figure 5.

Table 2: Constants of equation (6) for airflow over a tube bank of 20 or more rows [41] – excerpt

Configuration	Re_{max}	C_1	m
Staggered	10–10^2	0.90	0.40
Staggered	10^2–10^3	Approximate as a single (isolated) cylinder	
Staggered $S_T/S_L < 2$	10^3–2×10^5	$0.35(S_T/S_L)^{1/5}$	0.60
Staggered $S_T/S_L > 2$	10^3–2×10^5	0.40	0.60
Staggered	2×10^5–2×10^6	0.022	0.84

Table 3: Correction factor C2 of equation (6) for NL < 20 [41]

N_L	1	2	3	4	5	6	7	8	9
Aligned	0.64	0.80	0.87	0.9	0.92	0.94	0.96	0.98	0.99
Staggered	0.68	0.75	0.83	0.89	0.92	0.95	0.97	0.98	0.99

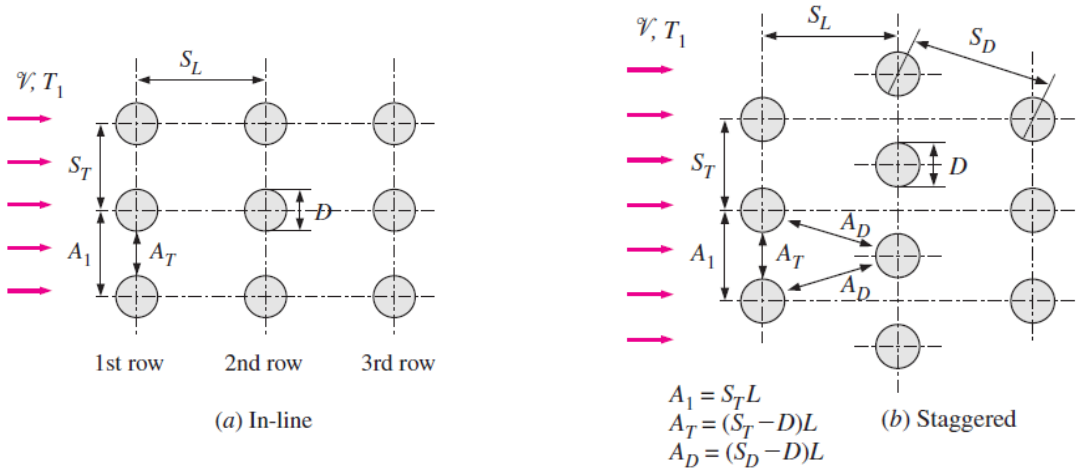

Figure 5: Tube arrangements in a bank (a) aligned and (b) staggered [42]

2.4 Thermal resistance from vapour pressure drop

The thermal resistance from vapour pressure drop (Rin in Figure 3) changes as the vapour pressure decreases as it flows from the evaporator to the condenser section. The expression used for the vapour pressure drop is that of Faghri [43] and takes the form:

$$R_v = \frac{8R_g\mu_v T_v^2}{\pi h_{fg}^2 P_v \rho_v}\left[\frac{(L_e + L_c)/2 + L_a}{r_i^4}\right] \tag{7}$$

Where R_g, h_{fg}, L_a, T_v, P_v, μ_v and ρ_v are the specific gas constant, latent heat of vaporisation of the working fluid, adiabatic section length and temperature, pressure, dynamic viscosity and density of the vapour phase, respectfully. The vapour temperature is the average temperature between the evaporator and condenser section temperatures and the vapour pressure is the saturation pressure correspondent to the vapour temperature.

2.5 Boiling heat transfer

Boiling regimes are dependent on the temperature difference between the bulk temperature of the fluid and the heating wall. In addition, evaporation on a pool of liquid is different from evaporation of a liquid film. The thermosyphons under study were all engineered to work in the nucleate pool boiling regime. The expression chosen to predict the heat transfer in nucleate pool boiling is that of Rohsenow & Hartnett [44], found to be the most comprehensive correlation as it holds remarkably well and has been reported by many researchers in the literature; Reay & Kew [7], Hagens et al. [13], Mroué et al. [37] and Ramos et al. [45] reported the use of Rohsenow & Hartnett's expression [46] to predict the heat transfer from nucleate pool boiling in thermosyphons. Rohsenow & Hartnett's expression for nucleate pool boiling has the form shown in equation (8).

$$q'' = \mu_l h_{fg}\left[\frac{g(\rho_l - \rho_v)}{\sigma}\right]^{1/2}\left(\frac{c_{p,l}(T_{sat} - T_s)}{c_{sf} h_{fg} {Pr_l}^n}\right)^3 \quad (W/m^2) \tag{8}$$

The subscript *l* refers to the liquid phase and *v* to the gas phase as during boiling there is a mix of both. The coefficient c_{sf} and the exponent n depend on the surface-liquid combination. The

thermosyphons under investigation are composed of carbon steel and filled with water having the following vales of c_{sf} = 0.006 and n = 1.0 [46].

The thermal resistance offered by the boiling process may be found by first converting the heat flux to heat transfer rate by multiplying it with the heat transfer area and then divide the difference in temperature by this value, as shown in equation (9):

$$R_{b,pool} = \frac{T_s - T_{sat}}{q'' A_{e,inside}} \quad (K/W) \tag{9}$$

It is important to note that the temperature of saturation of the fluid (T_{sat}) and the Temperature of the boundary (T_s) are required in order to solve the expressions related to the boiling and condensation of the working fluid. This is often resolved by employing thermocouples inside of the thermosyphon and on its surface.

2.6 Condensation heat transfer

Condensation is found to take place in the condenser section where the working fluid, upon coming into contact with the cooler walls, condenses and gives up its latent heat energy. For this heat transfer mechanism, the laminar condensation equation from Nusselt is used [47]:

$$h_{cond} = 0.943 \times \left(\frac{{k_l}^3 \rho_l (\rho_l - \rho_V) g \, h_{fg}}{\mu_l \, \theta \, l} \right)^{1/4} \tag{10}$$

Assuming that $\rho_l \gg \rho_v$ further simplifies the equation. Based on experiments, McAdams [48] also suggests a 20% increase to theoretical expressions due to the fact that experimental values are often larger, changing (10) into:

$$h_{cond} = 1.13 \times \left(\frac{{k_l}^3 {\rho_l}^2 g \, h_{fg}}{\mu_l \, \theta \, l} \right)^{1/4} \tag{11}$$

2.7 Predicting the performance of a thermosyphon-based heat exchanger

The heat exchanger under study is equipped with 6 thermosyphons arranged in parallel as shown in the schematic represented by “Parallel” refers to their arrangement within the thermal network analogy. From a heat transfer perspective, the total thermal resistance for the heat exchanger as shown in Figure 6 would assume the six thermosyphons are in parallel with each other. This means that the overall thermal resistance would be smaller the more thermosyphons are included in the assembly. This is represented analytically in the following way:

$$\frac{1}{R_{6\ thermosyphons\ (TS)}} = \frac{1}{R_i} + \frac{1}{R_{ii}} + \frac{1}{R_{iii}} + \frac{1}{R_{iv}} + \frac{1}{R_v} + \frac{1}{R_{vi}} \tag{12}$$

The thermosyphons (TS) are assumed to have the same average internal thermal resistance thus simplifying the equation to:

$$\frac{1}{R_{6\,TSs}} = \frac{1}{R_{1\,TS}} \times 6 \quad \therefore \quad R_{6\,TS} = \frac{R_{1\,TS}}{6} \tag{13}$$

When looking at the larger picture as displayed in Figure 6, the overall thermal resistance for the thermosyphon-equipped heat exchanger ($R_{th,TSHX}$) may be found through the following expression:

$$R_{th,TSHX} = R_{h,e} + R_{6\,TSs} + R_{h,c} \tag{14}$$

The subscript *TS* stands for thermosyphon, *e* for evaporator, *c* for condenser and *o* for outer.

Placing equation (13) into equation (14):

$$R_{th,TSHX} = R_{h,e} + \frac{R_{1\,TS}}{6} + R_{h,c} \tag{15}$$

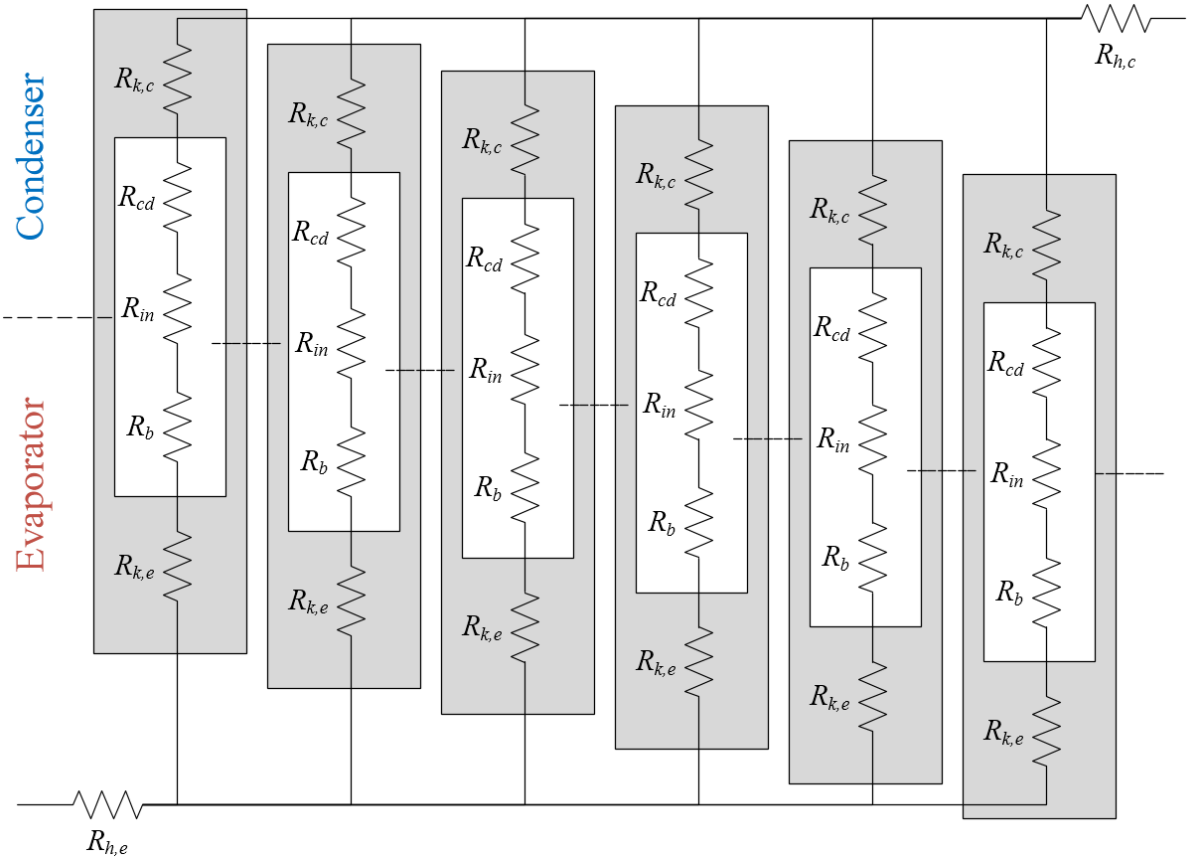

Figure 6: Schematic of the thermal resistances within the thermosyphons equipped in the heat exchanger

2.7.1 Determination of the thermal conductivity of a single thermosyphon

If the thermosyphon is assumed to be a solid super-conductor, this means that the total axial conductivity of a single thermosyphon may be taken as the axial conduction through a solid pipe:

$$R_{1\,TS} = \frac{L}{kA} \quad (K/W) \tag{16}$$

Where $R_{1\,TS}$ is the overall thermal resistance of a single thermosyphon, L is correlated to the length of the thermosyphon (in m), k is the effective thermal conductivity for a single thermosyphon (in W/mK) and A the cross sectional area (in m^2). Re-arranging the equation for k and considering the cross-sectional area of a circle, equation (17) is obtained:

$$k = \frac{L}{R_{1\,ts}\pi r^2} \quad (W/mK) \tag{17}$$

Equation (17) represents the thermal conductivity for a thermosyphon if it is assumed to be a solid super conductor. This value is used as a boundary condition in the CFD simulation.

2.8 The effectiveness-NTU (ε-NTU) prediction method applied to a TSHX

ε -NTU stands for effectiveness-Number of Transfer Units and it is a method of predicting the performance of a heat exchanger. The number of transfer units is a dimensionless parameter widely used in heat exchanger analysis, generally defined as:

$$\text{NTU} \equiv \frac{UA}{C_{min}} \tag{18}$$

Where U represents the overall heat transfer coefficient, A the total heat transfer area and C_{min} the minimum heat capacity rate between the hot and cold flows. The heat capacity rate is a measure of the mass flow rate (ṁ in kg/s) multiplied by the specific heat capacity (c_p in *J/kg.K*).

Effectiveness (ε) is the ratio of the actual heat transfer rate to the maximum possible heat transfer rate; which would be achieved if the temperature of the outlet of the cold flow would equal the inlet temperature of the hot flow [26]:

$$\varepsilon \equiv \frac{q_{act}}{q_{max}} \equiv \frac{C_c(T_{h,i} - T_{h,o})}{C_{min}(T_{h,i} - T_{c,i})} \quad \text{and} \quad \varepsilon = \frac{C_c(T_{c,o} - T_{c,i})}{C_{min}(T_{h,i} - T_{c,i})} \tag{19}$$

Where C_h and C_c represent the heat capacity of the hot and cold flows, respectively, and C_{min} the smallest between the two. By definition, effectiveness is dimensionless and must be valued between 0 and 1; theoretically only a heat exchanger of infinite length would be able to achieve an effectiveness of 1.

The ε-NTU analysis of a heat exchanger equipped with thermosyphons may be done by separating it into two separate heat exchangers, the condenser and the evaporator, and consider them coupled by the thermosyphon working fluid [6, 24, 38, 43]. The effectiveness of the evaporator and condenser sections of the heat exchanger is determined separately and is given by:

$$\varepsilon_e = 1 - e^{(-NTU_e)} \quad \text{and} \quad \varepsilon_c = 1 - e^{(-NTU_c)} \tag{20}$$

The number of transfer units for the evaporator and for the condenser is found through:

$$\text{NTU}_e = \frac{U_e A_e}{C_e} \quad \text{and} \quad \text{NTU}_c = \frac{U_c A_c}{C_c} \tag{21}$$

Where A refers to the total heat transfer area in the respective row or stage, and C_e and C_c represent the average heat capacity of the shell-side fluid. The overall heat transfer coefficient *U* must be found for each section using the thermal network analogy explained in a later chapter.

Faghri [43] defined the effectiveness of an individual thermosyphon to be related to the minimum and maximum values of effectiveness between the evaporator and the condenser sections:

$$\varepsilon_{ts} = \left(\frac{1}{\varepsilon_{min}} + \frac{C_r}{\varepsilon_{max}}\right), \quad C_r = \frac{C_{min}}{C_{max}} \tag{22}$$

Where ε_{min} and ε_{max} take the minimum and maximum values of ε_e and ε_c. C_r is the heat capacity ratio and C_{min} and C_{max} follow the same logic of the effectiveness, taking the minimum and maximum values of C_e and C_c, respectively.

The effectiveness of a multistage heat exchanger in counter flow for an n number of rows has been adapted from Incropera & DeWitt [47] in order to apply to thermosyphon-equipped heat exchangers.

$$\varepsilon_{e,n} = \frac{\left(\frac{1 - C_{r,e}\,\varepsilon_e}{1 - \varepsilon_e}\right)^n - 1}{\left(\frac{1 - C_{r,e}\,\varepsilon_e}{1 - \varepsilon_e}\right)^n - C_{r,e}} \tag{23}$$

$$\varepsilon_{c,n} = \frac{\left(\frac{1 - C_{r,c}\,\varepsilon_c}{1 - \varepsilon_c}\right)^n - 1}{\left(\frac{1 - C_{r,c}\,\varepsilon_c}{1 - \varepsilon_c}\right)^n - C_{r,c}} \tag{24}$$

Cr is the heat capacity ratio of the fluid streams on each side of the thermosyphon; the ratio between the heat capacity rate of the shell-side fluid to the heat capacity rate of the thermosyphon's working fluid. However, since the working fluid is at constant temperature, its specific heat and capacity rate is effectively infinite, making the variables $C_{r,e}$ and $C_{r,c}$ equal to zero [39]. Equations (23) and (24) are then simplified into the forms seen in equation (25) and (26), respectively:

$$\varepsilon_{e,n} = 1 - (1 - \varepsilon_e)^n \tag{25}$$

$$\varepsilon_{c,n} = 1 - (1 - \varepsilon_c)^n \tag{26}$$

The overall effectiveness depends on which fluid side has the largest heat capacity; if the heat capacitance of the evaporator side fluid is the largest; $C_e > C_c$:

$$\varepsilon_t = \left(\frac{1}{\varepsilon_{c,n}} + \frac{C_c/C_e}{\varepsilon_{e,n}}\right)^{-1} \tag{27}$$

On the other hand, if $C_c > C_e$:

$$\varepsilon_t = \left(\frac{1}{\varepsilon_{e,n}} + \frac{C_e/C_c}{\varepsilon_{c,n}}\right)^{-1} \tag{28}$$

Using the overall effectiveness of the heat exchanger, the outlet temperatures for the evaporator and the condenser can be predicted from:

$$T_{h,out} = T_{h,in} - \varepsilon_t \frac{C_{min}}{C_e}\left(T_{h,in} - T_{c,in}\right) \tag{29}$$

$$T_{c,out} = T_{c,in} + \varepsilon_t \frac{C_{min}}{C_c}\left(T_{h,in} - T_{c,in}\right) \tag{30}$$

3 Experimental set up

This chapter describes the physical design of the experimental rig, the working conditions of the heat exchanger, including the inlet temperatures and flow rates of both shell sides, as well as the control apparatus used.

3.1 Design of test rig

The experimental rig consisted of a heat exchanger equipped with six thermosyphons in a cross-flow arrangement. The design of the rig was based on a real heat exchanger used by the partner company, built with a modular design in mind in order to allow further investigation of different flow configurations and boiling regimes.

The test rig was equipped with six thermosyphons vertically arranged in two staggered rows. The thermosyphon tubes were made of carbon steel measuring 2m in length and with a diameter of 28mm. The surrounding wall had an average thickness of 2.5mm. The working fluid was distilled water and the filling ratio was 100% (of the evaporator section), which roughly translates into 0.7m in height from the bottom of the thermosyphon. All tubes were chemically treated before insertion of water to avoid corrosion.

As can be seen in Figure 7, the condenser section occupied the top 0.2m of the thermosyphons and the evaporator section the lower 0.6m. The remaining 1.2m were kept fully insulated as they served the adiabatic section of the heat pipe. Both the evaporator and the condenser were separated from the adiabatic section by a 10mm-thick division plate in order to prevent leaks.

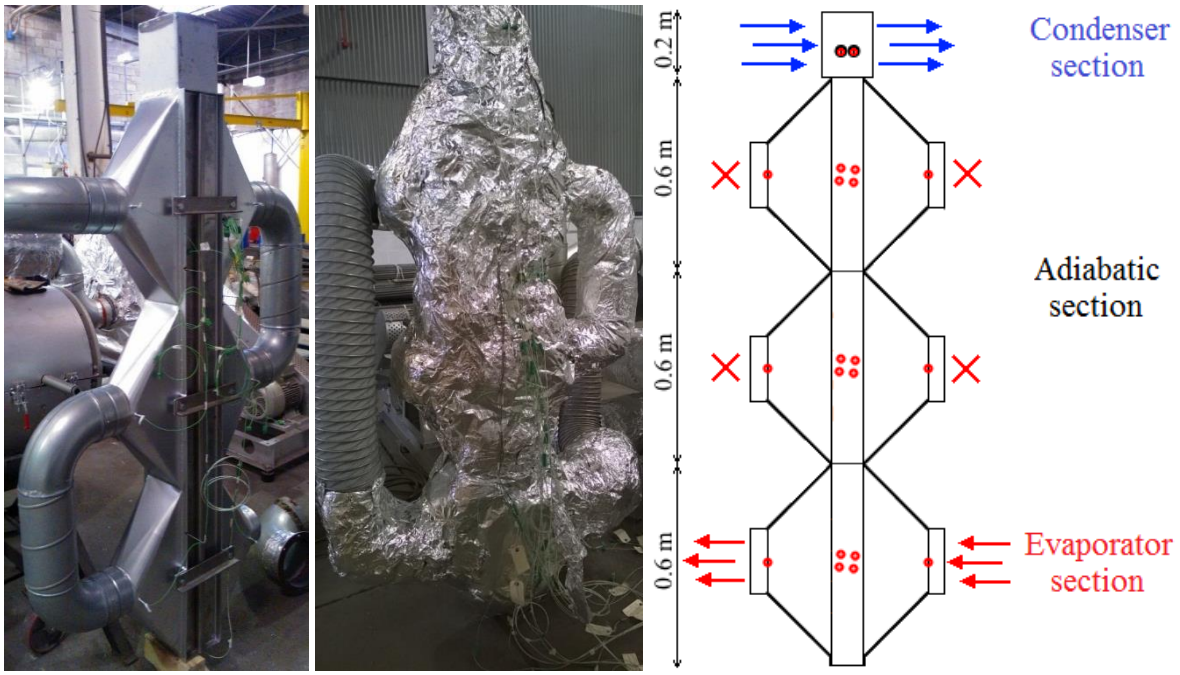

Figure 7: Experimental apparatus of the heat exchanger in cross flow
From left to right: the heat exchanger before installation; the heat exchanger after being thermally insulated; representative schematic of the thermosyphon heat exchanger and the size of its respective sections.

3.2 Experiment design

The experimental rig was divided between two circuits; a closed air circuit – the heat source – and an open water circuit – the heat sink –, both included in the schematic represented in Figure 8. The hot air circuit consisted of a closed air loop equipped by a fan and a heater. The flow was directed to pass through the fan and the heater and then to enter the heat exchanger. After leaving the heat exchanger, it was sucked into the fan once again, repeating the cycle. The fan frequency ranged between 10 and

50Hz in 10Hz increments. The mass flow rate was controlled by an analogue pitot tube installed at the inlet of the evaporator section and ranged between an average 0.05and 0.14kg/s in 0.03 increments.

The heater power could be regulated according to a desired temperature thanks to a feedback loop. The feedback loop controlled the heater power through a thermocouple located at the outlet of the heat exchanger. The temperature of the air varied between 100 and 300°C in 50°C increments. The higher temperatures correspond to the normal working conditions of the heat exchangers encountered in waste heat recovery [12]. The lower temperatures were employed to test the lower operating limits of the thermosyphons.

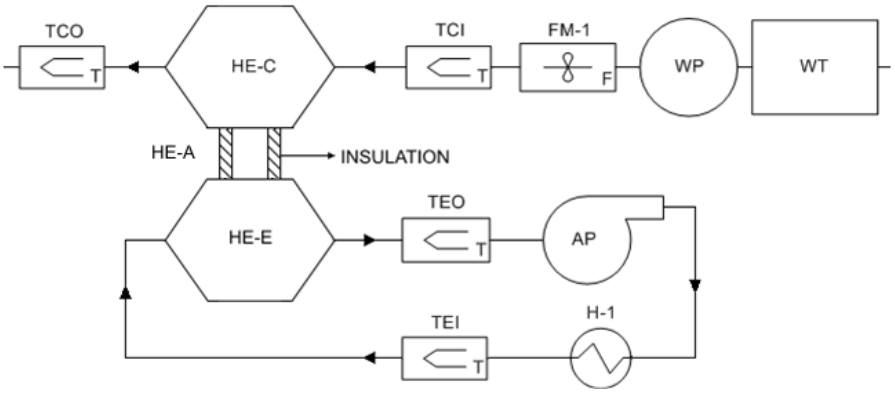

Figure 8: Schematic of the single pass test setup

Description: TCI/TCO – Thermocouples at inlet/outlet of condenser; HE-C/E/A – Thermosyphon heat exchanger Condenser/Evaporator/Adiabatic section; FM-1 – Turbine Flow Meter; WP – Water pump; WT – Water tank; TEI/TEO – Thermocouple at inlet/outlet of evaporator; AP – Air Pump; H-1 – Air Heater.

The cold water circuit consisted of an open loop and included a water tank to help regulate the inlet flow rate into the pump as can be seen in Figure 8. The mass flow rate of water was kept constant throughout the test at 0.08kg/s and at an average temperature of 10°C. After leaving the water tank, the water was pumped through the heat exchanger. After flowing through the heat exchanger, the warmed-up water would freely flow into another process. The flow inside the condenser section followed a U-shaped path as depicted in Figure 4.

3.3 Gathering and Processing of Data

20 k-type thermocouples were placed at specific locations in the heat exchanger to measure the temperature of the flows and the working temperatures of the thermosyphons. The thermocouples were placed in key sections, such as the inlet and outlet of both the evaporator and condenser sections, on the surface of each "corner" thermosyphon (numbered 1 to 4 in Figure 4), on the adiabatic section, and within the thermosyphons. The thermocouple placements are marked in red in the simplified schematic of Figure 7.

Four thermocouples were placed on the surface of each "corner" thermosyphon: one in the evaporator section, two in the adiabatic section and one in the condenser section. These thermocouples were brazed into the surface of the thermosyphon at 1mm depth. Two brazed thermocouples are shown in Figure 9.

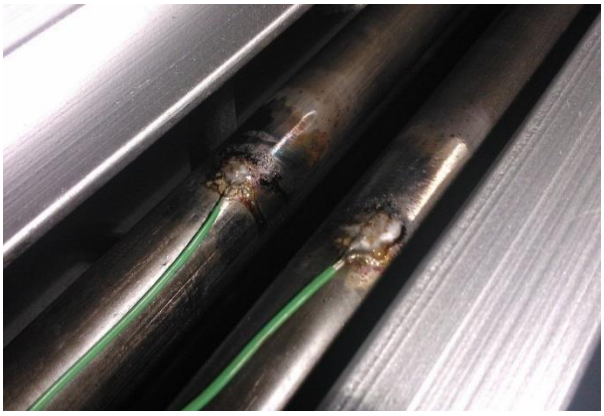

Figure 9: The brazed thermocouples on the surface of the thermosyphon

The experimental procedure was the same in all the tests and it is described as follows:

1. The cold water was allowed to run in the cold water circuit.
2. The air was then bled from the condenser section through the bleed valve located at the top.
3. After the condenser section was filled with water, the heater was turned on and the hot air flow was flowing in the evaporator section.
4. The temperature was set to 300°C. Data for this temperature setting would be recorded for a fan rate of 10, 20, 30, 40 and 50Hz. The same flow rates were then tested for 250, 200, 150, 100 and 50°C.
5. Data were recorded and collected for each setting every10 minutes at steady state conditions.

A total of 30 tests were conducted, one for each different inlet condition.

4 The CFD model

A 3 dimensional computational model was run in parallel with the experimental tests conducted on the heat exchanger. In this simplified model the thermosyphons were modelled as super-conductors whose thermal conductivity had been deduced according to the inlet conditions using the analytical method explained in chapter 2.

4.1 Assumptions

The following assumptions were made prior to running the simulation:

a) Constant mass flow rate across the heat exchanger in both flow sides
b) Neglectable axial heat transfer from conduction across the thermosyphon wall
c) No heat transfer across the walls of heat exchanger
d) No heat transfer at the adiabatic section of the thermosyphon
e) Constant inlet mass flow rate across inlet area
f) Same thermal conductivity for all the thermosyphons
g) The thermosyphons were assumed to be solid superconductors

4.2 Methodology

ANSYS Fluent was the computational fluid dynamics (CFD) software used to simulate the heat flow within the heat exchanger. The model was created with the purpose of assessing the potential of simulating heat pipes as solids rods of constant conductivity for the modelling of future heat exchangers. The realizable k-epsilon turbulence model (k-ε) was used in each of the simulations as it is found to be more accurate at higher Reynolds number and smaller pressure gradients [49, 50], which is the case in this particular experimental test range. A coupled pressure-based solver is also recommended as it is more efficient in steady-state simulations and offers better results for single-phase fluid flow [45,51].

The thermosyphons were modelled as solid objects using the value for thermal conductivity achieved from the method described in chapter 3. For the fluid properties, Fluent's own standard tables of

substance properties were used to determine the characteristics of the fluids simulated (water in the condenser and air in the evaporator).

4.3 Mesh selection

The mesh selection was done by running the same simulation with different mesh sizes and comparing the accuracy of the results. A mesh was deemed "good" if the maximum skewness is lower than 0.7 for hexahedron and tetrahedrons and 0.8 for triangular elements [20]. A comparison of the results is available in Table 4 and can be observed in Figure 10.

Table 4: Mesh Dependency.

Level	*No of Cells*	*Type of cells*	*Skewness*	*Time per iter.*
Coarse	*1,408,658*	*Hex + Tetra*	*avg: 26%, stdev: 16%*	*2-10 s*
Medium	*2,291,364*	*Hex + Tetra*	*avg: 21%, stdev: 13%*	*7-15 s*
Fine	*3,099,230*	*Hex + Tetra*	*avg: 21%, stdev: 13%*	*25-50 s*

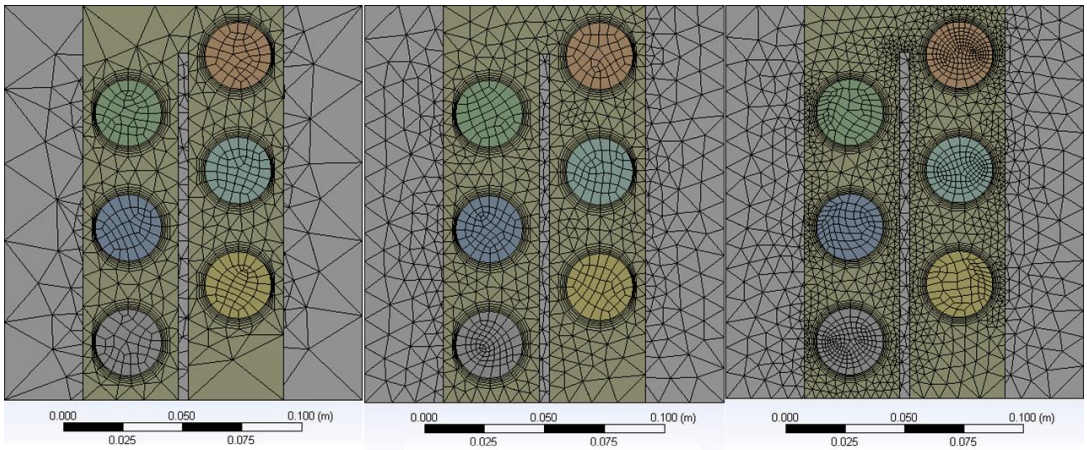

Figure 10: Comparison between the three different meshes – Coarse, Medium and Fine

It was found that a fine mesh would take 3 times longer to converge (on average) and the results would not be significantly more accurate (±0.8%); therefore the medium mesh was used in all the tests run in Fluent.

The relaxation factors were set at 1e-6 and the test allowed to run until no change was observed in the scaled residuals.

4.4 Boundary Conditions

The boundary conditions used in the CFD to describe the inlet and outlet of the heat exchanger model are displayed in Table 5. The CFD model was run several times for each different inlet condition to reduce the variance of the results.

Table 5: Boundary Conditions

	Type	*Mass flow rate (kg/s)*	*Temperature (°C)*
Evaporator Inlet	*Mass Flow Inlet*	*0.05 to 0.17 at 0.03 intervals*	*50 to 300 at 50 intervals*
Evaporator Outlet	*Mass Flow Inlet*	-	*Desired Output*
Condenser Inlet	*Mass Flow Inlet*	*Constant 0.0715*	*Constant 10.0 ± 0.3*
Condenser Outlet	*Mass Flow Inlet*	-	*Desired Output*

The boundary conditions used to simulate the inlets and outlets were of type "mass flow inlet", with the outlets having the opposite direction. This assumption is valid for both circuits: the air circuit

consisted of a closed system, as observed in Figure 8, so it was being "pulled" out of the evaporator outlet at the same rate it was pushed into the evaporator inlet.

At normal atmospheric conditions, water is incompressible. Since the condenser section had been completely purged of air prior to the start of any test, the assumption is that the mass flow rate of water at the exit of the condenser must be the same as the mass flow rate of water flowing into the condenser.

All the walls of the heat exchanger were insulated during the experimental test and were thus assumed to be adiabatic in the CFD simulation. The only contact between the hot and cold flows is made through the thermosyphons.

The thermosyphons were modelled not as two-phase devices, but as solid bars. The thermal conductivity of the tubes was predicted using the thermal network analogy described in chapter 2.

5 Results and discussion

This chapter presents the main results and includes a comparison between the experimental, theoretical and CFD results. First the results from the experimental tests are presented and then a comparison of the results obtained from the CFD and the numerical predictions is included.

5.1 Experimental Results

This section outlines the results for the experiment with six thermosyphons. Air was used as the evaporator-side fluid and water as the condenser-side fluid. The mass flow rate of air varied between 0.05 and 0.17kg/s and the inlet air temperature varied between 50 and 300°C. On the condenser side, the inlet temperature and the mass flow rate of water were both kept constant at approximately 7°C and 0.08kg/s respectively.

Figure 11 displays the temperature distribution within the heat exchanger for inlet temperatures of 50, 100, 150, 200, 250 and 300°C. The temperatures were logged from five different locations; namely at the inlet and outlet of the evaporator (T_{ein}, T_{eout}) and condenser sections (T_{cin}, T_{cout}) and inside the thermosyphons (T_{pipe}).

It can be seen that the trend is for the difference in temperature across the evaporator section to decrease as the mass flow rate of the incoming hot air increases. In the condenser section the difference in temperature increases with increasing mass flow rate on the evaporator side. From a thermodynamic perspective this is a logical outcome as the increasing mass flow rate of air into the evaporator increases the heat transfer coefficient which in turn increases the heat flow into the thermosyphon thus resulting in more heat being transferred to the water on the condenser section.

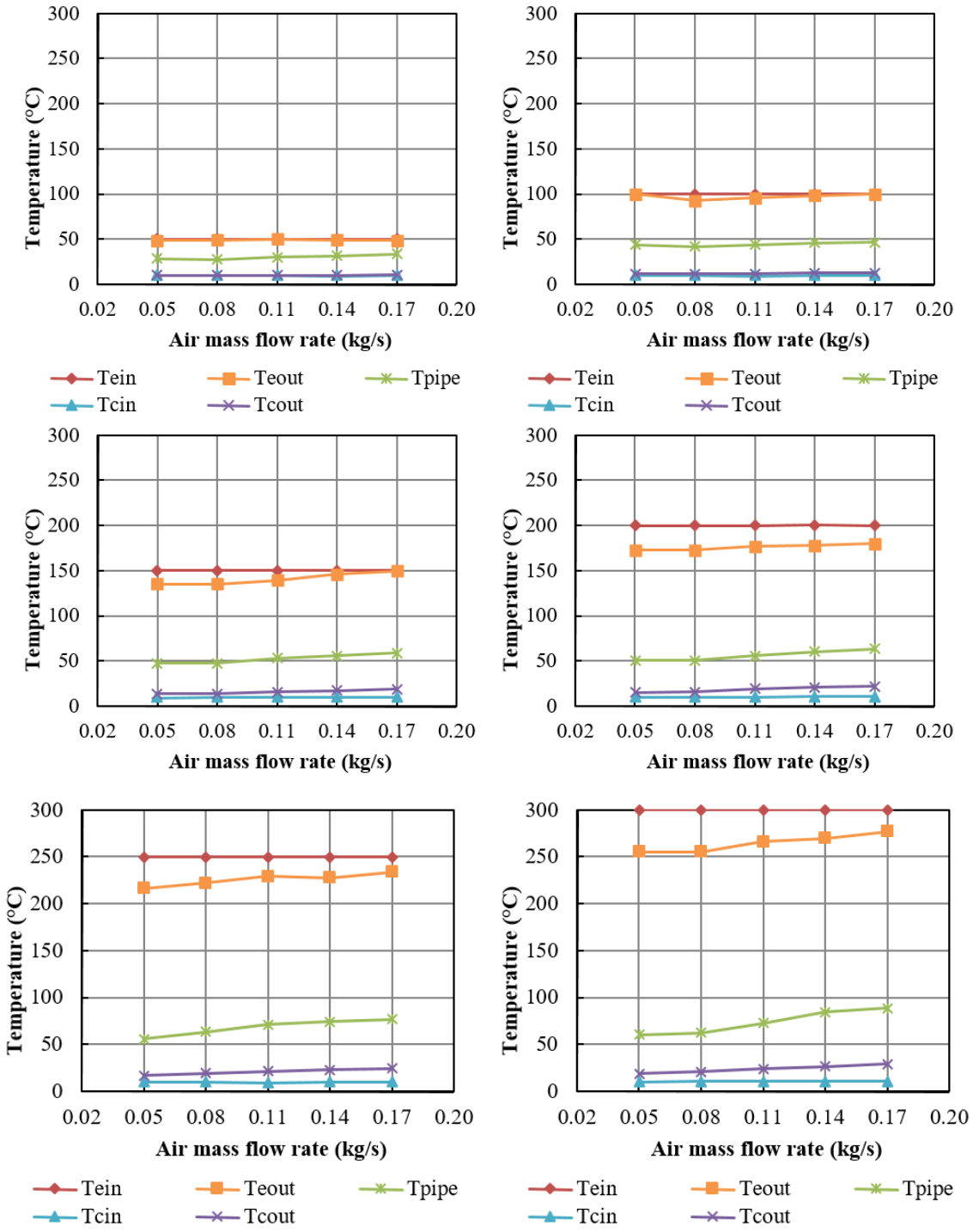

Figure 11: Temperature distribution within the heat exchanger for inlet air temperatures ranging from 50 to 300 °C

From the experimental results, a regular pattern emerged between the thermosyphon working temperature and the overall difference in temperature across the entire heat exchanger ($T_{e,avg} - T_{c,avg}$). A plot of the average working temperature of the thermosyphons against the overall difference in temperature between the evaporator and the condenser section for the range of mass flow rates tested is displayed in Figure 12. Data from the trend lines, shown in their respective colour, allowed the creation of equation (31) an expression able to predict the average working temperature of the thermosyphons for each different working conditions.

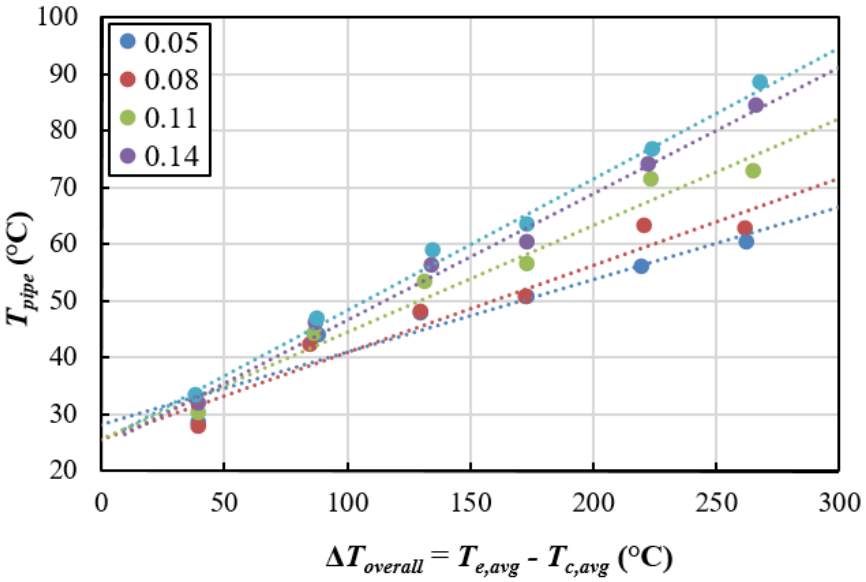

Figure 12: Average working temperature of the thermosyphons for different overall ΔT at different mass flow rates

$$T_{pipe} = 0.589\,\dot{m}^{0.5146}(\Delta T_{overall} - 40) + 32 \quad (°C) \tag{31}$$

Equation (31) is a correlation that allows the prediction of the average working temperature of the thermosyphons according to the mass flow rate of air on the evaporator side and the difference in temperature across the entire heat exchanger. The expression only applies to the heat exchanger under study with constant temperature and mass flow rate on the condenser side. The output of the applied correlation to the inlet conditions of the heat exchanger is presented in Figure 13 which seems to follow the tendency of Figure 12 with reasonable accuracy.

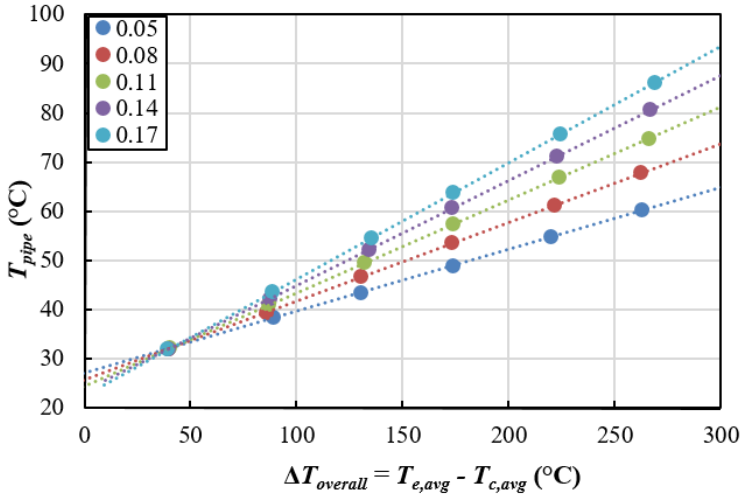

Figure 13: Predicted average working temperature of the thermosyphons for different overall ΔT at different mass flow rates

The heat transfer rate was found to be directly proportional to the inlet air mass flow rate and to the temperature of the flow at the inlet, as can be seen in Figure 14. The profile of the lines indicate that if

a higher mass flow rate was provided, the heat exchanger would be capable of transporting that much more heat, however, the lines also start to become more flat as the mass flow rate increases. The average maximum duty according to the data gathered was 900W maximum heat flux per heat pipe.

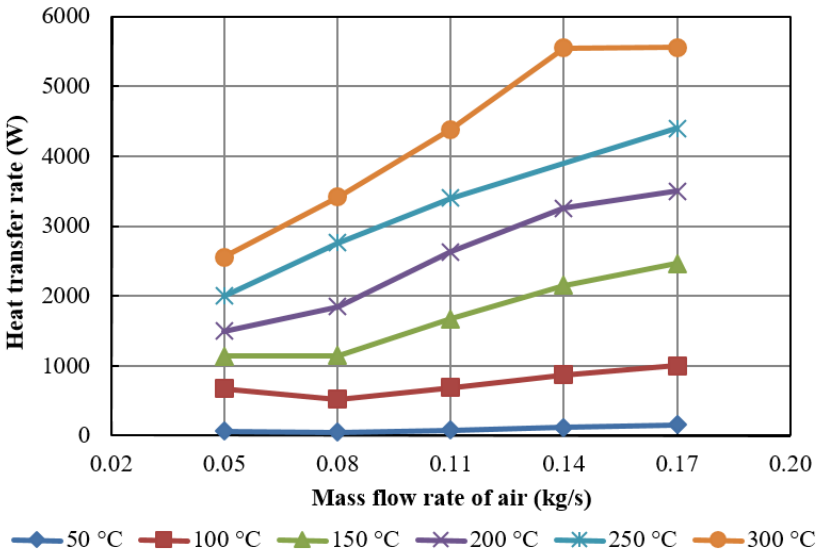

Figure 14: Total heat transfer rate of the heat exchanger

The thermal resistance from equation (18) was also plotted against the overall heat transfer rate as shown in Figure 15. A higher difference in temperature produced a lower overall thermal resistance in the heat exchanger due to the more stable boiling regime inside the thermosyphon. Once again, the results obtained at 50°C are the oddball with a thermal resistance higher than 0.2K/W. The other results have a lower value ranging between 0.05 and 0.1K/W. The plot clearly shows the thermal resistance is inversely proportional to the overall heat transfer coefficient.

An uncertainty study was conducted in order to find the error propagation from the measurement instruments used in the experimental rig. It was observed that for all the tests, the uncertainty when determining the Q_{out} is lower than 10%, which is an acceptable figure for engineering applications.

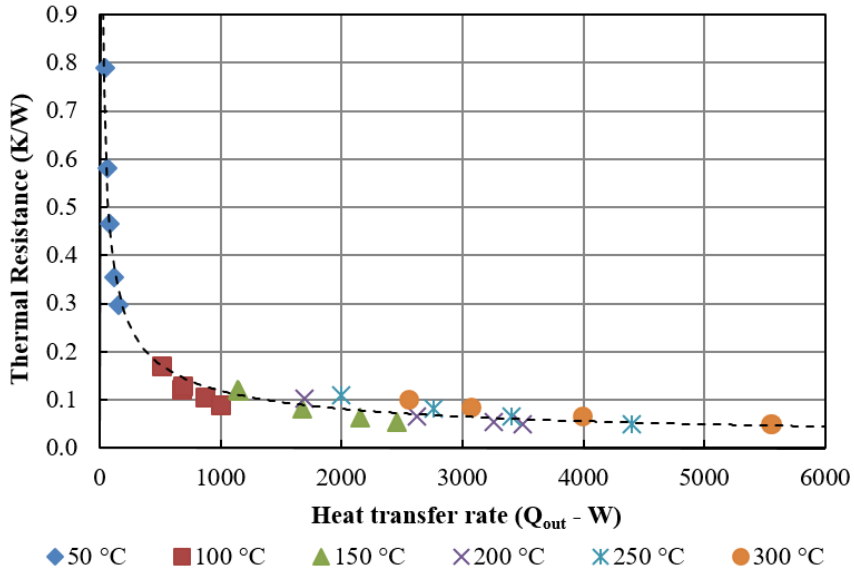

Figure 15: Relation between Q_{out} and the overall thermal resistance

5.2 Effectiveness

Effectiveness is a variable that is an integral part of the Effectiveness-Number of Transfer Units (ε-NTU) method and is a measure of a heat exchanger's heat transfer potential. The effectiveness is a rate of the actual heat transfer of a heat exchanger to the maximum possible heat transfer rate. Figure 16 represents a plot of the effectiveness of the heat exchanger against the mass flow rate of incoming air. A downward trend is observed in all of the results, as with the increased mass flow rate, the temperature difference between the inlet and the outlet of the condenser section is reduced, reducing the overall effectiveness. The plot is in agreement with Jouhara and Merchant [26] as higher inlet temperatures result in higher effectiveness.

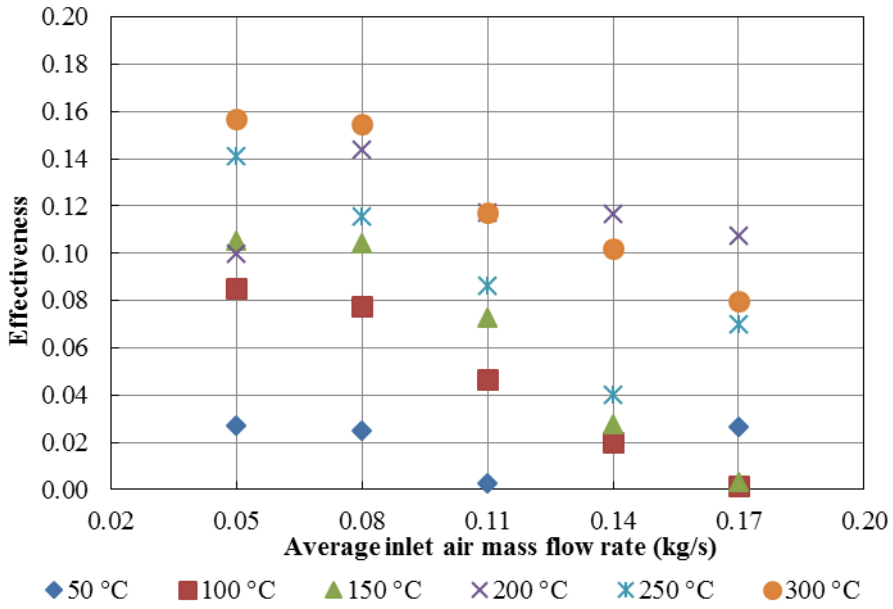

Figure 16: Effectiveness of the heat exchanger

The effectiveness was also plotted against the Number of Transfer Units (NTU) and it can be concluded that there is a quasi-linear relation in agreement with the literature for this type of plots [42,47] as seen in Figure 17. The heat exchanger under study had a small area of exposure and was incapable of transferring more than 0.2 transfer units, however, the trend shown in Figure 17 displays a linear increase. The effectiveness of the heat exchanger will increase at a rate of 9:10 to the number of transfer units until an effectiveness of 1 which at the current rate could be found at 1.2 NTU.

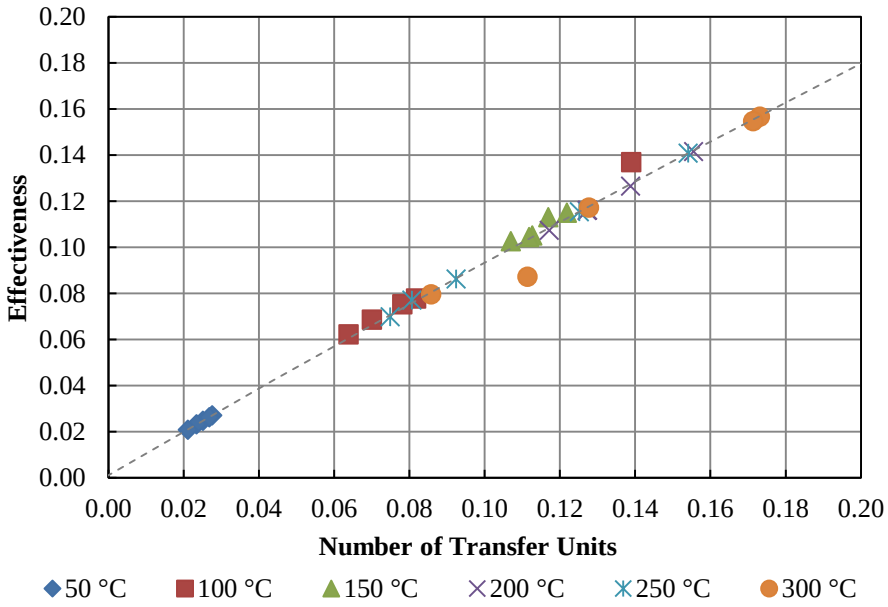

Figure 17: Comparison between the effectiveness and the NTU

5.3 Comparison of results

Regarding the temperature at the outlets, the CFD results compared well to the experimental results, with a maximum difference of 10% at the evaporator section and 15% at the condenser section as can be seen in Figure 18:

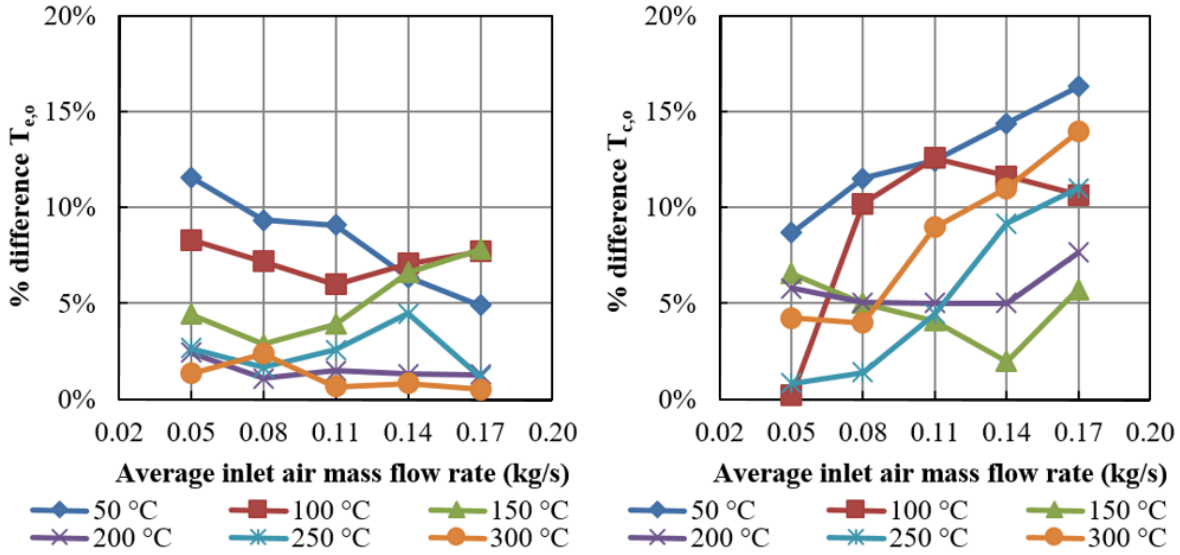

Figure 18: Percentage temperature difference at the outlets between the experimental test and the CFD simulation

Figure 19 portrays a more detailed comparison between the outlet temperature of the evaporator section and the condenser section; a good agreement is found on both as they tend towards the centre of the graph. According to Figure 19, it is found that the CFD simulation is slightly over-estimating the temperature at the outlet at low evaporator mass flow rates and under-estimating them as the mass flow rates increase.

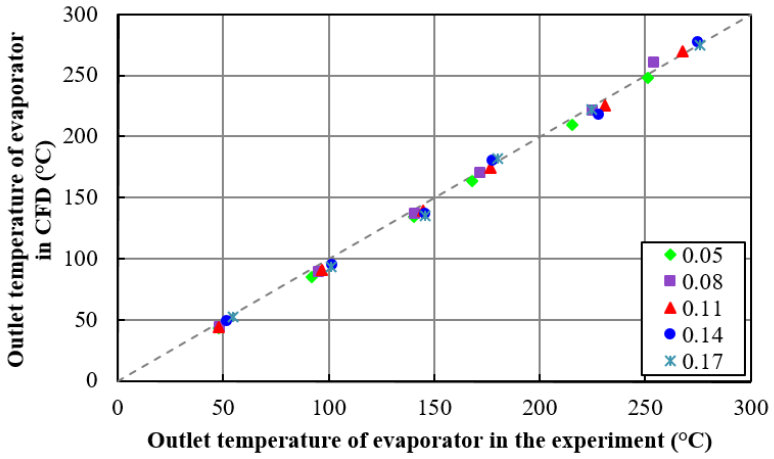

Figure 19: Comparison between experimental and CFD results for the temperature at the outlet of the evaporator at different mass flow rates.

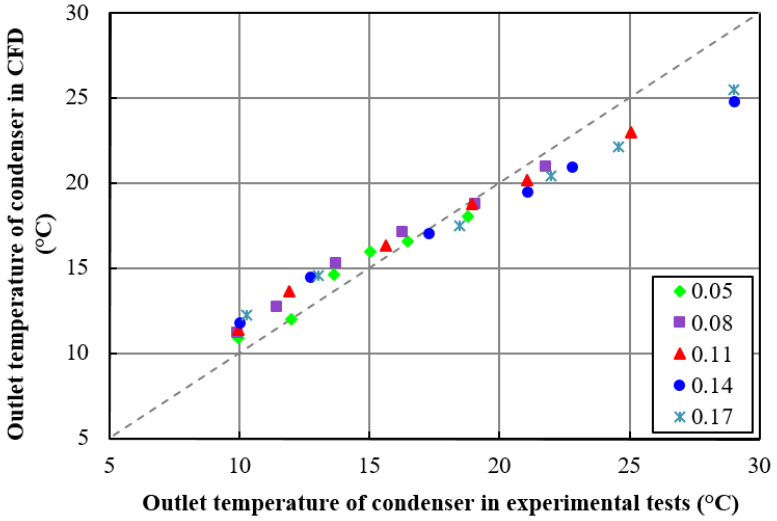

Figure 20: Comparison between experimental and CFD results for the temperature at the outlet of the condenser at different mass flow rates.

The heat transfer rate achieved in the CFD was compared with that found from the experimental results and plotted in figure 20. Following the same behaviour as figure 9, the CFD simulation over-estimates the performance of the heat exchanger. However, this is to be expected as in reality it is impossible to have an insulation that is completely adiabatic; particularly with the geometry of the heat exchanger under study. The CFD simulation also appears to be slightly under-estimating the performance of the heat exchanger at higher mass flow rates (10%); this may be due to higher inlet turbulence in the experimental rig as a result of an increased mass flow rate which is impossible to predict as an inlet boundary condition for the CFD model.

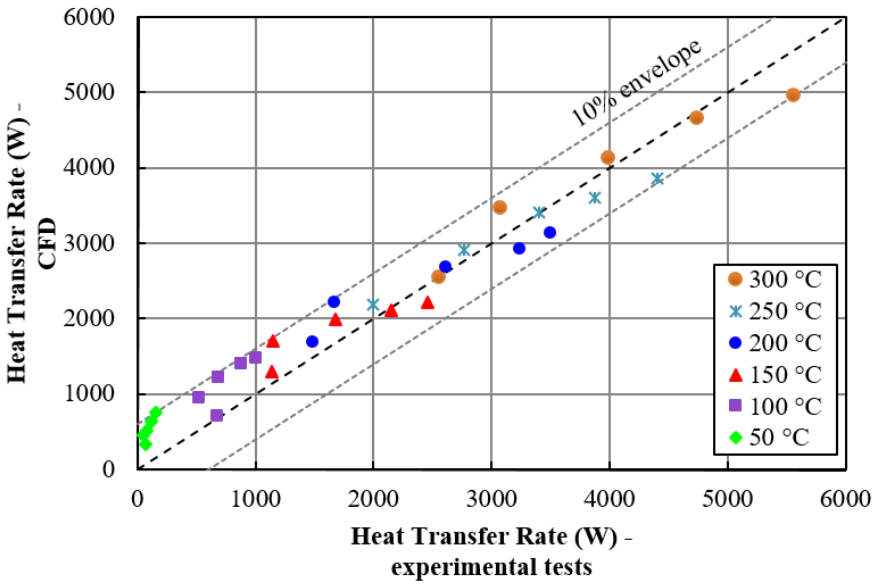

Figure 21: Comparison of the heat transfer rate between the experimental test and the CFD model for different operating temperatures.

The difference in temperature is partially reflected in the heat transfer rate. Figure 20 includes a comparison of the overall heat transfer rate between the experimental tests and CFD simulation. All the results are included within a 10% fluctuation showing a good correlation between the experimental data and the data obtained from the simulations. The theoretical results were plotted in a similar-type graph in Figure 22 and it was observed that the CFD simulation clearly follows the same trend. This leads to the conclusion that the inherent error is caused by the theoretical expressions which may require some fine tuning in order to better adapt to the problem at hand.

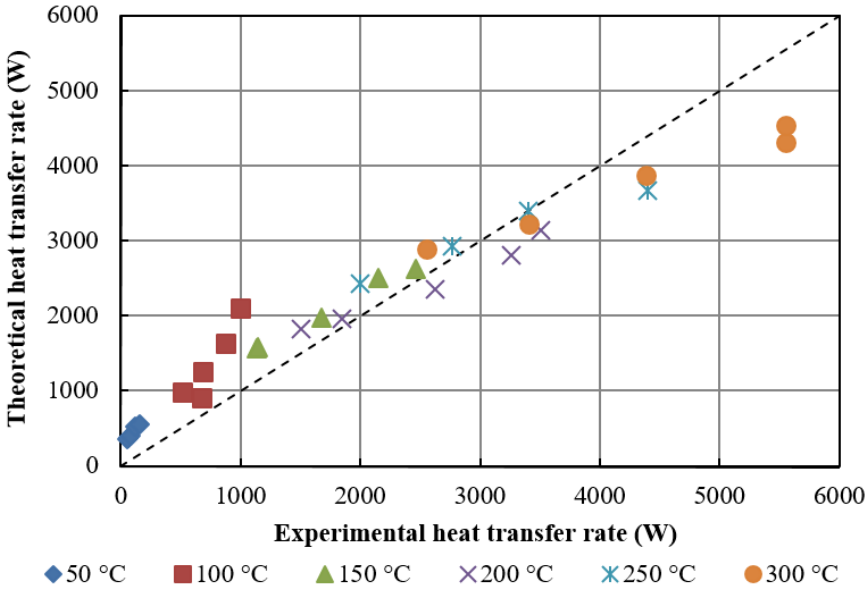

Figure 22: Direct comparison between the experimental and the predicted heat transfer rate.

5.4 Results from CFD simulation

CFD was useful as the visualisation of the problem allowed the identification of recirculation zones within the unique geometry of the heat exchanger. Figure 23 illustrates a vector plot of the velocity within the evaporator section of the heat exchanger. The higher velocities were found in the vicinity of the heat pipes. In this vector plot, the recirculation zones are clearly identifiable in blue at the top and bottom of the figure.

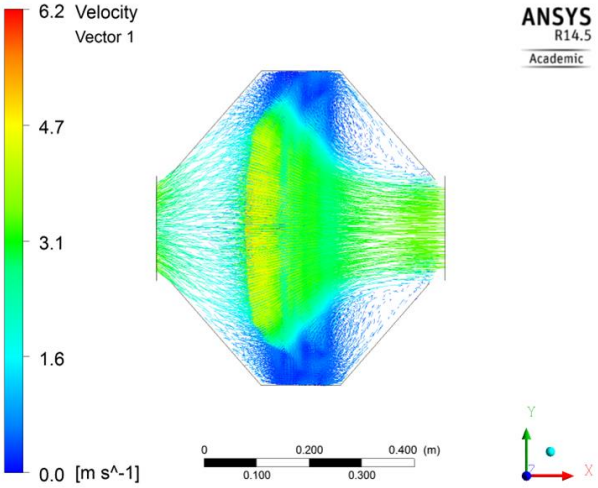

Figure 23: Vector velocity plot of the evaporator section

Figure 24 presents the average velocity profile within the condenser section. The inlet temperature and mass flow rate were kept constant in the condenser section allowing Figure 24 to represent the condenser section for all of the conditions tested. The blue areas represent re-circulation, common after the cylinders in parallel arrangements.

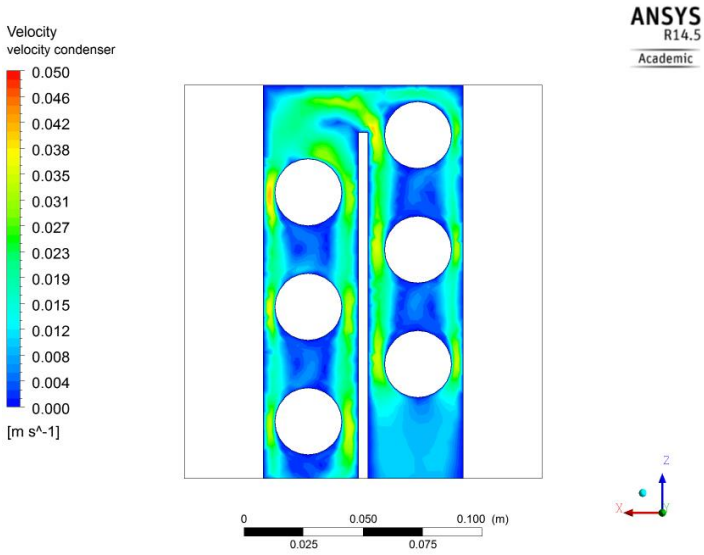

Figure 24: Velocity profile within the condenser section of the heat exchanger

A temperature contour of the evaporator is shown in Figure 25; the air is entering the evaporator at 300°C from the left and leaves the evaporator at approximately 255°C. Temperatures lower than 250°C are shown within the pipes. The variation of the temperature on the hot flow is particularly noticeable in this figure. The temperature of the thermosyphons at that particular height is also shown in its respective location.

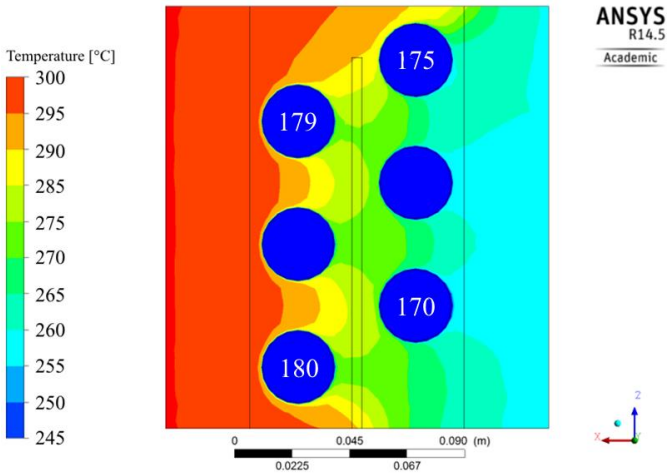

Figure 25: Average temperature contour of the air in the evaporator section at 300°C and 0.08m/s.

Figure 26 illustrates the temperature contour of the condenser section for the same inlet conditions as Figure 25. The water enters the condenser at 10°C and leaves the condenser at approximately 20°C. The numbers in the pipes represent the temperatures of the pipes at the condenser section. It can be observed that they diverge from the temperatures shown in Figure 25 and that is because the pipes are not isothermal within as a normal thermosyphon would be; their temperature varies along the y-axis due to the different fluid temperatures surrounding the pipes. The overall average temperature of the pipes, however, coincided with the saturation temperature of the pipes.

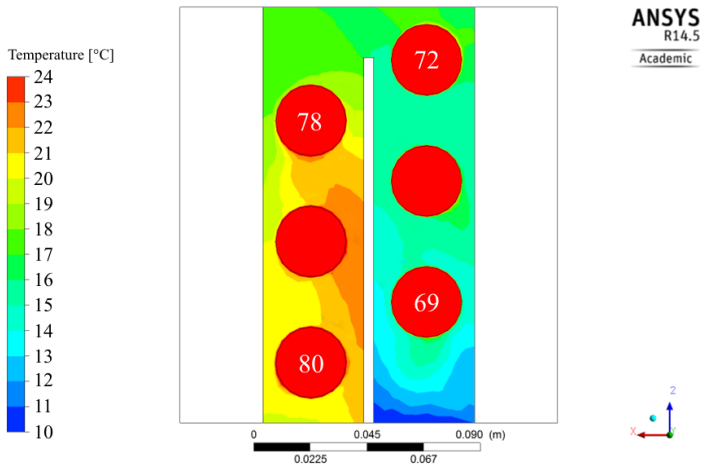

Figure 26: Average temperature contour of the water in the condenser for the evaporator conditions of 300°C and 0.08m/s

5.5 Error Propagation

An uncertainty study was conducted on the error propagation from the measurement instruments used in the experimental rig and the results are presented in Figure 27. The method is explained thoroughly in section 4.3.4.

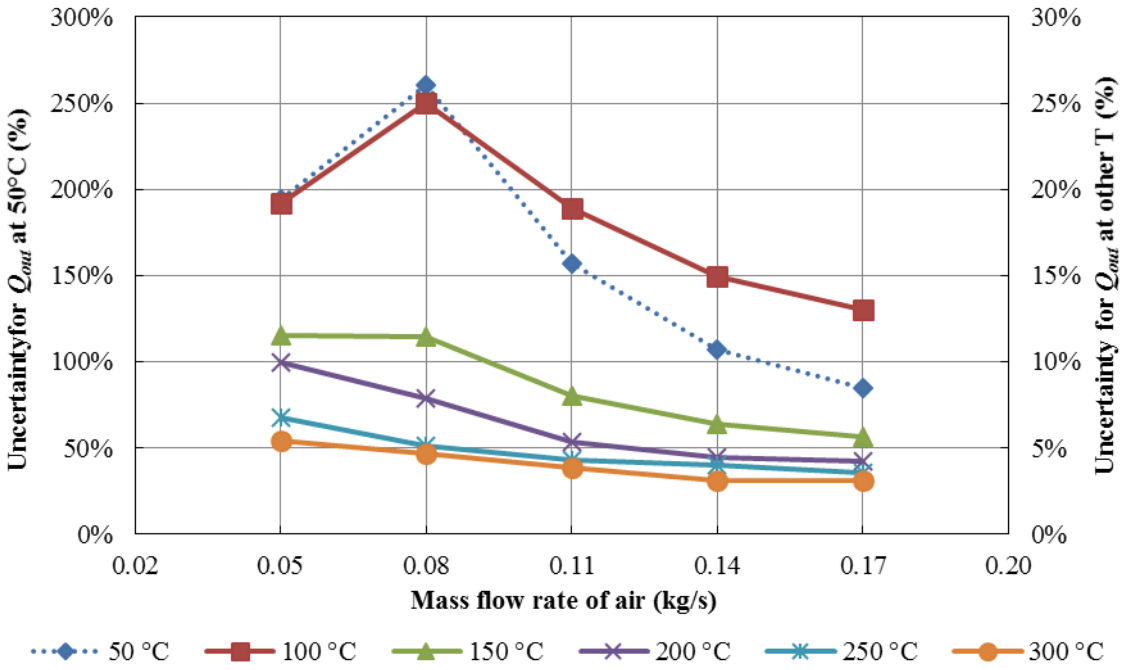

Figure 27: Error propagation for Q_{out}

It was observed that the smaller the difference in temperature between the inlet and the outlet temperatures, the higher the uncertainty. This is particularly striking at 50°C inlet air temperature where the uncertainty hovers the 300% due to the fact that the temperature variation is less than 1°C. At 100 °C the ΔTc already fluctuates close to 2°C and therefore the uncertainty propagation is reduced. For all the other tests the uncertainty when determining the Qout is lower than 10% and stays within the 5% range, which is a more acceptable range for most engineering applications.
Overall the trend is for the error propagation to reduce as the mass flow rate and the difference in temperatures increase, a trend seen in all the tests.

6 Conclusions

An experimental and a numerical investigation of a heat pipe-based heat exchanger was successfully carried out and verified through comparison with a real-world test experiment. The following conclusions were obtained according to the results:

- Higher temperatures and mass flow rates result in higher heat transfer rates up to a limit of 900W/pipe.
- Equations found in the literature seem to over-predict the results at low evaporator temperatures and under-predict at higher evaporator temperatures – an update is suggested.
- The modelling of the thermosyphons as solid bodies with a conductivity extracted from an analytical study involving the ε-NTU method has been tried and tested in a CFD simulation and the results proved very satisfactory.
- Good agreement between the experimental and numerical results for all temperatures was found for a wide range of flow conditions on the evaporator side; an average 5% temperature difference was observed between the numerical and experimental results in the evaporator section and 7% in the condenser section.

Acknowledgements
The authors would like to thank the funding bodies, the European Development Fund, and Econotherm UK Ltd. for their in kind contribution.

References
[1] C. Haddad, C. Périlhon, A. Danlos, M.-X. François and G. Descombes, "Some Efficient Solutions to Recover Low and Medium Waste Heat: Competitiveness of the Thermoacoustic Technology," Energy Procedia, vol. 50, pp. 1056-1069, 2014.
[2] Y. H. Yau, "The use of a double heat pipe heat exchanger system for reducing energy consumption of treating ventilation air in an operating theatre-A full year energy consumption model simulation," Energy and Buildings, vol. 40, no. 5, pp. 917-925, 2008.
[3] T. D. Swanson and G. C. Birur, "NASA thermal control technologies for robotic spacecraft," Applied Thermal Engineering, vol. 23, no. 9, pp. 1055-1065, June 2003.
[4] J. Choi, M. Jeong, J. Yoo and M. Seo, "A new CPU cooler design based on an active cooling heatsink combined with heat pipes," Applied Thermal Engineering, vol. 44, pp. 50-56, November 2012.
[5] H. Jouhara and R. Meskimmon, "Heat pipe based thermal management systems for energy-efficient data centres," Energy, vol. 77, pp. 265-270, 2014.
[6] A. Faghri, "Heat pipes: Review, Opportunities and Challenges," Frontiers in Heat Pipes, vol. 5, no. 1, pp. 1-48, 2014.
[7] D. Reay and P. Kew, Heat pipes: Theory, Design and Applications, Elsevier Limited, 2006.
[8] C. Han and L. Zou, "Study on the heat transfer characteristics of a moderate-temperature heat pipe heat exchanger," International Journal of Heat and Mass Transfer, vol. 91, pp. 302-310, 2015.
[9] H. Shabgard, M. J. Allen, N. Sharifi, S. P. Benn, A. Faghri and T. L. Bergman, "Heat pipe heat exchangers and heat sinks: Opportunities, challenges, applications, analysis, and state of the art," International Journal of Heat and Mass Transfer, vol. 89, pp. 138-158, 2015.
[10] H. Jouhara and R. Meskimmon, "Experimental investigatuion of wraparound loop heat pipe heat exchanger used in energy efficient air handling units," Energy, vol. 35, no. 12, pp. 4592-4599, 2010.
[11] A. Faghri, "Review and Advances in Heat Pipe Science and Technology," Journal of Heat Transfer, vol. 134, no. 12, 12 October 2012.
[12] Econotherm, "Econotherm - Waste Heat Recovery & Recycling Technology," 2012. [Online]. Available: http://www.econotherm.eu/index.html. [Accessed 1 2012].
[13] H. Hagens, F. Ganzevles, C. van der Geld and M. Grooten, "Air heat exchangers with long heat pipes: Experiments and predictions," Applied Thermal Engineering, no. 27, pp. 2646-2434, 2007.
[14] S. Noie, "Heat transfer characteristics of a two-phase closed thermosyphon," Applied Thermal Engineering 25, pp. 495-506, 2005.
[15] A. Nuntaphan, J. Tiansuwan and T. Kiatsiriroat, "Heat Transfer Coefficients of Thermosyphon Heat Pipe at Medium Operating Temperature," Thailand, 2001.
[16] L. Vasiliev, "Heat Pipes in modern heat exchangers," Elsevier, Belarus Minsk, Russia, 2005.
[17] J. T. Cieslinski and A. Fiuk, "Heat transfer characteristics of a two-phase thermosyphon heat exchanger," Applied Thermal Engineering, vol. 51, no. 1-2, pp. 112-118, 2012.
[18] Y. Yau and M. Ahmadzadehtalatapeh, "A review on the application of horizontal heat pipe heat exchangers in air conditioning systems in the tropics," Applied Thermal Engineering, vol. 30, no. 2-3, pp. 77-84, 2010.
[19] M. Ahmadzadehtalatapeh, "An air-conditioning system performance enhancement by using heat pipe based heat recovery technology," Scientia Iranica, vol. 20, no. 2, pp. 329-336, April 2013.
[20] T. Jadhav and M. Lele, "Theoretical energy saving analysis of air conditioning system using heat pipe heat exchanger for Indian climatic zones," Engineering Science and Technology, an International Journal, vol. 18, no. 4, pp. 669-673, 2015.
[21] F. Yang, X. Yuan and G. Lin, "Waste heat recovery using heat pipe heat exchanger for heating automobile using exhaust gas," Applied Thermal Engineering, vol. 23, no. 3, pp. 367-372, 2003.

[22] Y. Wang, X. Han, Q. Liang, W. He and Z. Lang, "Experimental investigation of the thermal performance of a novel concentric condenser heat pipe array," International Journal of Heat and Mass Transfer, vol. 82, pp. 170-178, March 2015.
[23] W. Srimuang and P. Amatachaya, "A review of the applications of heat pipe heat exchangers for heat recovery," Renewable and Sustainable Energy Reviews, vol. Volume 16, no. Issue 6, pp. 4303-4315, 2012.
[24] S. Noie, "Investigation of thermal performance of an air-to-air thermosyphon heat exchanger using ε-NTU method," Applied Thermal Engineering, vol. 26, no. 5-6, pp. 559-567, 2006.
[25] J. Danielewicz, M. A. Sayegh, B. Sniechowska, M. Szulgowska-Zgrzywa and H. Jouhara, "Experimental and analytical performance investigation of air to air two phase closed themrosyphon based heat exchangers," Energy, vol. 77, pp. 82-87, December 2014.
[26] H. Jouhara and H. Merchant, "Experimental investigation of a thermosyphon based heat exchanger used in energy efficient air handling units," Energy, pp. 82-89, 2012.
[27] A. Alizadehdakhel, M. Rahimi and A. Alsairafi, "CFD modeling of flow and heat transfer in a thermosyphon," International Communicaitons in Heat and Mass Transfer 37, pp. 312-318, 2010.
[28] B. Fadhl, L. C. Wrobel and H. Jouhara, "Numerical modelling of the temperature distribution in a two-phase closed thermosyphon," Applied Thermal Engineering, vol. 60, no. 1-2, pp. 122-131, 2013.
[29] H. Jouhara, B. Fadhl and L. C. Wrobel, "Three-dimensional CFD simulation of geyser boiling in a two-phase closed thermosyphon," International Journal of Hydrogen Energy, p. In press, 2016.
[30] K. Negishi and T. Sawada, "Heat transfer performance of an inclined two-phase closed thermosyphon," International Journal of Heat and Mass Transfer, vol. 26, pp. 1207-1213, 1983.
[31] I. Khazaee, R. Hosseini and S. Noie, "Experimental investigation of effective parameters and correlation of geyser boiling in a two-phase closed thermosyphon," Applied Thermal Engineering, vol. 30, no. 5, pp. 406-412, 2010.
[32] H. Shabgard, B. Xiao, A. Faghri, R. Gupta and W. Weissman, "Thermal characteristics of a closed thermosyphon under various filling conditions," International Journal of Heat and Mass Transfer, vol. 70, pp. 91-102, 2014.
[33] B. Hughes, H. Chaudhry and J. Calautit, "Passive energy recovery from natural ventilation air streams," Applied Energy, vol. 113, pp. 127-140, 2014.
[34] B. Selma, M. Désilets and P. Proulx, "Optimization of an industrial heat exchanger using an open-source CFD code," Applied Thermal Engineering, vol. 69, no. 1-2, pp. 241-250, 2014.
[35] H. Peng, X. Ling and J. Li, "Numerical simulation and experimental verification on thermal performance of a novel fin-plate thermosyphon," Applied Thermal Engineering, vol. 40, pp. 181-188, 2012.
[36] J. K. Calautita, H. N. Chaudhrya, B. R. Hughesa and S. A. Ghanib, "Comparison between evaporative cooling and a heat pipe assisted thermal loop for a commercial wind tower in hot and dry climatic conditions," Applied Energy, vol. 101, pp. 740-755, 2013.
[37] H. Mroué, J. Ramos, L. Wrobel and H. Jouhara, "Experimental and numerical investigation of an air-to-water heat pipe-based heat exchanger," Applied Thermal Engineering, vol. 78, no. ISSN 1359-4311, pp. 339-350, 2015.
[38] E. Azad and F. Geoola, "A design procedure for gravity assisted heat pipe heat exchanger," Heat Recovery System, vol. 4, no. 2, pp. 101-111, 1984.
[39] W. Kays and A. London, Compact Heat Exchanger Design, third ed. ed., New York: McGraw-Hill, 1984.
[40] A. Lukitobudi, A. Akbarzadeh, P. Johnson and P. Hendy, "Design, construction and testing of a thermosyphon heat exchanger for medium temperature heat recovery in bakeries," Heat Recovery Systems and CHP, vol. 15, no. 5, pp. 481-491, 1995.
[41] A. Zhukauskas, "Heat Transfer from Tubes in Cross Flow," in Advances in Heat Transfer, J. H. a. T. Irvine, Ed., New York, Academic Press, 1972.
[42] Y. A. Çengel, in Heat Transfer: A Practical Approach, McGraw-Hill, 2002, pp. 7, 515.
[43] A. Faghri, Heat Pipe Science and Technology, Taylor & Francis, 1995.
[44] W. Rohsenow, J. Hartnett and Y. Cho, Handbook of Heat Transfer, third ed. ed., McGraw-Hill, 1998.

[45] J. Ramos, A. Chong and H. Jouhara, “Numerical investigation of a cross flow air-to-water heat pipe-based heat exchanger used in waste heat recovery,” SusTEM 2015, Newcastle, 2015.
[46] W. M. Rohsenow, “A method of correlating heat-transfer data for surface boiling of liquids,” Trans. ASME, vol. 74, pp. 969-976, 1952.
[47] F. Incropera and D. DeWitt, Fundamentals of Heat and Mass Transfer, Fourth Edition ed., New York: John Wiley & Sons, 1996.
[48] W. McAdams, Heat Transmission, New York: McGraw Hill, 1954.
[49] ANSYS, “Ansys Fluent 14.5 Help,” 2012-2014. [Online]. [Accessed 2015].
[50] K. Ekambara, R. Sanders, K. Nandakumar and J. Masliyah, “CFD simulation of bubbly two-phase flow in horizontal pipes,” Chemical Engineering Journal, vol. 144, no. 2, pp. 277-288, 2008.
[51] Fluent Inc., “FLUENT 6.3 User's Guide,” 2014.
[52] J. Ramos, A. Chong, C. K. Tan, J. Matthews, M. A. Boocock and H. Jouhara, “Experimental Analysis of gas to water two phase closed thermosyphon based heat exchanger,” 10th International Conference on Heat Transfer, Fluid Mechanics and Thermodynamics, Orlando, USA, 2014.

Appendix B – CFD results

Condenser section temperature profile for 50°C inlet temperature and 0.05, 0.08, 0.11, 0.14 and 0.17 kg/s mass flow rate in the evaporator section, respectively.

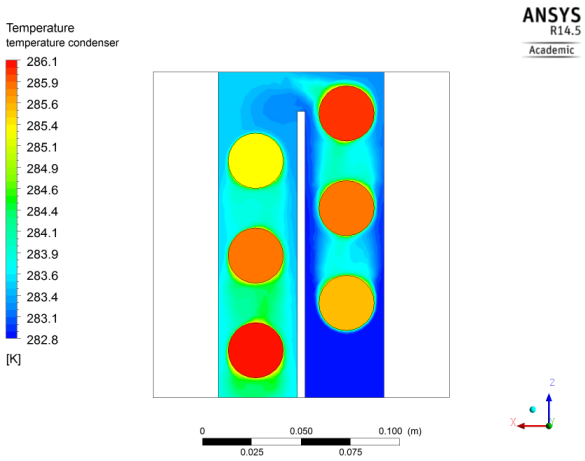

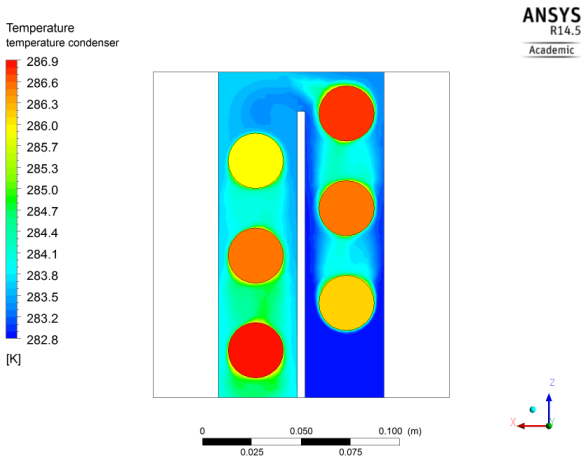

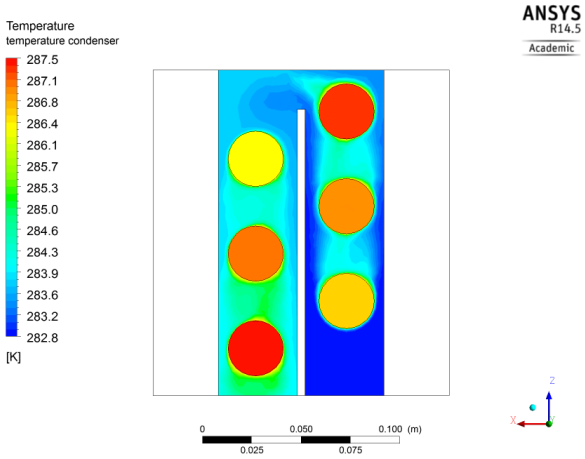

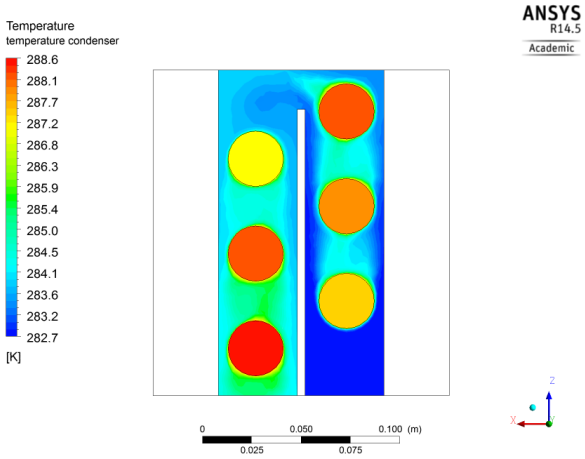

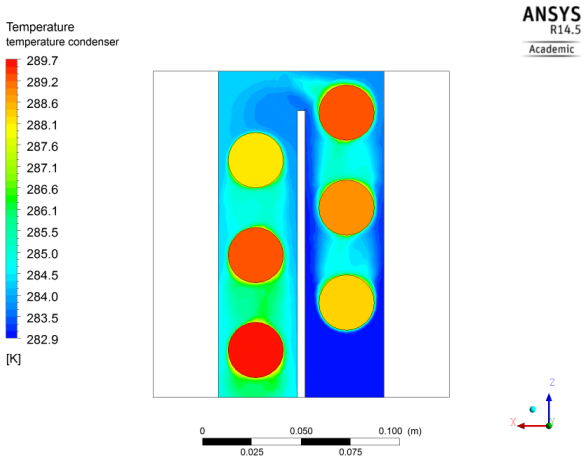

Condenser section temperature profile for 100°C inlet temperature and 0.05, 0.08, 0.11, 0.14 and 0.17 kg/s mass flow rate in the evaporator section, respectively.

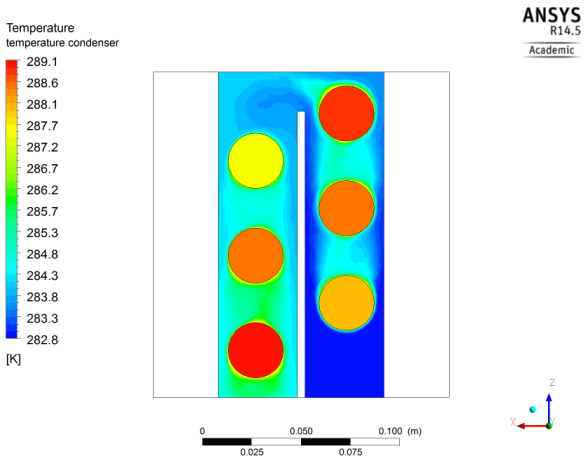

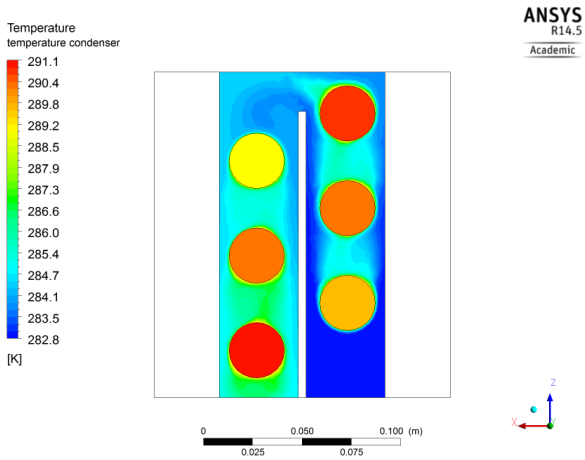

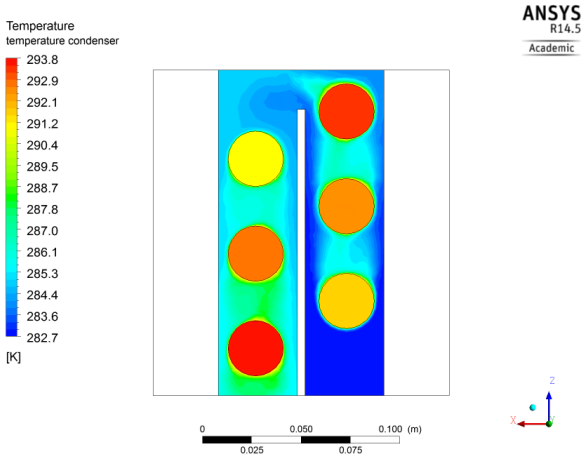

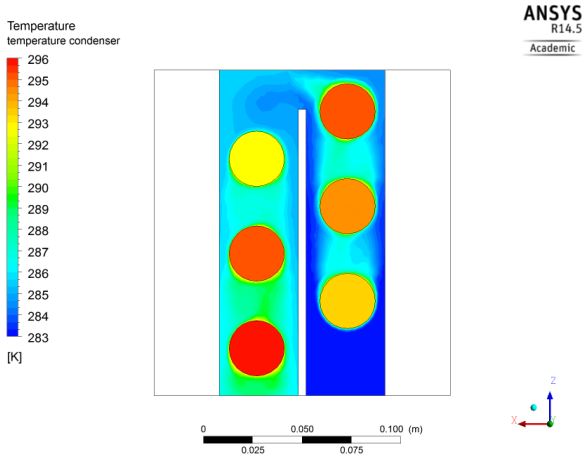

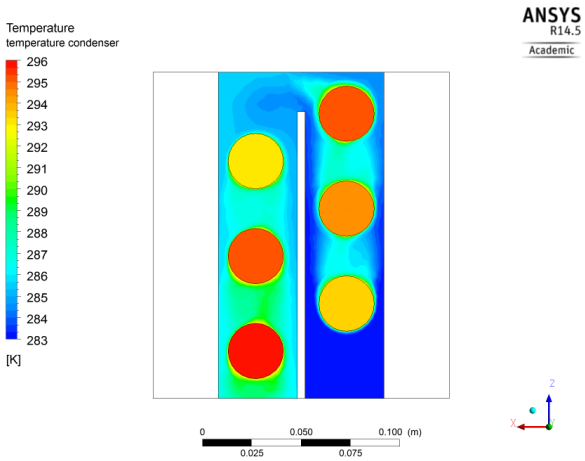

Condenser section temperature profile for 150°C inlet temperature and 0.05, 0.08, 0.11, 0.14 and 0.17 kg/s mass flow rate in the evaporator section, respectively.

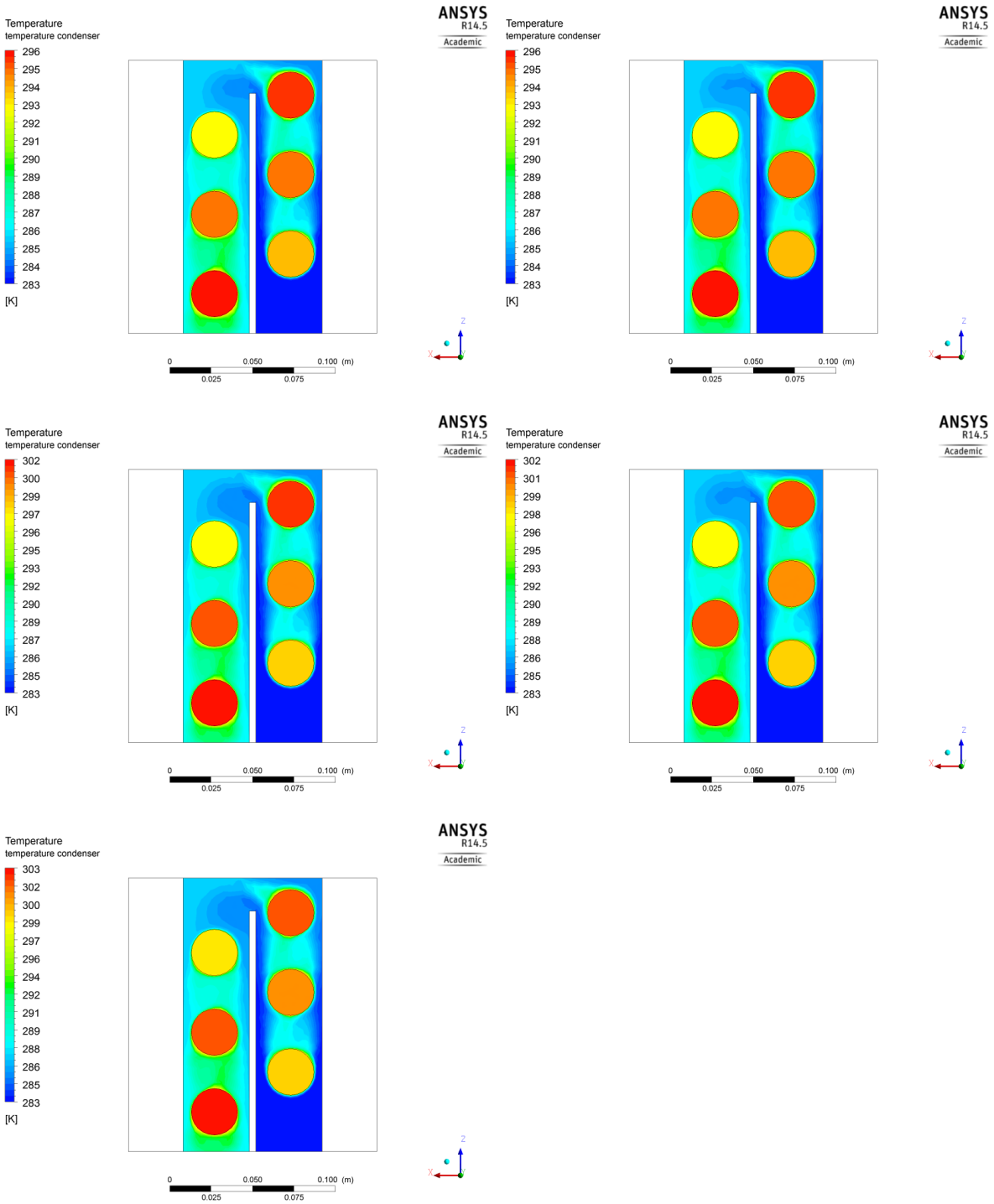

Condenser section temperature profile for 200°C inlet temperature and 0.05, 0.08, 0.11, 0.14 and 0.17 kg/s mass flow rate in the evaporator section, respectively.

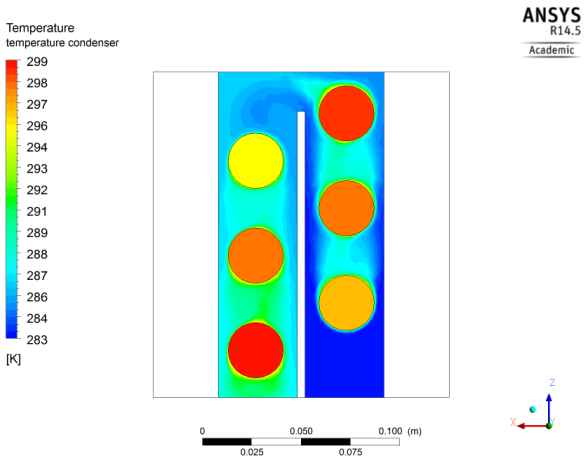

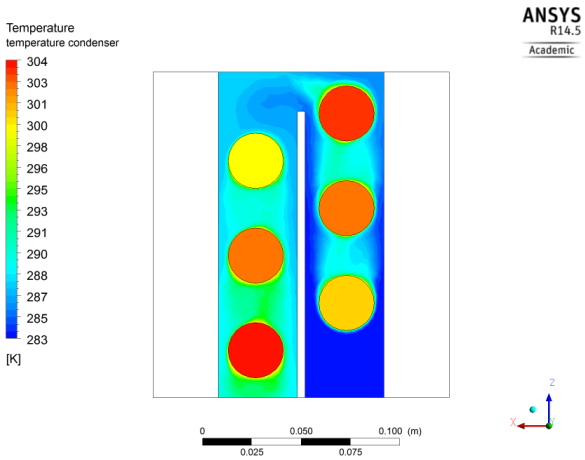

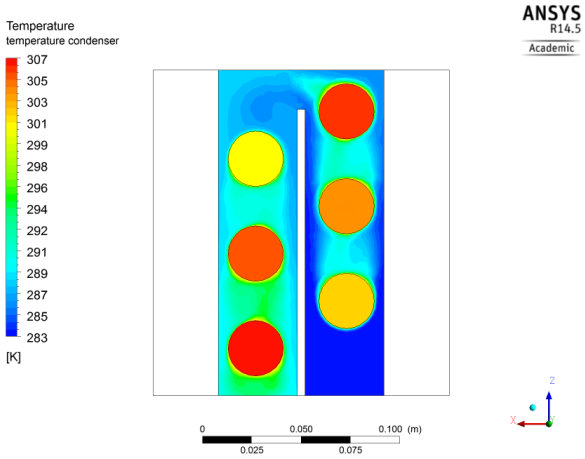

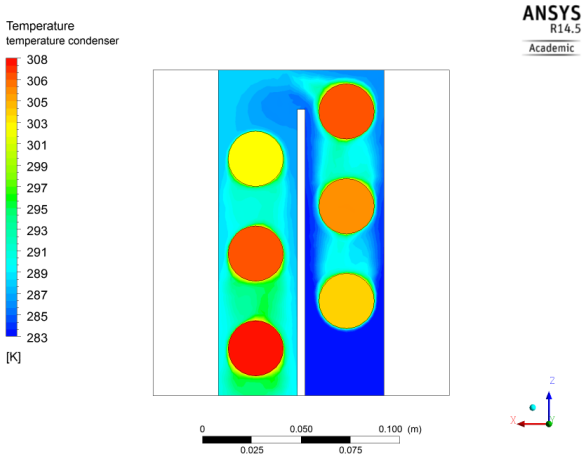

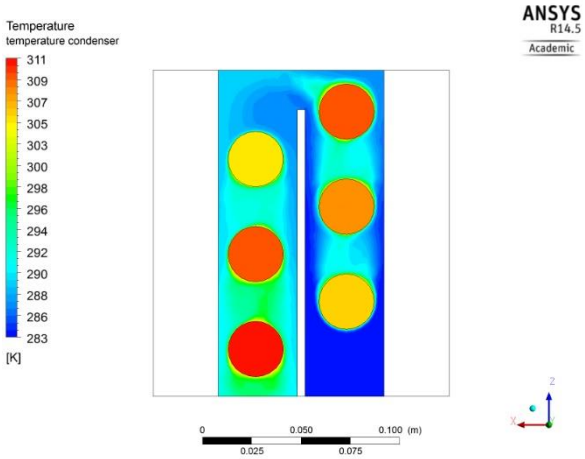

Condenser section temperature profile for 250°C inlet temperature and 0.05, 0.08, 0.11, 0.14 and 0.17 kg/s mass flow rate in the evaporator section, respectively.

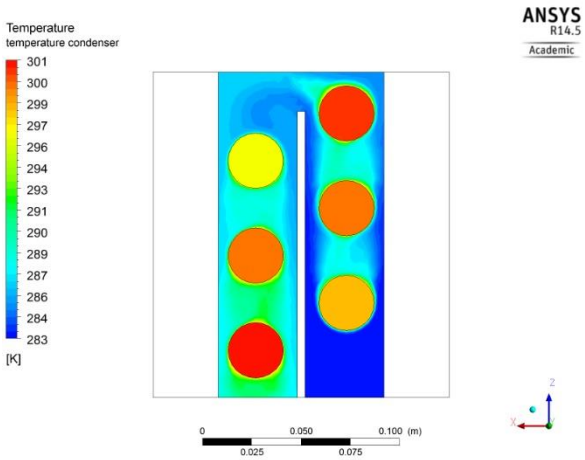

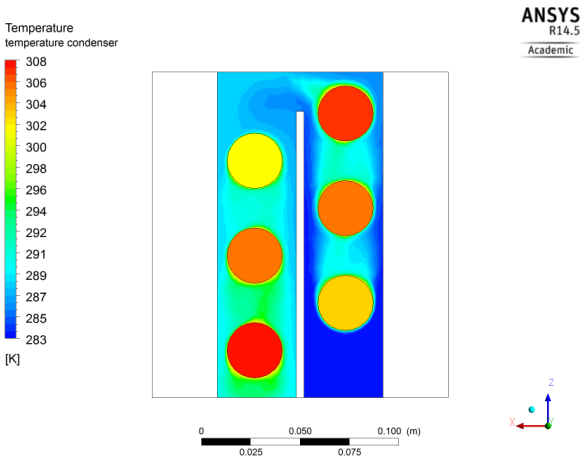

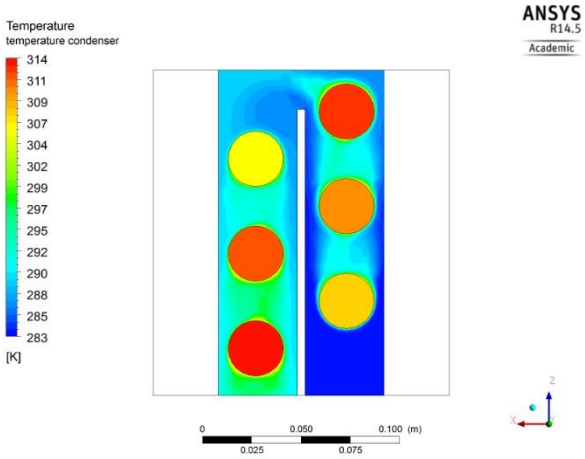

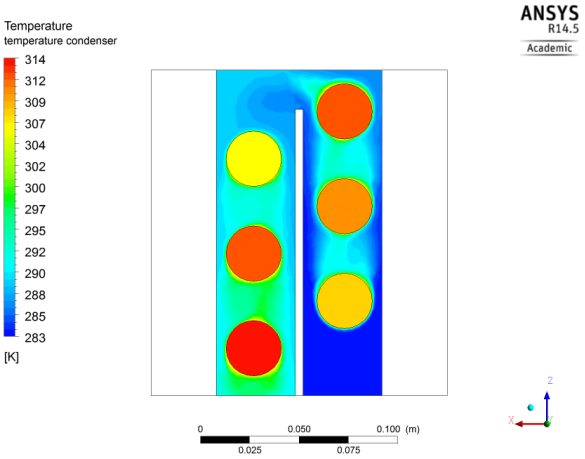

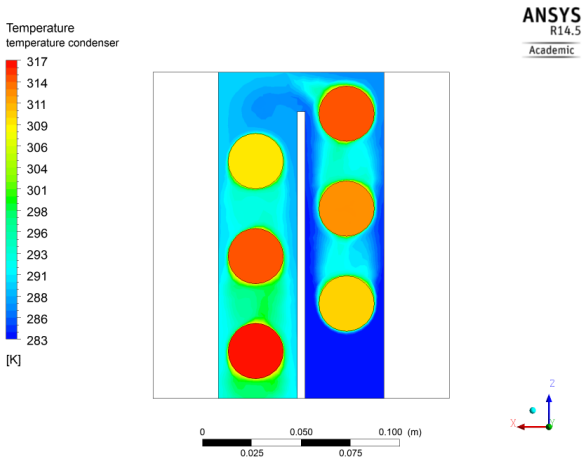

Condenser section temperature profile for 300°C inlet temperature and 0.05, 0.08, 0.11, 0.14 and 0.17 kg/s mass flow rate in the evaporator section, respectively.

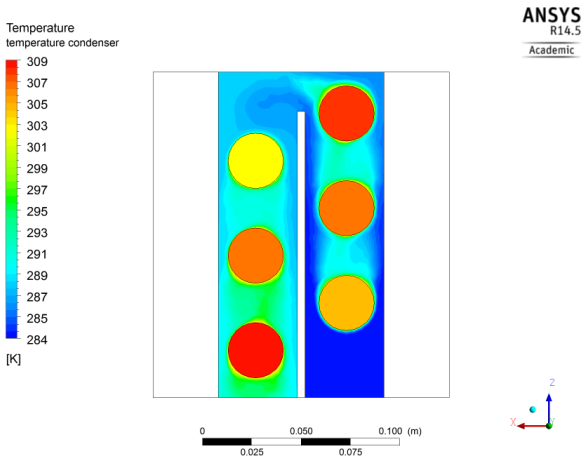

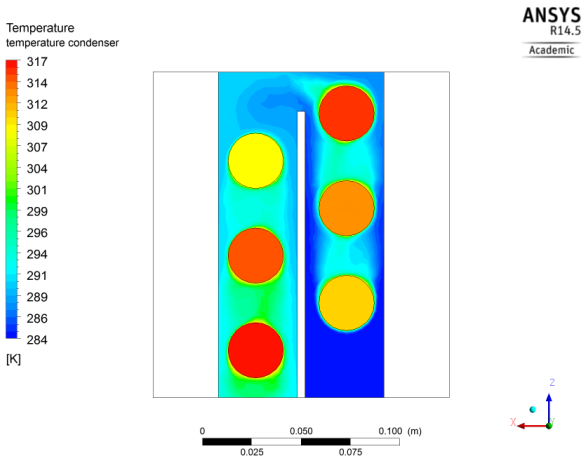

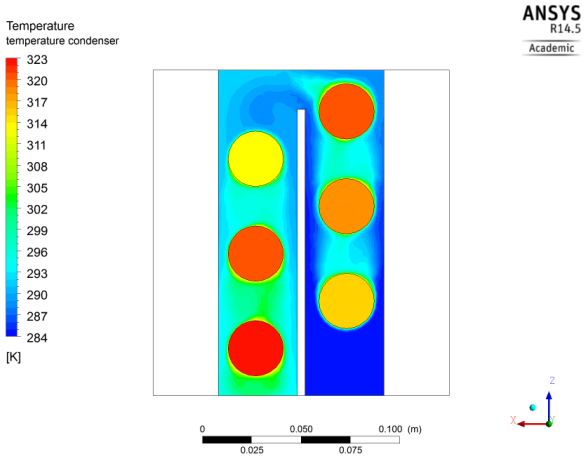

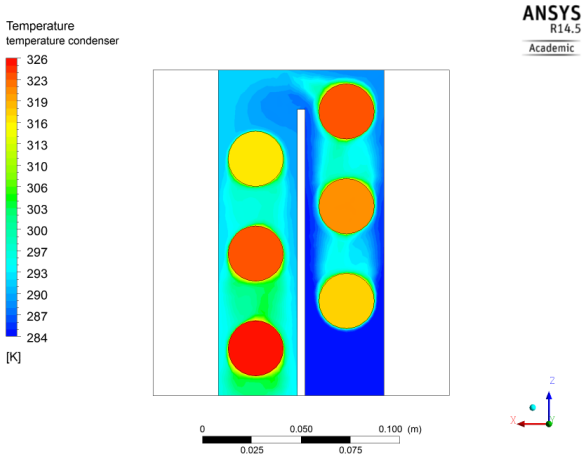

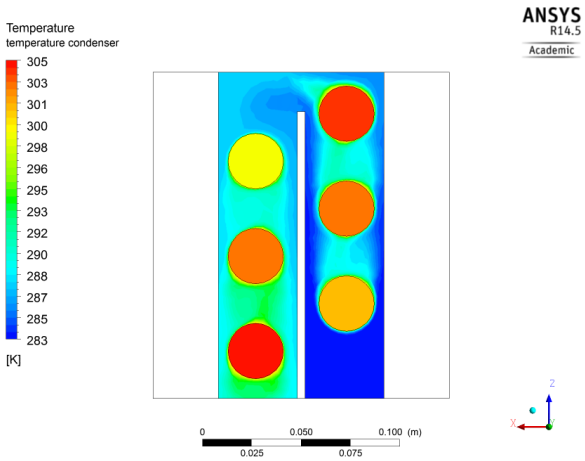

Evaporator section temperature profile for 50°C inlet temperature and 0.05, 0.08, 0.11, 0.14 and 0.17 kg/s mass flow rate, respectively.

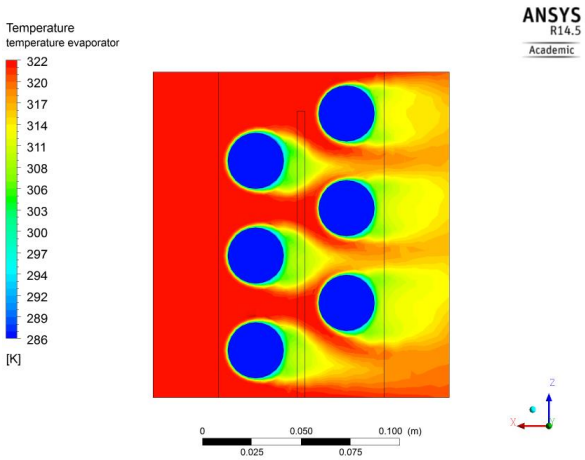

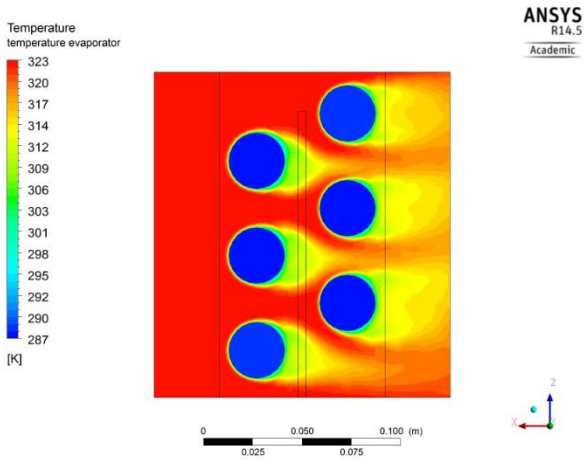

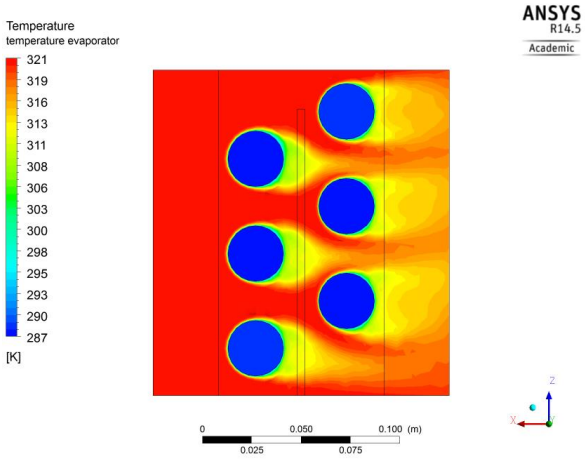

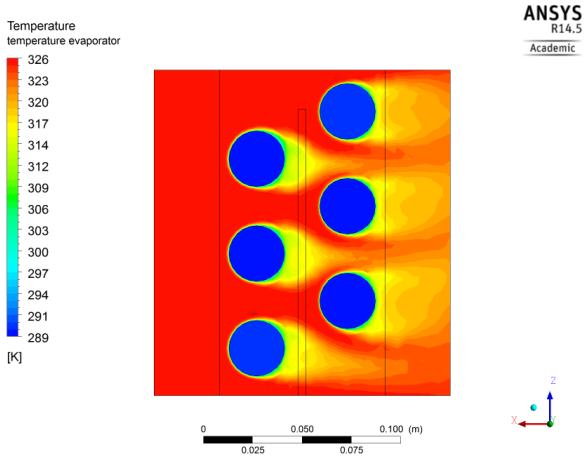

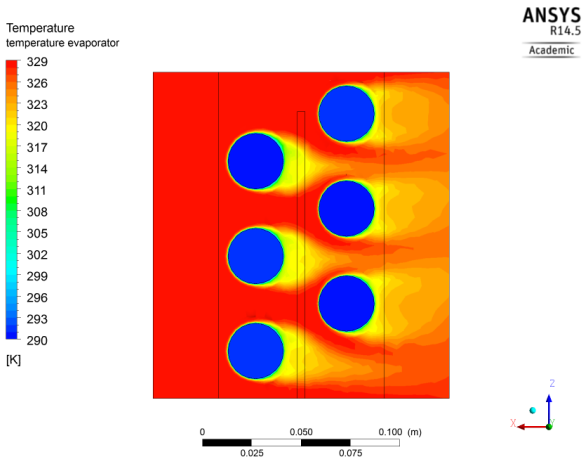

Evaporator section temperature profile for 100°C inlet temperature and 0.05, 0.08, 0.11, 0.14 and 0.17 kg/s mass flow rate, respectively.

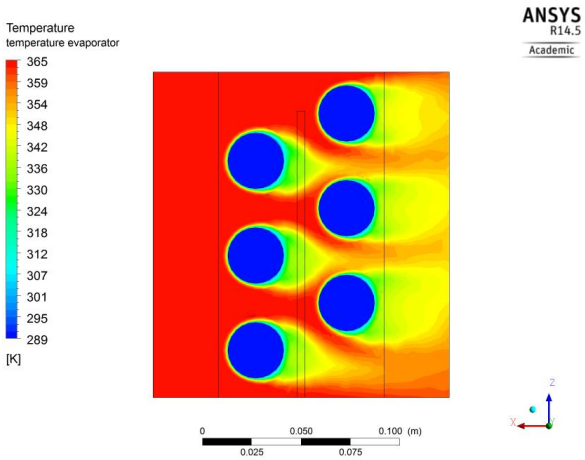

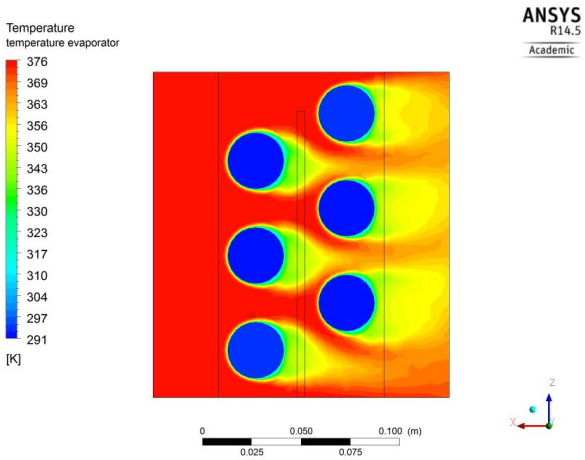

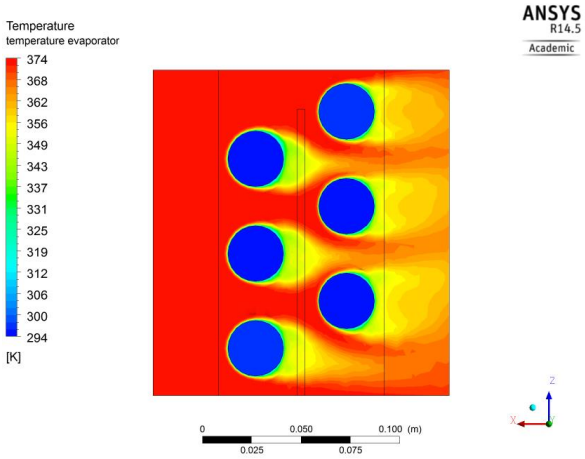

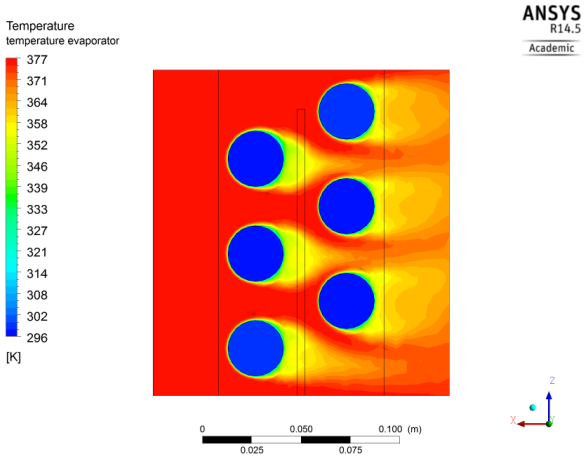

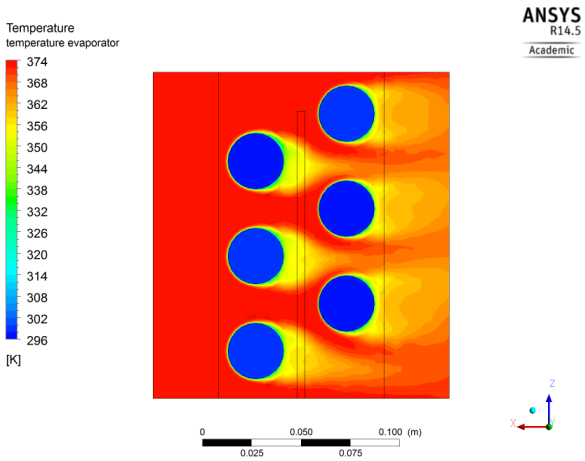

Evaporator section temperature profile for 150°C inlet temperature and 0.05, 0.08, 0.11, 0.14 and 0.17 kg/s mass flow rate, respectively.

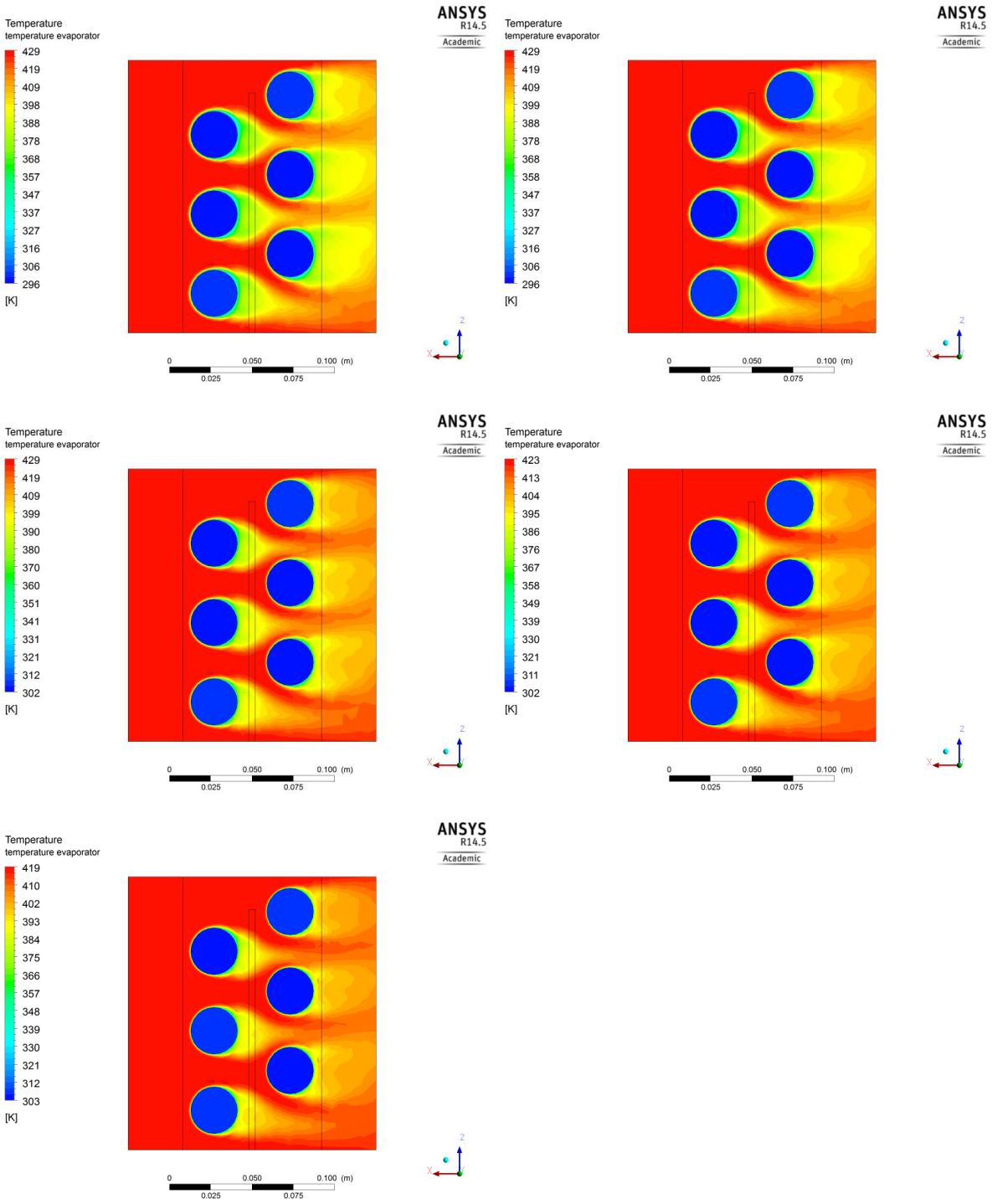

Evaporator section temperature profile for 200°C inlet temperature and 0.05, 0.08, 0.11, 0.14 and 0.17 kg/s mass flow rate, respectively.

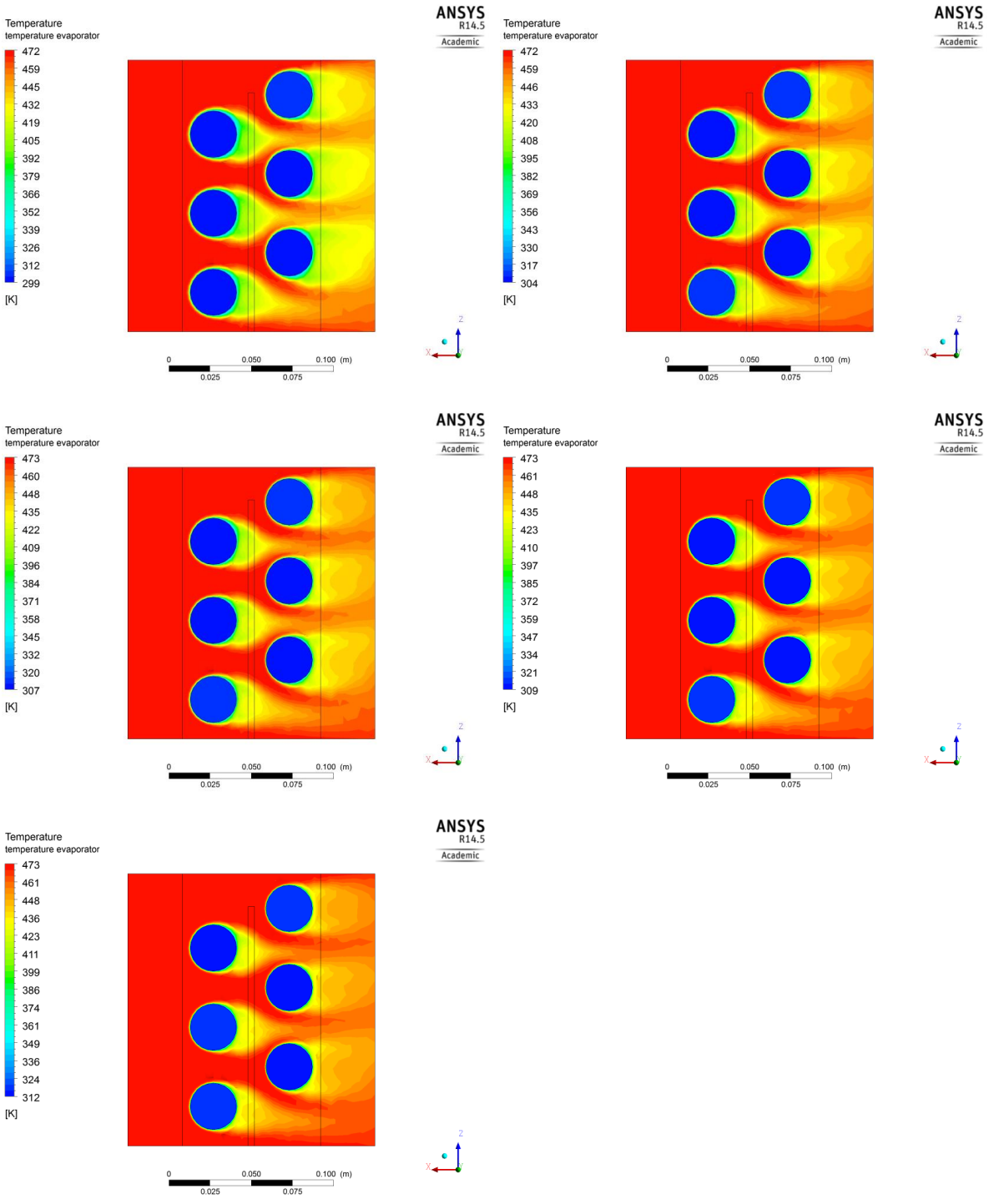

Evaporator section temperature profile for 250°C inlet temperature and 0.05, 0.08, 0.11, 0.14 and 0.17 kg/s mass flow rate, respectively.

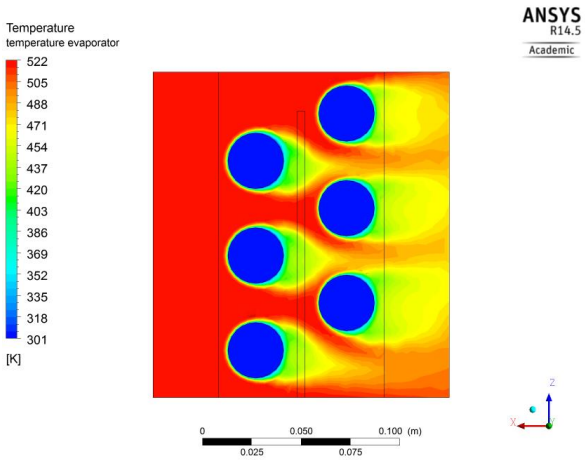

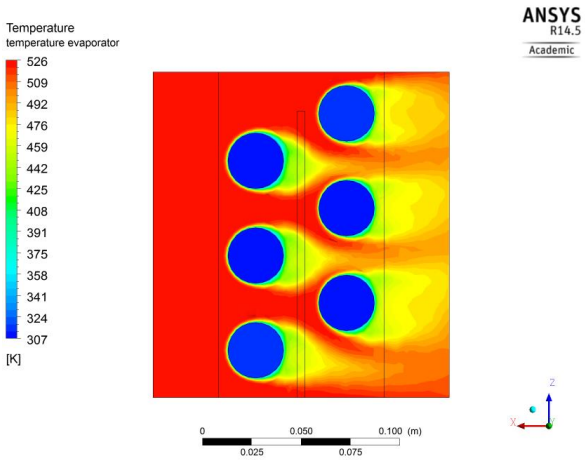

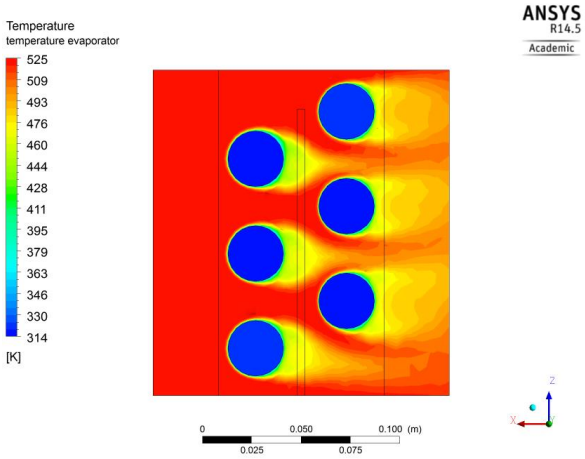

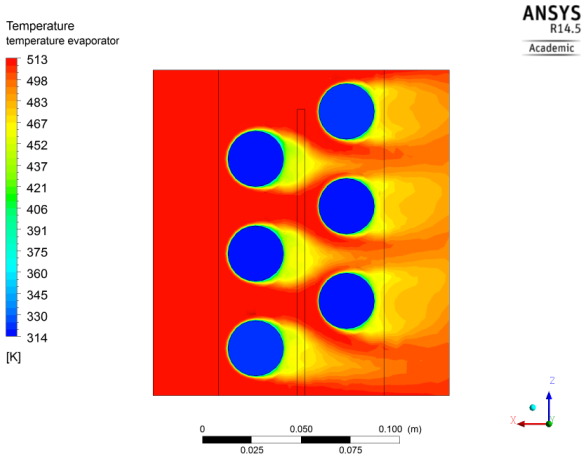

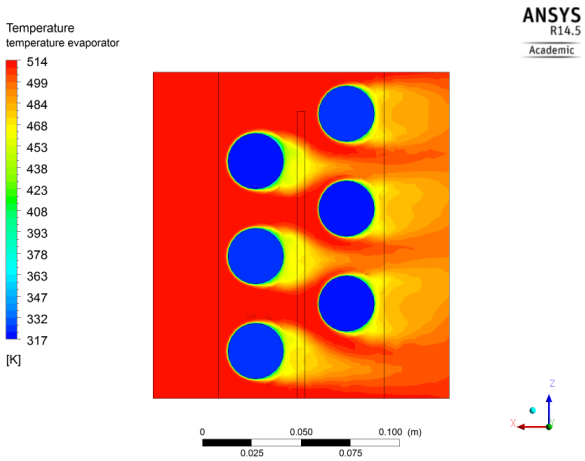

Evaporator section temperature profile for 300°C inlet temperature and 0.05, 0.08, 0.11, 0.14 and 0.17 kg/s mass flow rate, respectively.

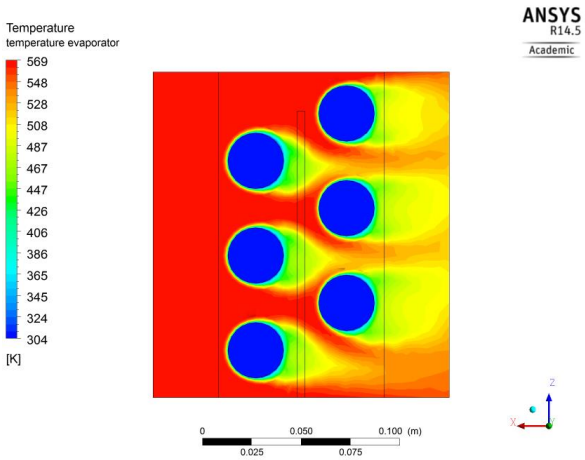

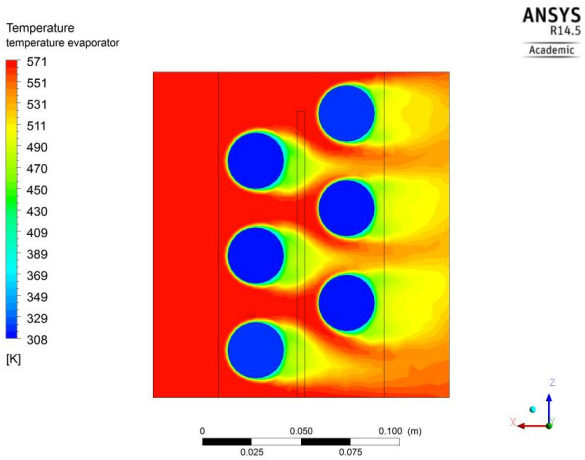

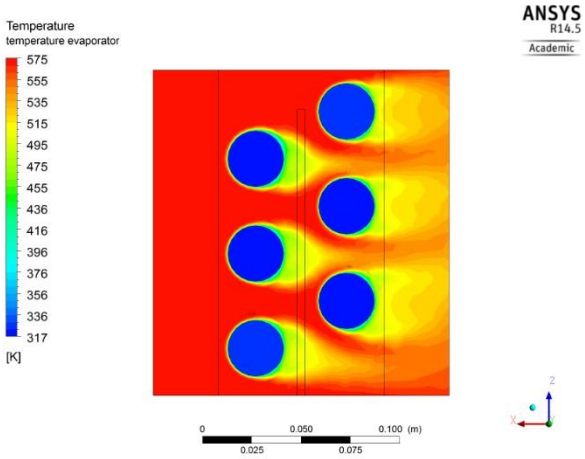

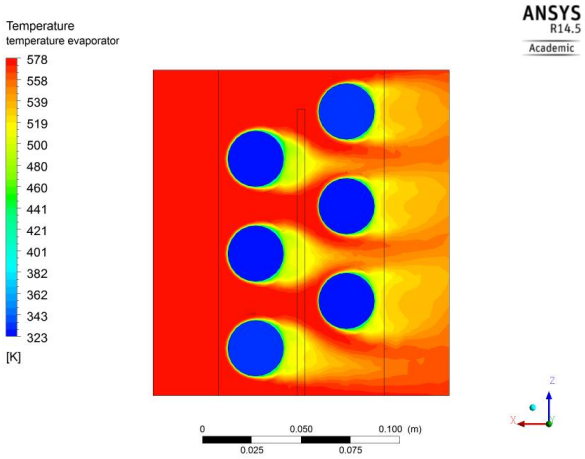

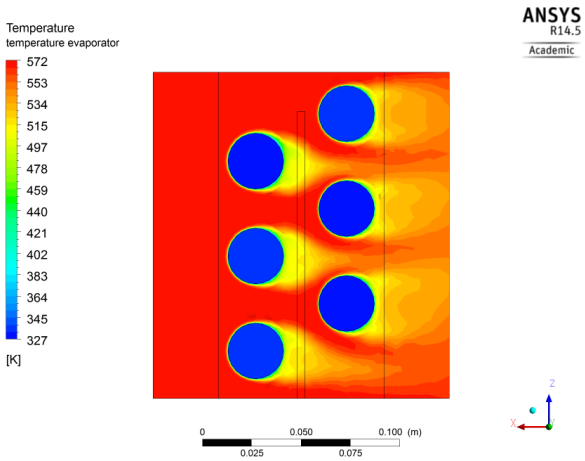

Temperature of the thermosyphons in the front row at 300°C and 0.05 kg/s:

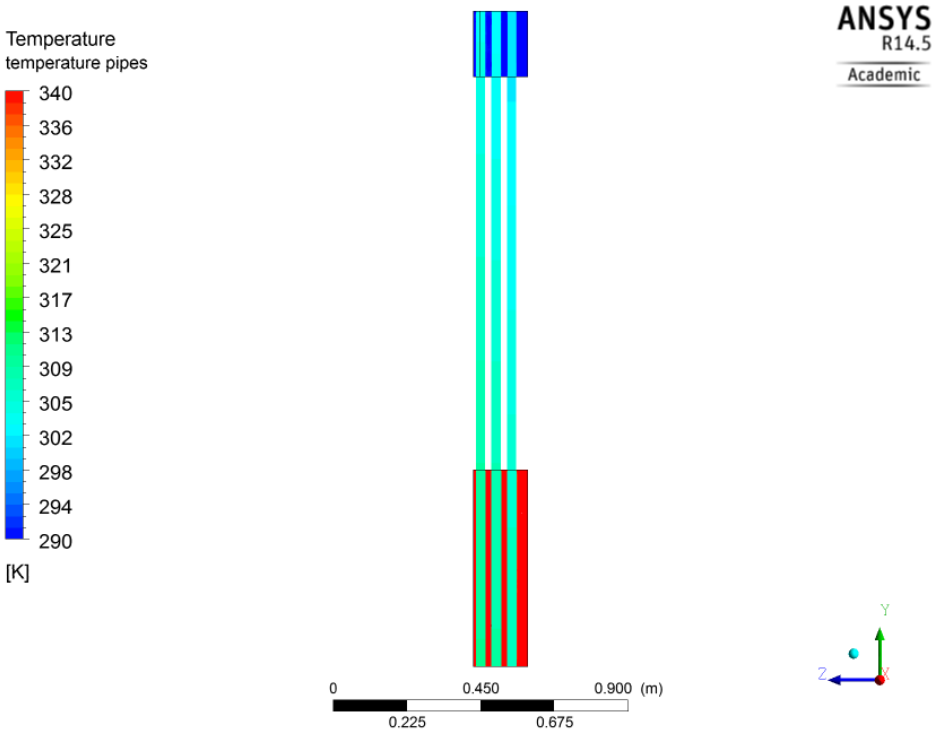

Temperature of the thermosyphons in the back row at 300°C and 0.05 kg/s:

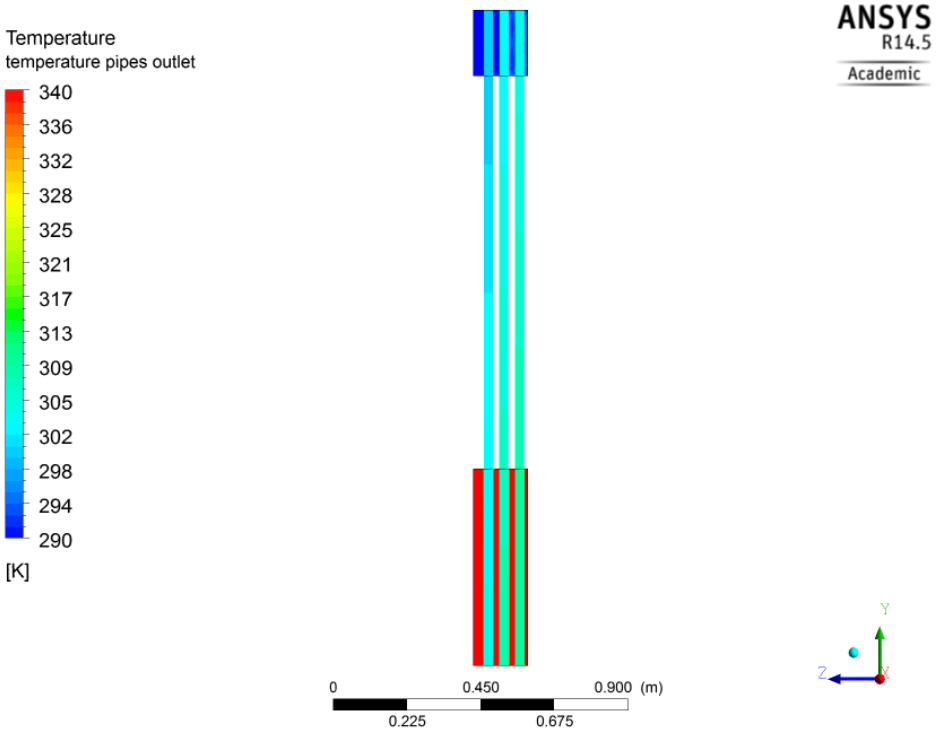

Temperature of the thermosyphons in the front row at 300°C and 0.08 kg/s:

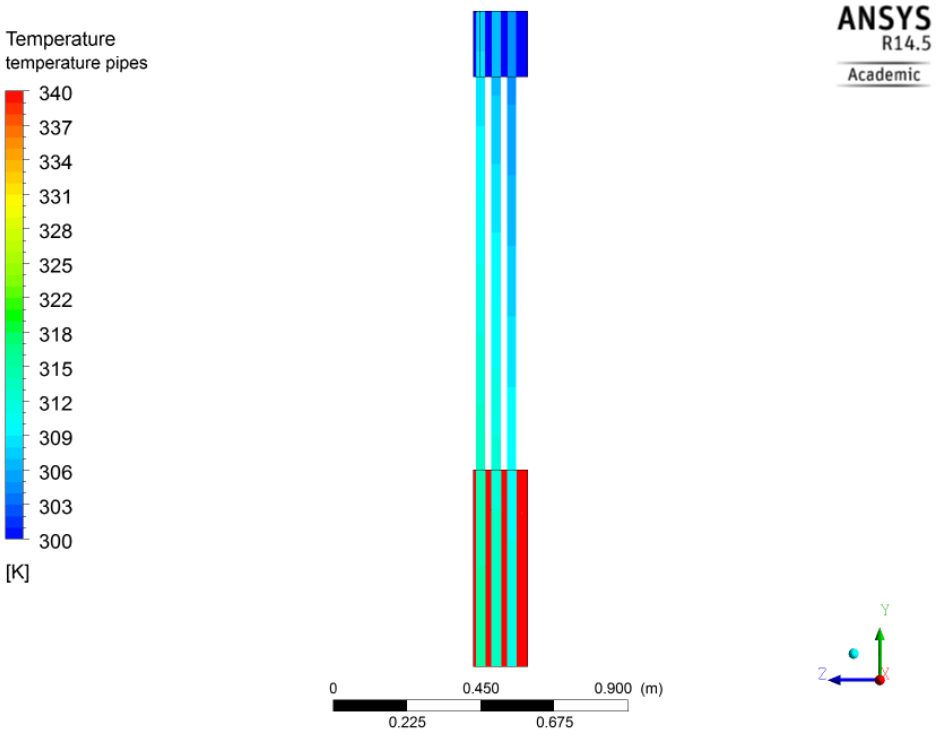

Temperature of the thermosyphons in the back row at 300°C and 0.08 kg/s:

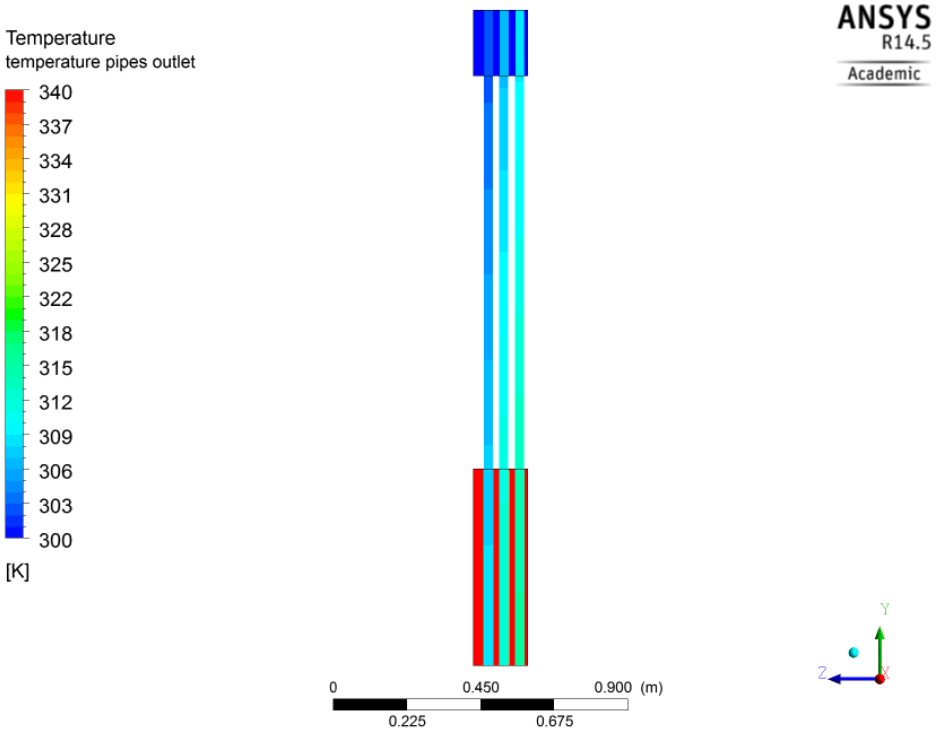

Temperature of the thermosyphons in the front row at 300°C and 0.11 kg/s:

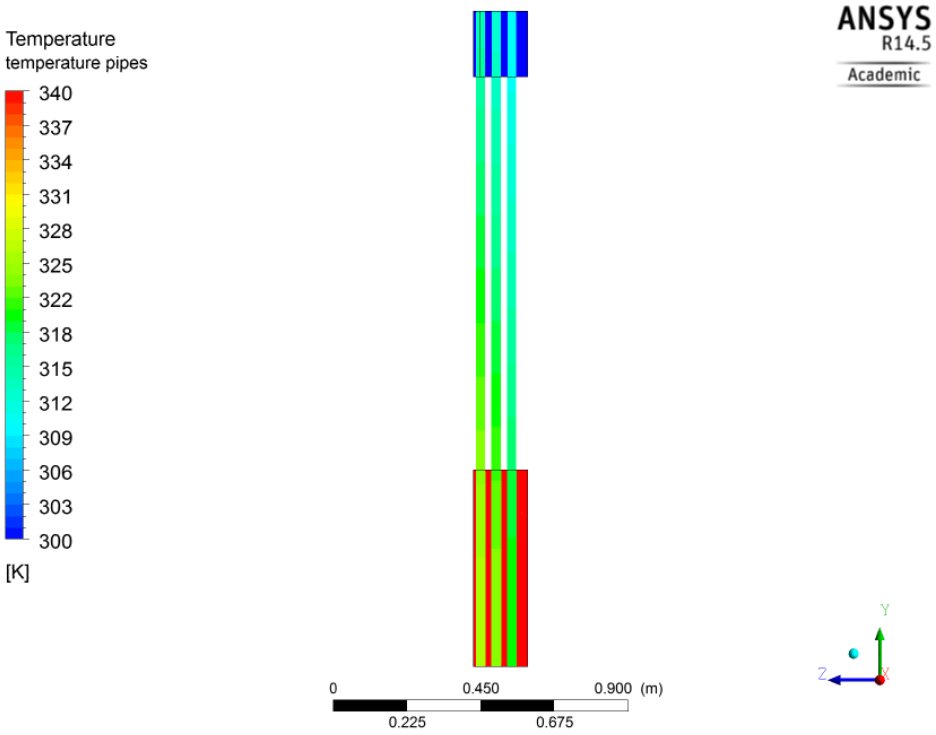

Temperature of the thermosyphons in the back row at 300°C and 0.11 kg/s:

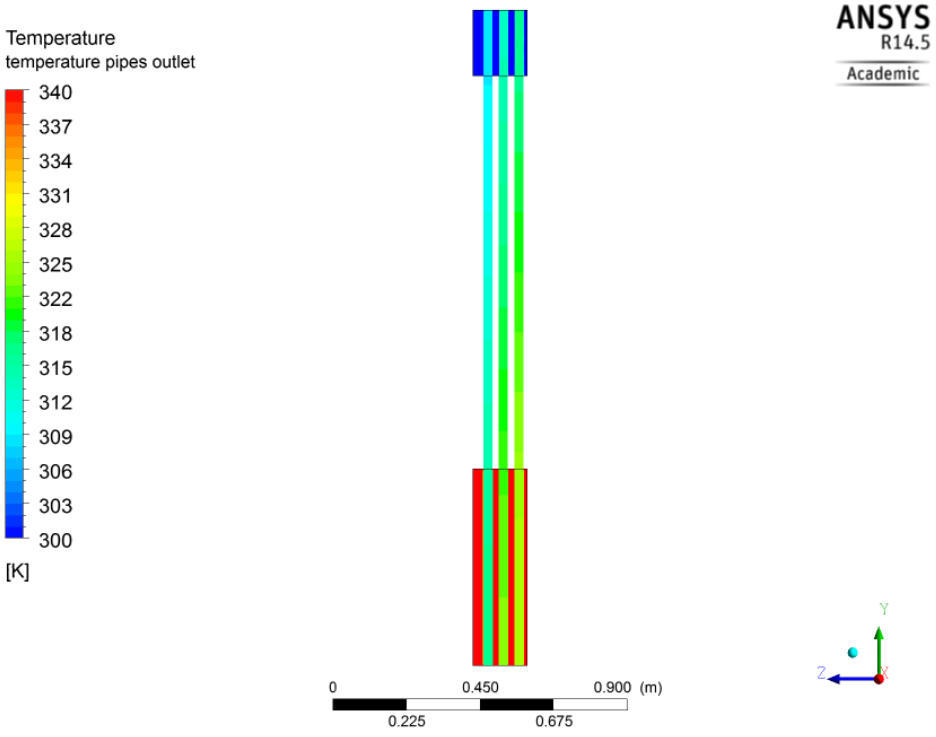

Temperature of the thermosyphons in the front row at 300°C and 0.14 kg/s:

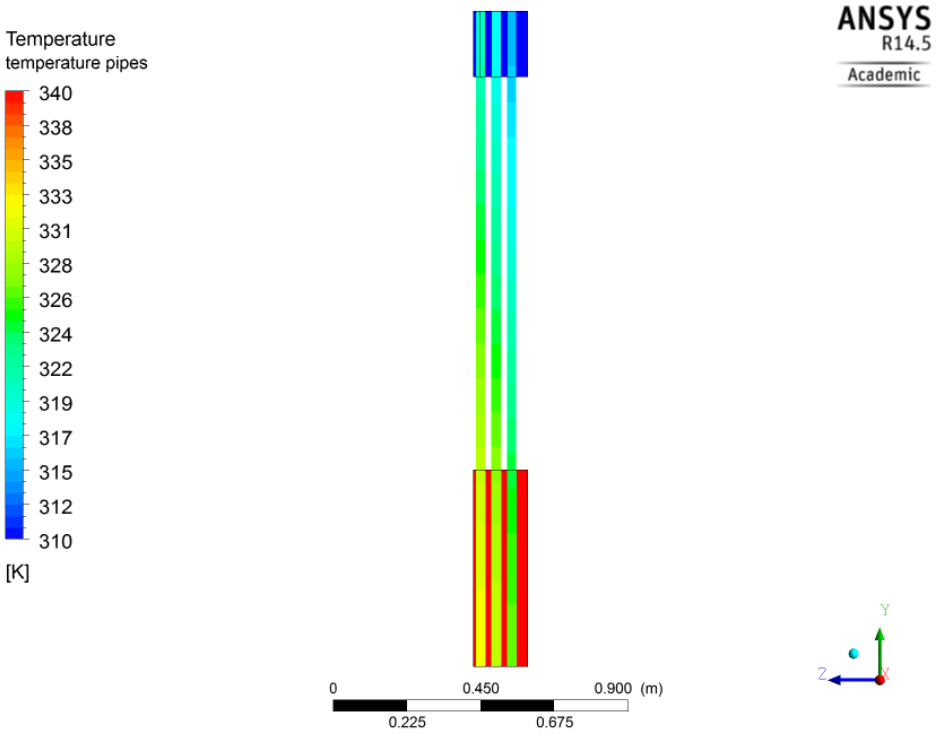

Temperature of the thermosyphons in the back row at 300°C and 0.14 kg/s:

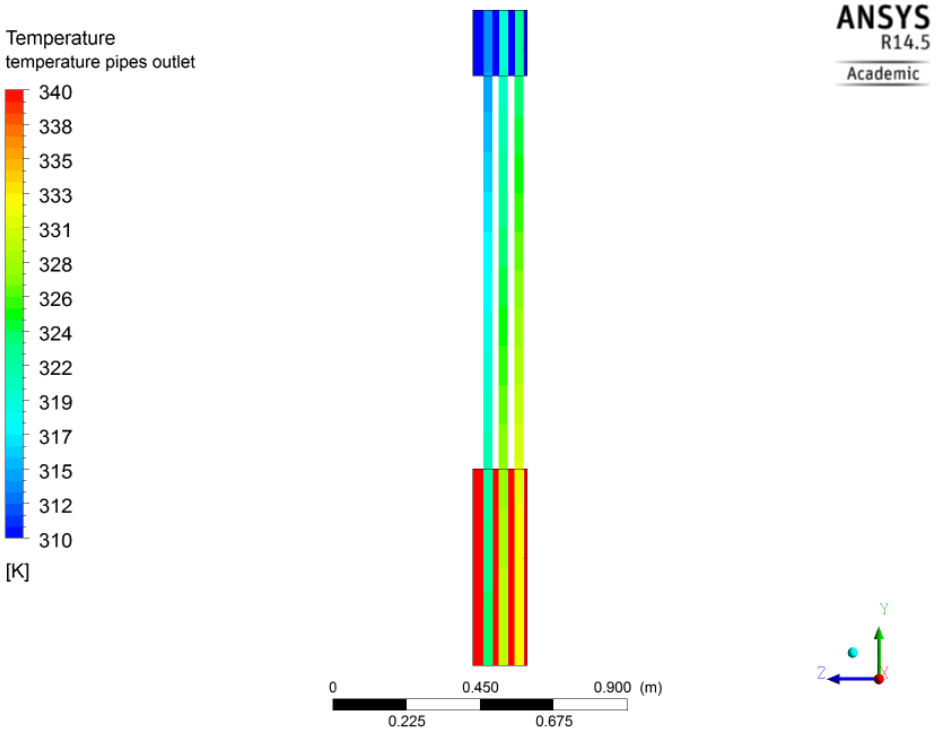

Temperature of the thermosyphon in the front row at 300°C and 0.17 kg/s:

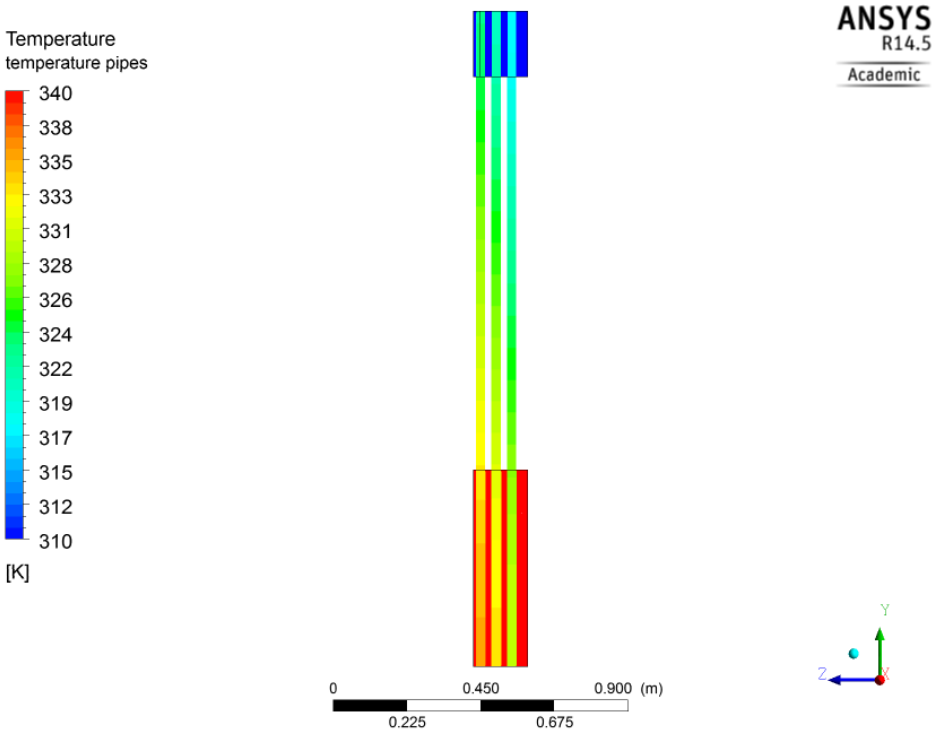

Temperature of the thermosyphon in the back row at 300°C and 0.17 kg/s: